Synthetic, Electrochemical and Thermodynamic Studies of Padlock Macrocyclic Nickel(II) Complexes

A thesis presented by Thomas James Cromie

to the University of St Andrews in application for

The Degree of Doctor of Philosophy

August 2001

Declarations

I, Thomas James Cromie, hereby certify that this thesis has been composed by myself, that it is a record of my work and that it has not been accepted in partial or complete fulfilment of any other degree or professional qualification.

Signed:_ Date: 4-9-01

I was admitted to the Faculty of Science of the University of St Andrews under Ordinance General No. 12 on the 1st April 1996 and as a candidate for the degree of Ph.D. on the 1st April 1997.

Signed:_ Date: 4-9-01

I hereby certify that the candidate has fulfilled the conditions of the Resolution and Regulations appropriate to the degree of Ph.D.

Signature of Supervisor: Date: 4-9-01

Copyright

Contents

Chapter 2

Padlock Macrocycles

Chapter 3

Electrocatalytic Activity

Chapter 4

Nickel(II) Pentaaza Macrocyclic Folding

Chapter 5

Miscellaneous Synthesis

Courses attended

The postgraduate courses I attended were: Advances in Synthetic Chemistry, Dr. F. G. Riddell, Advanced NMR Spectroscopy, Dr. R. K. Mackie and Presentation Skills, Dr. D. M. Smith.

Conferences

USIC '99, Heriot Watt	Presented a talk
RSC Dalton Meeting, St Andrews	Presented a poster
Macrocycles 2000, St Andrews	Presented a poster

Publications

1 R. W. Hay, J. A. Crayston, T. J. Cromie, P. Lightfoot and D. C. L. de Alwis, *Polyhedron*, 1997, **16**, 3557-3563.

2 R. W. Hay, T. J. Cromie and P. Lightfoot, *Transition Met. Chem.*, 1997, **22**, 510.

3 D. C. L. de Alwis, J. A. Crayston, T. J. Cromie, T. Eisenblätter, R. W. Hay, Ya. D. Lampeka, L. V. Tsymbal, *Electrochimica Acta*, 2000, **45**, 2061.

4 T. J. Cromie, R. W. Hay, P. Lightfoot, D. T. Richens and J. A. Crayston, *Polyhedron*, 2001, **20**, 307-312.

Acknowledgements

I wish to thank the University of St Andrews, School of Chemistry for funding this project.

I would like to express my gratitude to several people, first and foremost being Professor R. W. Hay. Professor Hay's support was unfailing and his enthusiasm infectious, he was an inspiration to everyone who met and worked with or for him, he is sadly missed by us all. Also a big thank you to Thomas Clifford and Andrew Danby whom I succeeded in Bob's group.

I would like to thank Dr. Richens and Dr. Crayston for taking over and guiding me through the last couple of years. Also on the thanks list are Professor Cole-Hamilton, Professor Irvine and all the technical staff for their support and encouragement. Thanks also go to Professor Lampeka and his research group, to Chanaka de Alwis and to Ann McConnell.

Outwith the department a debt of friendship and support is owed to all the guys in the fencing club, to my friend and mentor Duncan Pritchard and his wife Mandi, to Iain Munro, Andy Woodman, Richard Foster and Brian Fotheringham. Also to all the guys back home in particular Conor, Neal, Mark, Stuart and Rab and all their wives and families. Finally and most importantly to all of my family, including the Jarosz's, for moral and financial support and of course to my fiancée Emily, thank you one and all.

Either those reactions go or I will...

"The search for truth is in one way hard and in another way easy, for it is evident that no one can master it fully or miss it wholly. But each adds a little to our knowledge of nature, and from all the facts assembled there arises a certain grandeur."

- Aristotle

"The opposite of a correct statement is a false statement. The opposite of a profound truth may well be another profound truth."

- Niels Bohr

"The truth is more important than the facts."

- Frank Lloyd Wright

"I have come to believe that the whole world is an enigma, a harmless enigma that is made terrible by our own mad attempt to interpret it as though it had an underlying truth."

- Umberto Eco

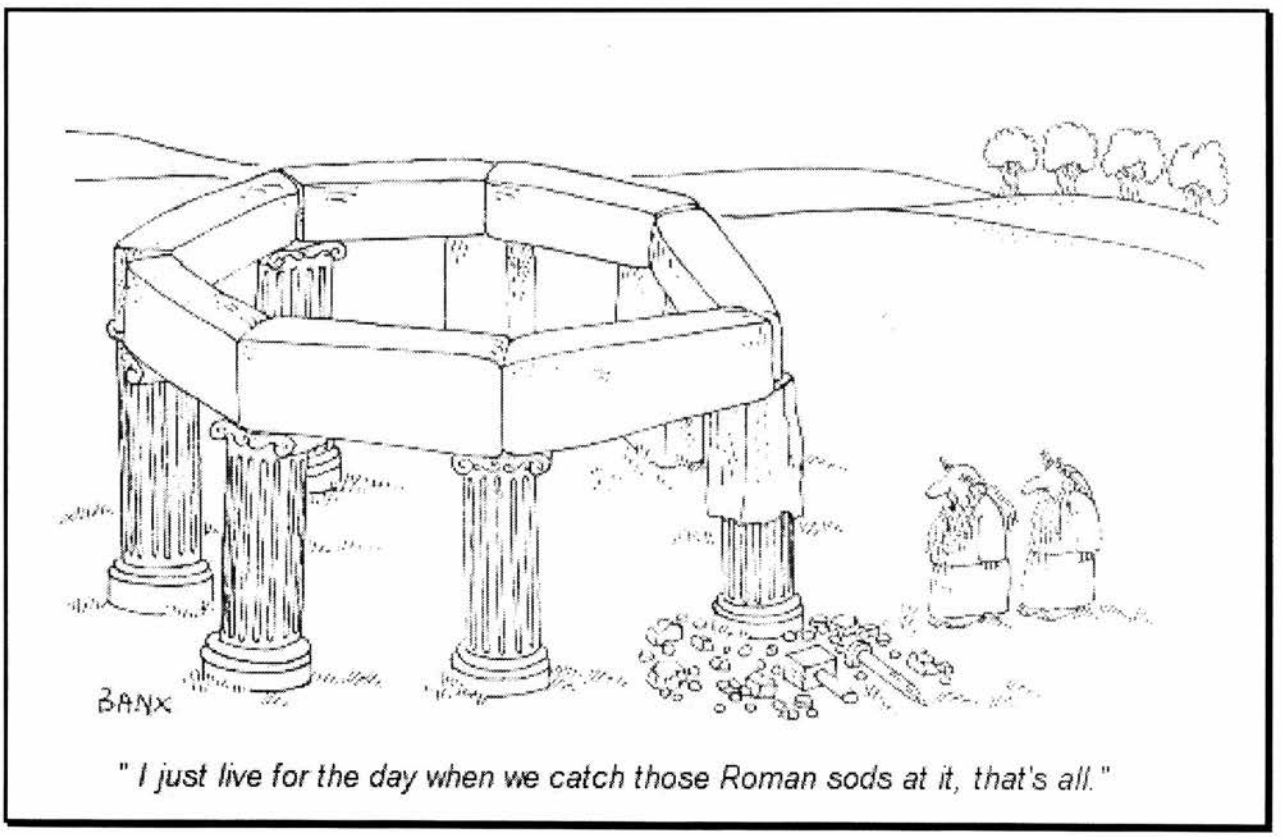

" I just live for the day when we catch those Roman sods at it, that's all."

Empirical Evidence...?

To my family, the memory of my Grandfather Stanley Cromie

and to my fiancée Emily

Abstract

The syntheses, structures and properties of novel padlock macrocycles, including data on the electrocatalytic reduction of CO_2 and adduct formation with 1,2-diaminoethane are described in this thesis. After a review of padlock macrocycles in Chapter 1 (76 references), the synthesis of a novel square planar hydroxyethyl pendant arm padlock macrocyclic Ni(II) complex and its octahedral *trans*-dichloro and *trans*-diisothiocyanato adducts is discussed in Chapter 2. In addition the preparation and characterisation of an octahedral *cis*-1,2-diaminoethane adduct is presented. X-ray crystal structures of all but the dichloro adduct are determined. In addition a benzyl pendant arm macrocycle, a hexaaza tricyclo macrocyclic complex and a dimeric macrocyclic complex are synthesised. The crystal structure of the hexaaza tricyclo macrocyclic complex is also presented. With the notable exception of the 1,2-diaminoethane adduct all the X-ray structures show that the macrocycle is in the most stable *trans*-III configuration, with the pendant arm, on the non-coordinating nitrogen, in the axial position. There is no interaction between the nickel(II) centre and the pendant arm either inter- or intramolecularly. They also show flattening of the uncoordinated bridgehead nitrogen atoms, which is typical for these pentaaza pendant arm macrocycles. Ni-N bond distances are comparable in all square planar structures except the tricyclo structure which has longer bonds to the tertiary nitrogen atoms. The bond lengths of the *trans*-diisothiocyanato adduct and the *cis*-1,2-diaminoethane adduct are typical for octahedral nickel(II) with the 1,2-diaminoethano adduct having slightly longer Ni-N bond distances due to the geometrical distortion of the macrocyclic folding.

The cyclic voltammetry behaviour of several padlock macrocycle complexes, and compares their electrocatalytic efficiency for the reduction of CO_2 is described in Chapter 3. Two types of electrochemical behaviour are noted. It seems that the Type 2 complexes all show low ΔE_P's (73-88 mV) for $Ni^{II/I}$ and reasonable catalytic currents for the reduction of carbon dioxide (17.5-

26.4 mA cm^{-2}). The pendant aminoethyl complex, $[Ni(L_5)]^{2+}$ started as Type 1 with a high ΔE_P and becomes a Type 2 species under reaction conditions as the pH drops to catalyse at a similar rate to Type 2 species. Of the other complexes tested, $[Ni(L_2)]^{2+}$ with the aromatic ring side arm is strongly Type 1 and has a high ΔE_P and a very low i_{cat}. An interesting correlation between peak separation and the catalytic current is noted for the pendant arm macrocycles and two other non-pendant arm complexes, 15aneN$_4$, $[Ni(L_3)]^{2+}$ and the binuclear complex, $[Ni_2(L_4)]^{4+}$. An explanation linking the catalytic current to the electrochemical kinetics is proposed.

In Chapter 4, a novel approach for determining the equilibrium parameters for ligand addition to square planar Ni(II) macrocyclic complexes is described which took into account the planar $\rightleftharpoons$ octahedral equilibrium. Parameters are reported for the reaction between a planar Ni(II) macrocycle ($[Ni(L_1)]^{2+}$) and 1,2-diaminoethane which gave a folded *cis*-octahedral complex. Further kinetic and thermodynamic investigations of this process using a range of chelating ligands is proposed.

Other syntheses are described in Chapter 5 which were not nickel(II) padlock macrocycles. These syntheses were of other interesting macrocycles and complexes, including three dipeptides, which were synthesised as preliminary investigations into other areas. Those projects were: *trans*-dioxocyclam based ligands and complexes, "Big Macs", synthesis of dipeptides for the study of metal promoted ester hydrolysis and copper(II) cyclen complexes. The X-Ray crystal structures of *trans*-dioxocyclam and nickel(II) *trans*-dioxocyclam were solved and discussed as well as an interesting crystal structure of a copper(II) cyclen complex in which a bromide is in the coordination sphere and a perchlorate has crystallised as the counter ion.

Chapter One

Introduction

1.1 Introduction

The vast family of macrocyclic ligands and their complexes has been established as an integral part of the general field of coordination chemistry[1]. The growth in this field since the 1960's has been such that it is now treated as a field separate from traditional acyclic ligand coordination chemistry. The preference for macrocycles over simple mono- or bidentate ligands, in certain cases, arises from the greater stability and inertness of their complexes as well as the extreme physical properties that are the result of their generally strong ligand fields, especially in the case of the aza macrocycles. In addition, entropy considerations favour complexation of metal centres by a single macrocycle over several mono or bidentate ligands, these factors taken together comprise what is known as the macrocyclic effect. We are interested in exploiting this effect to synthesise robust macrocyclic complexes.

Metal template syntheses of multidentate and macrocyclic ligands have been well established over the last two decades as offering high yielding and selective routes to new ligands and their complexes. A template effect arises from the stereochemistry imposed by the metal ion coordination of some of the reactants. This arrangement of reactants promotes a series of controlled steps. This is the *coordination* or *kinetic* template effect and provides routes to products not formed in the absence of the metal ion. In addition, the *thermodynamic* template effect refers to reactions that proceed in the absence of the metal ion but here the metal ion promotes formation of the desired products by removing them from the equilibrium. An equilibrium effect has also been identified, where aspects of both these effects combine; the distinctive feature of this is the formation of different products in the absence of a metal ion[1a].

This thesis is concerned with a particular type of template reaction where a ring closure is brought about by the addition of various "padlocking" nucleophiles. This type of reaction was first identified in 1966 by Thewalt and Weiss, Figure 1[2].

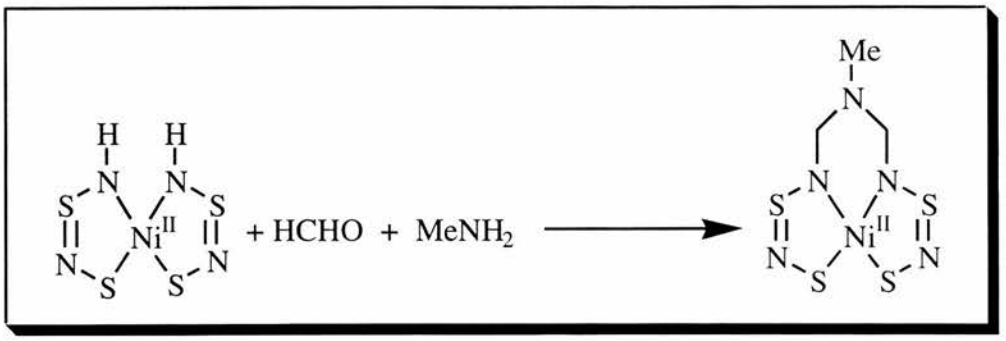

Figure 1

The formaldehyde condenses with the amine to form the imine, then methylamine adds to the imine (analogous to Michael addition) to "lock" the structure together.

Padlock syntheses are simple "one pot" reactions, which makes them both cheap and efficient. They have resulted in the synthesis of a large variety of macrocyclic complexes. The redox properties of macrocyclic complexes are of considerable interest because of their relationship to molecules of biological and environmental importance. For example, the reduction of CO_2 to CO has been achieved using macrocyclic complexes of nickel and cobalt. This is related to processes occurring both in photosynthetic membranes and methanogenic bacteria.

The general mechanism, Figure 2, for the formation of padlock macrocycles is believed to proceed as follows, shown here for the case of an amine nucleophile[3].

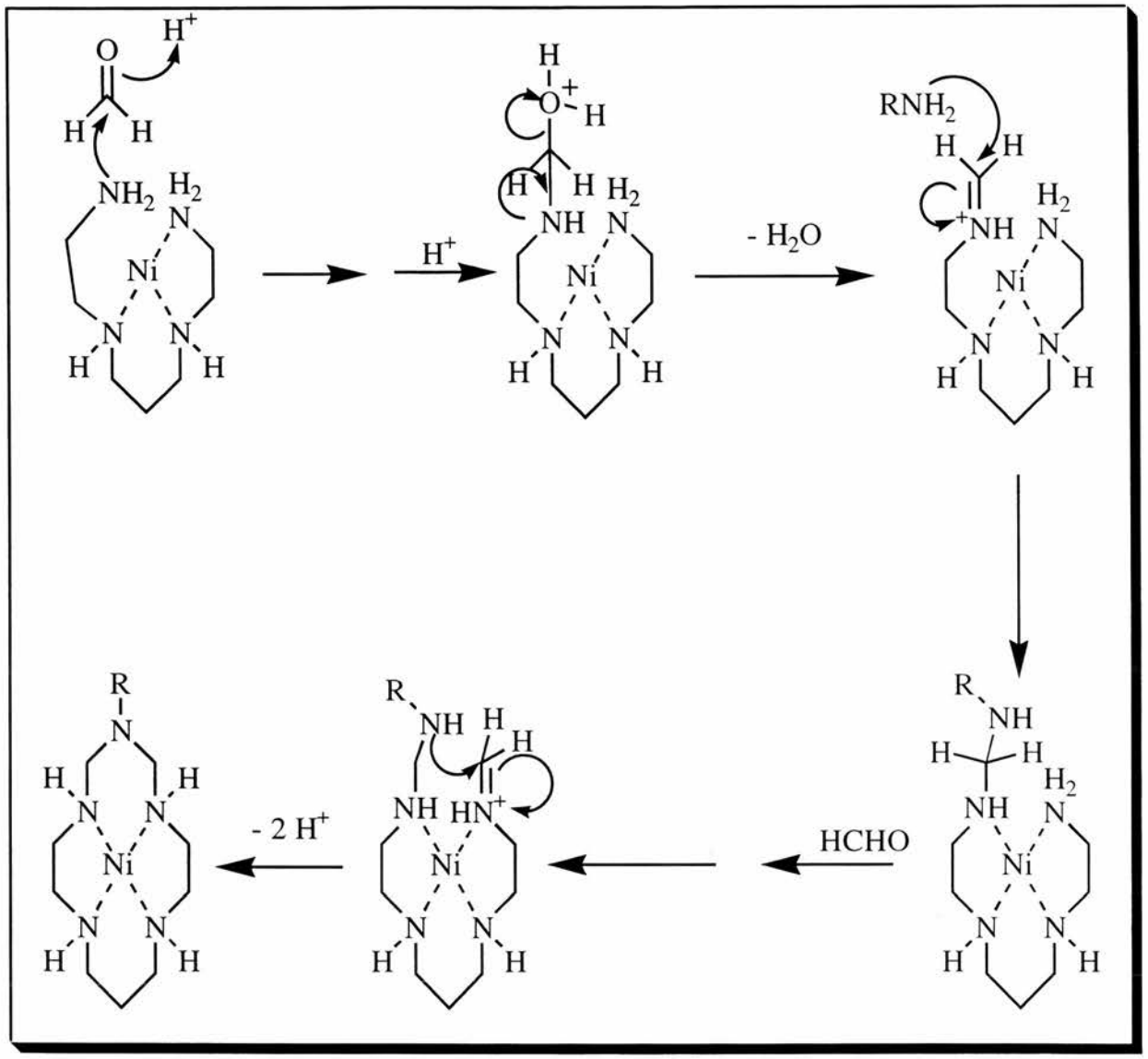

Figure 2

A wide variety of padlocking nucleophiles have been employed and the main categories can be classified as follows, Figure3:

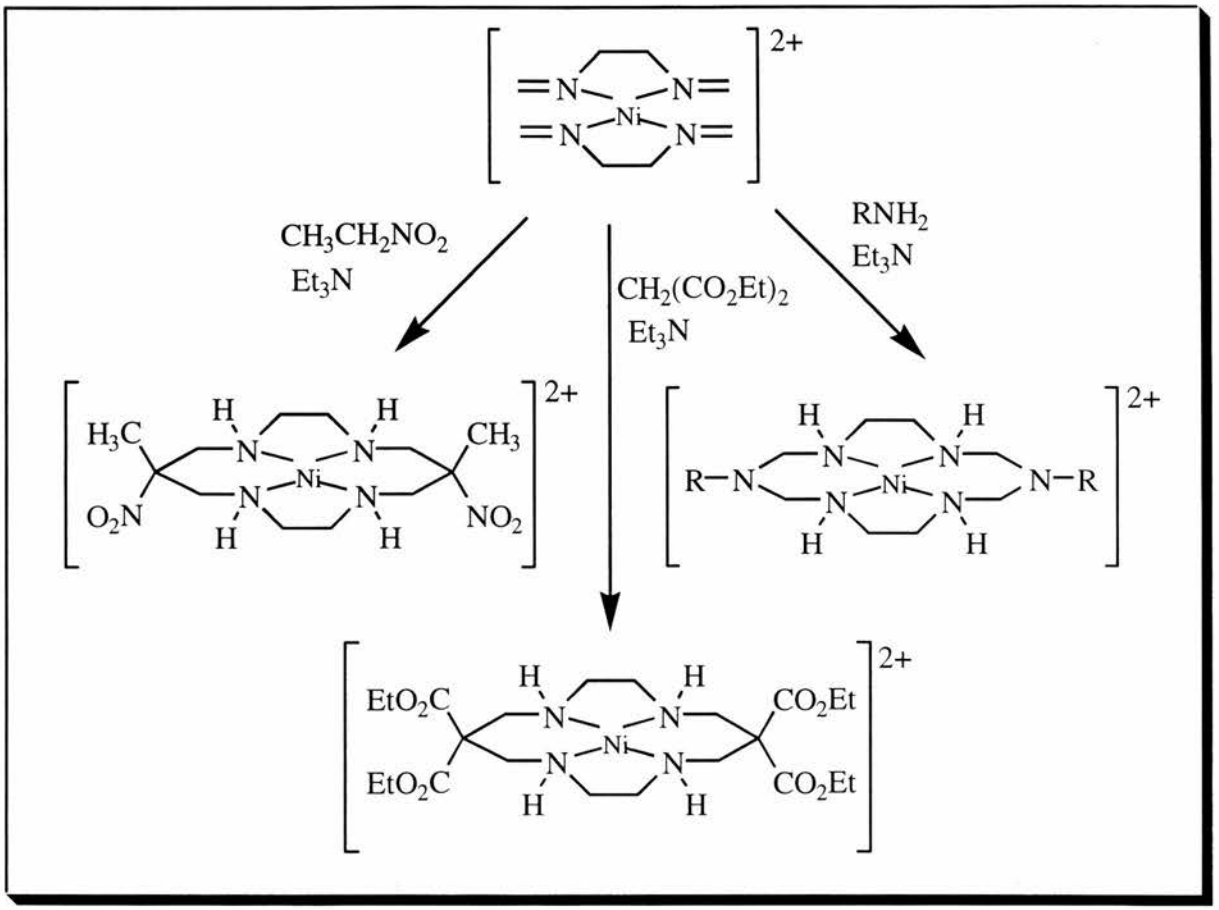

Figure 3

All of these nucleophiles have two acid protons on the α carbon and the stronger the acid the faster the template process (where nitroethane is the strongest acid)[23];

Interest in the template reactions described lies in the possibility of using a nucleophile carrying a desirable functionality as a locking fragment such as a "pendant arm" which can coordinate to the metal or influence the properties of the complex in other ways.

The main aims of this thesis are as follows:

1. To introduce new pentaaza padlock macrocycles and discuss their synthesis, properties and structures.
2. To examine their electrochemical and electrocatalytic properties.
3. To study the thermodynamics of the *cis*-folding of the new pendant arm pentaaza macrocycle, 3-(2-hydroxyethyl)-1,3,5,8,12-penta-azacyclotetradecane nickel(II) perchlorate.
4 To present other interesting macrocycles and discuss their synthesis and structure.

In this chapter the history of padlock macrocycles and advances in the field will be reviewed.

1.2 Caged Macrocycles

1.2.1 Inert Metal Ions

During the late 1970s and early 1980s detailed studies of template condensation reactions involving carbon acids and amine complexes of the inert metal ions Co^{3+}, Rh^{3+}, Ir^{3+} and Pt^{4+} were reported[3,4]. Reactions of these metals first to give the *tris*(ethane-1,2-diamine) complexes and then with formaldehyde and nitroethane produced macrobicyclic cage complexes, Figure 4:

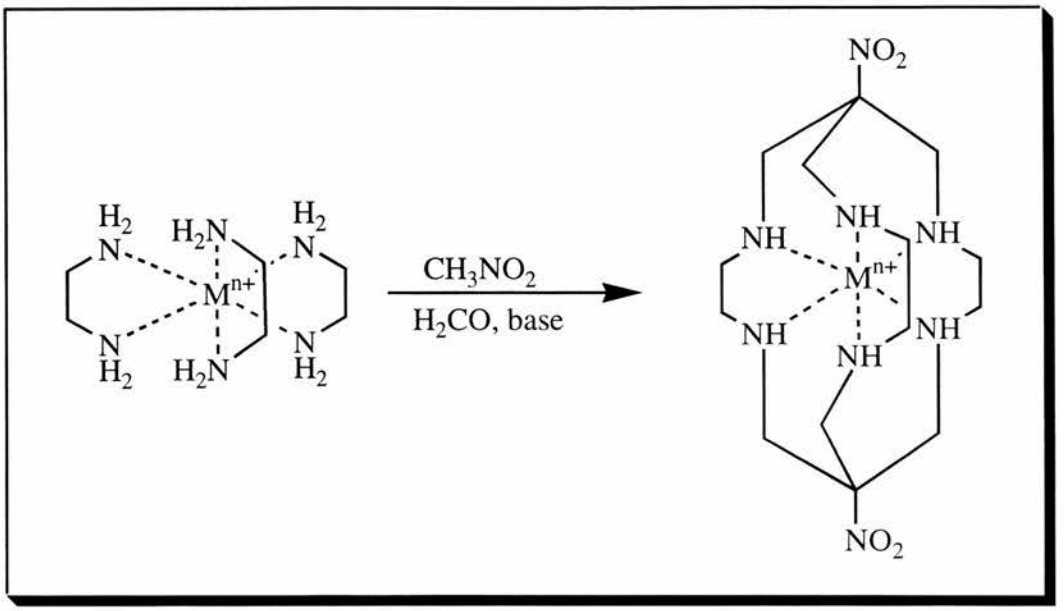

Figure 4

The pendant nitro group can be easily reduced to a primary amine, thus providing a site for additional chemistry and an additional potential coordinating site. Similarly, if NH_3 is used instead of nitroethane then the cage is capped with a donor N atom, Figure 5:

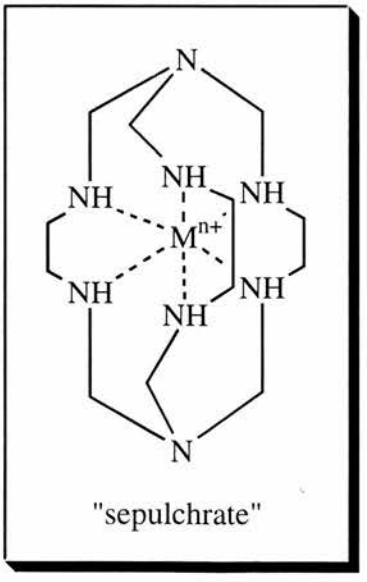

Figure 5

The cavities are appropriate for many M(II), M(III) and M(IV) ions, since very stable complexes with all the first row metal ions in one or more of these oxidation states have been prepared by insertion of the metal ion into the free macrobicyclic ligand isolated from the cobalt complex[58-60].

1.2.2 Labile Metal Ions

Following the reactions discussed in the previous section, attempts were made to perform the same condensation reactions around labile metal ions. These proved less successful. The first published attempt of this type of reaction isolated only a 1% yield of (**1**) by reaction of $[Ni(en)_3]^{2+}$, formaldehyde and ammonia[8]. The major products of the reaction were the mauve, triplet ground state Ni(II) complex of a hexadentate tripodal "half capped" ligand (**2**), and an orange, square planar complex of ligand (**3**), Figure 6:

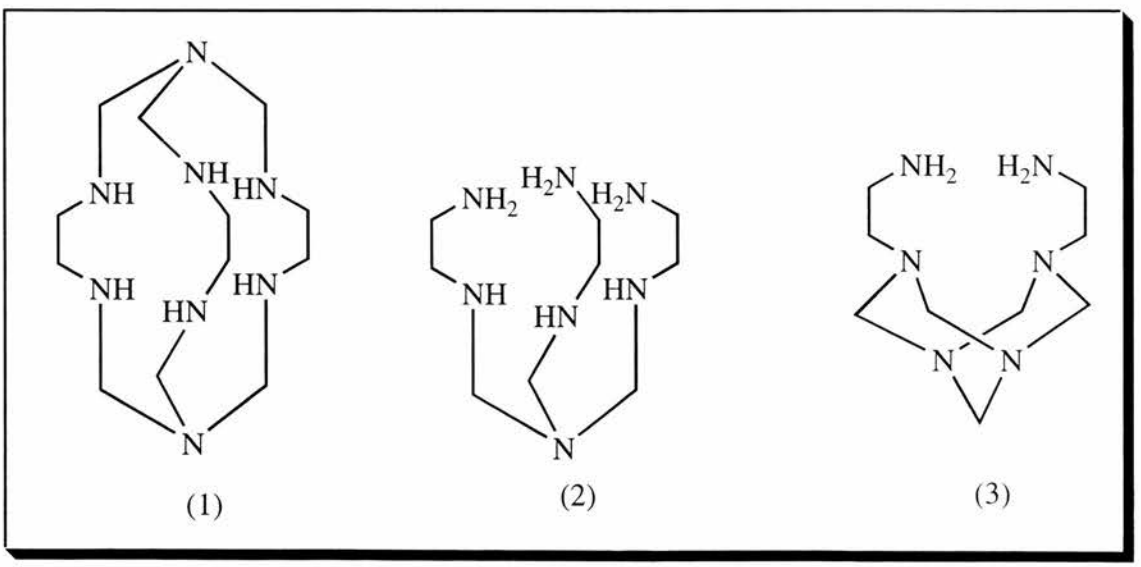

Figure 6

With inert octahedral $[M(en)_3]^{n+}$ complexes, reactions of the above type presumably involve the formation of an imine and subsequent nucleophilic attack by $^-CH_2NO_2$ or NH_3 at the imine carbon. This process leads in a stepwise manner to complete capping of each open octahedral face to form a macrobicyclic complex. With the labile metal ion Cu^{2+}, Jahn-Teller distortions may direct the chemistry towards the formation of square planar complexes. For example, $[Cu(en)_3]^{2+}$ reacts with formaldehyde and nitroethane to form complexes of **(4)** and **(5)** as sole products[9] Figure 7:

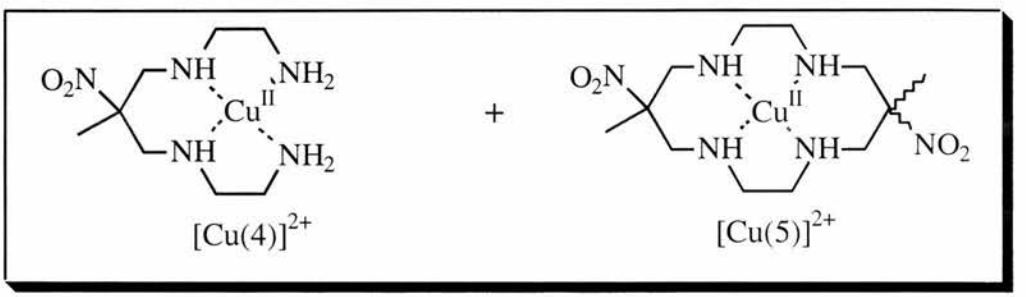

Figure 7

Notably, Ni^{2+} can direct the same chemistry leading to square planar complexes, with the ion $[Ni(\mathbf{5})]^{2+}$ readily prepared[7]. Even the octahedral ion $[Ni(\mathbf{2})]^{2+}$, when heated in dimethyl sulfoxide with excess formaldehyde and ammonia undergoes rearrangement to the square planar complex $[Ni(\mathbf{3})]^{2+}$. The high field ligands generated in these reactions promote square planar geometry for Ni^{2+} rather than octahedral.

1.3 Tetraazamacrocycles

1.3.1 Dinemac (6,13-dimethyl-6,13-dinitro-1,4,8,11-tetraazacyclotetradecane)

Cu[dinemac]$^{2+}$ (**6**) is prepared in a facile one pot high yielding synthesis, Figure 8[17]:

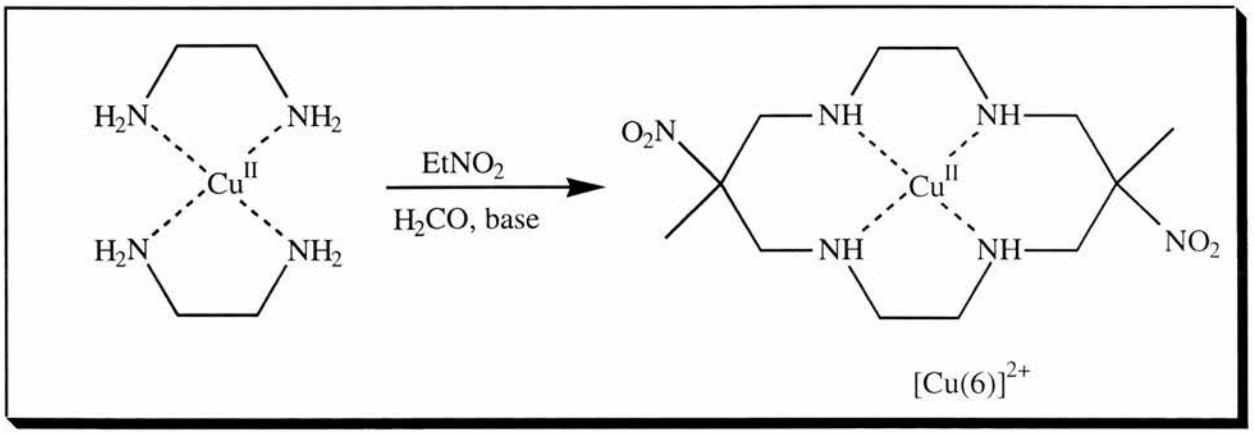

Figure 8

Condensation about $[Cu(en)_2]^{2+}$ in methanol with formaldehyde and the carbon acid nitroethane proceeds readily. In common with Cu^{2+} complexes of most saturated macromonocyclic tetramines, the dinemac complex is stable for long periods in quite strong acid. Analogous synthesis can be performed with nitropropane as the carbon acid.

1.3.2 Reduction of Dinemac

Reduction and demetallation occur simultaneously if excess powdered zinc and concentrated HCl are used, giving diammac(**7**)[17], Figure 9:

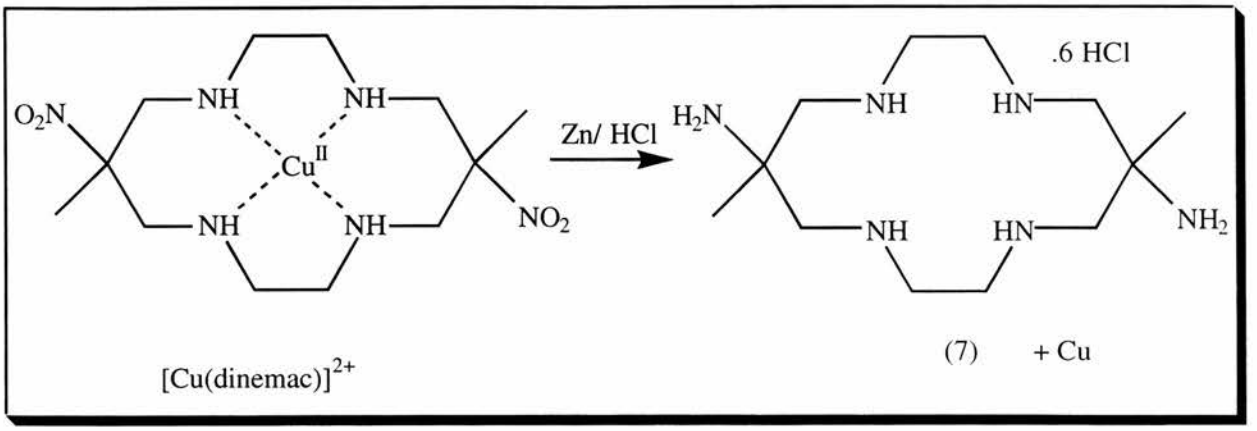

Figure 9

The Zn/HCl reduction removes the metal to generate the free ligand, which can then be reacted with a metal of choice. The reactions described also occur about Ni^{2+} [19].

1.3.3 Other Metal Centres

The most popular template padlock reactions of those described above are the reaction of $[Cu(en)_2]^{2+}$ or $[Ni(en)_3]^{2+}$ with formaldehyde and nitroethane to form the substituted macrocycle **(5)** as the M^{2+} complex in high yield[9]. Reduction of the nitro groups yields **(7)**, which is a substituted cyclam. The chemistry has been investigated and the structures determined, for complexes of **(7)** with a variety of metal ions including: Fe^{3+}, Co^{3+}, Cr^{3+}, Rh^{3+}, Zn^{2+}, Ni^{2+} and Cu^{2+} [9-14].

It should be noted that although a variety of metal ion centres have been studied, the standard synthetic approach for making diammac macrocycles involves using either the Ni^{2+} or Cu^{2+} as the template. This is followed by demetallation as described above, and then the free ligand is reacted with one of the previously mentioned metal ions.

Although diammac may complex in a hexadentate manner **(8)**, other modes of coordination have been observed, including pentadentate **(9)** and tetradentate **(10)** coordination. Both examples arise from protonation of one or both pendant primary amine groups, Figure 10[11].

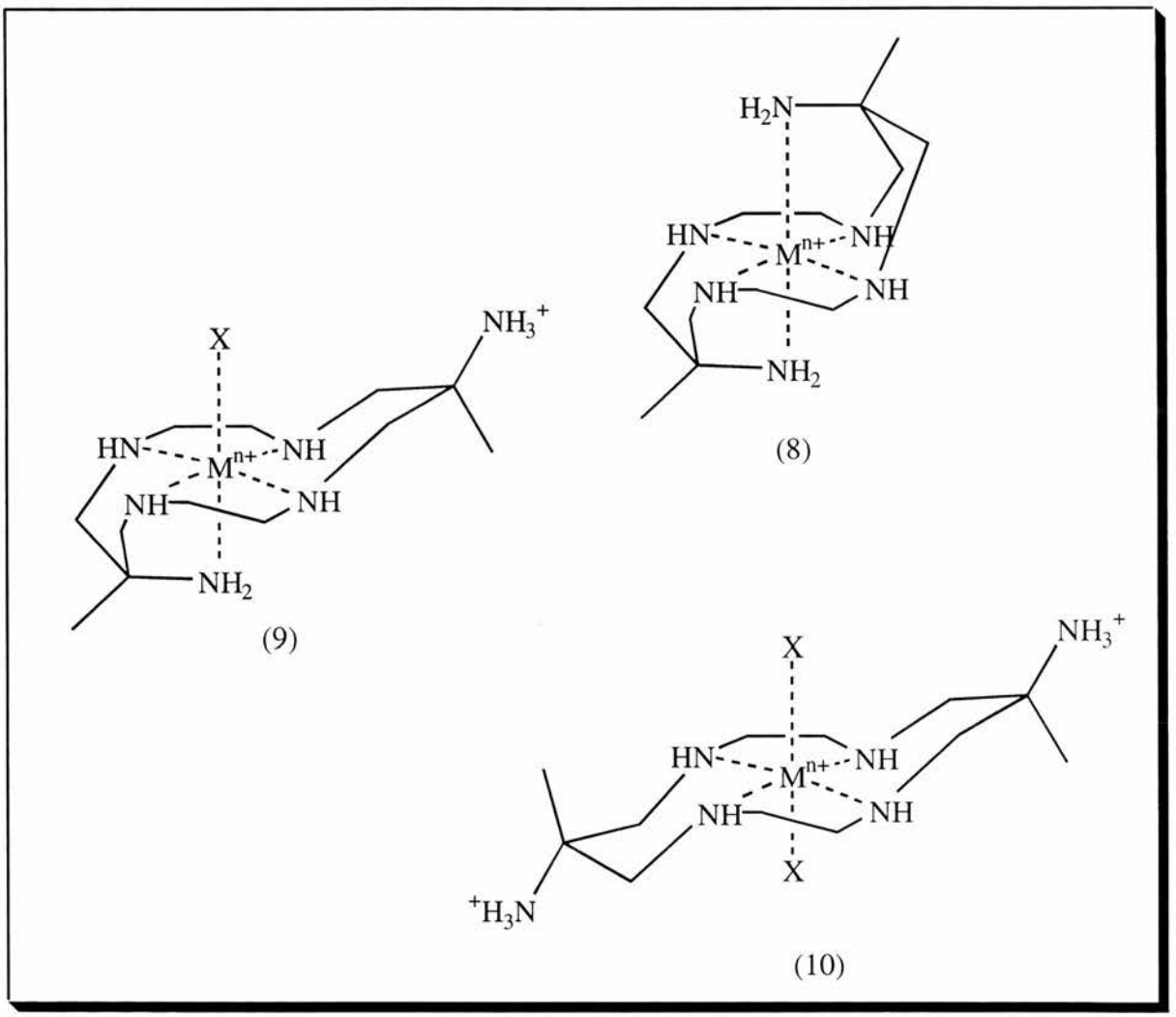

Figure 10

Molecular mechanics calculations on $[Co(diammac)]^{3+}$ showed that the exceptionally short Co-N bond lengths are a result of ligand demands[15]. In other words, a minimisation of intraligand strain leads to a relatively small deviation of the Co-N bonds from anticipated "strain-free" distances (*ca.* 1.925Å). Similar observations have been observed for other metal centres,

although electronic effects may also influence the outcome. This bond compression is reflected in physical properties, with electronic maxima shifted to a high energy resulting in the M^{3+} to M^{2+} redox potential having a large negative value. Importantly, when less than six of the amine donors are coordinated in complexes of diammac, the M-N bond lengths are not particularly unusual.

The Cu^{2+}, d^9 complex differs from the aforementioned metal ions as it displays the Jahn-Teller tetragonal elongation. This makes complexation with the pendant primary amine groups energetically disfavoured relative to arrangements in which these groups engage in other types of lattice interactions such as intermolecular hydrogen bonding. For this reason all isolated Cu^{2+} complexes have the pendant primary amine groups uncoordinated. In other respects the macrocyclic conformation and Cu-N distances (2.021, 2.027) closely resemble those of $[Cu(cyclam)]^{2+}$ [16].

1.4 Structure and Properties of Diammac Complexes

1.4.1 *Cis* and *trans* Isomers

The synthesis of diammac as previously described generates two isomeric forms, *trans*-(**11**) and *cis*-(**12**) isomers, in which the pendant amines lie on opposite sides or the same side of the macrocycle ring respectively, Figure 11:

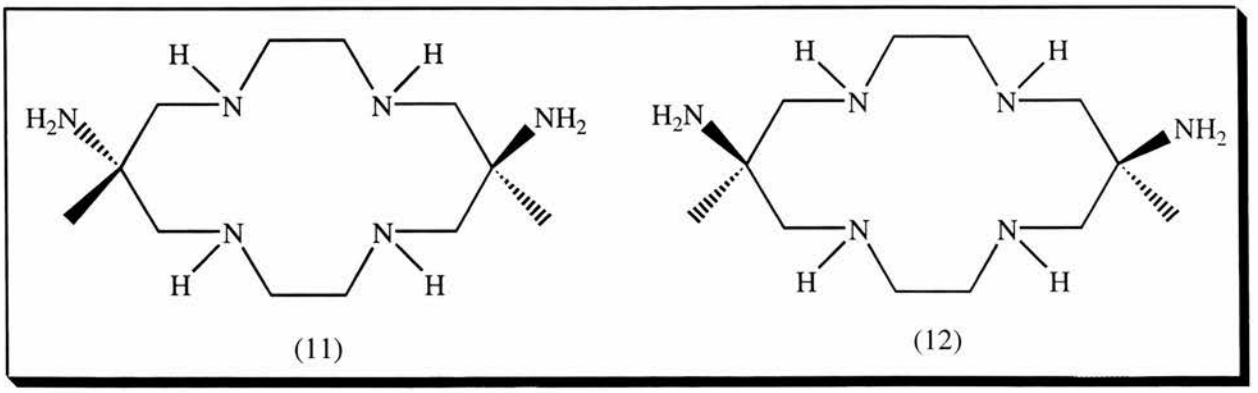

Figure11

The X-ray crystal structure of the Cu^{2+} complex [Cu(**11**)]$(ClO_4)_2$ was reported in 1986 but the evidence for the presence of isomer (**12**) was based only on subtle differences in the infra-red spectra exhibited by the Cu^{2+} complexes of (**11**) and (**12**).

The two isomers were reported to have been isolated in the *trans*:*cis* ratio of 4:1. It should be noted that the geometric isomers of the nitro-substituted macrocycle products have not been separated. It has only been possible to separate the reduced ligands. It was not until 1992 that the identification, isolation and X-ray crystal structure of (**12**) were determined[17]. This was achieved by complexing the *cis* ligand with Cd^{2+}.

Diammac was prepared as previously described and the isomers isolated using a column (100x3 cm) of Dowex 50W x 2 cation exchange resin. The *cis* isomer was then added to a solution of tricadmium sulfate octahydrate and sodium perchlorate monohydrate and the pH raised to 6 with sodium hydroxide solution. Colourless crystals suitable for X-ray structure determination formed upon slow evaporation of the solution at room temperature. The crystal structure of [Cd(diammac)]$(ClO_4)_2$ *trans* isomer confirmed hexadentate coordination of diammac. The

macrocyclic moiety of diammac is folded and the pendant primary amines occupy positions within the coordination sphere.

In order to discuss the origins of the selectivity in formation of the *trans* isomer in preference to the *cis* isomer, one must return to the precursor dinitro-substituted complex $[Cu(dinemac)]^{2+}$, since the ratio of *trans* to *cis* isomers for this complex is necessarily the same as that found for the diammac complex. Therefore, this suggests that the original template synthesis of $[Cu(dinemac)]^{2+}$ must be the source of stereoselectivity[17]. The two isomers of $[Cu(dinemac)]^{2+}$ are equally likely if the relative stabilities are considered. There is no significant difference between the steric bulk of a nitro group and that of a methyl group, so whether the nitro groups are on the same side or opposite sides of the macrocycle ring is immaterial when the relative strain energies of the two complexes are considered. Hence, the observed isomer ratio is a result of kinetic control. There is an intermediate step which favours the formation of the *trans* isomer, as shown in the proposed mechanism below, Figure 12:

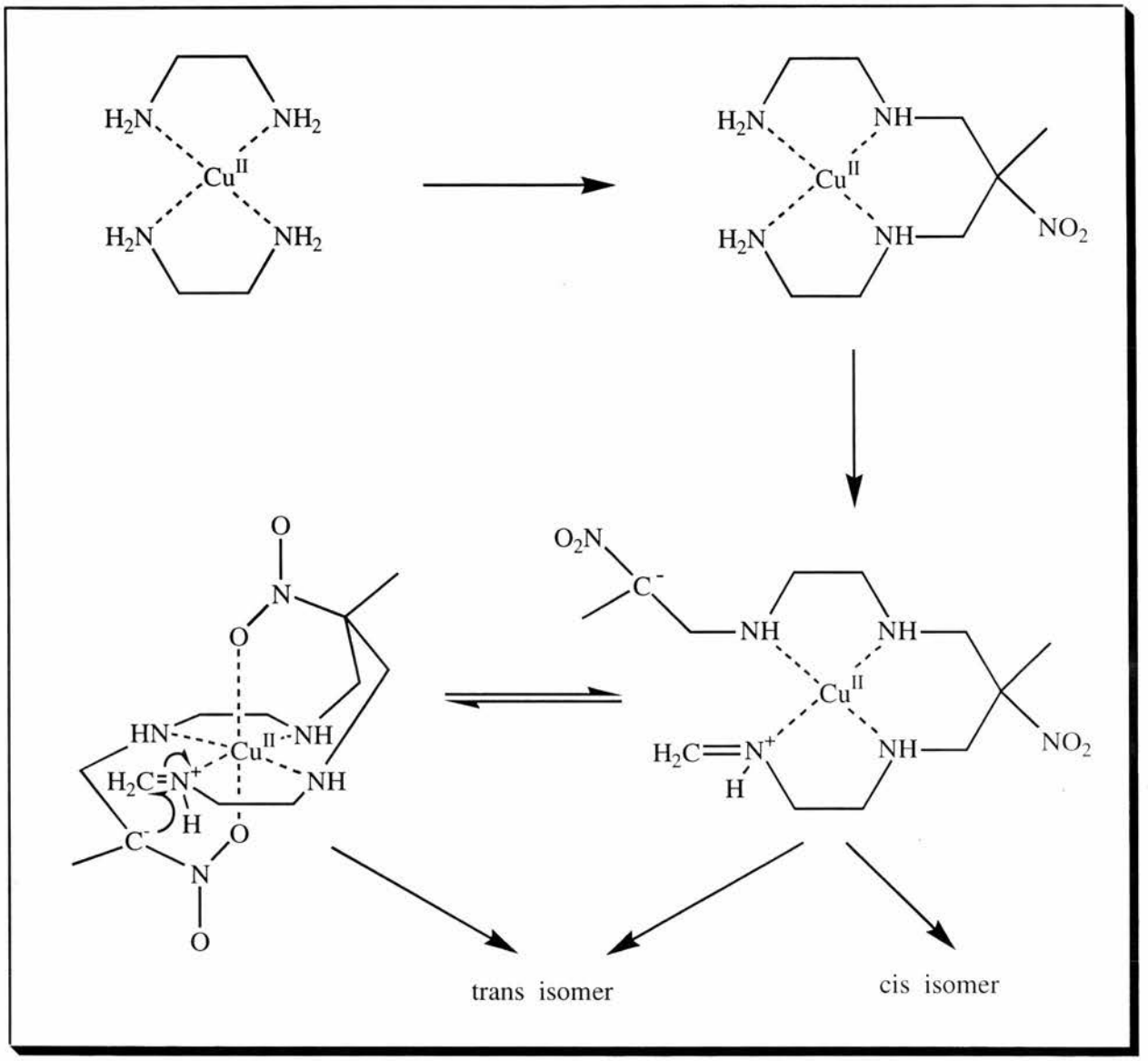

Figure 12

The critical step is the introduction of the second nitroethane residue into the acyclic mononitro complex. The orientation of the nitro group at the time that cyclisation of the second six membered chelate ring occurs determines whether the *trans* or *cis* isomer is formed. For there to be a preference (4:1) of *trans* to *cis* it is proposed that the coordination of both nitro groups is the factor which results in the observed ratio of products.

Although axial coordination of nitro groups to the Cu^{2+} metal centre has not been positively identified in solution, it has been observed in crystal structures of Cu^{2+} complexes bearing pendant nitro groups[18].

As already noted, the crystal structures of complexes of the hexadentate coordinated *trans* isomer of diammac have revealed shorter than average M-N bonds due to ligand constraints. Notably, this has not occurred in the case of $[Cd(diammac)]^{2+}$; in fact, the Cd-N bond lengths were slightly larger than average for a hexaamine cadmium(II) complex[17].

This discovery of shorter than average M-N bonds in hexadentate diammac complexes has been supported further by work carried out in 1993 by Bernhardt, Comba and Hambley[20]. The synthesis, spectroscopic and structural characterisation of the Cr(II), Co(II) and Ni(II) complexes of *trans*-diammac were reported. Here the spectroscopic and structural properties of the isomeric (*cis* and *trans*) systems were examined with the angular overlap model (AOM) and molecular mechanics (MM) calculations and the X-ray crystal structure of $[Cr(cis\text{-diammac})(ClO_4)_3].2H_2O$ was also reported.

The results presented demonstrated that complexes of the two isomeric, hexadentate macrocyclic ligands display quite different physical and structural properties as a result of the mode of coordination dictated by the ligand. Specifically, the $[M(trans\text{-diammac})]^{n-}$ complexes display exceptionally short M-N bond lengths, high energy electronic transitions and particularly negative $M^{3+/2+}$ redox couples, whereas the $[M(cis\text{-diammac})]^{2+}$ isomers do not.

The axial elongation of M-N (pendant) bonds relative to the equatorial M-N (secondary) increases with increasing metal-ion size throughout the series of hexadentate coordinated

complexes of *trans* diammac. In addition, the N (pendant) - M-N (secondary) bite angle becomes increasingly acute as the metal becomes larger.

It can be seen that this concomitant elongation and lateral displacement of the M-N (pendant) bond must eventually result in its breaking. On identification of the *cis*-$[Cu(diammac)]^{2+}$ isomer, the metal ion size limit for hexadentate coordination of *trans*-$[M(diammac)]^{2+}$ lies between Zn(II) and Cd(II)[17].

1.4.2 α and β isomers of $[Ni(diammac)]^{2+}$

$[Ni(dinemac)]^{2+}$ **(13)**, prepared in an analogous fashion to the $[Cu(dinemac)]^{2+}$, can be reduced to $[Ni(diammac)]^{2+}$ **(14)** with the major isomer having the *trans* arrangement, Figure 13:

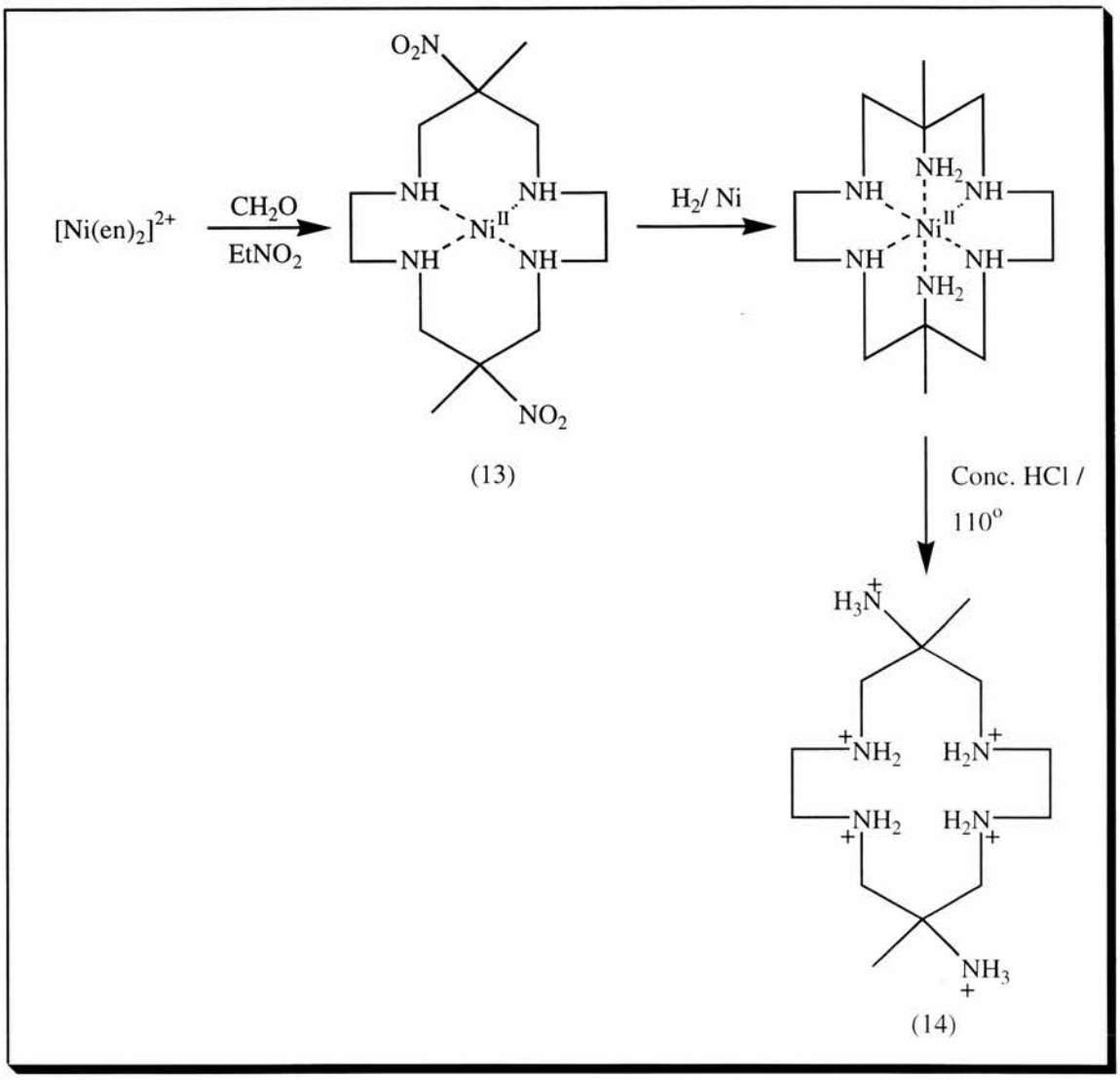

Figure 13

The (*trans*-6,13-diamino-6,13-dimethyl-1,4,8,11-tetraazacyclotetradecane)nickel(II) has been isolated in approximately equal amounts of the two isomeric forms, designated α (with R,S,R,S configuration of the chiral nitrogen centres) and β (with the R,R,S,S configuration) Figure 14[19]:

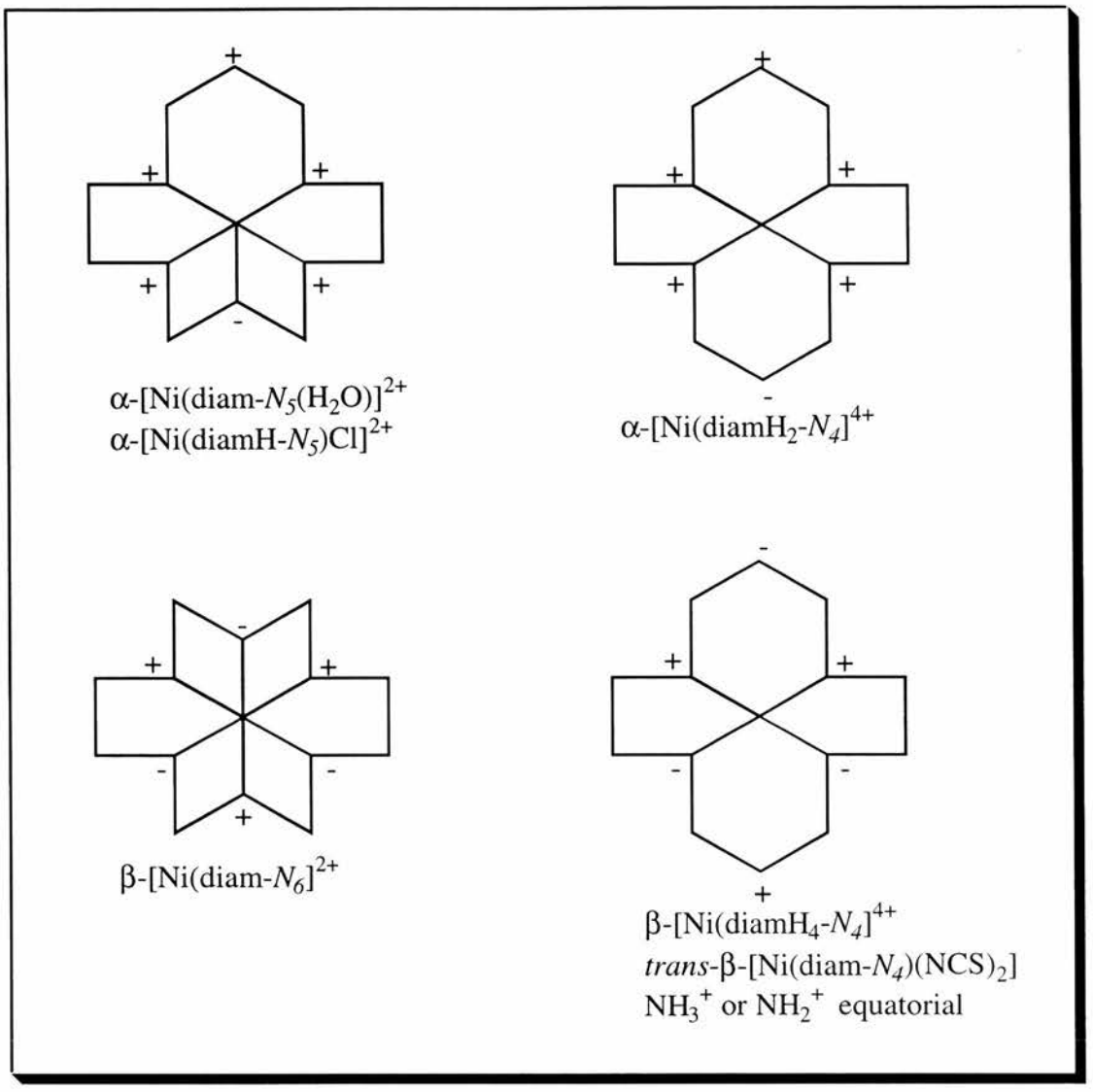

Figure 14

The symbols α and β refer to the orientation of the secondary amine NH group, or the primary amino substituents, with respect to the (flattened) molecular plane.

The diammac ligand for α-isomer compounds of neutral or monoprotonated diammac is normally five coordinate, with one primary amino group coordinated, with an additional ligand, usually water *trans* to the amino substituent, completing octahedral coordination about the Ni(II).

The non-coordinated primary amine group is readily protonated. In strongly acidic solutions the diprotonated ligand occurs as the yellow, singlet ground state, square planar cation.

The β-isomer cation has six coordinate diammac with both primary amino substituents coordinated, unless the amino substituents are displaced by "strong" ligands with small steric demands, such as cyanide or thiocyanate. In acid solution the diprotonated ligand is formed with water or thiocyanate completing the octahedral coordination. In high concentrations of salts with large, singly charged anions such as perchlorate the diprotonated cation occurs as a yellow, singlet ground state, square planar cation. The α-isomer slowly transforms to the β-isomer in solution and is, therefore, probably the major or possibly the only direct product of the reduction.

The coordinated primary amine groups of both isomers of $[Ni(diammac)]^{2+}$ are labile, but the macrocycle secondary amine groups are very resistant to acid demetallation. The α-isomer shows very slow demetallation in acid at ambient temperatures at a rate insignificant compared with acid-catalysed isomerisation to the β-isomer. The β-isomer is very resistant to acid, although the ligand is obtained by demetallation of the complex cation by heating in concentrated hydrochloric acid.

1.5 Further Tetraazamacrocycles

1.5.1 Synthesis of a Tetraazamacrocycle from trien

Reaction of $[Cu(trien)]^{2+}$ or $[Ni(trien)]^{2+}$ in basic methanol with aqueous formaldehyde and RNO_2 (R= C_2H_5 or CH_3) results in the ready formation of complexes of the macromonocyclic ligands 12-methyl-12-nitro-1,4,7,10-tetraazacyclotridecane **(15)** and 12-ethyl-12-nitro-1,4,7,10-tetrazacyclotridecane **(16)** in high yield, Figure 15:

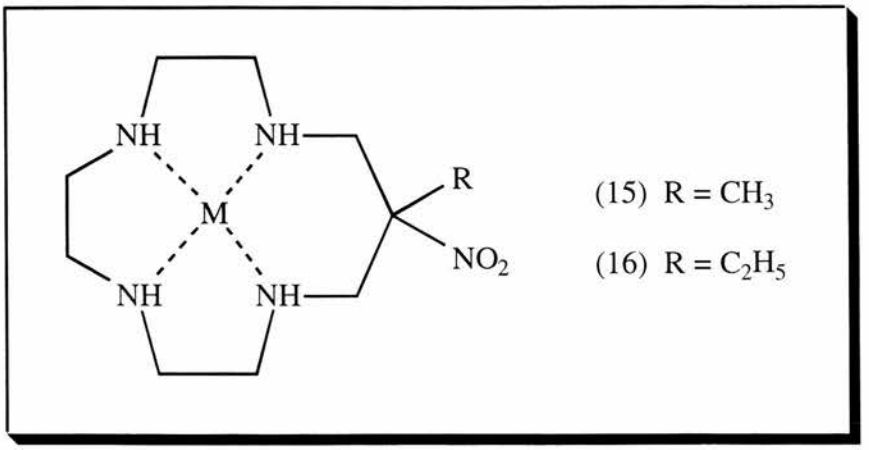

Figure 15

The equivalent chemistry has been extended to the Cu(II) complexes of a range of tetraazaalkanes to produce 14-, 15- and 16-membered macrocycles and a strapped 15-membered macrocycle, Figure 16[61-64]:

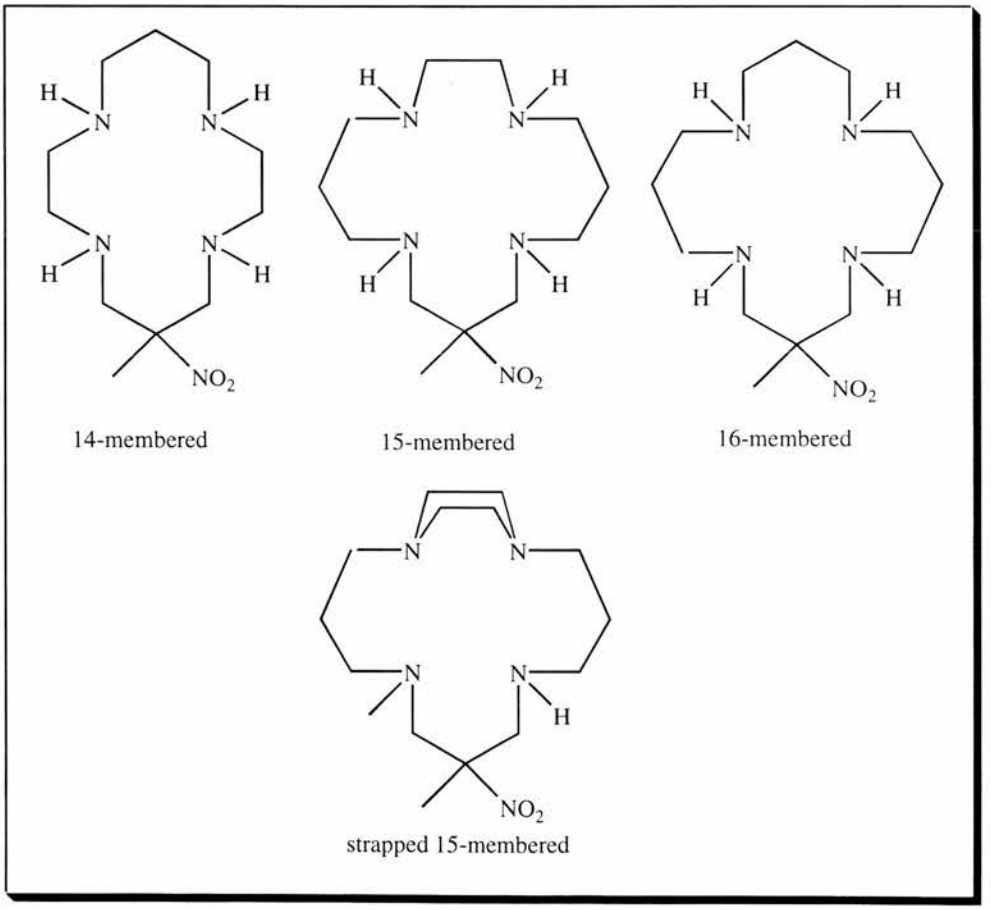

Figure 16

1.5.2 Synthesis of Tetraazamacrocycles using Dimethylmalonate as the padlocking Nucleophile

Bis(1,2-diaminoethane) complex cations of Cu(II) and Ni(II) react with formaldehyde and diethyl-(or dimethyl)malonate to form complexes of the 6,6,13,13-tetracarbomethoxy-1,4,8,11-tetraazacyclotetradecane macrocycle (17)[22]. These hydrolyse in base to give tetracarboxy-substituted cations (18), which decarboxylate in acid to E-6,13-dicarboxy-substituted cations (19). These isomeric dicarboxy-substituted cations esterify to form perchlorate salts of the isomeric Cu(II) compounds of the E-dicarbomethoxy-substituted cations (20). The compounds can be demetallated very slowly in acid, allowing the isolation of free E-6,13-dicarboxy-1,4,8,11-tetracyclotetradecane, Figure 17:

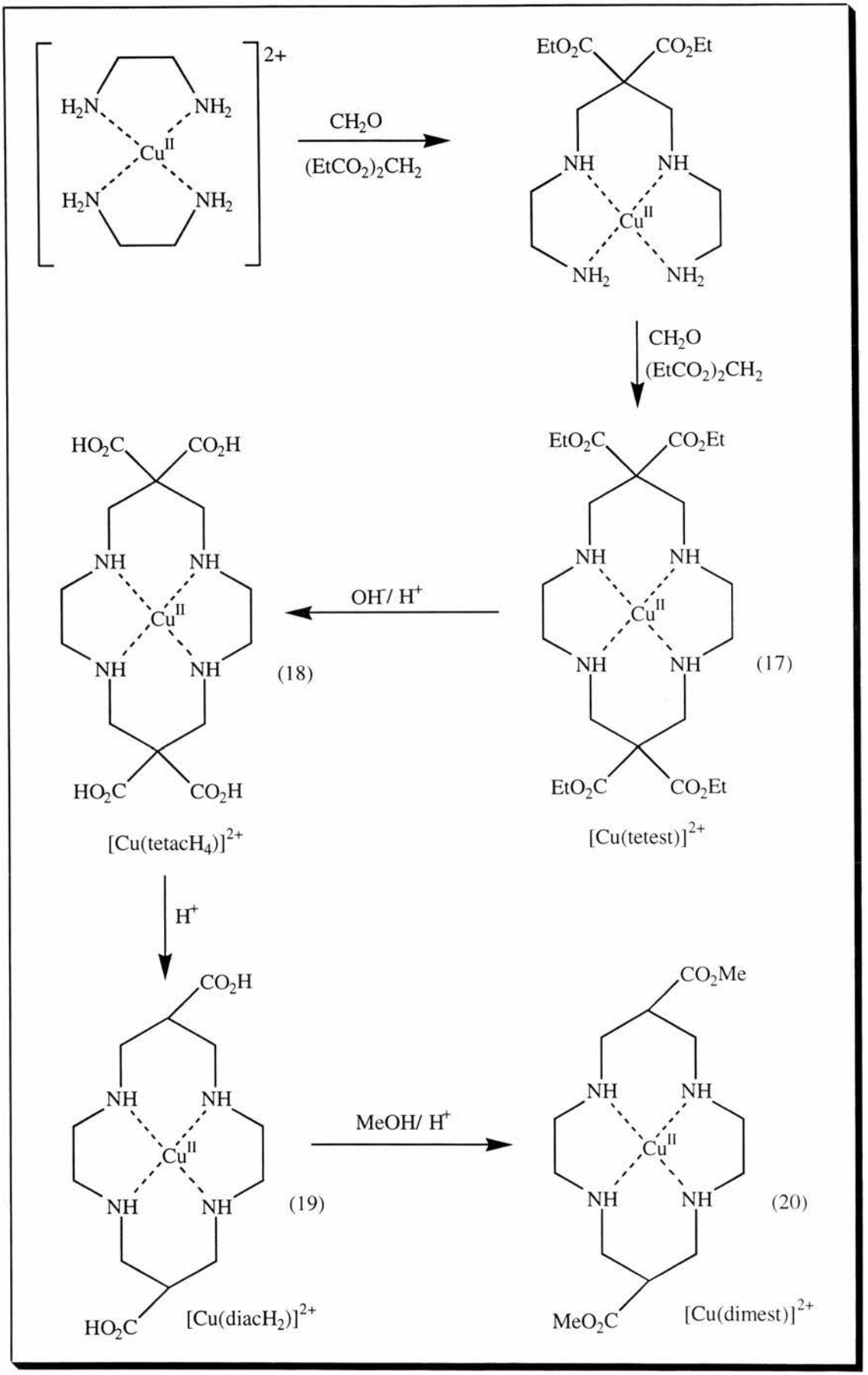
2+
H_2N
NH_2
Cu^{II}
CH_2O
$(EtCO_2)_2CH_2$
EtO_2C
CO_2Et
NH
NH_2
OH^-/ H^+
HO_2C
CO_2H
(18)
(17)
$[Cu(tetacH_4)]^{2+}$
$[Cu(tetest)]^{2+}$
H^+
$MeOH/ H^+$
CO_2Me
MeO_2C
(19)
(20)
$[Cu(diacH_2)]^{2+}$
$[Cu(dimest)]^{2+}$

Figure 17

Work carried out in 1992 by Li Xin *et al.* reported a 12% yield of these Cu(II) compounds[21]. Further work carried out during 1996 by Fabbrizzi *et al.* reported a 21% yield of the $[Cu(tetest)]^{2+}$ [22]. Although the overall yield is relatively low the simple one pot reaction involving inexpensive reagents makes this a convenient method for the preparation of carboxy substituted cyclams and their derivatives. A variation on this synthesis has been carried out using benzaldehyde rather than formaldehyde as the building block, Figure 18[3,22]:

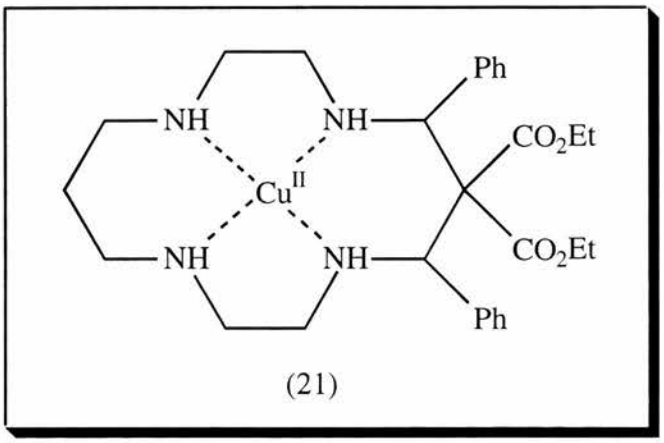

(21)

Figure 18

This introduces a functionalisation on the ring, modifying and enriching the activity of the metal centre. A relatively high yield is reported for this reaction, 70%, but due to the instability of the C=N bonds, water must be excluded from the reaction medium. In anhydrous conditions the anion of diethylmalonate attacks successfully the C=N bond, ensuring the formation of a stable tetraaza ring. This macrocycle also displays the typical inertness of tetraazamacrocyclic complexes towards acid catalysed demetallation and in particular they survive in strongly acidic solutions.

1.5.3 Synthesis of a Tetraazamacrocycle using Diethylmalonate and Nitroethane as Padlocking Nucleophiles in the same Molecule

Another variation is the use of diethylmalonate and nitroethane condensation the same molecule. In a multiple step process commencing with $[Cu(en)_2]^{2+}$, capping using diethylmalonate was employed to produce **(22)**, Figure 19:

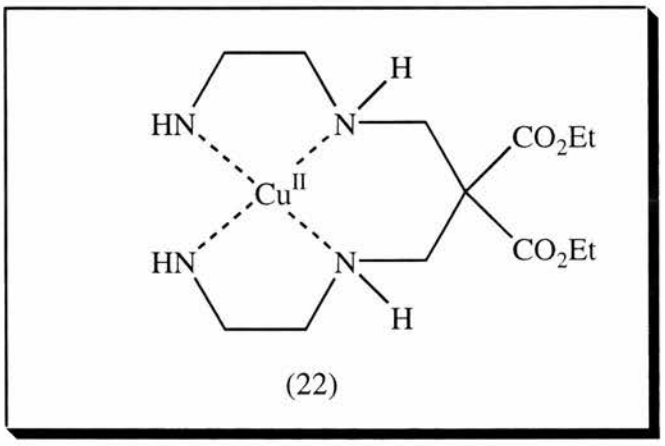

(22)

Figure 19

This species is then stabilised by conversion to the methylester derivative **(23)** by hydrolysis in basic methanol, Figure 20:

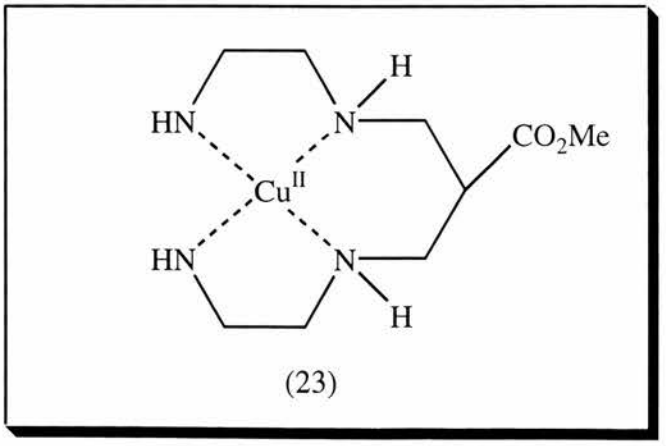

(23)

Figure 20

The other pair of primary amines of the intermediate complex molecule are then capped using nitroethane, the methyl ester being hydrolysed in the process. The resulting complex **(24)** is a cyclam derivative with both nitro and carboxylate pendant groups which, after reduction to convert the nitro to an amine and to remove the metal **(25)**, is capable of encapsulating a wide range of octahedral metal ions as a hexadentate ligand, Figure 21[65,66].

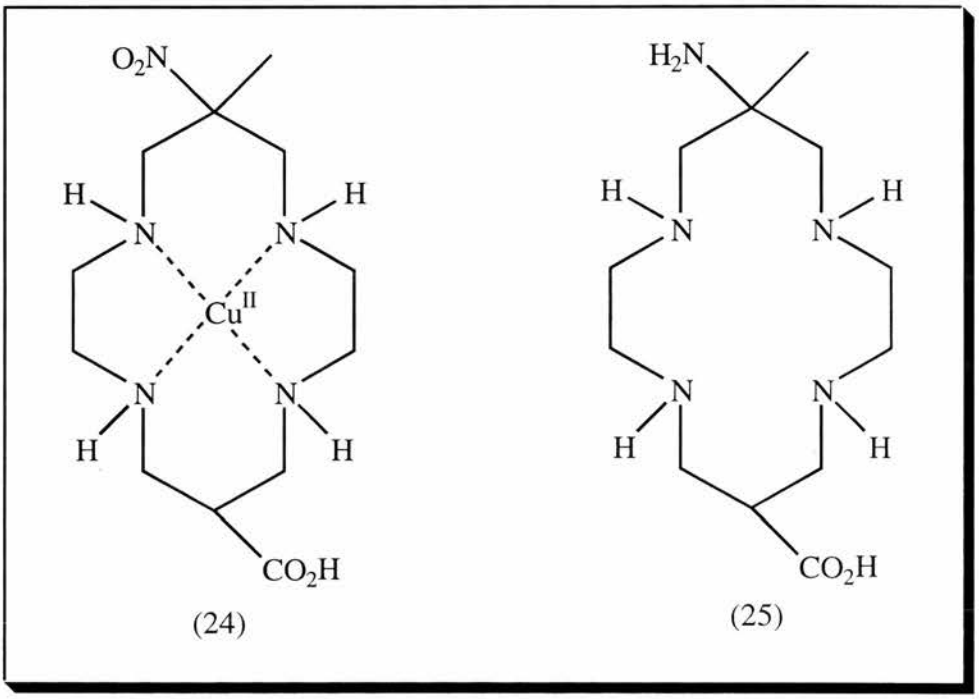

Figure 21

1.5.4 Cyano Tetraaza Complexes

The synthesis of cyano complexes has been carried out using NC-CH_2-CN as the padlocking nucleophile, Figure 22:

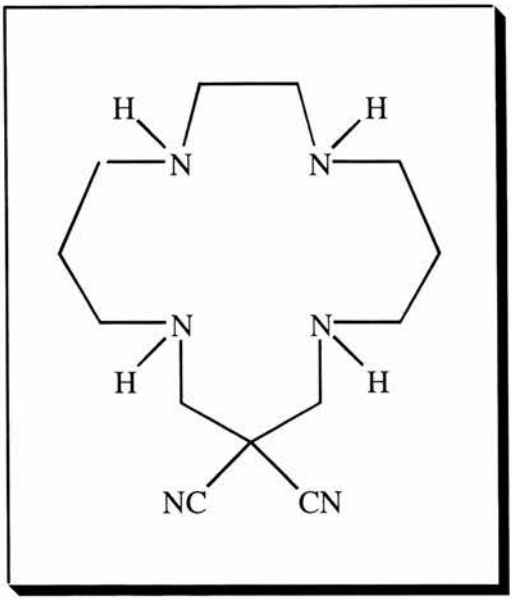

Figure 22

The stability of the pendant groups is not apparently great and the product has not been definitely confirmed[67].

1.5.5 Complexes of tetraazamacrocycles from Bis(propane-1,2-diamine) and Bis(2-methylpropane-1,2-diamine)

The reaction of bis(1,2-diamine)copper(II) complexes of racemic propane-1,2-diamine (pn) and 2-methylpropane-1,2-diamine (dmen) with formaldehyde and nitroethane in methanol under basic conditions yields minor macrocyclic condensation products ((**26**) and (**27**), respectively) in addition to the major acyclic products, Figure 23[23]:

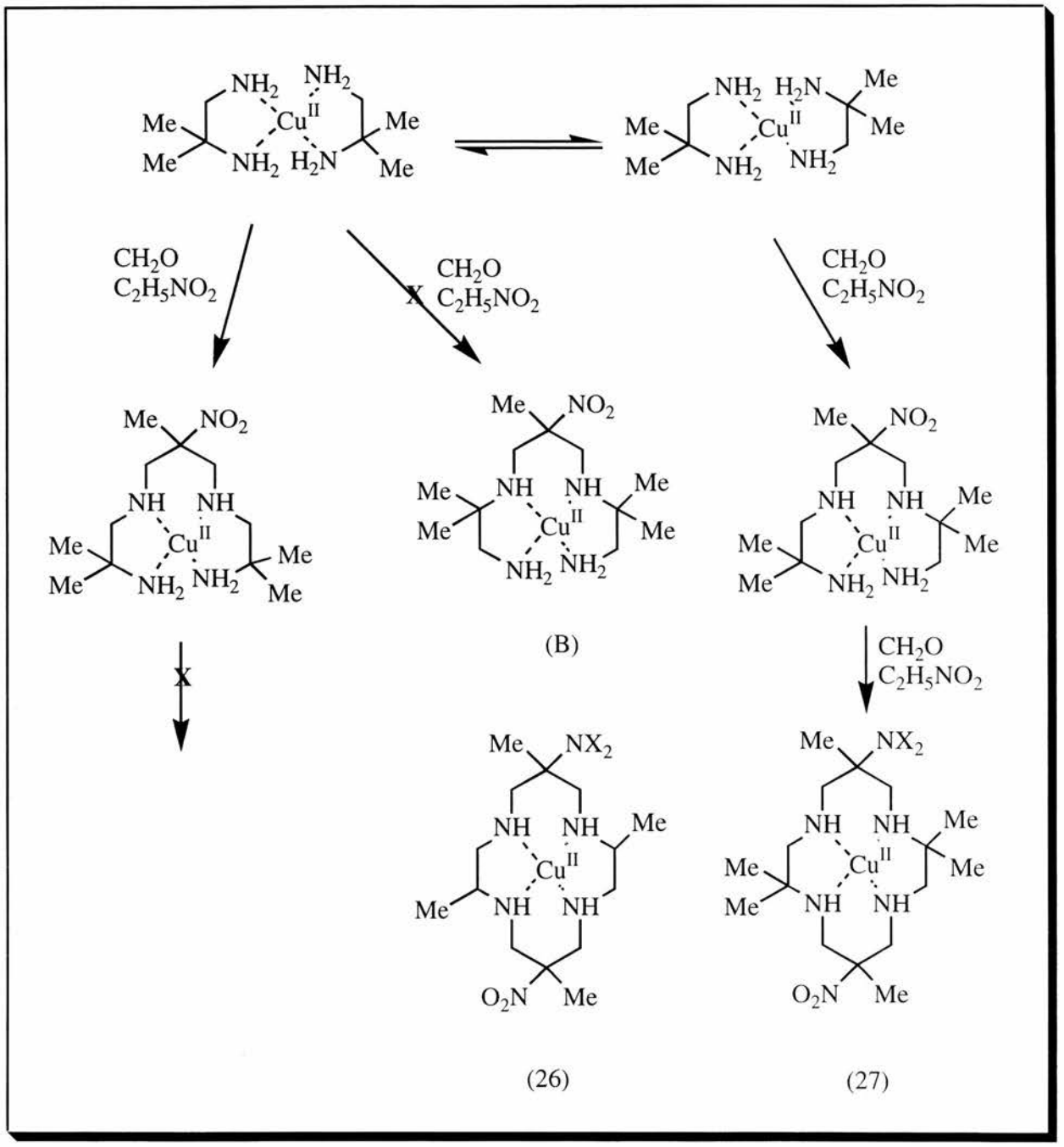

Figure 23

It is the steric effects introduced by the bulky gem-dimethyl substituents around the primary amines that are considered to result in these low yields and even non-existent intermediates such as (**B**). Both macrocycles (**26**) and (**27**) are demetalised using Zn/ HCl. Macrocycle (**26**) has been crystallised and its Cu-N distances determined. They are not unusual for Cu(II)

tetraazamacrocycles of this type. The geometry is very similar to the centrosymmetric structures of $Cu(cyclam)^{2+}$, suggesting that the additional methyl groups in the pn residues have little influence on the copper environment.

1.5.6 Swollen Macrocycles

As already described, diammac has been previously prepared by condensation around Cu(II) and Ni(II), but this does not permit synthesis of larger ring macrocycles. The bis(diamine) palladium(II) cations (diamine = ethane-1,2-diamine, propane-1,3-diamine or butane-1,4-diamine) all undergo condensation reactions with formaldehyde and nitroethane to produce (**28-30**), Figure 24[51a]:

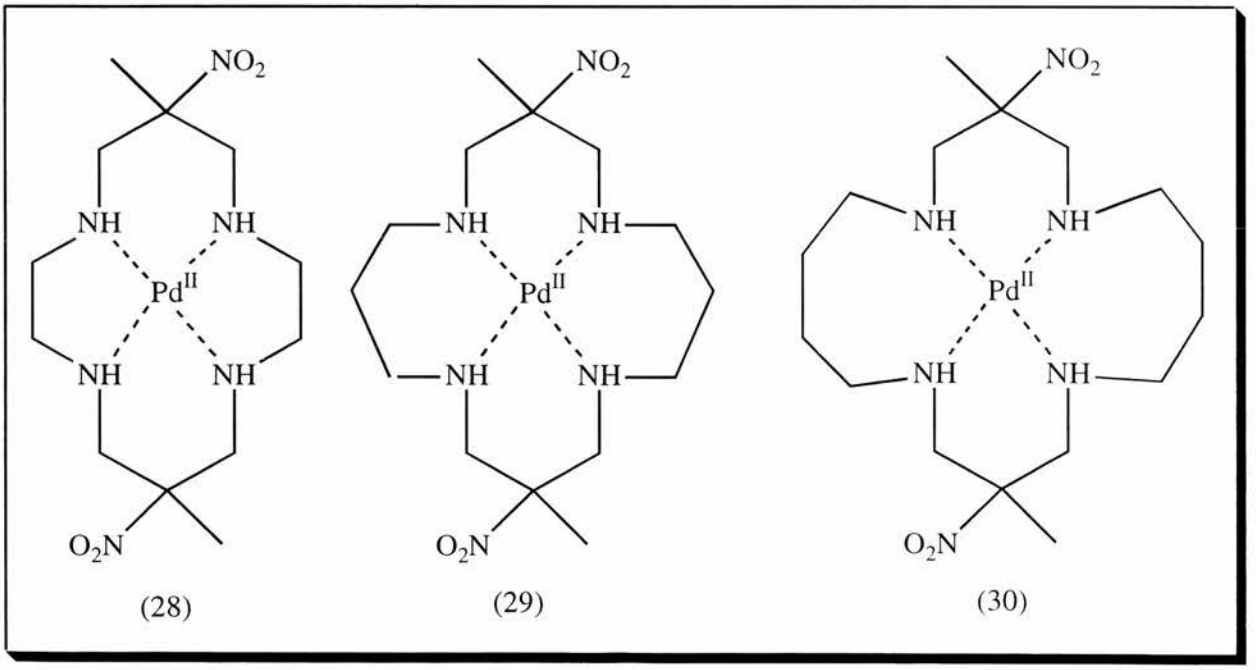

Figure 24

In the case of **(28)**, only the *trans* isomer was isolated in high yield, suggesting that only a small percentage of the *cis* isomer forms, ratios were not reported[51a]. The stereoselectivity parallels the behaviour in the analogous copper(II) based chemistry for this reaction. In the case of **(29)** and **(30)**, the more readily crystallised dominant product is the *cis* isomer. These results indicate that there appears to be a trend for a preference from the *trans* isomer to the *cis* isomer with increasing ring size. The "swelling" also leads to an increase in Pd-N distance. An irreversible $Pd^{II/IV}$ oxidation occurs at approximately +1.0 V (vs Ag/ AgCl), varying slightly with ring size. A multi-electron nitro group reduction is also observed near -0.8 V in each case.

1.5.7 Gold(III) Template Synthesis of a Pendant-arm Macrocycle

Gold(III) directed condensation of 1,2-diaminoethane with nitroethane and formaldehyde yields the gold coloured macrocyclic complex (*cis*-6,13-dimethyl-6,13-dinitro-1,4,8,11-tetraazatetradecan-1-ido)gold(III) **(31)** and the orange acyclic complex (1,9-diamino-5-methyl-5-nitro-3,7-diazanonan-3-ido)gold(III) **(32)** in good yields (>50%)[52]. Unlike the Cu and Ni analogues the pendant nitro groups are diposed on the same side of the macrocycle in a *cis* geometry, as confirmed by crystal structure analysis. This is probably du to the strongly square planar nature of gold(III) which would limit octahedral intra-complexation and, therefore, favour cis- ring closure see Figure 12[52]. In both complexes the gold ion lies in a square-planar environment of four nitrogen donors, Figure 25:

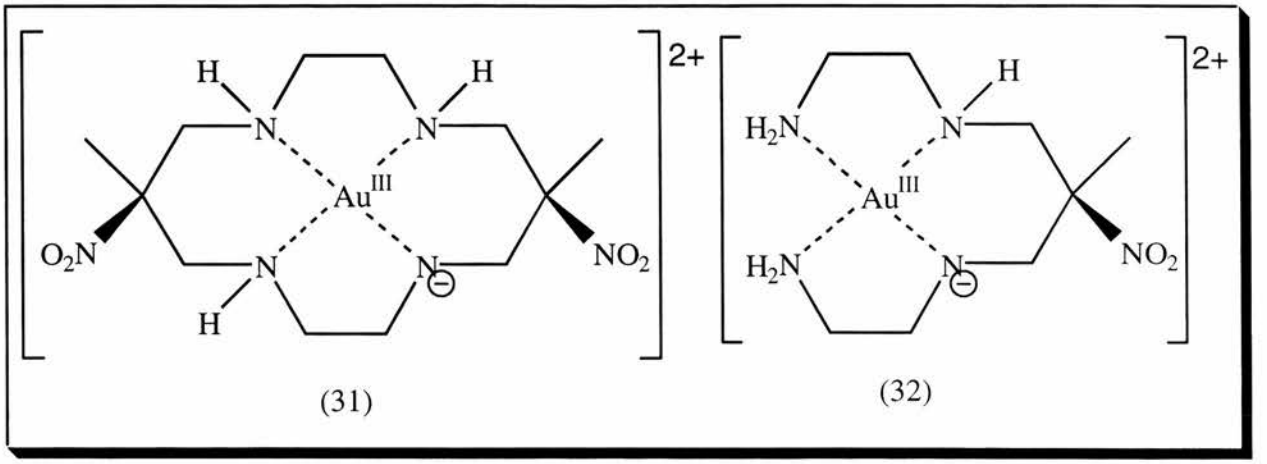

Figure 25

1.5.8 Other Tetraaza Nitroalkanes

Reaction of a range of nitro substituted molecules of the form R-CH_2-NO_2 (where R is an alkyl or a substituted alkyl group), formaldehyde and base with copper(II) and nickel(II) complexes of 4,7-diazadecane-1,10-diamine and 3,6-diazaoctane-1,8-diamine respectively produces a range of 13 and 15-membered macrocyclic products ((**33**) and (**34**)) with one nitro pendant and the R group remaining as the other pendant group. This chemistry is largely unaffected by the choice of R group, Figure 26[68]:

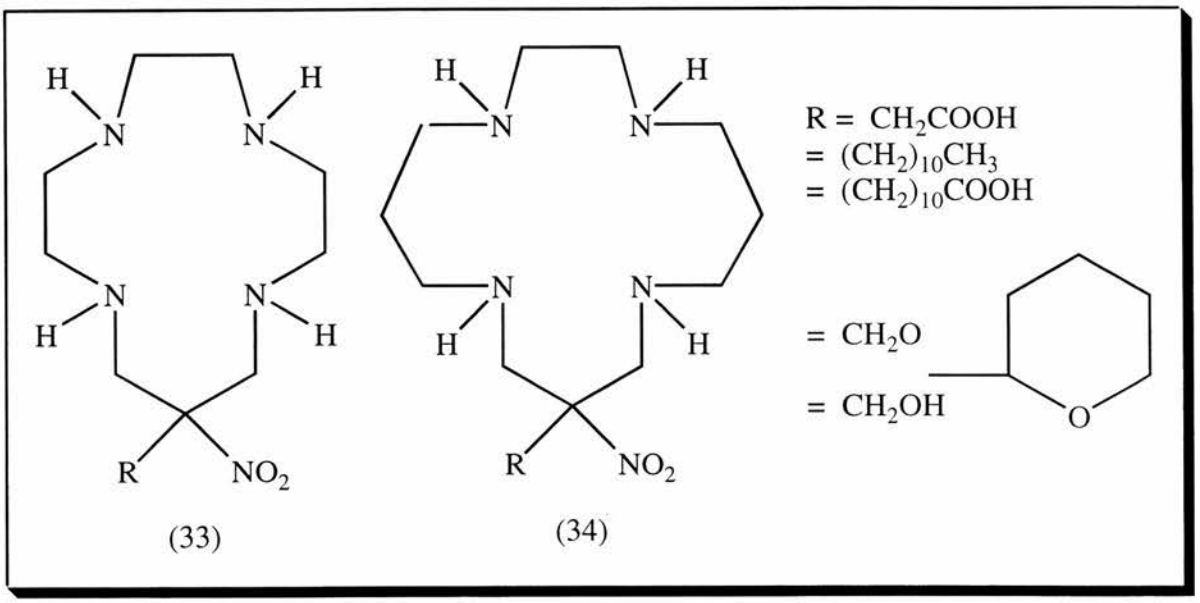

Figure 26

1.6 Pentaazamacrocycles

1.6.1 [Ni(II)(azacyclam)]$(ClO_4)_2$

In 1991 Fabbrizzi *et al.* carried out an analogous template condensation to those previously described, involving the open chain tetraamine 2,3,2-tet, formaldehyde and methylamine to give the low spin pentaaza macrocyclic complex [Ni(II)(azacyclam)]$(ClO_4)_2$ (**35**), Figure 27[24]:

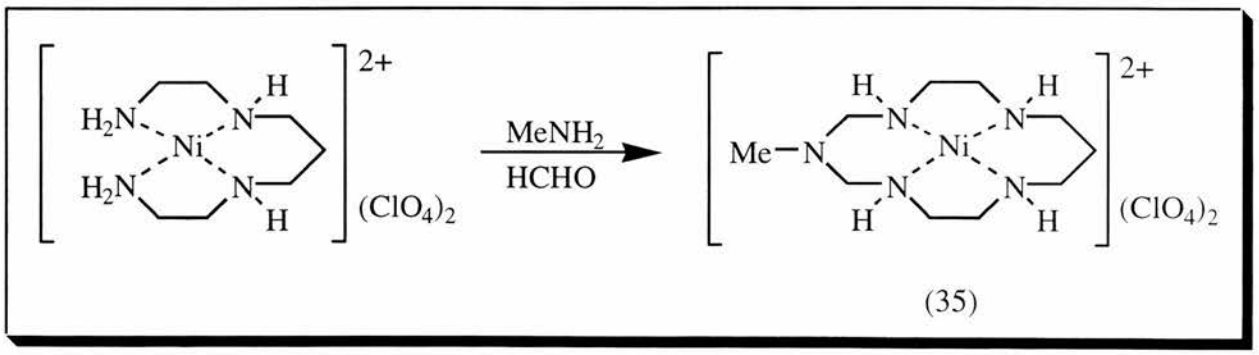

Figure 27

X-ray investigation showed that the tertiary nitrogen atom of the pentaaza macrocycle is not coordinated and that azacyclam displays coordinating tendencies (in terms of bond distances and angles) strictly similar to those of cyclam in analogous complexes.

The tertiary amine group appears as distinctly flattened thus presenting a pronounced sp^2 rather than sp^3 character. This reduces its basicity drastically, being protonated only in a strong acid solution of concentration 1 mol dm^{-3} or higher. This demonstrates that the fifth nitrogen atom introduced by template synthesis of the type described exerts a purely structural function and does not alter the cyclam like donor properties of the macrocycle.

Therefore, the [Ni(II)(azacyclam)]$(ClO_4)_2$ complex displays the same distinctive solution properties as the corresponding $[Ni(II)(cyclam)]^{2+}$ complex: i) inertness towards demetalation; ii) easy access to the Ni(II). It should be noted that the azacyclam ring is more fragile than that of cyclam. Attempts to demetalate $[Ni(azacyclam)]^{2+}$ complexes with sulfide or with boiling cyanide failed; demetalation was accompanied by macrocycle fragmentation.

1.6.2 Efficient Molecular Padlocks for Template Synthesis of Azacyclam

The crucial step of macrocycle formation is the attack of the deprotonated primary amine on the $N=CH_2$ imine bonds, derived from the Schiff base condensation of the terminal $-NH_2$ groups of coordinated 2,3,2-tet with formaldehyde. This suggests that electron withdrawing R groups, which make the attached $-NH_2$ group of the locking fragment more acidic, would favour cyclisation, Figure 28:

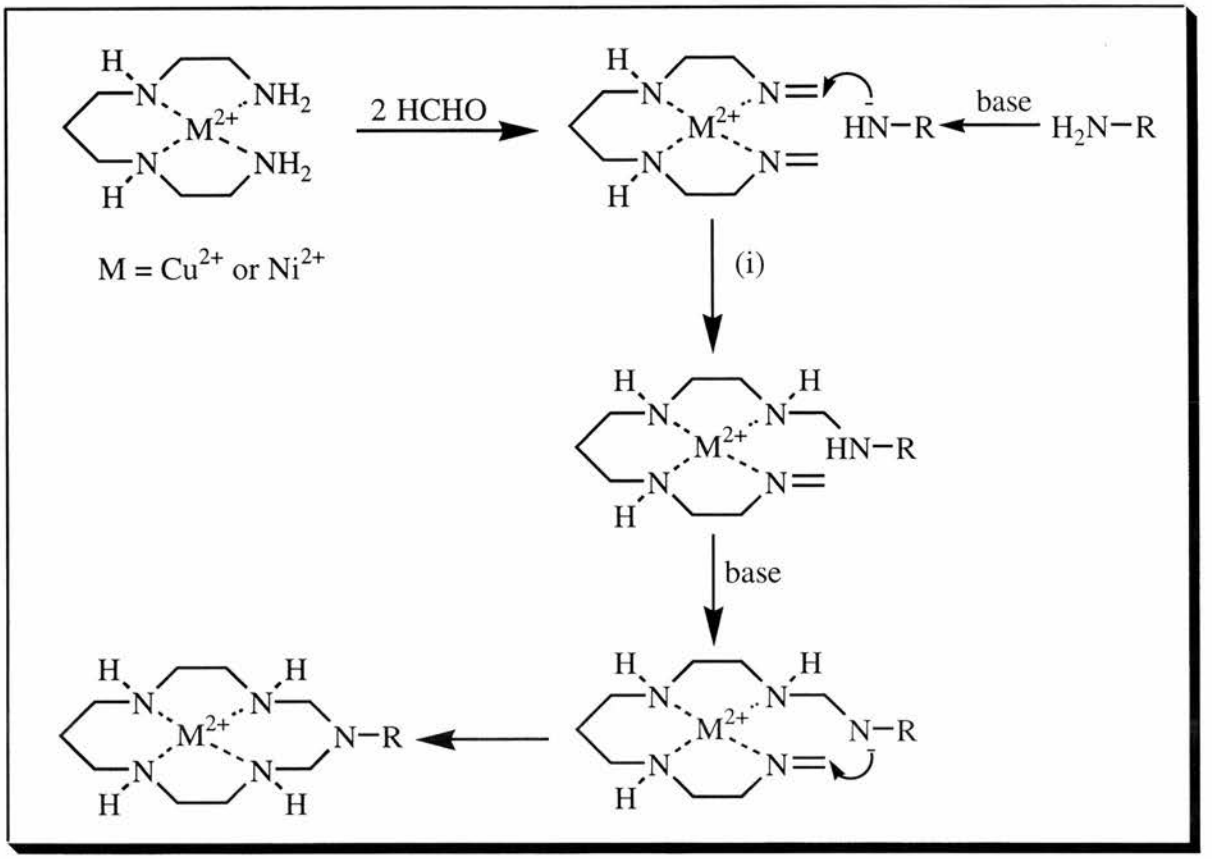

Figure 28

This hypothesis was tested by substituting R by the following groups[25]:

COMe, COPh, SO_2Ph, $SO_2C_6H_4Me$-p, $SO_2C_6H_4CO_2H$-p, SO_2-$C_{10}H_7$

All the obtained complexes displayed typical macrocyclic thermodynamic stability. Addition of strong acid, hydrochloric or perchloric, to their aqueous (when soluble) ethanol or acetonitrile solutions did result in any ring fragmentation, with the additional advantage that the templating metal centre (Ni(II)) can be removed from the ring by an acid wash and the free macrocycle recovered. The following plot represents % yields vs time profiles obtained for the reactions involving some selected locking fragments, Figure 29. Two well-known diprotic carbon acids, nitroethane and diethylmalonate are also considered:

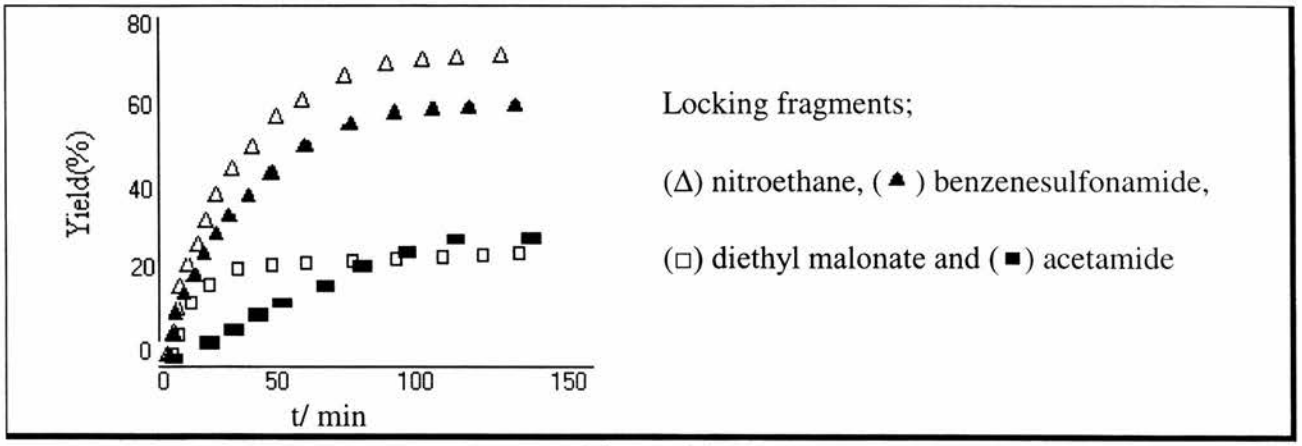

Figure 29

A linear relationship between the slope of the above graphs against the rate of the slowest step of the process (in this case one looks to any correlation with the acidity (pKa) of the diprotic nucleophile, used as a locking fragment) is shown below, Figure 30:

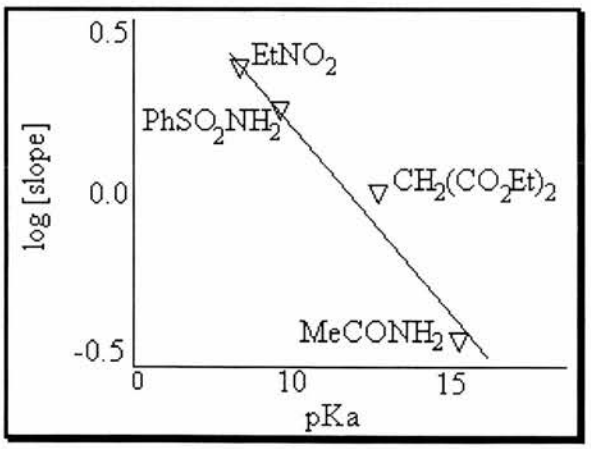

Figure 30

The lower the pKa of the nucleophile, the faster is the template process. Therefore, process (i) in the above scheme is the rate determining step of the overall template reaction. The rate of process (i) should depend linearly upon the concentration of the anion responsible for the nucleophilic attack, RNH^-, and this concentration is in turn linearly related to the acidity constant K_a.

The efficiency of the padlock reactions decreases along the series:

Nitroethane> sulfonamides> carboxamides> amines> diethylmalonate

These pentaaza template reactions provide the possibility to use molecules with acidic α hydrogens as a locking fragment, carrying a desirable functionality. In this sense amides and sulfonamides are very promising fragments to produce cyclam-like functionalised macrocycles through a one-pot procedure.

The redox potentials of the Ni(II) complexes of the azacyclam containing carboxamide or sulfonamide functional groups are reported to be influenced by the nature of the functional group[25]. In particular, the amide fragment controls the reduction potential for the $Ni^{III/II}$ and $Ni^{II/I}$ redox couples, which may be attributed to the d_{π}-p_{π} interaction between the nickel ion and the amido group.

1.6.3 Synthesis of a Pentaazamacrocycle using two Different Padlocks

Square planar Ni(II) complexes with various 1-alkyl **(36-38)** and 1-hydroxyalkyl **(39-41)** derivatives of the 14-membered pentaaza macrocycle 8-ethyl-8-nitro-1,3,6,10,13-pentaazacyclotetradecane can be synthesised by a two step metal template condensation reaction of 1,2-diaminoethane, nitroethane, formaldehyde and appropriate primary amines, Figure 31[30]:

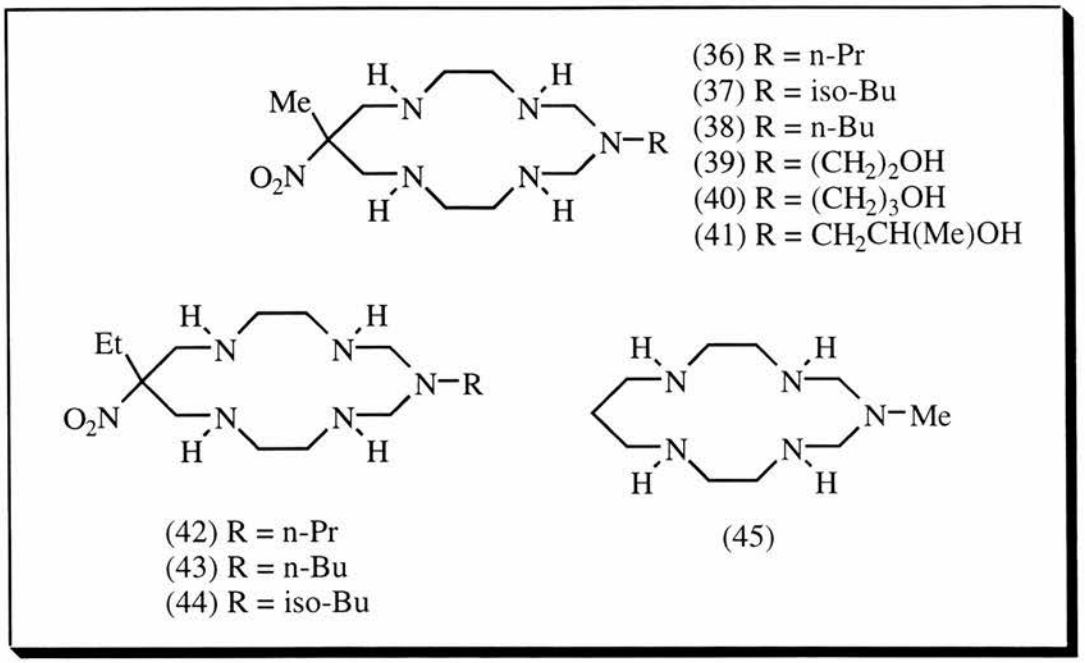

Figure 31

Compounds **(42)**, **(43)** and **(44)**, prepared in a similar manner as macrocycles **(36-41)**, exhibit chemical properties distinctly different from those of **(45)**, as would be expected given the absence of nitro functionalised pendant arm[24,30,31]. No nitro group and or hydroxyl group coordination is involved in the above mentioned macrocycles.

The electronic spectra for **(36-38)** are not varied significantly with the N-alkyl group and are quite similar to those for **(42-44)**. This indicates that the ligand field strength of the complexes is not affected significantly by the variation of the alkyl group attached to the carbon and uncoordinated nitrogen atom. The spectra of **(39-41)** containing one N-hydroxyalkyl pendant arm are also similar to those of **(36-38)**, strongly indicating that the hydroxyl group in each complex is not coordinated to the central metal ion. Analysis of the redox potentials also showed that the electron density on the metal ion of **(36-42)** is not affected significantly by the variation of alkyl groups attached to carbon and uncoordinated nitrogen:

Table 1.6.4.1: *Spectroscopic and electrochemical data for the nickel(II) complexes (**36**)–(**42**).*

Complex	λ_{max} nm (ε, M^{-1} cm^{-1})	$[Ni(L)]^{2+} \rightarrow [Ni(L)]^{3+}$ Volt *vs.* SCE
$[Ni(36)](ClO_4)_2$	453(62)	+1.09
$[Ni(37)](ClO_4)_2$	453(62)	+1.08
$[Ni(38)](ClO_4)_2$	453(61)	+1.07
$[Ni(39)](ClO_4)_2$	453(81)	+1.07
$[Ni(40)](ClO_4)_2$	453(74)	+1.09
$[Ni(41)](ClO_4)_2$	450(68)	+1.07
$[Ni(42)](ClO_4)_2$	455(69)	+1.04

Although various different alkyl substituents on the uncoordinated nitrogen atom of the previous compounds **(36-41)** did not affect the oxidation potentials of the Ni complex, a study involving copper complexes has shown that the oxidation potentials can vary on comparison of the following complexes **(46-51)**, Figure 32[32]:

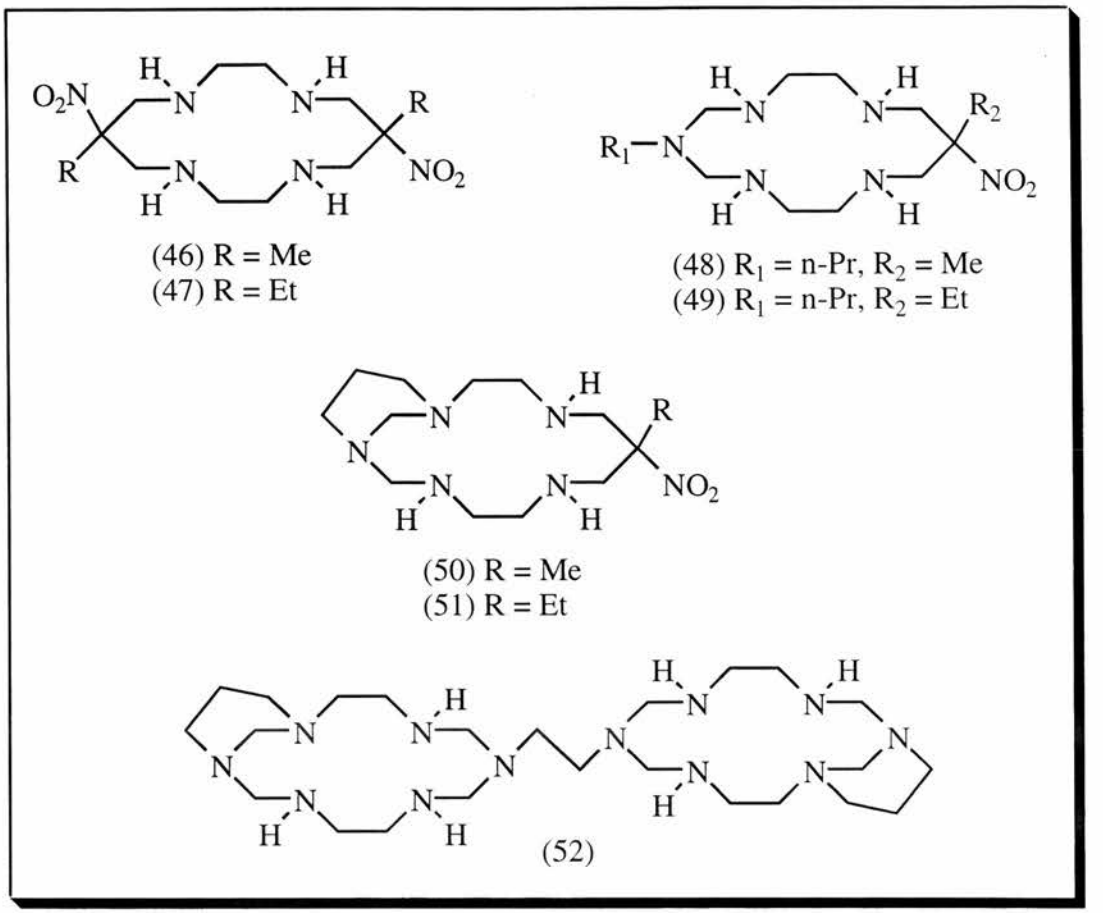

Figure 32

Table 1.6.4.2: *Electrochemical data for the copper(II) complexes (**46**)-(**52**).*

Complex	$[Cu(L)]^{2+} \rightarrow [Cu(L)]^{3+}$ (V)
$[Cu(46)](ClO_4)_2$	+1.58
$[Cu(47)](ClO_4)_2$	+1.56
$[Cu(48)](ClO_4)_2$	+1.48
$[Cu(49)](ClO_4)_2$	+1.48
$[Cu(50)](ClO_4)_2$	+1.56
$[Cu(51)](ClO_4)_2$	+1.55
$[Cu(52)](ClO_4)_2$	+1.34

In summary, the oxidation potentials of the Ni compounds **(36-41)** do not change significantly when the N-alkyl chain is varied, but the above study does indicate that the oxidation potentials

of Cu complexes of this type do vary significantly when different N-groups (indicated in the diagrams) are substituted, implying coordination of the pendant groups.

1.7 Hexaazamacrocycles

1.7.1 Instability of Methylenediamine Linkages

In 1987 Suh *et al.* attempted to synthesise macrocycle **(53)** from the condensation reaction of 1,2-diaminoethane, formaldehyde and ammonia using nickel(II) as the template, Figure 33[33]:

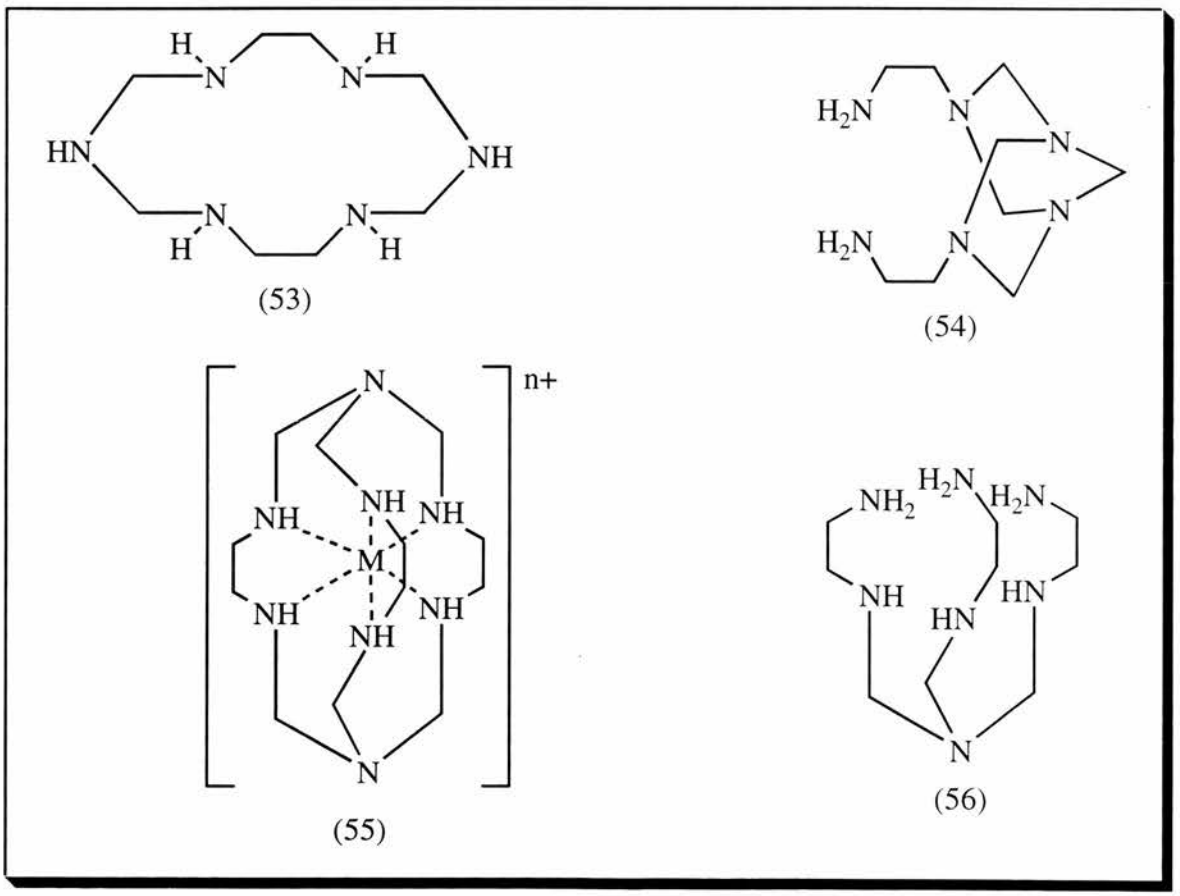

Figure 33

However, **(53)** was not obtained, instead the Ni(II) complex of the noncyclic tetradentate ligand **(54)** was recovered as the major product, in addition to the macrocyclic complex **(55)** and the Ni(II) complex with a noncyclic hexadentate ligand **(56)** as the minor products from the reaction, Figure 33[33].

In these reactions formaldehyde links two amine moieties, forming methylenediamine linkages (-N-CH_2-N-). The methylenediamine linkages are unstable when they contain primary and secondary amines and thus secondary nitrogens of methylene diamines in the Ni(II) complexes of **(55)** and **(56)** are stabilised by the coordination to the metal ion. The failure to synthesise the complex of **(53)** is, therefore, ascribed to the instability of methylenediamine linkages containing uncoordinated nitrogens.

1.7.2 Complexes of 14-Membered Hexaazamacrocyclic Ligands with Various Alkyl Pendant Arms at the Uncoordinated Nitrogens

Following the previous results, in 1988 Suh *et al.* prepared new Ni(II) and Cu(II) complexes of the 14-membered hexaazamacrocycles **(57)** and **(58)** by the template condensation of 1,2-diaminoethane, formaldehyde and alkylamines, Figure 34[34]:

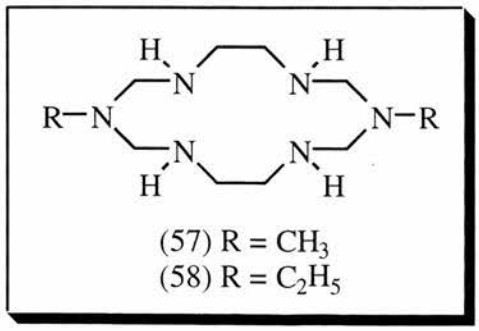

(57) R = CH_3
(58) R = C_2H_5

Figure 34

In these cases the methylenediamine linkages contain tertiary amines and are, therefore, stable. The hexaazamacrocyclic complexes [M(II)(**57**)]$(ClO_4)_2$ and [M(II)(**58**)]$(ClO_4)_2$ are extremely stable in the crystalline state and in solution are stable against ligand dissociation even in highly acidic solutions.

The electronic spectra of $[Ni(\mathbf{57})]^{2+}$ and $[Ni(\mathbf{58})]^{2+}$ are comparable to those of square planar Ni(II) complexes with saturated tetraazamacrocycles, indicating that the hexaaza ligands of these complexes do not differ significantly from the tetraaza ligands with respect to the ligand field strength. Similarly, the spectra of $[Cu(\mathbf{57})]^{2+}$ and $[Cu(\mathbf{58})]^{2+}$ are also comparable to those of other square planar Cu(II) complexes with tetraazamacrocyclic ligands.

Oxidation and reduction potentials of the Ni(II) and Cu(II) complexes of (**57**) and (**58**) do not differ significantly from those of [14]aneN_4 complexes. This suggests that macrocycles (**57**) and (**58**) have Lewis basicities and hole sizes similar to those of the [14]aneN_4 ligand in spite of the structural differences.

All efforts to obtain free ligands from the complexes by treating the complexes with excess NaCN, H_2S gas or strong acid were unsuccessful due to ring fragmentation. Free ligands (**57**) and (**58**) must be unstable because they contain methylenediamine moieties with secondary nitrogens.

This work was extended further in 1989 when Suh *et al.* prepared compounds (**59-63**) by heating the methanol solutions of 1,2-diaminoethane, formaldehyde and appropriate primary amines in the presence of Ni(II) or Cu(II) chloride followed by addition of excess perchloric acid, Figure 35[35]:

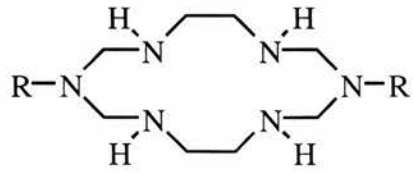

(59) R = $CH_2CH_2CH_3$
(60) R = $CH_2CH_2CH_2CH_3$
(61) R = $CH_2CH(CH_3)_2$
(62) R = $CH_2CH(CH_2CH_3)CH_2CH_2CH_2CH_3$
(63) R = $CH_2C_6H_5$

Figure 35

The synthetic routes for the complexes may be similar to those of **(57)** and **(58)** but the yields were much lower, 20-35%.

The spectroscopic and electrochemical properties of complexes **(59-63)** are similar to those of tetraazamacrocyclic complexes and are not affected significantly by the nature of the alkyl group.

1.7.3 Small Ring Moieties Fused to Hexaazamacrocycles

The Ni(II) complexes of **(64-67)** have been synthesised by the simple template condensation of formaldehyde and appropriate amines, Figure 36[50,51]:

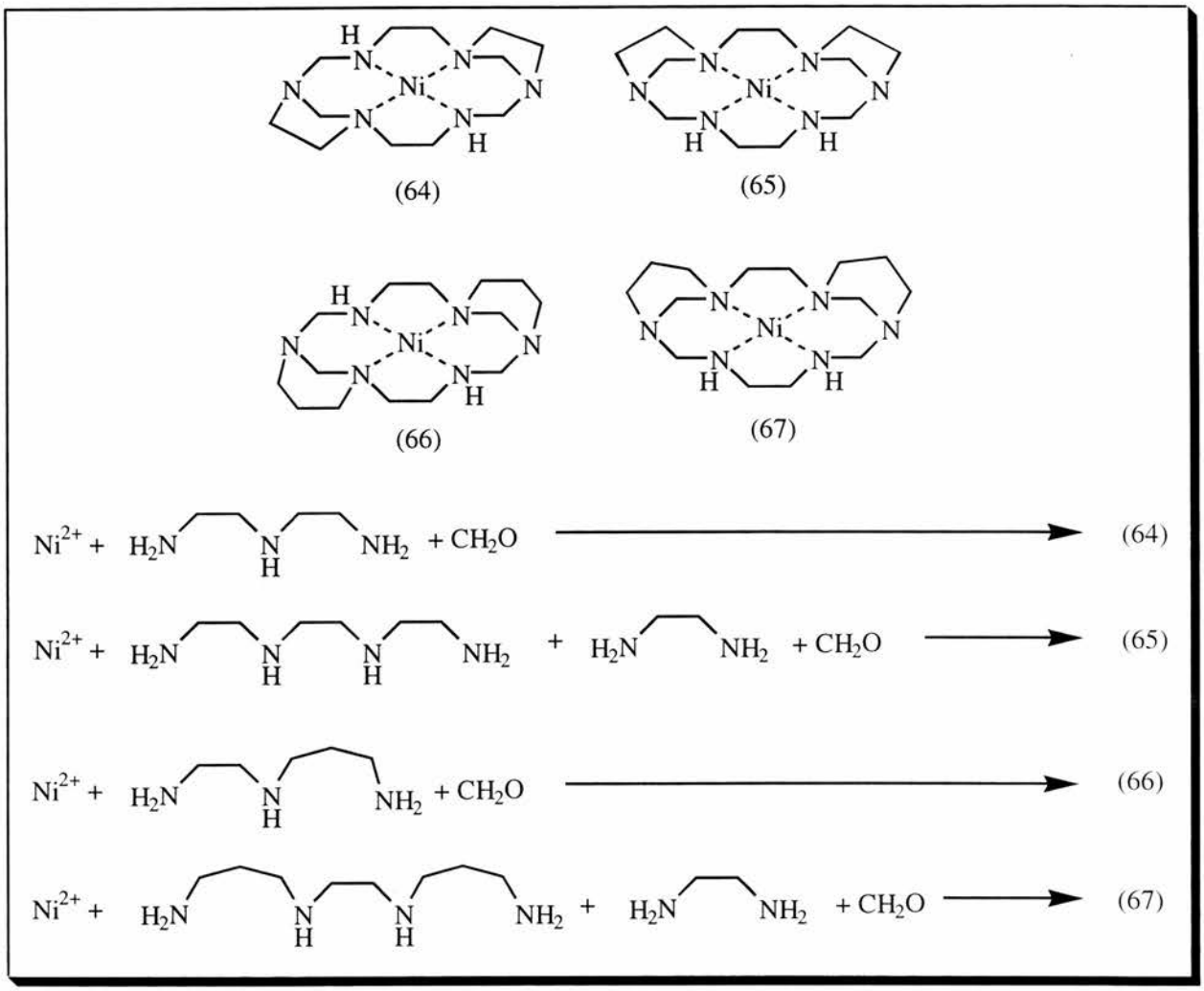

Figure 36

These complexes are extremely stable and decompose only slightly in highly acidic media.

For these macrocyclic complexes **(64-67)**, which retain the same 14-membered macrocyclic framework, the size of the sub-ring moieties affects the spectroscopic properties of the complexes. The complexes of **(64)** and **(65)** contain uncommon 1,3-diazacyclopentane sub-rings and **(66)** and **(67)** contain 1,3-diazacyclohexane sub-rings in the hexaazamacrocyclic framework[50,51]. The Ni(II) complexes of **(66)** and **(67)** exhibit λ_{max} values at approximately 20 nm longer wavelength than those of **(64)** and **(65)**, indicating the weaker ligand field strength of

(66) and **(67)**. The weaker interaction between the Ni(II) ion and the macrocyclic ligand with 1,3-diazacyclohexane sub-ring moieties is related to the Ni-N bond distances in **(66)** and **(67)**, which are longer by 0.03Å than those in **(64)** and **(65)**. There is a qualitative relationship between Ni-N bond distances and λ_{max} values. As the Ni-N bond distances increase, the λ_{max} value increases.

1.7.4 Complexes of 14-Membered Hexaazamacrocyclic Ligands with Pendant Functional Groups.

The Ni(II) complexes of hexaazamacrocyclic ligands **(68-72)**, which incorporate functional groups such as OH and CN into the pendant arms attached at the uncoordinated bridgehead nitrogen atoms, have been synthesised by the simple template condensation of 1,2-diaminoethane, formaldehyde and primary amines with the appropriate functional groups, Figure 37[35,36]:

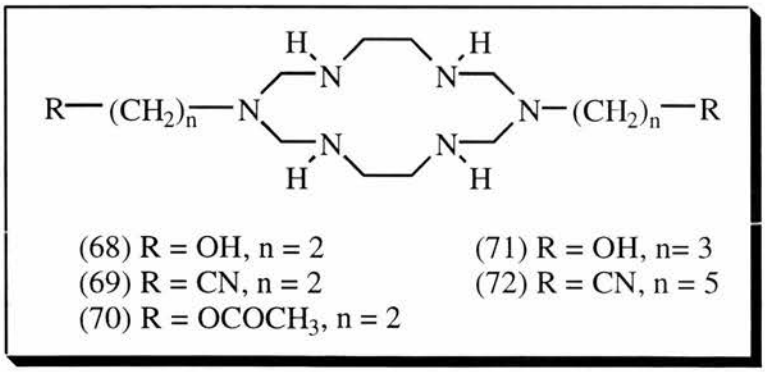

(68) R = OH, n = 2
(69) R = CN, n = 2
(70) R = $OCOCH_3$, n = 2
(71) R = OH, n= 3
(72) R = CN, n = 5

Figure 37

The hydroxyl pendant groups in the Ni(II) complex of **(68)** react with acetic anhydride to produce the Ni(II) complex of **(70)**.

The Ni(II) complexes of **(68-72)** are square planar in solution. Their uv/vis spectra and electrochemical data are slightly affected by the type of functional group and the length of the pendant chain. The oxygen atoms of the pendant hydroxyl groups form hydrogen bonds with the secondary NH's of the neighbouring macrocyclic ligands[39].

1.7.4.1 Formation of a Coordination Polymer

The Ni(II) complex with macrocycle **(72)** forms a coordination polymer on crystallisation, Figure 38[37]. Each Ni(II) ion in the macrocycle unit is coordinated by two nitrile groups of the neighbouring macrocycles. The Ni(II) atom is virtually in an octahedral geometry:

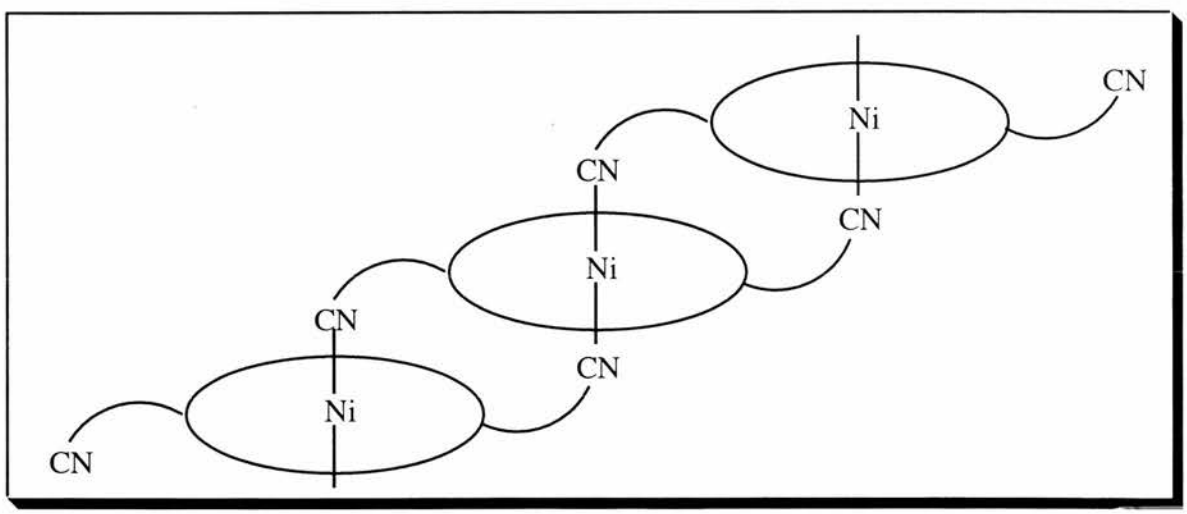

Figure 38

It is expected that various coordination polymers may be designed and synthesised if the functional groups and the chain length are appropriately varied.

1.7.5 Hexaazamacrocycle Synthesised using an Acetamide Padlock

The synthesis of 14 and 16-membered hexaazamacrocycles can be achieved by the template condensation of 1,2-diaminoethane or 1,3 diaminopropane with formaldehyde and acetamide in a 1:2:1 molar ratio in the presence of metal chlorides[38]:

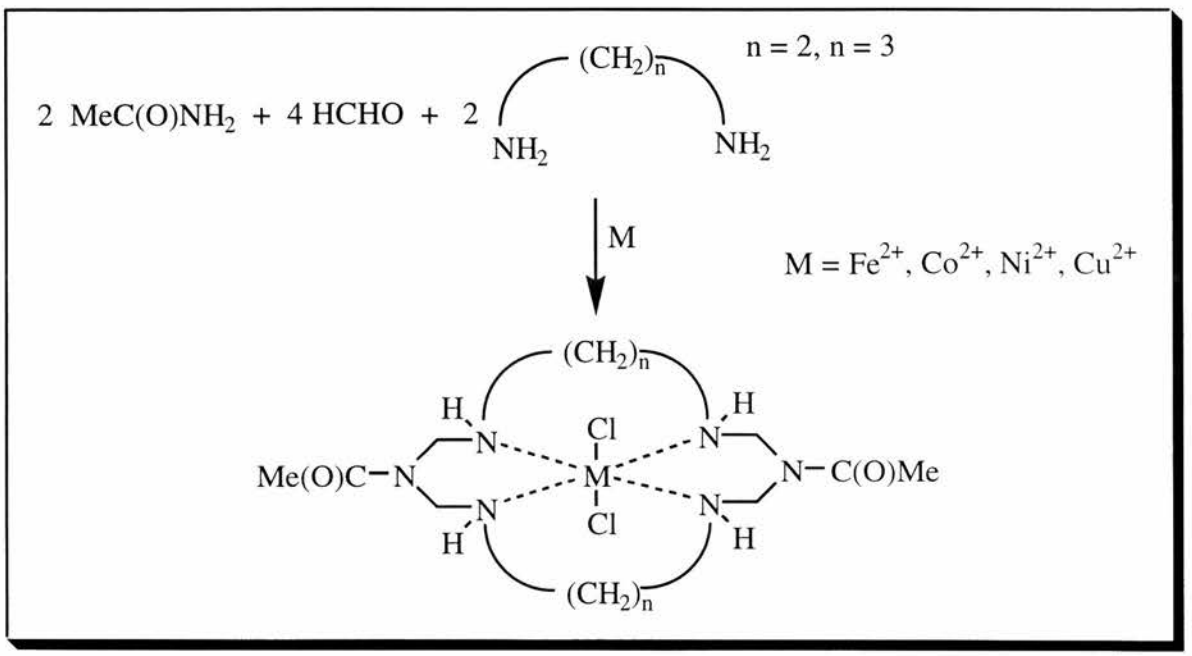

Figure 39

A facile $Cu^{II/I}$ reduction is observed in these complexes, whereas the $Cu^{II/III}$ oxidation process does not occur and hence the present macrocyclic complexes are able to stabilise the Cu^{+} oxidation state rather than the Cu^{3+} state.

1.7.6 Hexaaza Gold(III) Complexes

Ni(II), Cu(II) and Co(III) complexes of various saturated polyazamacrocyclic ligand have been synthesised by metal template condensation reactions with formaldehyde and amines. In order to prepare the complexes of other metal ions, it would be useful to prepare free macrocycles. However, the macrocyclic ligands with -N-CH_2-N- (methylenediamine) linkages are unstable when they are not coordinated to a metal ion. Therefore, there is considerable interest in finding other metal ions that can be utilised in the metal template reactions.

In 1996 Suh *et al.* synthesised two gold(III) complexes of the hexaazamacrocyclic ligand 1,8-bis(2-hydroxyethyl)-1,3,6,8,10,13-hexaazacyclotetradecane (**73**), four coordinate [Au(**73**)]$(ClO_4)_2$ 1/2 H_2O) and six coordinate [Au(**73**)Cl_2]$AuCl_4$, Figure 40[39]. These complexes were synthesised in high yield from the template condensation of 1,2-diaminoethane, formaldehyde and ethanolamine in the presence of gold(III) ion. The gold(III) template cyclisation is extremely fast compared with the corresponding Ni(II) template reaction:

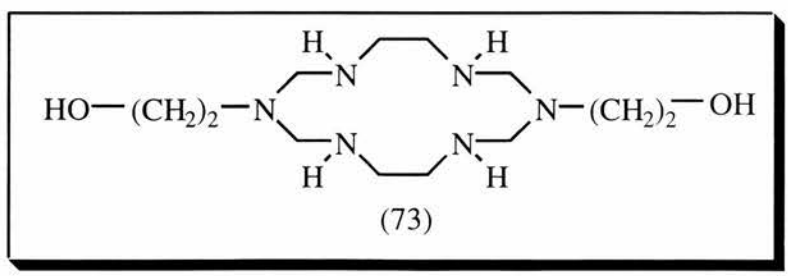

(73)

Figure 40

The complexes incorporate the hydroxyethyl pendants onto the bridgehead nitrogens but the hydroxyl groups are not involved in intra or inter molecular coordination.

1.7.7 Ni(III) Hexaaza Complexes

The six coordinate Ni(III) macrocyclic complexes $[Ni^{III}(L)X_2]^+$ where L = 1,8-bis(2-hydroxyethyl)-1,3,6,8,10,13-hexaazacyclotetradecane (**74**), 1,8-bis(2-cyanoethyl)-1,3,6,8,10,13-hexaazacyclotetradecane (**75**) or 1,8-dimethyl-1,3,6,8,10,13-hexaazacyclotetradecane (**76**) and X = Cl^-, Br^- or NO_3^- have been prepared by the oxidation of the square-planar Ni(II) complexes of the corresponding macrocyclic ligands, Figure 41[40]. Although the macrocyclic ligands (**74**) and (**75**) contain potentially coordinating pendant groups as well as the tertiary nitrogens at the bridgehead position, none of them coordinates the Ni(III) ion. Hence the Ni(III) species are stabilised by the extra axial ligand:

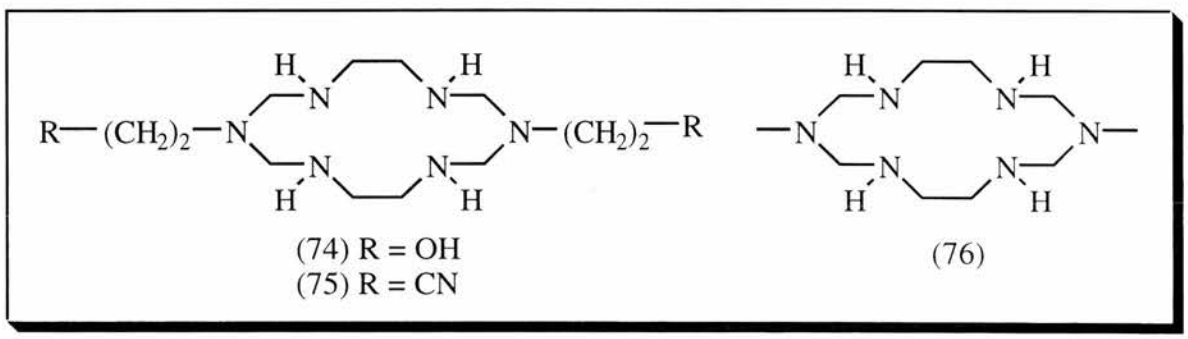

Figure 41

The Ni(III) ions are in a low spin d^7 state with the unpaired electron residing in the dz^2 orbital to adopt tetragonally distorted octahedral geometry.

1.8 Binuclear Macrocycles

1.8.1 Binuclear Macrocycles from fully Saturated 14-Membered Hexaazamacrocyclic Subunits

There has been considerable interest in the synthesis of binuclear macrocyclic complexes, since the complexes often represent a helpful tool in the study of metal-metal interaction and multi-metal centred catalysts[42-46].

In order to obtain binuclear macrocyclic complexes several synthetic strategies have been employed:

(i) Synthesis of macrocycles containing functional groups.

(ii) Synthesis of large macrocycles able to incorporate two metal ions.

(iii) Synthesis of double ring macrocycles in which two macrocyclic subunits are linked together.

Each binuclear macrocyclic system exhibits its own unique properties. In particular, double ring macrocycles do not alter significantly the properties of each macrocyclic subunit itself and thus most of the advantages of the monomers, such as kinetic inertness and thermodynamic stability, remain intact.

Until the late 1980s and early 1990s most synthetic routes for these binuclear species required several steps. In 1991 Kang *et al.* synthesised new Ni(II) and Cu(II) complexes with various alkyl derivatives of 1,2-bis(1,3,6,8,10,13-hexaaza-1-cyclotetradecyl)ethane, in which two fully

saturated 14-membered hexaazamacrocyclic subunits were linked together by and ethylene chain, Figure 42[41].

This synthesis is a one step template condensation of formaldehyde and 1,2-diaminoethane and appropriate primary alkyl amines in the presence of the metal ions:

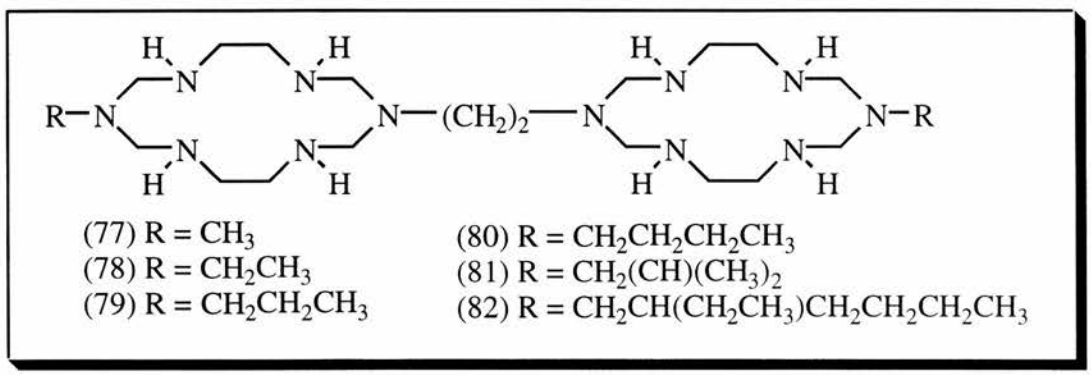

Figure 42

The binuclear complexes are very stable in solid state and in solution. The properties of these double ring macrocyclic complexes are very similar to those of their monomeric analogues. This strongly indicates that metal-metal interactions of the binuclear complexes, in which the uncoordinated nitrogen atoms of two hexaazamacrocyclic units are linked together by an ethylene chain, are not significant.

1.8.2 Synthesis of Dinickel(I) Complexes of Bis-macrocyclic Ligands.

In 1993 a bis-macrocyclic Ni(I) complex was synthesised by the simple template condensation method of their Ni(II) analogues followed by reduction with Na(Hg) in MeCN to give (**83**) and (**84**), Figure 43[47]:

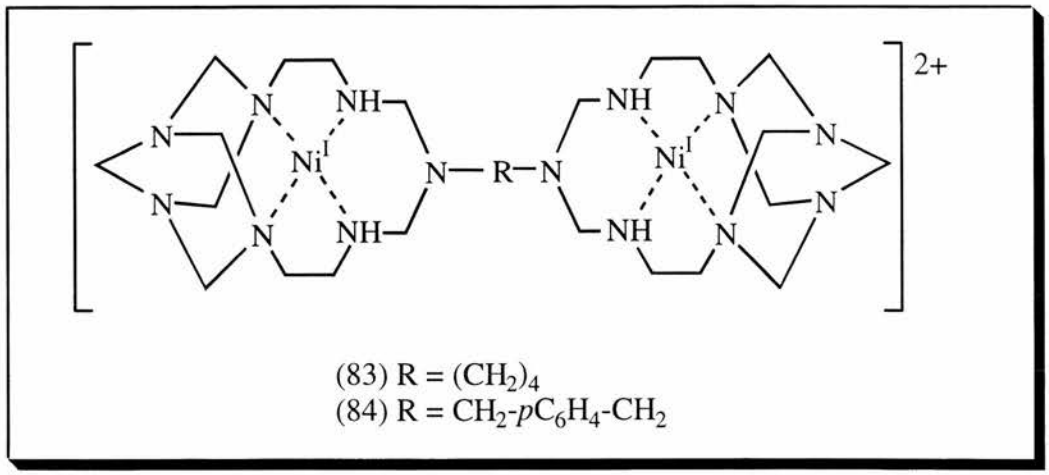

Figure 43

These complexes were the first examples of Ni(I) complexes with bis-macrocyclic ligands. The isolation of Ni(I) macrocyclic complexes is quite rare and only a few complexes of monomacrocyclic ligands have been reported[48,49]. The bis-macrocyclic ligands of (**83**) and (**84**) stabilise two Ni(I) ions and metal-metal interactions are absent.

1.8.3 Binuclear Macrocycles from fully Saturated 14-membered Pentaazamacrocyclic Subunits

Template condensation of $[M(2,3,2\text{-tet})]^{2+}$ (M = Ni or Cu, 2,3,2-tet = 3,7-diazanonane-1,9-diamine) with formaldehyde and aliphatic diamines $H_2N(CH_2)_nNH_2$ (n = 2-5) results in dinickel and dicopper bis(macrocyclic) complexes in which two 1,4,6,8,11-pentaazacyclotetradecane subunits are linked by polymethylene chains of various lengths through the uncoordinated nitrogen bridgehead atoms, Figure 44[53]:

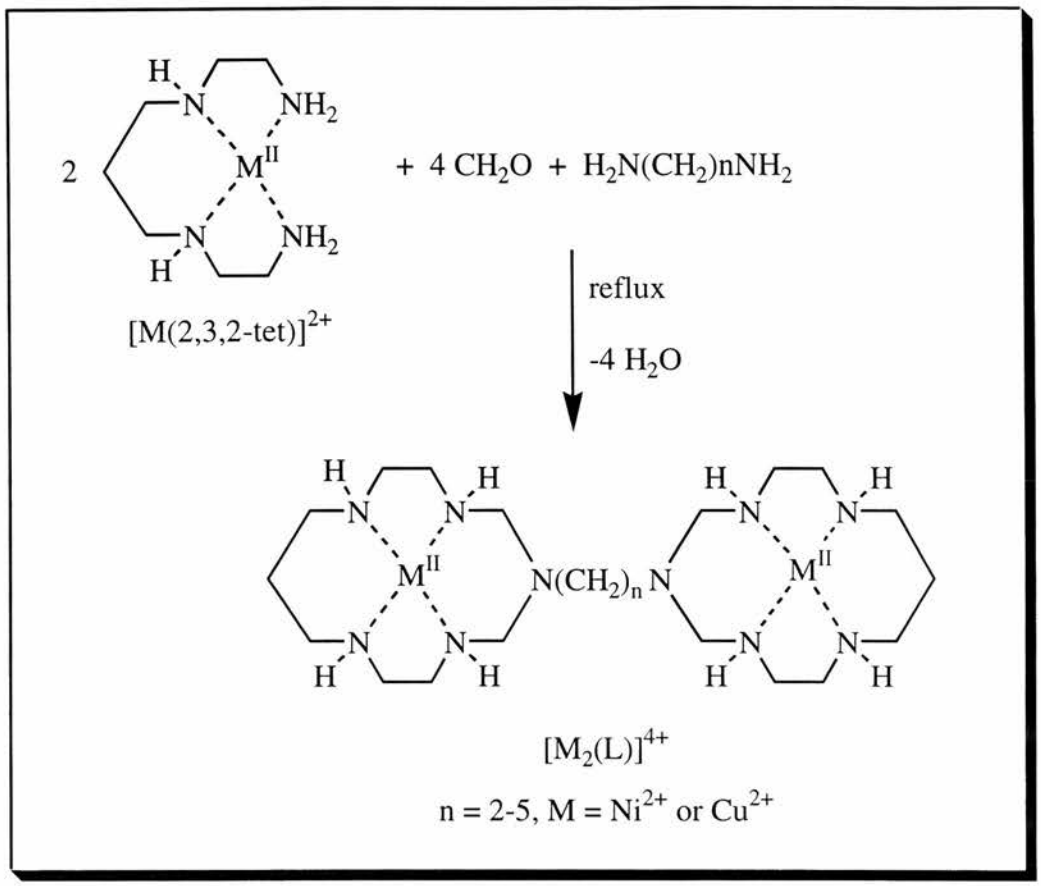

Figure 44

In this case the geometric structure of these compounds (in particular the length of the polymethylene bridges between the macrocyclic subunits) substantially influences the thermodynamic parameters of interaction of diamines with copper complexes and the electrochemical properties of the $Ni^{II/I}$ and $Ni^{III/II}$ redox reactions (ΔE_p's are dramatically increased >250 mV)[53a].

1.8.4 Synthesis of Binuclear Macrocycles from fully Saturated Hexaazamacrocyclic Subunits Containing Small Ring Moieties

A one pot condensation reaction of 1,4,8-triazaoctane, 1,2-diaminoethane and formaldehyde in the presence of Ni(II) produces a dinuclear Ni(II) complex of the bis-macrocyclic ligand, $[Ni_2(\mathbf{85})](ClO_4)_4$, in which two fully saturated hexaazamacrocycles are linked together by an ethylene chain, Figure 45[54,55]:

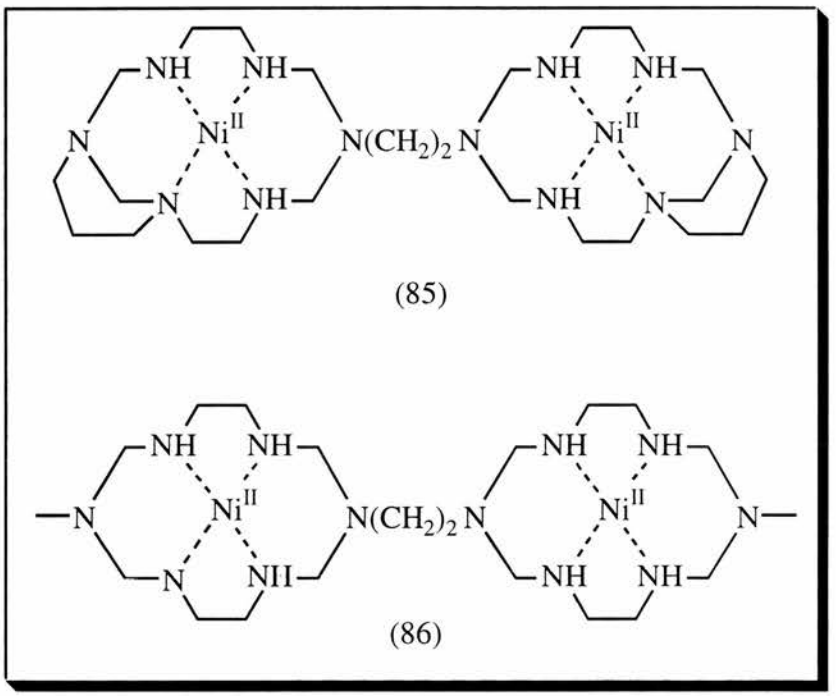

Figure 45

Each macrobicyclic subunit of the complex **(85)** contains one 1,3-diazacyclohexane ring and has a square-planar geometry with a 5-6-5-6 chelate ring sequence. The electrochemical properties show that metal-metal interactions of dinuclear complex **(85)** are negligible since there is no splitting of the $Ni^{III/II}$ wave. Comparisons of the spectral and chemical properties of **(85)** and **(86)** show that the number of 1,3-diazacyclohexane ring moieties fused to the ligands largely affects

these properties. This is due to the distortion that these rings exert on the environment of the nickel(II) ion as can be seen in the crystal structures of these types of macrocycles, see Chapter 2.

1.8.5 Synthesis of a Binuclear Macrocycle Linked by a Biphenyl Group

Novel binuclear compounds have been prepared by the template condensation reaction of 1,2-diaminoethane or 1,3-diaminopropane with formaldehyde and benzidine followed by Schiff base condensation with acetyl acetone or dibenzoylmethane or phthalaldehyde, Figure 46[55-57]:

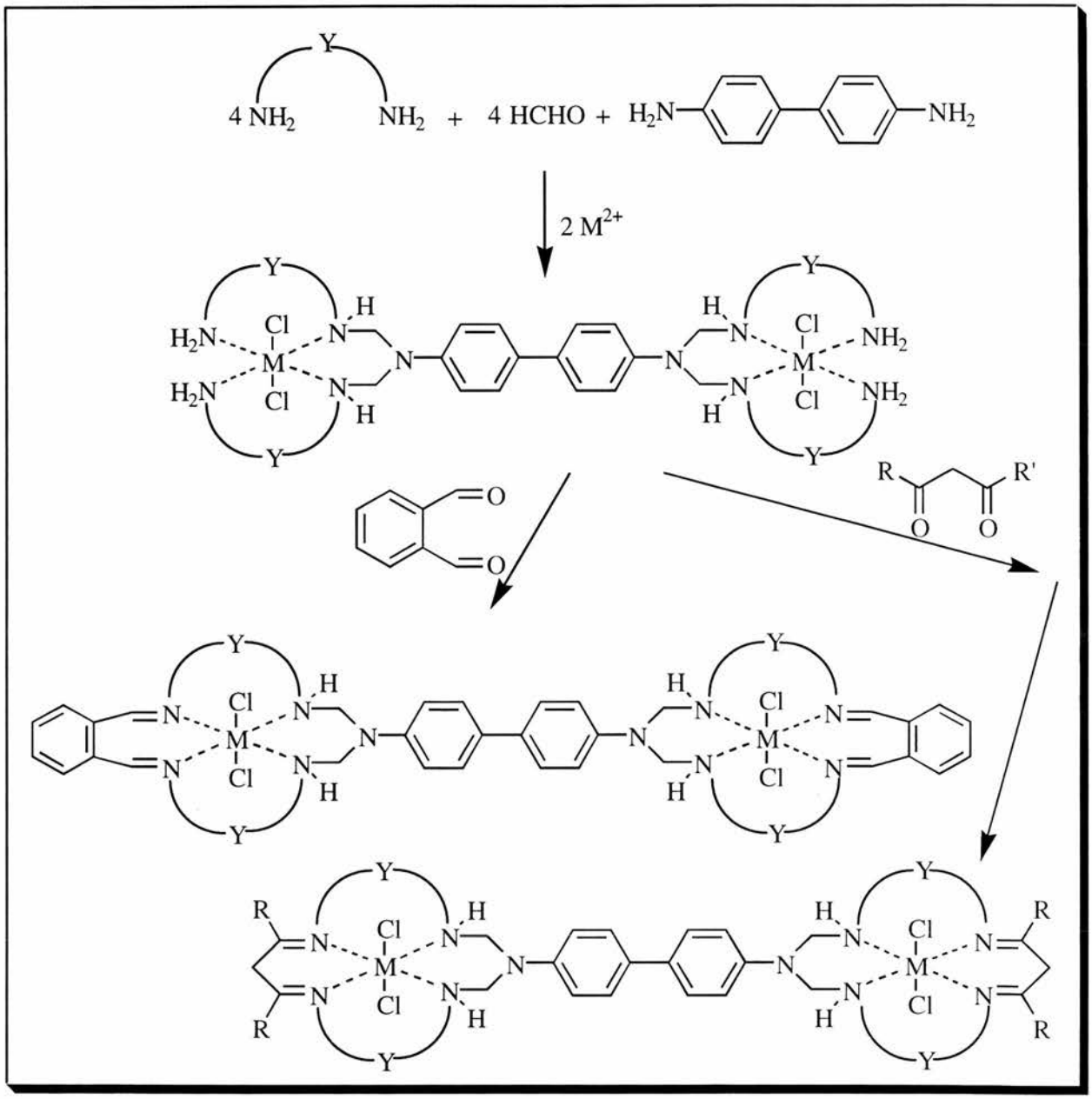

Figure 46

Where M = Fe^{2+}, Co^{2+}, Ni^{2+}, Cu^{2+}, Zn^{2+},

And the variable substituents are:

(87) Y = $(CH_2)_2$, R = CH_3

(88) Y = $(CH_2)_3$, R = CH_3

(89) Y = $(CH_2)_2$, R = C_6H_5

(90) Y = $(CH_2)_3$, R = C_6H_5

(91) Y = $(CH_2)_2$

(92) Y = $(CH_2)_3$

In this case the macrocyclic rings are far away from each other and the two metal centres act independently of each other.

A similar type of reaction involving the template condensation of triethylenetetraamine, formaldehyde and benzidine produces the macrocycle (**93**), Figure 47[57b]:

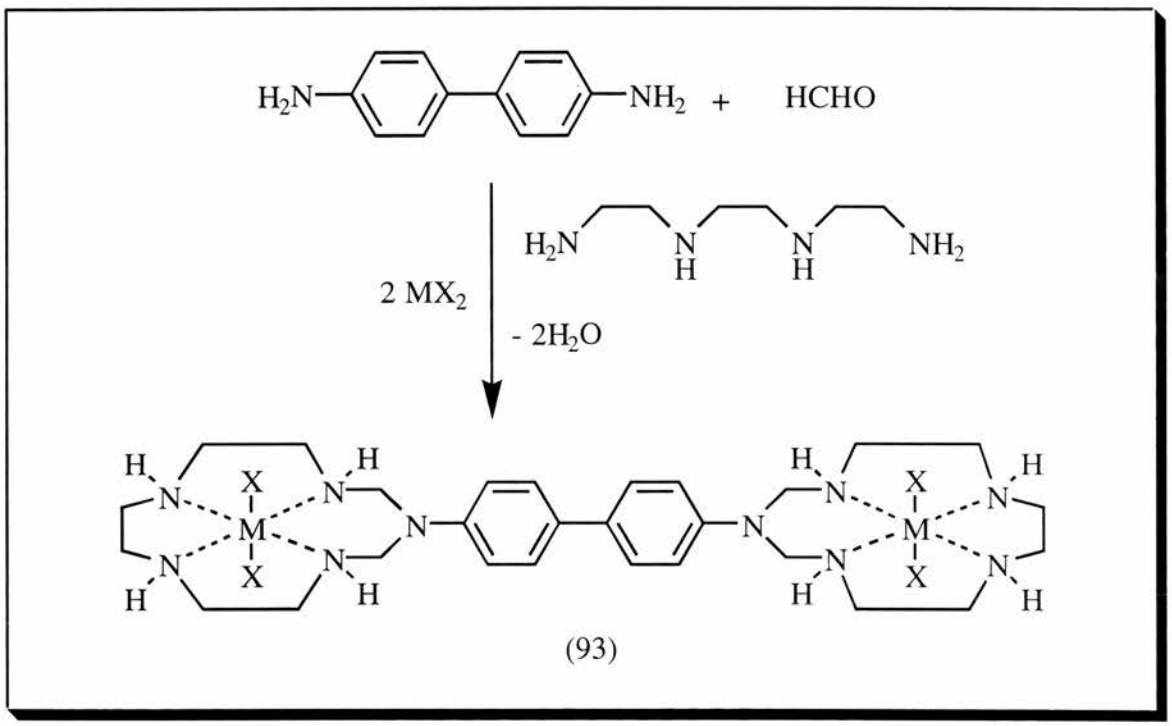

Figure 47

The electronic absorption bands of all these bis-macrocyclic binuclear complexes, in comparison to those of the similar mono-nuclear complexes, do not show appreciable differences. The magnetic moment values of the complexes also agree well with their mononuclear analogues. This similarity in spectral and magnetic properties suggests that the metal centres are non-interacting in these complexes in solutions.

1.9 Conclusion

Compounds with acidic protons of varying nature and of general formula H_2A, can act as efficient molecular padlocks in the presence of formaldehyde, in closing open chain amines around a labile metal centre (e.g. Cu^{2+} and Ni^{2+}). Metal complexes of cyclam-like macrocycles are thus synthesised in a very convenient (one pot) manner and using inexpensive reagents[3]. However, the metal pentaaza and hexaaza complexes cannot be considered analogues of the corresponding cyclam complexes. The standard synthetic approach for making tetraaza macrocycles involves using either Ni^{2+} or Cu^{2+} as the template. The free ligand is then inserted with one of the previously mentioned metal ions. Demetalation in pentaaza and hexaaza macrocycles is accompanied by macrocycle fragmentation due to the instability of the methylenediamine linkages[33].

Around inert octahedral metal ions, saturated and usually macrobicyclic molecules are readily accessible. Around more labile metal ions, such as Cu(II), Ni(II) and Pd(II) there is a tendency to form usually saturated macromonocyclic molecules, directed by a preference for four coordination and square-planarity with strong field ligands in those cases[17,51a].

Interest in the template reactions described in this work rather lies in the possibility to use as a locking fragment a diprotic acid carrying a desirable functionality. Applications of previously mentioned macrocycles lies in their use in the electrocatalytic reduction of CO_2 to CO and for DNA cleavage[69-72]. The reduction of CO_2 is an important objective in the development of alternative fuel sources. Among various possible approaches, the electrochemical reduction of CO_2 appears to be an attractive method.

1.9.1 Aims of the Project and Organisation of the Thesis

This thesis discusses the synthesis of new macrocycles around a nickel(II) centre (Chapter 2) using the techniques outlined in this chapter. The range of macrocycles include single pendant arm macrocycles prepared from 2,3,2-tet (see section 1.6), a hexaaza macrocycle with two sub-rings (see section 1.7.3), a binuclear bis-macrocycle (see section 1.8) and a discussion of some attempted syntheses. We discuss aspects of their chemical and physical properties and their structures[27,53a,71,73].

Chapter 3 is an investigation of the electrocatalytic reduction of CO_2 to CO using a series of these complexes (see section 1.1). A possible correlation between the effect of the side arm on the electrochemical kinetics is also explored[70,71,73]. The discovery of a relationship between electrochemical kinetics and catalytic current is reported.

Chapter 4 is a thermodynamic study of the square planar – *cis*-octahedral folding of the pendant arm macrocycle 3-(2-hydroxyethyl)-1,3,5,8,12-pentaaza-cyclotetradecane nickel(II) perchlorate. Folding of macrocycles is well known and Billo and Margerum have studied the kinetics of the *cis*-folding of $[Ni(cyclam)]^{2+}$ but the thermodynamics have not been studied in any depth to date[73-75].

In Chapter 5 the synthesis and characterisation of a range of other interesting macrocycles are discussed. Crystal structures were determined for *trans*-dioxocyclam dihydrate, nickel(II) *trans*-dioxocyclam and a pendant arm *trans*-dioxocyclam is presented. Large hexaazamacrocycles are discussed and two Schiff bases are reported, metal ion promoted dipeptide ester hydrolysis is discussed and three dipeptides are presented. Cyclen is discussed and two copper complexes are

presented and the crystal structure of the copper(II) cyclen complex: [Cu(cyclen)Br](ClO_4).$NaClO_4$.H_2O is also presented.

1.10 References

1. P. V. Bernhardt, *Ph.D. Thesis*, University of Newcastle, 1990.

1a. See for example; O. Costisor and W. Linert, *Reviews in Inorganic Chemistry*, 2000, **20**, 63.

2. U. Thewalt and J. Weiss, *Z. Anorg. Chem.*, 1996, **348**, 238.

3. L. Fabbrizzi, M. Licchelli, A. M. M. Lanfredi and O. Vassalli, *Inorg. Chem.*, 1996, **35**, 1582.

4. A. M. Sargeson, *Chem. Brit.*, 1979, **15**, 23.

5. R. J. Geue, T. W. Hambley, J. M. Harrowfield, A. M. Sargeson and M. R. Snow, *J. Am. Chem. Soc.*, 1984, **106**, 5478.

6. J. M. Harrowfield, PhD Thesis, Australian National Uni. 1998.

7. H. A. Boucher, G. A. Lawrance, P. A. Lay, A. M. Sargeson, A. M. Bond, D. F. Sangster and J. C. Sullivan, *J. Am. Chem. Soc.*, 1983, **105**, 4652.

8. M. P. Suh, W. Shin, D. Kim and S. Kim, *Inorg. Chem.*, 1984, **23**, 618.

9. P. Comba, W. F. Curtis, G. A. Lawrance, M. A. O'Leary, B. W. Skelton and A. H. White, *Inorg. Chem.*, 1986, **25**, 4269.

10. P. V. Bernhardt, P. Comba, T. W. Hambley and G. W. Lawrance, *Inorg. Chem.*, 1991, **30**, 942-946.

11. P. V. Bernhardt, T. W. Hambley and G. W. Lawrance, *J. Chem. Soc., Dalton Trans.*, 1989, 1059.

12. N. F. Curtis, G. J. Gainsford, T. W. Hambley, G. A. Lawrance, K. R. Morgan and A. Sirwardena, *J. Chem. Soc., Chem. Commun.* 1987, 295.

13. P. V. Bernhardt, P. Comba, T. W. Hambley, G. W. Lawrance, N. F. Curtis, M. Maeder and A. Sirwardena, *Inorg. Chem.*, 1990, **29**, 3208.

14. P. V. Bernhardt, T. W. Hambley and G. W. Lawrance, *J. Chem. Soc., Dalton Trans.*, 1990, 983.

15. T. W. Hambley, *Inorg. Chem.*, 1988, **27**, 2496.

16. G. A. Lawrance, B. W. Skelton, A. H. White and P. Comba, *Aust. J. Chem.*, 1986, **39**, 1101.

17. P. V. Bernhardt, P. Comba, T. W. Hambley, G. A. Lawrance, N. and V. Katain, *J. Chem. Soc., Dalton Trans.*, 1992, 355.

18. G. A. Lawrance, B. W. Skelton, A. H. White, P. Comba, N. F. Curtis and M. A. O'Leary, *J. Chem. Soc., Dalton Trans.*, 1988, 2145.

19. N. F. Curtis, G. J. Gainsford, D. C. Weatherburn and A. Sirwardena, *Aust. J. Chem.*, 1993, **46**, 755.

20. P. V. Bernhardt, P. Comba, T. W. Hambley, *Inorg. Chem.*, 1993, **32**, 2804.

21. L. Xin, N. F. Curtis, D. C. Weatherburn, *Trans. Met. Chem.*, 1988, **17**, 147.

22. L. Fabbrizzi, M. Licchelli, A. Poggi, O. Vassalli, L. Ungaretti and W. Sardone, *Inorg. Chim. Acta.*, 1996, **246**, 379.

23. M. Rossignoli, P. V. Bernhardt, G. A. Lawrance and M. Maeder, *Aust. J. Chem.*, 1997, **50**, 529.

24. L. Fabbrizzi, A. M. Manotti, P. Pallavicini, A. Perotti, A. Taguetti and F. J. Ugozzoli, *J. Chem. Soc., Dalton Trans.*, 1991, 3263.

25. A. Blas, G. Santis, L. Fabbrizzi, A. M. M. Lanfredi, M. Licchelli, P. Morosini, P. Pallavini and F. Ugozzoli, *J. Chem. Soc., Dalton Trans.*, 1993, 1411.

26. C. C. A. Rossignoli, T. W. Hambley, G. A. Lawrance and M. Maeder, *Inorg. Chem.*, 1996, **35**, 4961.

27. R. W. Hay, T. J. Cromie and P. Lightfoot, *Trans. Met. Chem.*, 1997, **22**, 510.

28. C. I. Smith, J. A. Crayston and R. W. Hay, *J. Chem. Soc., Dalton Trans.*, 1993, 3267.

29. R. W. Hay, A. Danby, P. Lightfoot and Y. D. Lampeka, *Polyhedron*, 1997, **16**.

30. S. G. Kang, S. K. Jung, *J. Sci. Edu. Taegue Univ.*, 1992, **5**, 87.

31. S. G. Kang, J. S. Choi, *Bull. Korean Chem. Soc.*, 1994, **15**, 374.

32. S. G. Kang, J. S. Choi and K. Ryu, *Bull. Korean Chem. Soc.*, 1994, **15**, 1305.

33. M. P. Suh, W. Shin, H. Kim and C. H. Koo, *Inorg. Chem.*, 1987, **26**, 1846.

34. M. P. Suh and S. G. Kang, *Inorg. Chem.*, 1988, **27**, 2544.

35. M. P. Suh, S. G. Kang and S. K. Jung, *Bull. Korean Chem. Soc.*, 1989, **10**, 362.

36. R. W. Hay, M. J. Armstrong and M. Hassan, *Trans. Met. Chem.*, 1992, **17**, 270.

37. M. P. Suh, B. Y. Shim and T. S. Yoon, *Inorg. Chem.*, 1994, **33**, 5509.

38. M. Shakir, A. K. Mohamed, S. P. Varkey and Z. A. Siddiqi, *Trans. Met. Chem.*, 1996, **21**, 162.

39. M. P. Suh, S. Kim, B. Y. Kim, D. Hong and T. S. Yoon, *Inorg. Chem.*, 1996, **35**, 3595.

40. M. P. Suh, Y. E. Lee and B. Y. Shin, *Inorg. Chim. Acta*, 1998, **269**, 337.

41. S. G. Kang, S. K. Jung, J. K. Kweon, *Bull. Korean Chem. Soc.*, 1991, **12**, 219.

42. A. Buttafava, L. Fabbrizzi, A. Perotti, A. Poggi and B. Seghi, *Inorg. Chem.*, 1984, **23**, 3917.

43. L. Fabbrizzi, F. Forlini, A. Perotti and B. Seghi, *Inorg. Chem.*, 1984, **23**, 807.

44. L. Fabbrizzi, L. Montagna, A. Poggi, T. A. Kaden and L. C. Siegfried, *J. Chem. Soc., Dalton Trans.*, 1987, 2631.

45. L. Fabbrizzi, L. Montagna, A. Poggi, T. A. Kaden and L. C. Siegfried, *Inorg. Chem.*, 1986, **25**, 2671.

46. M. P. Suh and S. G. Kang, *Inorg. Chem.*, 1988, **27**, 2544.

47. M. P. Suh, S. G. Kang and S. K. Kim, *Inorg. Chem.*, 1993, **32**, 3562.

48. M. P. Suh, H. K. Kim, M. J. Kim, *Inorg. Chem.*, 1992, **31**, 3620.

49. C. O. Dietrich-Buchner, J. Kern, *J. Chem. Soc., Chem. Commun.*, 1985, 760.

50. M. P. Suh, W. Shin, S. G. Kang and T. M. Chung, *Inorg. Chem.*, 1989, **28**, 1602.

51. M. P. Suh, J. W. Choi, S. G. Kang and W. C. Shin, *Inorg. Chem.*, 1989, **28**, 1763.

51a M. Rossignoli *et al.*, *Inorg.Chem.*, 1996, **35**, 4961.

52. M. Rossignoli, P. V. Bernhardt, G. A. Lawrance and M. Maeder, *J. Chem. Soc., Dalton Trans.*, 1997, 323.

53. S. V. Rosokha, Y. D. Lampeka and I. M. Maloshtan, *J. Chem. Soc., Dalton Trans.*, 1993, 631.

53a C. de Alwis, J. A. Crayston, T. J. Cromie, T. Eisenblätter, R. W. Hay, Ya. D. Lampeka, L. V. Tsymbal, *Electrochimica Acta*, 2000, **45**, 2061.

54. S. G. Kang, S. K. Jung, J. K. Kweon and M. S. Kim, *Polyhedron*, 1993, **12**, 353.

55. S. G. Kang, K. Ryu, S. K. Jung and C. S. Kim, *Bull. Korean. Chem. Soc.*, 1996, **17**, 331.

56. M. Shakir, A. K. Mohamed, S. P. Varkey, O. S. M. Nasman, *Indian Journal of Chemistry*, 1996, **35A**, 935.

57. M. Shakir, A. K. Mohamed, S. P. Varkey and O. S. M. Nasman, *Synth. React. Inorg. Met. Org. Chem.*, 1998, **28**, 135.

57b T. A. Khan, M. A. Rather, N. Jahan, S. P. Varkey and M. Shakir, *Synth. React. Inorg. Met. Org. Chem.*, 1997, **27**, 843.

58. P. Comba, A. M. Sargeson, L. M. Englehardt, J. M. Harrowfield, A. M. White, E. Horn and M. R. Snow, *Inorg. Chem.*, 1985, **24**, 2325.

59. P. Comba, L. M. Englehardt, J. M. Harrowfield, G. A. Lawrance, L. L. Martin, A. M. Sargeson and A. M. White, *J. Chem. Soc., Chem. Commun.*, 1985, 174.

60. I. I. Crewer, L. R. Gahan, J. M. Harrowfield, G. A. Lawrance, L. L. Martin and A. M Sargeson, unpublished results.

61. G. A. Lawrance, M. Rossignoli, B. W. Skelton and A. H. White, *Aust. J. Chem.*, 1987, **40**, 1441.

62. G. A. Lawrance and M. O'Leary, *Polyhedron*, 1987, **6**, 1291.

63. P. Comba, N. F. Curtis, G. A. Lawrance, M. O'Leary, B. W. Skelton and A. H. White, *J. Chem. Soc., Dalton Trans.*, 1988, 2145.

64. L. M. Engelhardt, G. A. Lawrance, T. M. Manning and A. H. White, *J. Chem. Soc.*, 1989, **43**, 1859.

65,66. T. W. Hambley, G. A. Lawrance, M. Maeder and E. N. Wilkes, *J. Chem. Soc., Dalton Trans.*, 1992, 1283.

67. G. A. Lawrance and M. A. O'Leary, unpublished results.

68. P. V. Bernhardt, P. Comba, L. R. Gahan and G. A. Lawrance, *Aust. J. Chem.*, 1990, **43**, 2035.

69. M. Beley, J. P. Collin, R. Ruppert and J. P. Sauvage, *J. Am. Chem. Soc.*, 1986, **108**, 7461.

70. J. P. Collin, A. Jouaiti and J. P. Sauvage, *Inorg. Chem.*, 1998, **27**, 1986.

71. R. W. Hay, J. A. Crayston, T. J. Cromie, P. L. Lightfoot and D. C. L. de Alwis, *Polyhedron*, 1997, **16**, 3557.

72. Y. Ishikawa, Y. Morishita, T. Yamamoto, H. Kurosaki, M. Goto, H. Matsuo and M. Sugiyamg, *Chem. Letters*, 1998, 39.

74 T. J. Cromie, R. W. Hay, P. Lightfoot, D. T. Richens and J. A. Crayston, *Polyhedron*, 2001, **20**, 307.

75 E. J. Billo, Inorg. Chem., 1984, **23**, 2223.

Chapter Two

Padlock Macrocycles

2.1 Introduction

The term "Molecular Padlock" was first used by Thewalt and Weiss in 1966 to describe their synthesis of the polydentate N_2S_2 ligand Scheme 2.1[1].

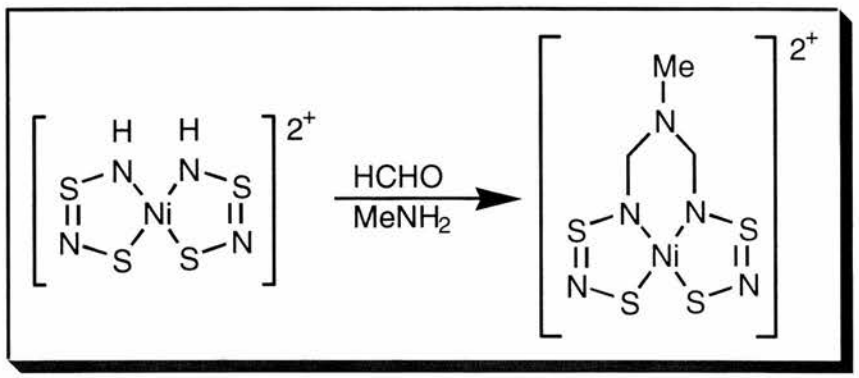

Scheme 2.1

The formaldehyde condenses with the amine to form the imine and then another molecule of amine, in this case methylamine, adds to the imine to lock or cap the structure together. The reaction can be regarded as a special type of Michael addition reaction as the imine bond is quite highly polarised by the metal ion which acts as a Lewis acid. Since then a variety of padlock macrocycles have been prepared in this manner within this group using the methods outlined in Scheme 2.2[2].

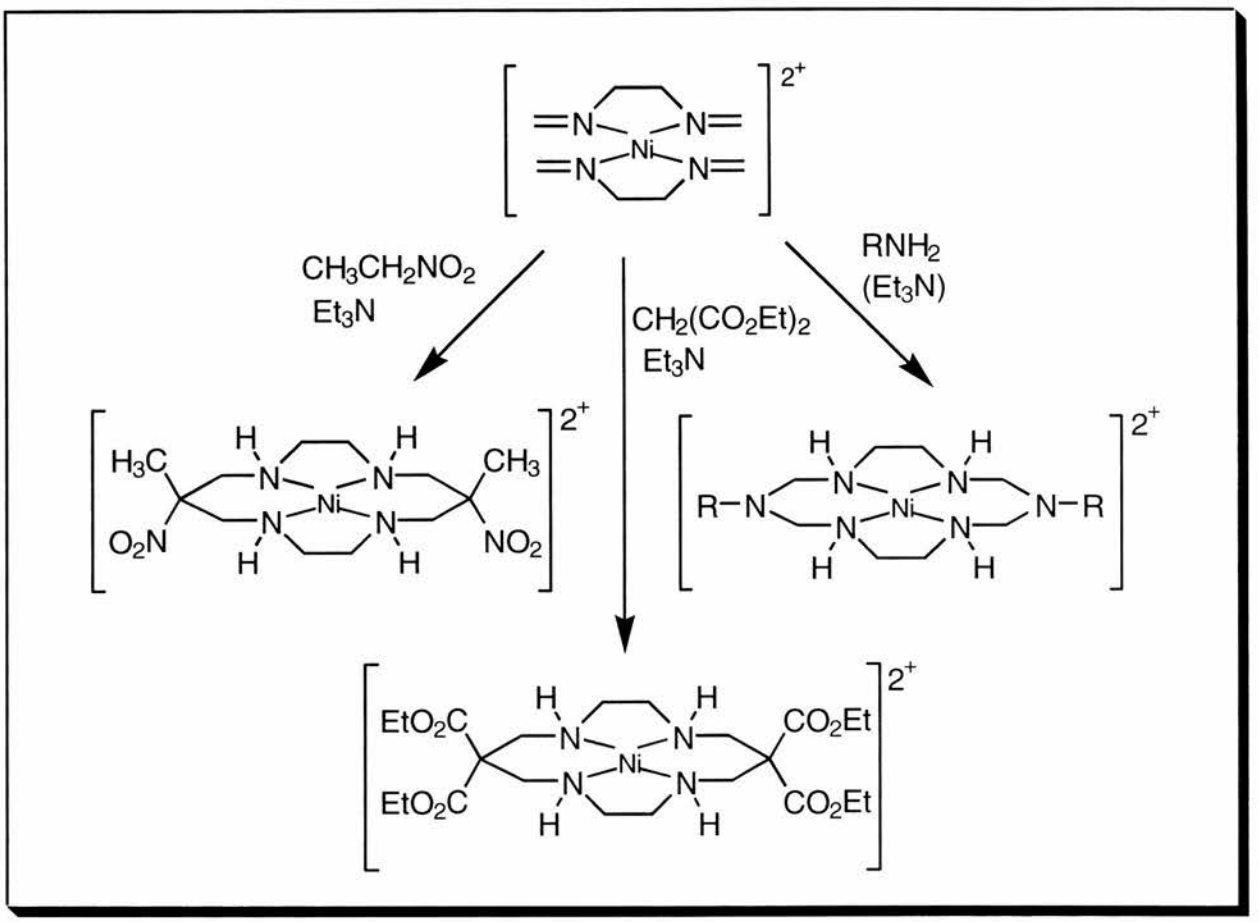

Scheme 2.2: *Examples of padlock macrocycles*

In these examples two molecules of 1,2-diaminoethane co-ordinate the nickel(II) and 4 equivalents of formaldehyde are used to generate the imines[3]. As shown in Scheme 2.2 this locking up of the macrocycles is not exclusive to amines and is just as easily achieved with carbanions. In the cases where amines are used, the presence of base often promotes the formation of the padlock but is not always necessary. In the two carbanion examples, removal of one of the acidic protons is required by base (Et_3N) to generate the reactive carbanion.

When 1,2-diaminoethane is used to co-ordinate the metal the resulting padlock macrocycle can have two pendant arms on either side giving a symmetrical complex with bifunctionality[5-12]. When 1,9-diamino-3,7-diazanonane (2,3,2-tet) is used, (and other aza-amines of this type), as the

co-ordinating ligand prior to reaction with formaldehyde the resultant, padlocked, macrocycle has only one pendant arm (Scheme 2.3)[13].

In this Chapter our attempts to synthesise several of the pentaaza one-pendant arm macrocycles, a hexaaza macrocycle and one with bifunctionality will be described[14-16]. The general synthesis of the padlock macrocycles is relatively simple. A nickel(II) salt, typically nickel(II) chloride hexahydrate, is dissolved in ethanol and the other reagents added with stirring, i.e. the co-ordinating 1,2-diaminoethane or polyaza-amine, capping amine, formaldehyde and base (where required)[14,17]. This mixture is heated for 24 hr, cooled and the product is obtained directly from the reaction mixture by precipitation of the perchlorate salt on adding a saturated solution of sodium perchlorate in ethanol. The products are normally orange crystals typical of square planar nickel(II) complexes having typical λ_{max} values for square planar nickel(II) at ~450 nm.

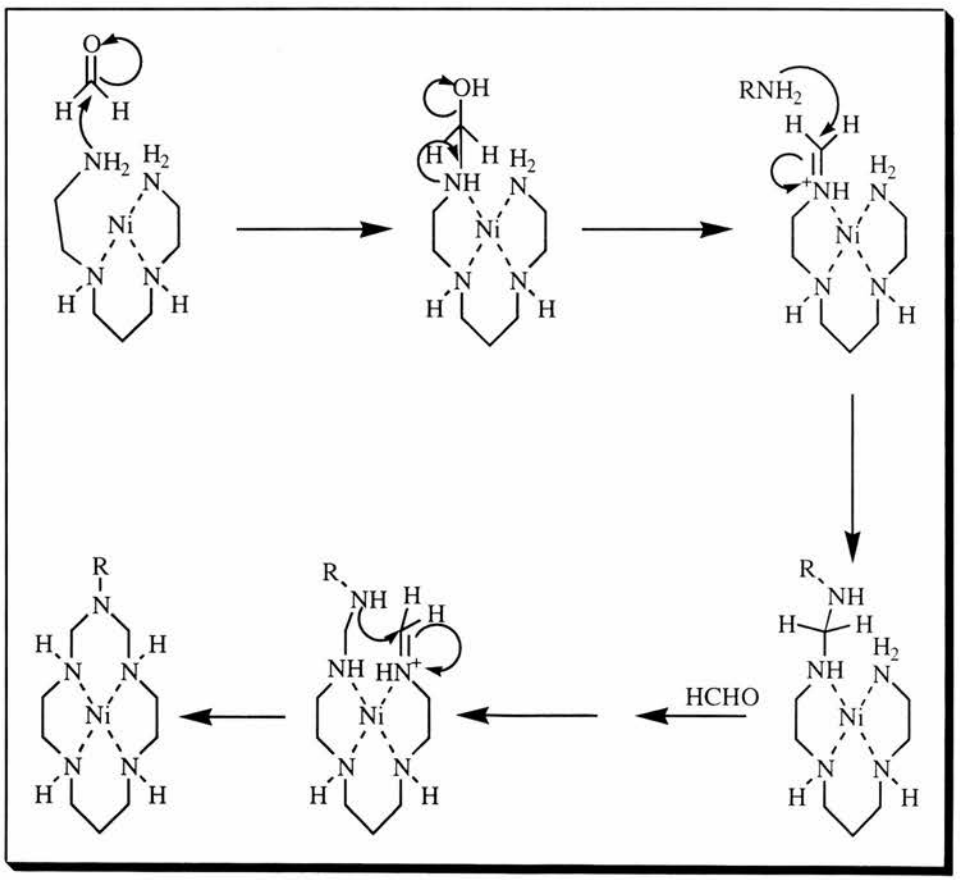

Scheme 2.3: *Mechanistic scheme for the formation of Padlock Macrocycles.*

These one pendant arm macrocycles bear a strong structural resemblance to cyclam, a well studied catalyst for the reduction of carbon dioxide[18-21]. There is considerable interest in the effect of the pendant arm on this catalysis and this will be discussed further in Chapter 3.

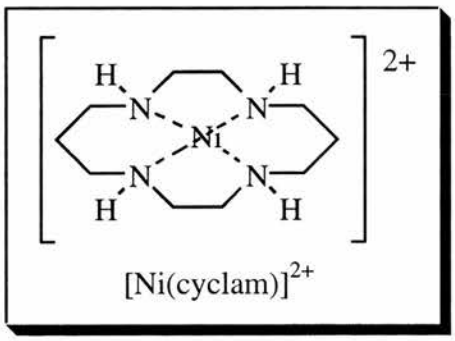

Figure 2.1

2.2 Nickel(II) pentaaza Padlock Macrocyclic Complexes

2.2.1 3-(2-hydroxyethyl)-1,3,5,8,12-penta-azacyclotetradecane)nickel(II) perchlorate; $[Ni(L_1)(ClO_4)_2]$

The reaction of formaldehyde and ethanolamine with the nickel(II) complex of 1,9-diamino-3,7-diazanonane (2,3,2-tet) gives the nickel(II) complex of the macrocycle 3-(2-hydroxyethyl)-1,3,5,8,12-penta-azacyclotetradecane $[NiL_1]^{2+}$ which can be readily isolated as the planar orange perchlorate salt (Figure 2.2)[14]. In nitromethane solution the complex has λ_{max} = 454 nm (ε = 60 $dm^3\ mol^{-1}\ cm^{-1}$) attributable to the $d_{xy} \rightarrow d_x^2\text{-}_y^2$ transition. The N atom carrying the hydroxyethyl group is very weakly basic which probably arises due to the difficulty of protonating a complex carrying a dipositive charge.

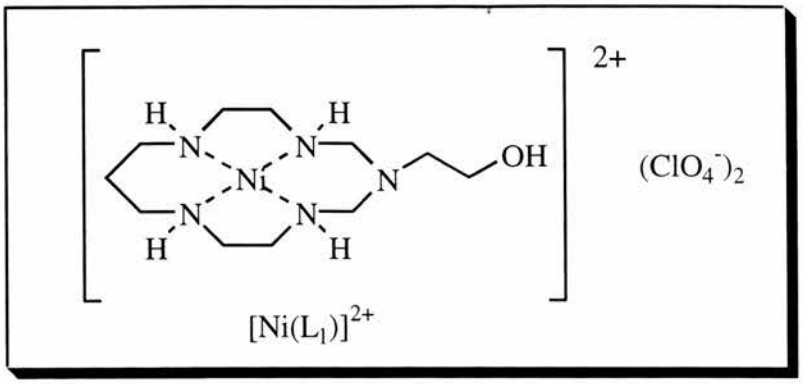

Figure 2.2: *3-(2-hydroxyethyl)-1,3,5,8,12-penta-azacyclotetradecane)nickel(II) perchlorate*

In aqueous solution there is evidence for a square planar ⇌ octahedral equilibrium:

$$[NiL]^{2+} + 2\ H_2O \rightleftharpoons [NiL(OH_2)_2]^{2+}$$

The ^1H NMR in CD_3NO_2 is quite sharp as expected for a diamagnetic planar d^8 complex, Figure 2.4, see experimental section for assignments. Addition of one drop of D_2O to the solution leads to a pronounced paramagnetic line broadening as axial addition gives the paramagnetic octahedral complex whose NMR spectrum is shown in Figure 2.5 overleaf[14]. Addition of concentrated hydrochloric acid to a concentrated aqueous solution of $[Ni(L_1)]^{2+}$ gives the blue-violet dichloro-complex in solution, *trans*-$[Ni(L_1)Cl_2]$ (Figure 2.3). The visible spectrum of the octahedral complex in aqueous solution has λ_{max} at 516 and 672 nm, Figure 2.6.

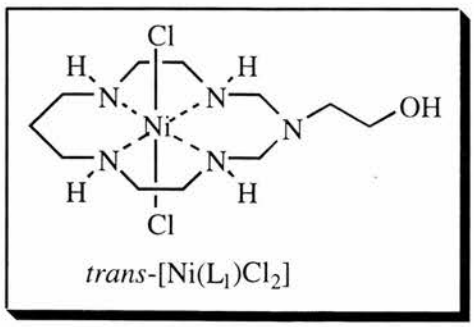

Figure 2.3

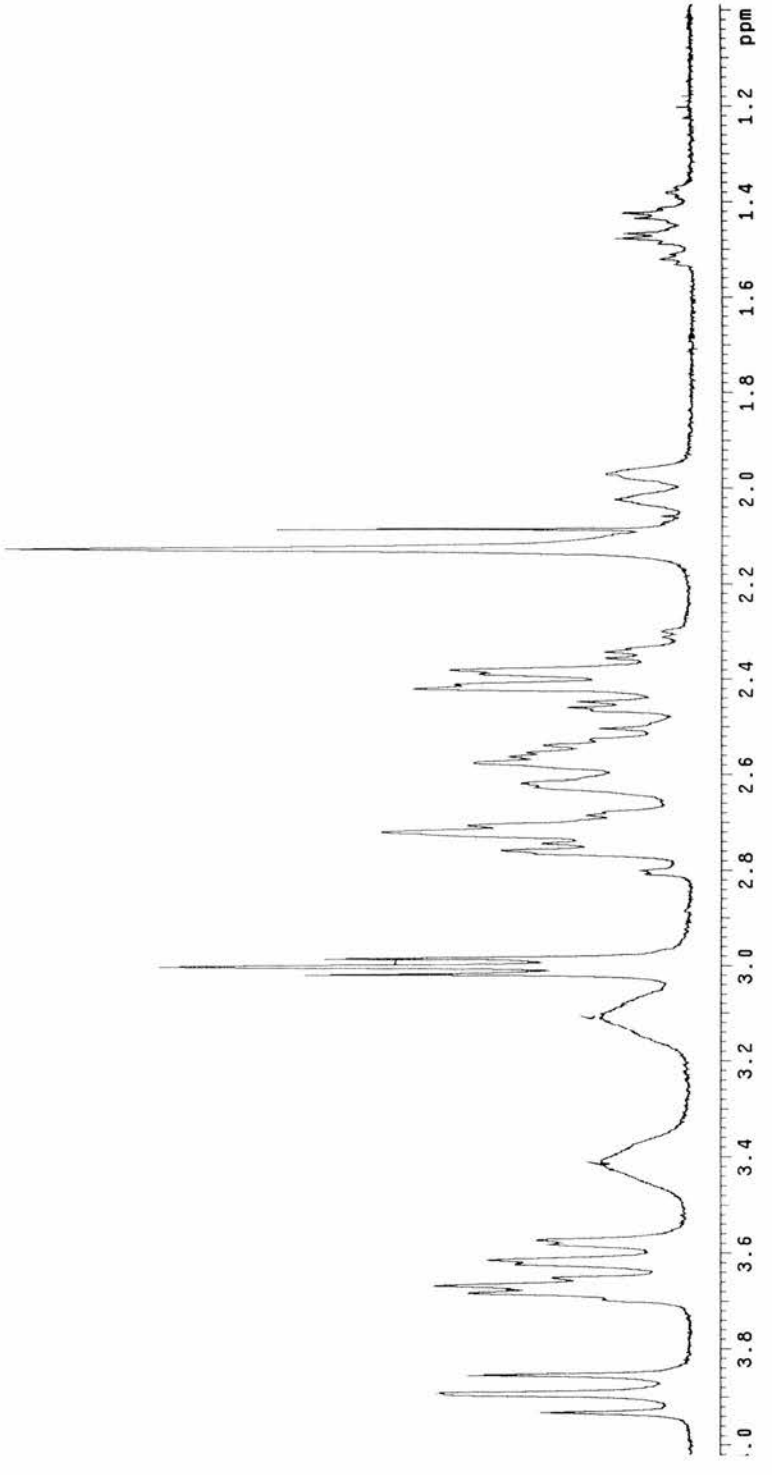

Figure 2.4: *^1H NMR of* trans-*$[Ni(L_1)](ClO_4)_2$ in CD_3NO_2 solution.*

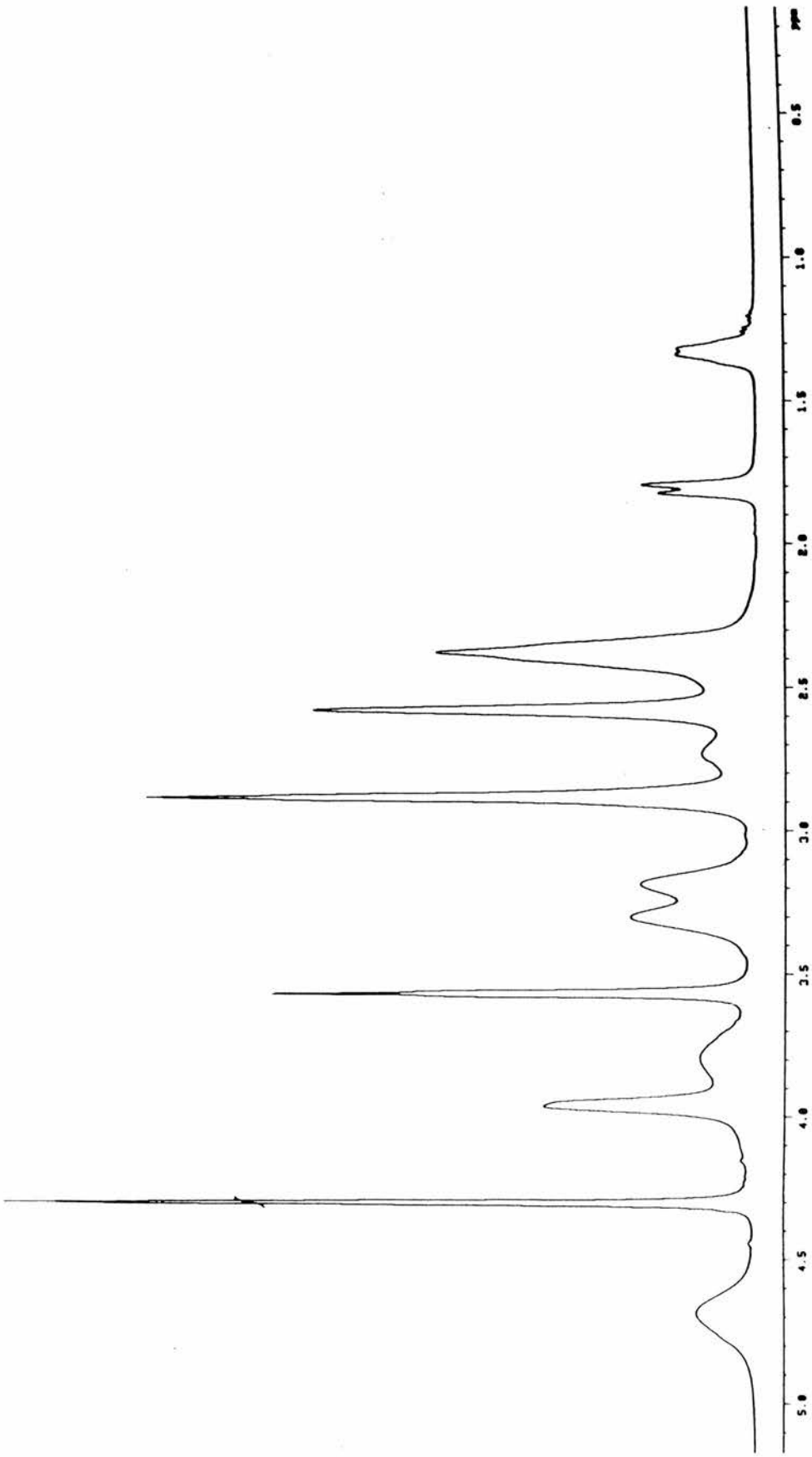

Figure 2.5: *^1H NMR of* trans-*$[Ni(L_1)](ClO_4)_2$ in CD_3NO_2 on addition of one drop of D_2O*

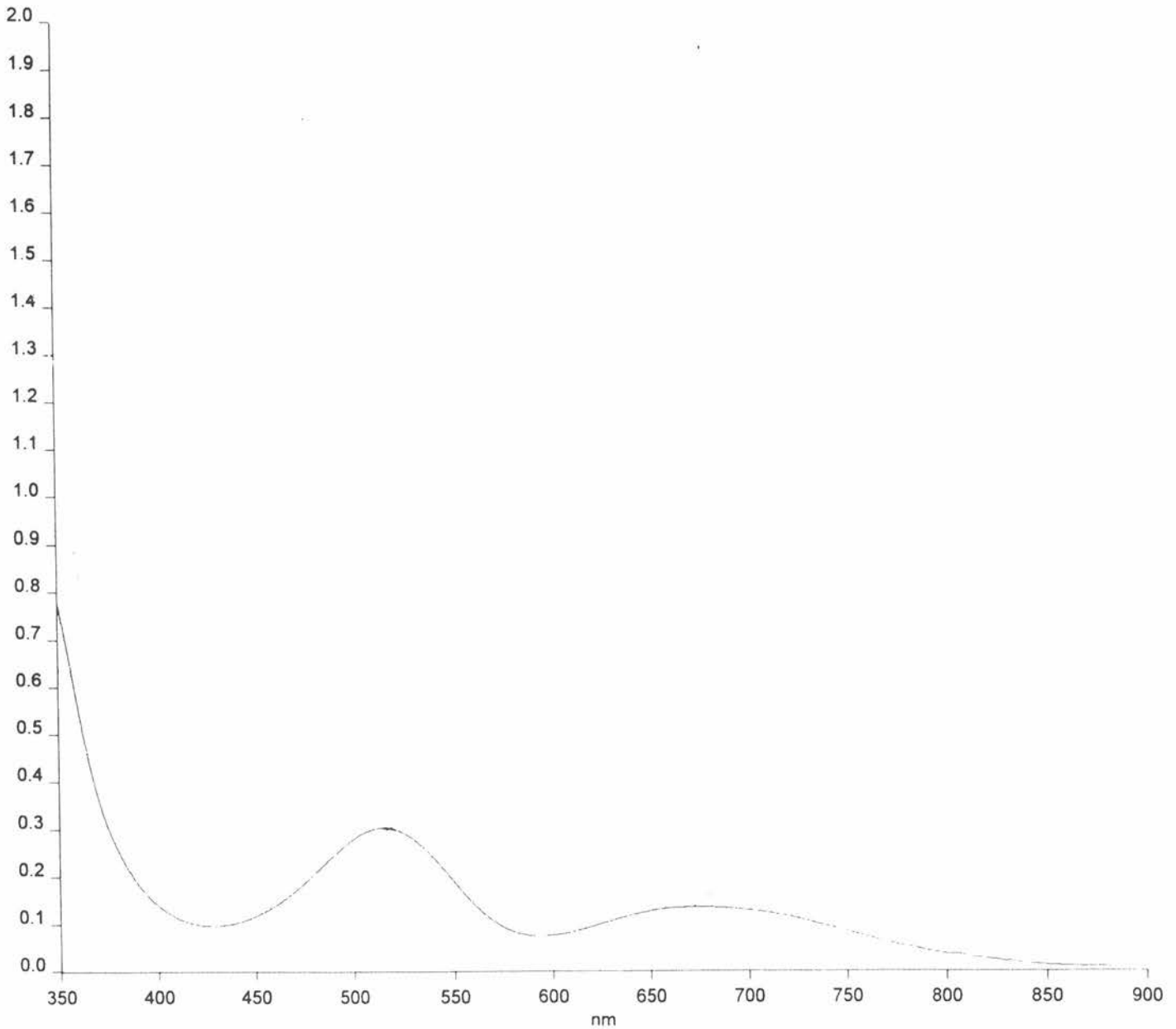

Figure 2.6: *Uv/vis spectrum of* $[Ni(L_1)Cl_2]$ *in water*

Addition of a concentrated aqueous solution of potassium thiocyanate to a concentrated aqueous solution of $[Ni(L_1)]^{2+}$ gives *trans*-$[Ni(L_1)(NCS)_2]$ (Figure 2.6) which precipitates from the aqueous solution and is readily isolated[15]. The visible spectrum was obtained in nitromethane and crystals suitable for X-Ray diffraction studies were also obtained from nitromethane by slow crystallisation. In nitromethane the complex has λ_{max} at 498 (ε = 12.7), 799 (ε = 6.7) and 923 nm (ε = 10.7 dm^3 mol^{-1} cm^{-1}), which are typical values for octahedral nickel(II).

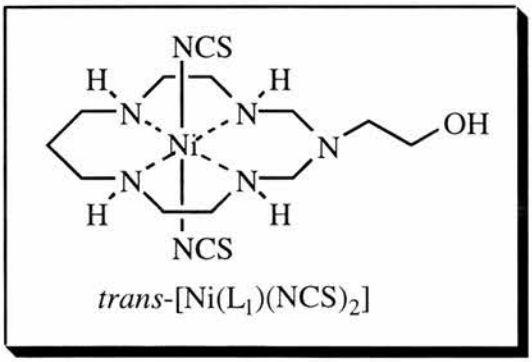

trans-$[Ni(L_1)(NCS)_2]$

Figure 2.7

On addition of a chelating ligand, the macrocycle undergoes an interesting folding reaction into the *cis*-configuration. This can be achieved, for example, by the addition of neat 1,2-diaminoethane to a concentrated aqueous solution of $[Ni(L_1)]^{2+}$ to give the adduct (Figure 2.7) and is characterised by a distinct colour change in the solution from orange (square planar Ni^{2+}) to blue-violet (octahedral Ni^{2+})[23]. The visible spectrum of *cis*-$[Ni(L_1)(en)]^{2+}$ in water has λ_{max} at 535 (ε = 8.8) and 865 nm (ε= 10.4 dm^3 mol^{-1} cm^{-1}) which are attributed to the $^3A_{2g} \rightarrow {}^3T_{1g}$ and $^3A_{2g} \rightarrow {}^3T_{2g}$ transitions respectively. The maximum at 865 nm has evidence of some splitting which indicates a reduction of symmetry away from the regular octahedral geometry at the Ni^{2+} centre. Crystals of this complex suitable for X-Ray diffraction studies were obtained by slow crystallisation from water over several weeks.

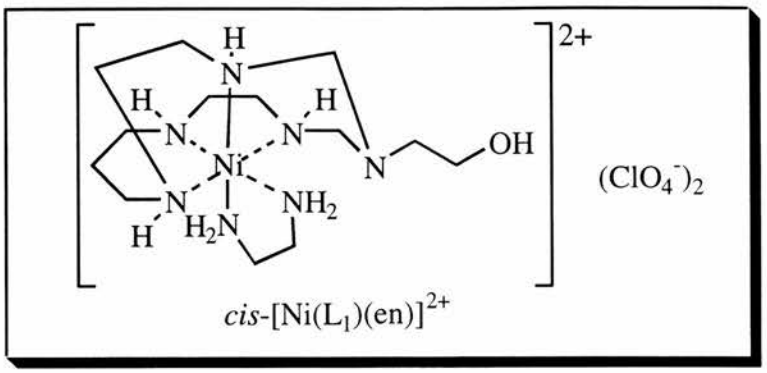

Figure 2.8: *Showing the folding of the macrocycle away from being square planar around the Ni^{2+} centre upon chelating to 1,2-diaminoethane.*

2.2.2 [(3-benzyl-1,3,5,8,12-pentaazacyclotetradecane)nickel(II)] perchlorate

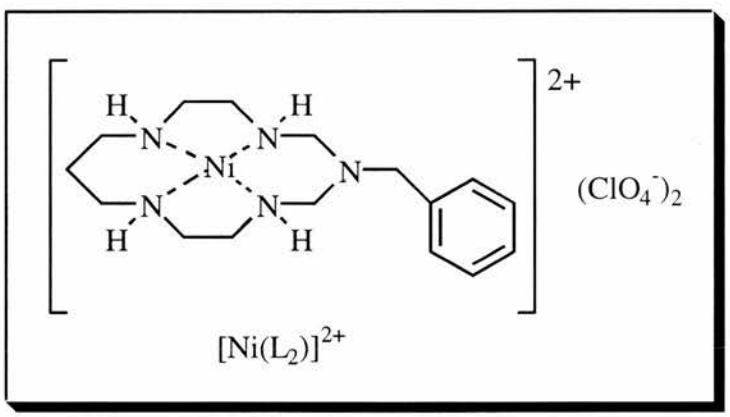

Figure 2.9

This was prepared in an identical manner to the aminopyridine derivative, discussed in section 2.2.5, using aminomethyl benzene as the capping amine. The macrocycle was readily isolated and displayed none of the behaviour of the pyridine derivative on exposure to air (see section 2.2.5).

2.2.4 [((*R,R,S,S*)-1,3,6,8,12,15-hexaazatricyclo[13.3.1.1]eeicosane)nickel(II)] perchlorate

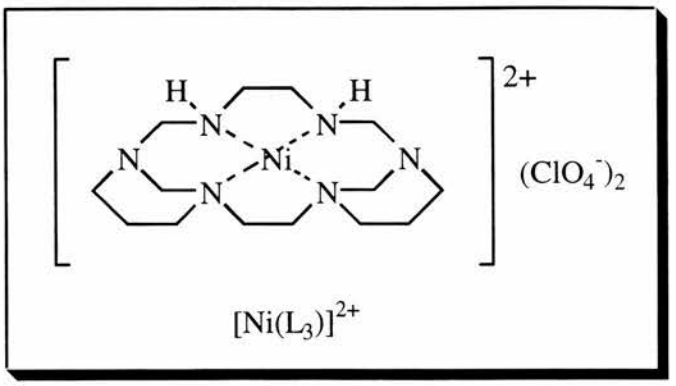

Figure 2.10

The perchlorate salt of this complex was prepared following the procedure reported by M. P. Suh and co-workers resulting in large red block crystals[24]. The reported synthesis described the preparation of the thermodynamically unfavoured *R,S,R,S* isomer and they reported the kinetics of the isomerisation to the thermodynamically favoured *R,R,S,S* isomer. Suh *et al.* described two methods by which they isolated the *R,S,R,S* isomer. Several attempts to isolate this isomer using both of the described routes have failed.

Method 1: Solid $[Ni(L_3)](ClO_4)_2$ was mixed with pulverised $KOH_{(s)}$ and acetonitrile was slowly added. The mixture was stirred for a time, the solution should undergo a colour change from yellow to deep purple. The solution was filtered and distilled water added to the filtrate, the resulting precipitate of $Ni(OH)_2$ was removed by filtration and the filtrate was reduced by half volume. Dark red crystals of *R,S,R,S*-$[Ni(L_3)](ClO_4)_2$ should appear on standing at room temperature.

Method 2: This was an attempt to obtain *R,S,R,S*-$[Ni(L_3)](ClO_4)_2$ directly from the reaction mixture of the template synthesis of the macrocycle. A methanolic solution of $NiCl_2.6H_2O$,

N,N'-bis(3-aminopropyl)ethane-1,2-diamine, paraformaldehyde and 1,2-diaminoethane is refluxed for 3 hours. The solution was filtered whilst hot and allowed to cool. A saturated solution of $NaClO_4$ was added to the filtrate and the solution is allowed to stand in a refrigerator, the orange-red precipitate is filtered. This crude product was then suspended in hot water and a small volume of MeCN is added until all the solid matter dissolves. The solution then stood at room temperature overnight. The resulting orange precipitate of *R,R,S,S*-$[Ni(L_3)](ClO_4)_2$ was filtered and the filtrate stands in the refrigerator until the dark red crystals of the *R,S,R,S* complex form.

In our experiments, however, we were unable to isolate any *R,S,R,S*-$[Ni(L_3)](ClO_4)_2$, instead all the precipitates were exclusively *R,R,S,S*-$[Ni(L_3)](ClO_4)_2$. The orange powder precipitates and large red crystals were both *R,R,S,S*-$[Ni(L_3)](ClO_4)_2$, and the uv/vis spectra showed there to be only *R,R,S,S*-$[Ni(L_3)](ClO_4)_2$ having a λ_{max} 470 nm (ε = 88 dm^3 mol^{-1} cm^{-1}), X-Ray crystallography revealed that the dark red crystals were of the *R,R,S,S* isomer and not of the *R,S,R,S* isomer as reported[24]. We cannot explain, at this time, why we were unable to repeat the reported isomerisation.

2.2.5 [1,1'-Butyl bis(1,3,6,10,13-pentaazacyclotetradecane)]dinickel(II) perchlorate

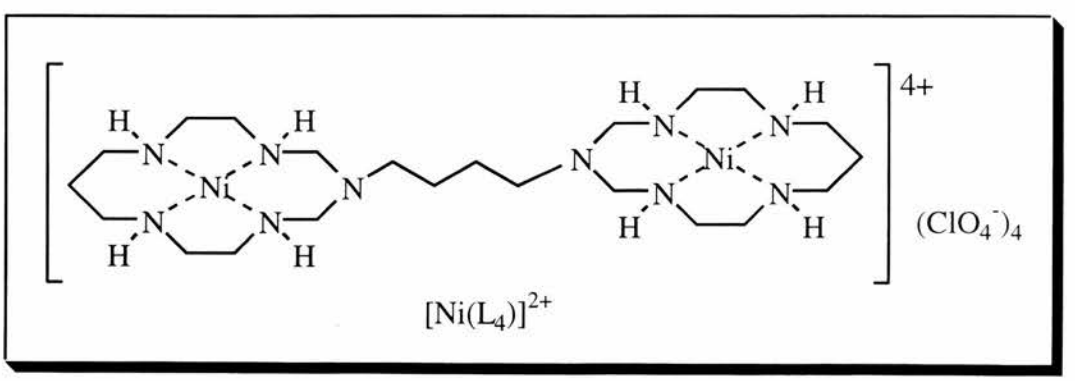

Figure 2.11

This binuclear bis-macrocyclic Nickel(II) complex $[Ni_2(L_4)]^{4+}$ was synthesised in collaboration with Y. D. Lampeka and followed the standard padlocking procedure with two equivalents of 2,3,2-tet to one equivalent of the diamine[16,25]. The yield was low and purification was difficult due to solubility problems. The macrocycle was tested with a range of other padlock macrocycles for catalytic activity in the reduction of CO_2 to CO and the results are discussed in Chapter 3.

2.2.5 The attempted synthesis of other nickel(II) pendant arm macrocycles

The synthesis of several other padlock macrocycles was attempted with limited success. The first of these was the 2-aminomethyl pyridine derivative:

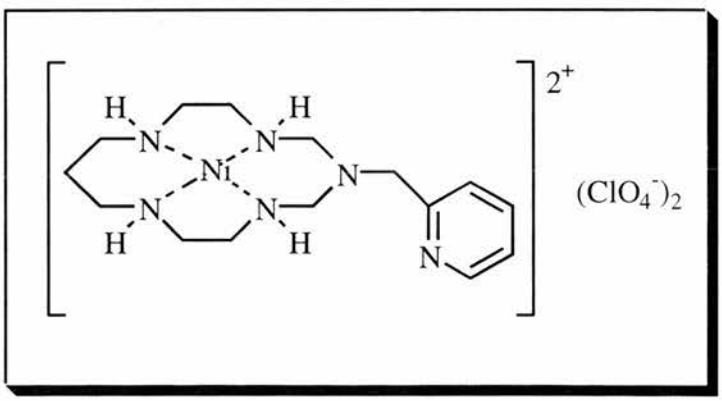

Figure 2.12: *2-aminomethyl pyridine analogue of* $[Ni(L_2)](ClO_4)_2$.

This complex was prepared in a manner identical to that for the hydroxyethyl $[Ni(L_1)]^{2+}$ and benzyl $[Ni(L_2)]^{2+}$ derivatives but here used 2-aminomethyl pyridine as the padlock nucleophile. On addition of the saturated solution of sodium perchlorate in ethanol an orange precipitate was initially formed which was assumed to be the perchlorate salt of the required complex. However, on filtration the orange material degraded to a black tar on contact with the atmosphere and

seemed exceptionally hygroscopic. This product has so far proved very difficult to isolate and purify. Successful synthesis of the corresponding benzyl analogue $[Ni(L_2)]^{2+}$ (2.2.2) indicates that the problems are associated with the presence of the nitrogen atom in the aromatic ring.

The synthesis of another padlock macrocycle with two pendant arms deriving from ethyl acetoacetate was attempted using the bis(1,2-diaminoethane)nickel(II) complex see Scheme 2.2. Here the addition of base is required to generate the carbanion of ethyl acetoacetate[26].

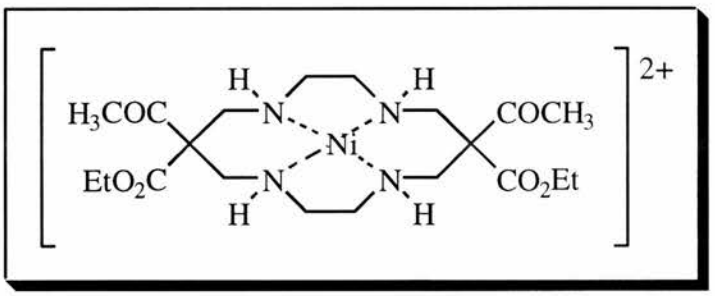

Figure 2.13: *Bifunctional two-pendant arm complex of ethyl acetoacetate.*

The interesting feature of this derivative is that after base hydrolysis of the ethyl ester the two carboxylic acids should spontaneously (or with heating) decompose to give off carbon dioxide (see Chapter 1, p. 20). This would leave a macrocycle with two acyl functionalities on either side. Attempts to isolate this complex proved difficult and crystallisation from concentrated perchloric acid was unsuccessful.

The synthesis of a sixteen membered pentaaza padlock macrocycle was also attempted from the precursor 3,3,3-tet (1,11-diamino-4,8-diazaundecane). This starting ligand chelates the nickel(II) ion centre in the same manner as 2,3,2-tet but forms three six membered rings around the metal centre whereas 2,3,2-tet chelates such that one six membered ring and two five membered rings

are formed. When the ligand complex is capped the metal ion will be surrounded by four six membered rings, Figure 2.14.

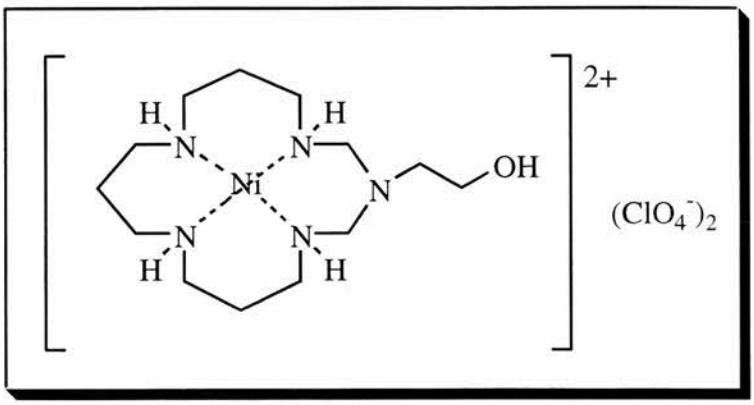

Figure 2.14: *3-(2-hydroxyethyl)-1,3,5,9,13-penta-azacyclohexadecane)nickel(II) perchlorate.*

The synthesis of this macrocycle followed the previous syntheses and used ethanolamine as the capping amine. After 24 hr of reflux the reaction mixture was reduced to half volume under reduced pressure and cooled in an ice bath. After a saturated solution of sodium perchlorate was added, there was no immediate precipitation but on leaving in the fridge for several days a gelatinous blue precipitate appeared which may be the octahedral diaqua complex. This is perhaps not an unsurprising result since with four six-membered chelate rings the ligand field is significantly weaker and, therefore, octahedral diaqua complexes might be expected to form more extensively.

2.3 Crystal Structure Determinations using X-ray Diffraction

2.3.1 Crystal Structure Determination of 3-(2-hydroxyethyl)-1,3,5,8,12-pentaazacyclotetradecane)nickel(II) perchlorate

Suitable crystals for X-Ray diffraction studies were obtained by slow crystallisation of the perchlorate salt from aqueous/ ethanol solution. The ORTEP view of the molecule with the ring numbering system is shown in Figure 2.14. The nickel atom is in a planar environment with N_2, N_5, N_8 and N_{12} acting as donor atoms with the Ni-N bond distances in the range 1.930 to 1.938 Å which is quite normal for low spin planar nickel(II) complexes. The hydroxyethyl side arm on N_1 does not interact with the central nickel. The ligand has a *trans* III configuration of the *sec*-NH centres which is the most thermodynamically favoured configuration of the 1,4,8,11-tetra-azacyclotetradecane (cyclam) ring system leading to chair six-membered rings and gauche five-membered rings. The hydroxyethyl substituent on N_1 is axial and a similar stereochemistry has been observed in the N-Me and N-Et derivatives with nickel(II). The elipsoids of the pendant hydroxyl group are large and indicate a certain amount of movement within the lattice. The two perchlorate anions lie in the axial sites with Ni-O bond distances of 2.836(3) and 3.028(3) Å indicating that there is no interaction between O_4 and O_7 and the central nickel atom in the solid state. Summaries of the atomic coordinates, bond distance and bond angles are given in Tables 2.1 to 2.3.

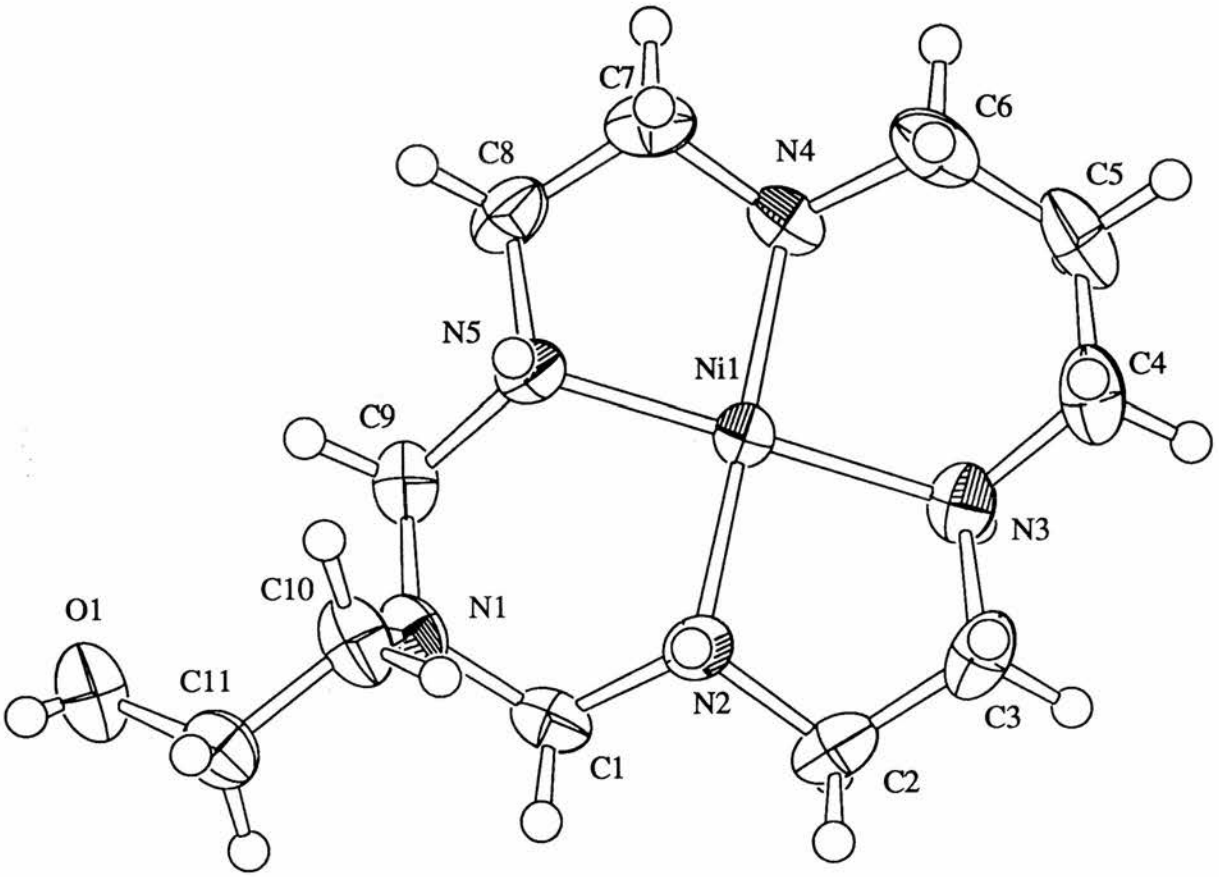

Figure 2.15: *ORTEP of* $[Ni(L_1)](ClO_4)_2$

2.3.1.1 Data Collection

An orange block crystal of $C_{11}H_{27}N_5O_9Cl_2Ni$ having approximate dimensions of 0.40 x 0.20 x 0.15 mm was mounted on a glass fibre. All measurements were made on a Rigaku AFC7S diffractometer with graphite monochromated Mo-Kα radiation.

Cell constants and an orientation matrix for data collection, obtained from a least-squares refinement using the setting angles of 25 carefully centred reflections in the range $24.13 < 2\theta < 24.93°$ corresponded to a primitive monoclinic cell with dimensions:

$a = 9.598(4)\text{Å}$

$b = 13.688(3)\text{Å}$ $\beta = 94.60(2)°$

$c = 14.830(3)\text{Å}$

$V = 1942.1(9)\text{Å}^3$

For Z = 4 and F.W. = 502.97, the calculated density is 1.72 g/cm^3. The systematic absences of:

$h0l: h+l \neq 2n$

$0k0: k \neq 2n$

uniquely determine the space group to be:

$\{P\ 2_1/n\ (\#14)\}$

The data were collected at a temperature of 20 ± 1 °C using the ω-2θ scan technique to a maximum 2 theta value of 50.0°.Omega scans of several intense reflections, made prior to data collection, had an average width at half-height of 0.29° with a take-off angle of 6.0°. Scans of (1.26 + 0.35 tan θ)° were made at a speed of 16.0° /min (in omega). The weak reflections ($I < 15.0\sigma(I)$) were rescanned (maximum of 4 scans) and the counts were accumulated to ensure good counting statistics. Stationary background counts were recorded on each side of the reflection. The ratio of peak counting time to background counting time was 2:1. The diameter of the incident beam collimator was 1.0 mm and the crystal to detector distance was 235 mm, The computer-controlled slits were set to 9.0 mm (horizontal) and 13.0 mm (vertical).

2.3.1.2 Data Reduction

Of the 3802 reflections which were collected, 3578 were unique ($R_{int} = 0.037$). The intensities of three representative reflection were measured after every 150 reflections. No decay correction was applied.

The linear absorption coefficient, μ, for Mo-Kα radiation is 13.3 cm^{-1}. An empirical absorption correction based on azimuthal scans of several reflections was applied which resulted in *trans*mission factors ranging from 0.82 to 1.00. The data were corrected for Lorentz and polarization effects.

2.3.1.3 Structure Solution and Refinement

The structure was solved by direct methods[27] and expanded using Fourier techniques[28]. The non-hydrogen atoms were refined anisotropically. Some hydrogen atoms were refined isotropically, the rest were included in fixed positions. The final cycle of full-matrix least-squares refinement[29]

was based on 2824 observed reflections ($I > 3.00\sigma(I)$) and 257 variable parameters and converged (largest parameter shift was 0.05 times its esd) with unweighted and weighted agreement factors of:

$$R = \Sigma \, ||Fo| - |Fc|| \, / \, \Sigma \, |Fo| = 0.037$$

$$R_w = \sqrt{(\Sigma w \, (|Fo| - |Fc|)^2 \, / \, \Sigma w \, Fo^2)} = 0.033$$

The standard deviation of an observation of unit weight[30] was 2.88. The weighting scheme was based on counting statistics. Plots of $\Sigma w \, (|Fo| - |Fc|)^2$ versus $|Fo|$, reflection order in data collection, $\sin\theta/\lambda$ and various classes of indices showed no unusual trends. The maximum and minimum peaks on the final difference Fourier map corresponded to 0.53 and -0.40 $e^-/ Å^3$, respectively.

Neutral atom scattering factors were taken from Cromer and Waber[31]. Anomalous dispersion effects were included in Fcalc[32]; the values for $\Delta f'$ and $\Delta f''$ were those of Creagh and McAuley[33]. The values for the mass attenuation coefficients are those of Creagh and Hubbel[34]. All calculations were performed using the teXsan[35] crystallographic software package of Molecular Structure Corporation.

Table 2.1 Atomic coordinates

atom	x	y	z
Ni(1)	0.04917(5)	0.21811(3)	0.34418(3)
Cl(1)	0.0226(1)	0.31746(7)	0.07717(6)
Cl(2)	0.0956(1)	0.29816(8)	0.61086(7)
O(1)	0.4694(4)	0.5520(3)	0.3743(2)
N(1)	0.2342(3)	0.4230(2)	0.3394(2)

N(2)	0.0042(3)	0.3538(2)	0.3638(2)
N(3)	-0.1502(3)	0.1934(2)	0.3348(2)
C(1)	0.0868(4)	0.4304(3)	0.3187(2)
C(2)	-0.1484(4)	0.3682(3)	0.3393(3)
C(3)	-0.2201(4)	0.2794(3)	0.3724(3)
C(4)	-0.2044(4)	0.1015(4)	0.3743(3)
C(5)	-0.1366(5)	0.0121(3)	0.3381(3)
C(10)	0.2889(4)	0.4567(3)	0.4299(3)
C(11)	0.3529(4)	0.5560(3)	0.4275(3)

Table 2.2 Bond Lengths(Å)

atom	atom	distance	atom	atom	distance
Ni(1)	N(2)	1.934(3)	Ni(1)	N(3)	1.938(3)
Ni(1)	N(4)	1.937(3)	Ni(1)	N(5)	1.930(3)
O(1)	C(11)	1.422(5)	N(1)	C(1)	1.427(5)
N(1)	C(9)	1.426(5)	N(1)	C(10)	1.475(4)
N(2)	C(1)	1.503(4)	N(2)	C(2)	1.494(4)
N(3)	C(3)	1.486(5)	N(3)	C(4)	1.498(5)
N(4)	C(6)	1.470(5)	N(4)	C(7)	1.488(5)
N(5)	C(8)	1.498(4)	N(5)	C(9)	1.503(4)
C(2)	C(3)	1.498(6)	C(4)	C(5)	1.505(6)
C(5)	C(6)	1.509(6)	C(7)	C(8)	1.485(6)
C(10)	C(11)	1.492(5)			

Table 2.3 Bond Angles(°)

atom	atom	atom	angle	atom	atom	atom	angle
N(2)	Ni(1)	N(3)	87.0(1)	N(2)	Ni(1)	N(4)	178.5(1)
N(2)	Ni(1)	N(5)	92.1(1)	N(3)	Ni(1)	N(4)	94.2(1)
N(3)	Ni(1)	N(5)	179.1(1)	N(4)	Ni(1)	N(5)	86.7(1)
C(1)	N(1)	C(9)	114.5(3)	C(1)	N(1)	C(10)	116.6(3)
C(9)	N(1)	C(10)	115.9(3)	Ni(1)	N(2)	C(1)	118.1(2)
Ni(1)	N(2)	C(2)	108.4(2)	C(1)	N(2)	C(2)	110.0(3)

Ni(1)	N(3)	C(3)	107.9(2)	Ni(1)	N(3)	C(4)	119.4(3)
C(3)	N(3)	C(4)	109.7(3)	Ni(1)	N(4)	C(6)	119.1(2)
Ni(1)	N(4)	C(7)	107.7(2)	C(6)	N(4)	C(7)	110.1(3)
Ni(1)	N(5)	C(8)	108.5(2)	Ni(1)	N(5)	C(9)	117.5(2)
C(8)	N(5)	C(9)	110.0(3)	N(1)	C(1)	N(2)	113.8(3)
N(2)	C(2)	C(3)	106.3(3)	N(3)	C(3)	C(2)	106.7(3)
N(3)	C(4)	C(5)	111.7(3)	C(4)	C(5)	C(6)	112.6(4)
N(4)	C(6)	C(5)	112.2(3)	N(4)	C(7)	C(8)	106.6(3)
N(5)	C(8)	C(7)	105.7(3)	N(1)	C(9)	N(5)	113.3(3)
N(1)	C(10)	C(11)	112.4(3)	O(1)	C(11)	C(10)	108.7(4)

2.3.2 Crystal Structure Determination of $[Ni(L_1)(NCS)_2]$ (L_1 = 3-hydroxyethyl-1,3,5,8,12-pentaazacyclotetradecane).

Two ORTEP views of the complex *trans*-$[Ni(L_1)(NCS)_2]$ are shown in Figure 2.15 and these confirm the *trans* stereochemistry of the complex with N-bonded thiocyanate in the axial sites and the Ni-NCS bond distances of 2.106 and 2.145 Å. The equatorial sites on nickel are occupied by N_1, N_2, N_4 and N_5 with Ni-N bond distances of 2.053 to 2.076 Å, which are typical for octahedral Ni(II) azamacrocyclic complexes with a triplet ground state. Atomic coordinates, bond distances and bond angles are given in Tables 2.4 to 2.6 The ligand has the thermodynamically stable *trans* III configuration of the sec-NH centres, leading to chair six-membered chelate rings and gauche five-membered rings. The hydroxyethyl group on N_3 is axial. A similar configuration has been observed in the perchlorate salts of the NMe and NEt azacyclams and is also found in $[Ni(L_1)](ClO_4)_2$ see Section 2.3.1. There is no evidence for hydrogen bonding interactions involving the hydroxyethyl group in the crystal lattice.

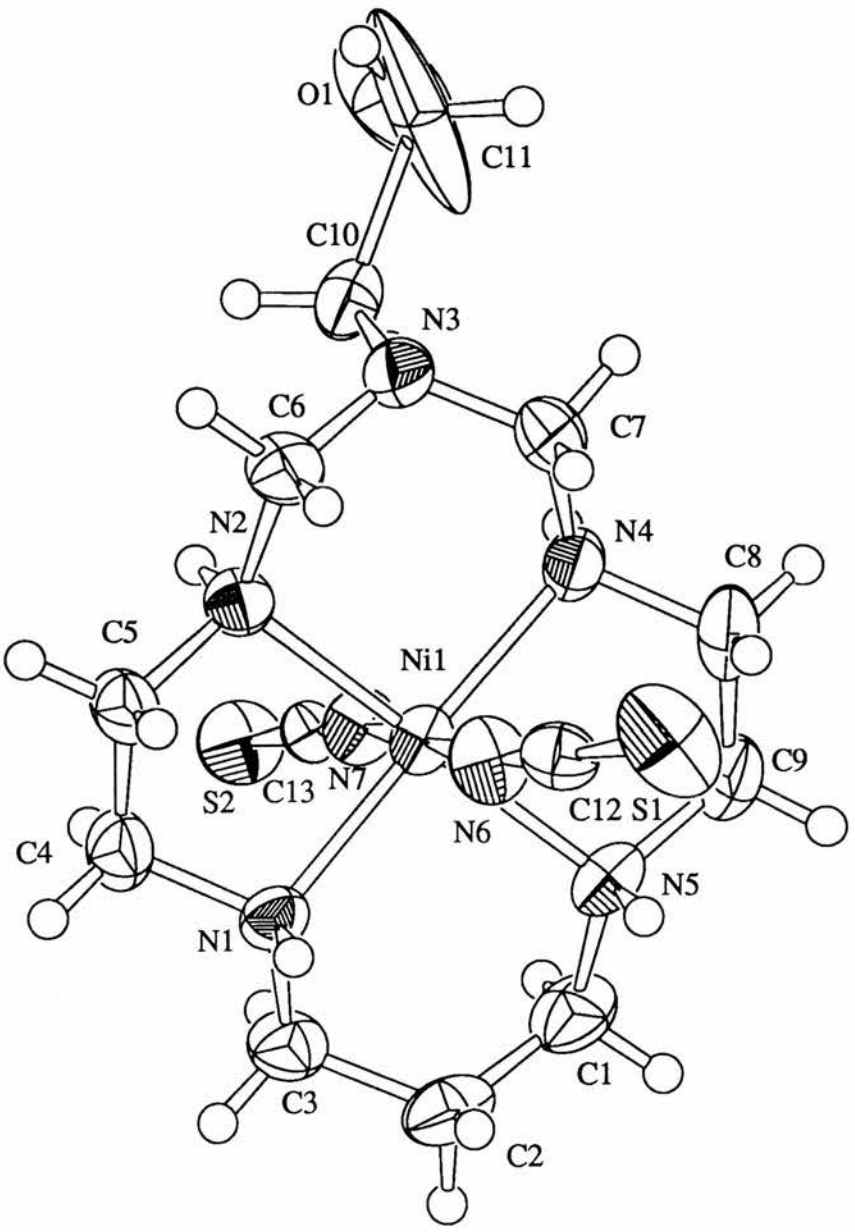

Figure 2.16: *ORTEP of trans-[Ni(L_1)($NCS)_2$]($ClO_4)_2$.*

2.3.2.1 Data Collection

A purple block crystal of $C_{13}H_{27}N_7ONiS_2$ having approximate dimensions of 0.50 x 0.40 x 0.35 mm was mounted on a glass fibre. All measurements were made on a Rigaku AFC7S diffractometer with graphite monochromated Mo-Kα radiation.

Cell constants and an orientation matrix for data collection, obtained from a least-squares refinement using the setting angles of 20 carefully centred reflections in the range $10.39 < 2\theta < 13.65°$ corresponded to a primitive monoclinic cell with dimensions:

$a = 7.934(4)Å$

$b = 29.067(5)Å \qquad \beta = 108.81(3)°$

$c = 8.583(4)Å$

$V = 1873(1)Å^3$

For Z = 4 and F.W. = 420.22, the calculated density is 1.49 g/cm^3. The systematic absences of:

$h0l: h \neq 2n$

$0k0: k \neq 2n$

uniquely determine the space group to be:

$\{P\ 2_1/a\ (\#14)\}$

The data were collected at a temperature of 20 ± 1 °C using the ω-2θ scan technique to a maximum 2θ value of 50.1°.Omega scans of several intense reflections, made prior to data collection, had an average width at half-height of 0.28° with a take-off angle of 6.0°. Scans of (0.79 + 0.35 tan θ)° were made at a speed of 16.0° /min (in omega). The weak reflections ($I < 15.0\sigma(I)$) were rescanned (maximum of 4 scans) and the counts were accumulated to ensure good counting statistics. Stationary background counts were recorded on each side of the reflection. The ratio of peak counting time to background counting time was 2:1. The diameter of the incident beam collimator was 1.0 mm and the crystal to detector distance was 235 mm, The computer-controlled slits were set to 9.0 mm (horizontal) and 13.0 mm (vertical).

2.3.2.2 Data Reduction

Of the 3645 reflections which were collected, 3396 were unique ($R_{int} = 0.110$). The intensities of three representative reflection were measured after every 150 reflections. No decay correction was applied.

The linear absorption coefficient, μ, for Mo-Kα radiation is 12.7 cm^{-1}. An empirical absorption correction based on azimuthal scans of several reflections was applied which resulted in *trans*mission factors ranging from 0.32 to 1.00. The data were corrected for Lorentz and polarization effects. A correction for secondary extinction was applied (coefficient = 2.77188e-07).

2.3.2.3 Structure Solution and Refinement

The structure was solved by direct methods[27] and expanded using Fourier techniques[28]. The non-hydrogen atoms were refined anisotropically. Some hydrogen atoms were refined isotropically, the rest were included in fixed positions. The final cycle of full-matrix least-squares refinement[29] was based on 2681 observed reflections ($I > 3.00\sigma(I)$) and 218 variable parameters and converged (largest parameter shift was 0.35 times its esd) with unweighted and weighted agreement factors of:

$$R = \Sigma \, ||Fo| - |Fc|| \, / \, \Sigma \, |Fo| = 0.079$$

$$R_w = \sqrt{(\Sigma w \, (|Fo| - |Fc|)^2 \, / \, \Sigma w \, Fo^2)} = 0.086$$

The standard deviation of an observation of unit weight[30] was 5.36. The weighting scheme was based on counting statistics. Plots of $\Sigma w \, (|Fo| - |Fc|)^2$ versus $|Fo|$, reflection order in data collection, $\sin\theta/\lambda$ and various classes of indices showed no unusual trends. The maximum and minimum peaks on the final difference Fourier map corresponded to 1.72 and -1.48 $e^-/ Å^3$, respectively.

Neutral atom scattering factors were taken from Cromer and Waber[31]. Anomalous dispersion effects were included in Fcalc[32]; the values for $\Delta f'$ and $\Delta f''$ were those of Creagh and McAuley[33]. The values for the mass attenuation coefficients are those of Creagh and Hubbel[34]. All calculations were performed using the teXsan[35] crystallographic software package of Molecular Structure Corporation.

Table 2.4 Atomic coordinates

Atom	x	y	z
Ni(1)	0.1971(1)	0.11825(3)	0.9743(1)
S(1)	0.4168(4)	0.0031(1)	0.6795(3)
S(2)	-0.0983(3)	0.23027(8)	1.2188(3)
O(1)	0.210(1)	0.2954(5)	0.634(1)
N(1)	0.2985(8)	0.0913(2)	1.2071(8)
N(2)	0.4187(8)	0.1606(2)	1.0420(8)
N(3)	0.3724(9)	0.1861(2)	0.7570(8)
N(4)	0.0981(9)	0.1431(2)	0.7378(8)
N(5)	-0.0203(9)	0.0742(2)	0.9030(8)
N(6)	0.3353(10)	0.0652(3)	0.8905(9)
N(7)	0.0555(9)	0.1687(2)	1.0572(8)
C(1)	-0.105(1)	0.0656(3)	1.031(1)
C(2)	0.025(1)	0.0477(3)	1.189(1)
C(3)	0.165(1)	0.0811(3)	1.291(1)
C(4)	0.436(1)	0.1241(3)	1.300(1)
C(5)	0.544(1)	0.1383(3)	1.1932(10)
C(6)	0.495(1)	0.1673(3)	0.905(1)
C(7)	0.239(1)	0.1549(3)	0.6614(10)
C(8)	-0.028(1)	0.1079(3)	0.643(1)
C(9)	-0.140(1)	0.0926(3)	0.745(1)
C(10)	0.309(1)	0.2329(3)	0.779(1)
C(11)	0.306(3)	0.2639(5)	0.601(2)
C(12)	0.371(1)	0.0390(3)	0.809(1)
C(13)	-0.0058(10)	0.1941(3)	1.1234(9)

Table 2.5 Bond Lengths(Å)

atom	atom	distance	atom	atom	distance
Ni(1)	N(1)	2.053(6)	Ni(1)	N(2)	2.069(7)
Ni(1)	N(4)	2.056(7)	Ni(1)	N(5)	2.076(6)
Ni(1)	N(6)	2.145(7)	Ni(1)	N(7)	2.106(7)

S(1)	C(12)	1.643(9)	S(2)	C(13)	1.644(8)
O(1)	C(11)	1.28(2)	N(1)	C(3)	1.492(10)
N(1)	C(4)	1.474(10)	N(2)	C(5)	1.503(10)
N(2)	C(6)	1.502(9)	N(3)	C(6)	1.43(1)
N(3)	C(7)	1.44(1)	N(3)	C(10)	1.48(1)
N(4)	C(7)	1.51(1)	N(4)	C(8)	1.48(1)
N(5)	C(1)	1.48(1)	N(5)	C(9)	1.48(1)
N(6)	C(12)	1.136(10)	N(7)	C(13)	1.133(9)
C(1)	C(2)	1.51(1)	C(2)	C(3)	1.52(1)
C(4)	C(5)	1.50(1)	C(8)	C(9)	1.50(1)
C(10)	C(11)	1.76(2)			

Table 2.6 Bond Angles(°)

atom	atom	atom	angle	atom	atom	atom	angle
N(1)	Ni(1)	N(2)	85.6(2)	N(1)	Ni(1)	N(4)	177.9(3)
N(1)	Ni(1)	N(5)	94.6(3)	N(1)	Ni(1)	N(6)	88.3(3)
N(1)	Ni(1)	N(7)	91.2(3)	N(2)	Ni(1)	N(4)	95.1(3)
N(2)	Ni(1)	N(5)	178.0(3)	N(2)	Ni(1)	N(6)	92.4(3)
N(2)	Ni(1)	N(7)	89.3(3)	N(4)	Ni(1)	N(5)	84.7(3)
N(4)	Ni(1)	N(6)	89.7(3)	N(4)	Ni(1)	N(7)	90.8(3)
N(5)	Ni(1)	N(6)	85.6(3)	N(5)	Ni(1)	N(7)	92.6(3)
N(6)	Ni(1)	N(7)	178.2(3)	Ni(1)	N(1)	C(3)	115.5(5)
Ni(1)	N(1)	C(4)	105.6(5)	C(3)	N(1)	C(4)	112.6(7)
Ni(1)	N(2)	C(5)	104.6(5)	Ni(1)	N(2)	C(6)	112.2(5)
C(5)	N(2)	C(6)	114.3(6)	C(6)	N(3)	C(7)	115.5(7)
C(6)	N(3)	C(10)	113.5(7)	C(7)	N(3)	C(10)	115.8(7)
Ni(1)	N(6)	C(12)	161.6(7)	Ni(1)	N(7)	C(13)	170.3(7)
N(5)	C(1)	C(2)	112.4(7)	C(1)	C(2)	C(3)	117.3(8)
N(1)	C(3)	C(2)	110.2(7)	N(1)	C(4)	C(5)	108.6(7)
N(2)	C(5)	C(4)	107.3(7)	N(2)	C(6)	N(3)	114.4(7)
N(3)	C(10)	C(11)	105.8(7)	O(1)	C(11)	C(10)	91(1)
S(1)	C(12)	N(6)	176.2(8)	S(2)	C(13)	N(7)	178.8(7)

2.3.3 Crystal Structure Determination of [(1,3,6,8,12,15-hexaazatricyclo[13.3.1.1]eicosane)nickel(II)] perchlorate.

The ORTEP view of the cation for (R,R,S,S)-$[Ni(L_3)](ClO_4)_2$ is shown in Figure 2.16 and is looking down the axial axis of the complex. Tables 2.7 to 2.9 summarise the atomic coordinates, bond distances and bond angles. The nickel atom is in a planar environment, with slight distortions, with N_1, N_2, N_4 and N_5 acting as donors , N1 and N2 are both secondary nitrogen donors and N_4 and N_5 are both tertiary nitrogen donors, with Ni-N bond distances in the range 1.940(3) and 1.971(3) Å. The Ni-N bond lengths involving the tertiary nitrogen donors are significantly longer than those involving the secondary nitrogen donors, Ni-N_4 at 1.971 and Ni-N_1 at 1.940 Å. The average Ni-N bond distance of (*R,R,S,S*)-$[Ni(L_3)](ClO_4)_2$ is 1.954 Å compared to 1.935 Å for $[Ni(L_1)](ClO_4)_2$ where all the nitrogen donors are secondary amines. In general, tertiary nitrogens do not bind nickel(II) as strongly as secondary nitrogens, therefore, the corresponding Ni-N bonds are often longer. The ligand has a trans III configuration leading to chair six-membered rings and gauche five-membered rings. The bite angles of the five membered rings are 85.6(1) and 88.0(1)° and of the six membered rings are 93.0(1) and 93.4(1)°. The C-N bond distances of the uncoordinated bridgehead amines N3 and N6 range from 1.414 Å to 1.441 Å which is shorter than for normal aliphatic C-N bond distances of 1.52 Å. The bond angles around N3 and N6 are 111.6 to 117.2°. This flattening of the bond angles and shortening of the C-N bond distances at the bridgehead tertiary nitrogen has been observed for other polyaza macrocycles see Section 2.3.1, $[Ni(L_1)](ClO_4)_2$, N-C bond distance 1.427(5) Å and C-N-C bridgehead bond angle 114.5(3)°.

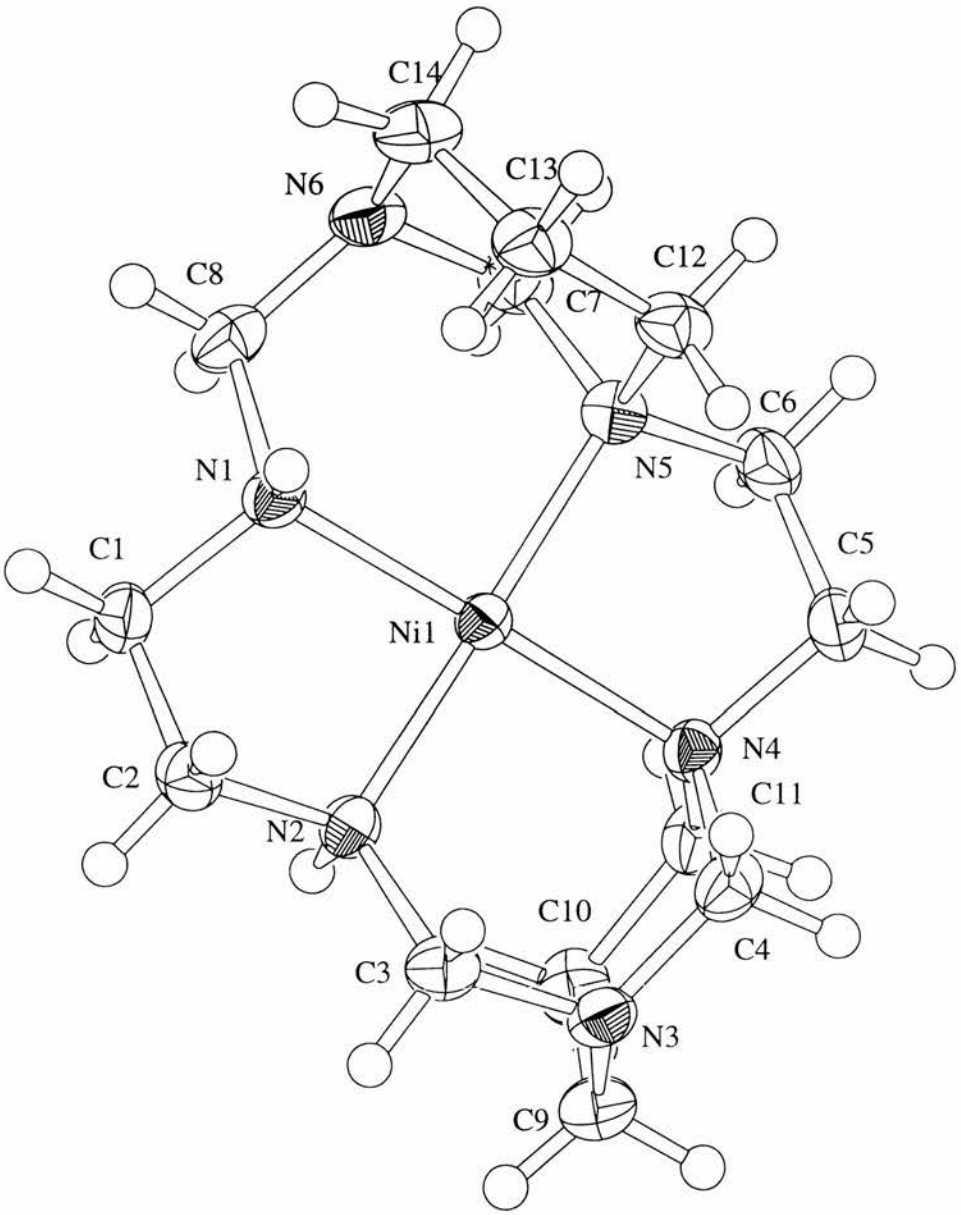

Figure 2.17: *ORTEP view of* $[Ni(L_3)](ClO_4)_2$

2.3.3.1 Data Collection

A red block crystal of $C_{14}H_{31}N_6O_{8.50}Cl_2Ni$ having approximate dimensions of 0.50 x 0.45 x 0.30 mm was mounted on a glass fibre. All measurements were made on a Rigaku AFC7S diffractometer with graphite monochromated Mo-Kα radiation.

Cell constants and an orientation matrix for data collection, obtained from a least-squares refinement using the setting angles of 25 carefully centred reflections in the range $24.26 < 2\theta < 24.84°$ corresponded to a C-centred monoclinic cell with dimensions:

$a = 32.577(4)\text{Å}$

$b = 9.585(5)\text{Å}$ $\quad \beta = 111.32(2)°$

$c = 14.461(4)\text{Å}$

$V = 4206(2)\text{Å}^3$

For Z = 8 and F.W. = 549.04, the calculated density is 1.73 g/cm^3. Based on the systematic absences of:

hk1: $h+k \neq 2n$

h01: $1 \neq 2n$

packing considerations, a statistical analysis of intensity distribution, and the successful solution and refinement of the structure, the space group was determined to be:

C2/c (#15)

The data were collected at a temperature of 20 ± 1 °C using the ω-2θ scan technique to a maximum 2 theta value of 50.0°.Omega scans of several intense reflections, made prior to data collection, had an average width at half-height of 0.29° with a take-off angle of 6.0°. Scans of (1.42 + 0.35 tan θ)° were made at a speed of 16.0° /min (in omega). The weak reflections ($I < 15.0\sigma(I)$) were rescanned (maximum of 4 scans) and the counts were accumulated to ensure good counting statistics. Stationary background counts were recorded on each side of the reflection. The ratio of peak counting time to background counting time was 2:1. The diameter of the incident beam collimator was 1.0 mm and the crystal to detector distance was 235 mm, The computer-controlled slits were set to 9.0 mm (horizontal) and 13.0 mm (vertical).

2.3.3.2 Data Reduction

Of the 4028 reflections which were collected, 3953 were unique ($R_{int} = 0.020$). The intensities of three representative reflection were measured after every 150 reflections. No decay correction was applied.

The linear absorption coefficient, μ, for Mo-Kα radiation is 12.4 cm^{-1}. An empirical absorption correction based on azimuthal scans of several reflections was applied which resulted in *trans*mission factors ranging from 0.87 to 1.00. The data were corrected for Lorentz and polarization effects. A correction for secondary extinction was applied (coefficient = 5.76712e-07).

2.3.3.3 Structure Solution and Refinement

The structure was solved by direct methods[27] and expanded using Fourier techniques[28]. The non-hydrogen atoms were refined anisotropically. Some hydrogen atoms were refined isotropically, the rest were included in fixed positions. The final cycle of full-matrix least-squares refinement[29] was based on 3133 observed reflections ($I > 3.00\sigma(I)$) and 298 variable parameters and converged (largest parameter shift was 0.45 times its esd) with unweighted and weighted agreement factors of:

$$R = \Sigma \, ||Fo| - |Fc|| \, / \, \Sigma \, |Fo| = 0.038$$

$$R_w = \sqrt{(\Sigma w \, (|Fo| - |Fc|)^2 \, / \, \Sigma w \, Fo^2)} = 0.045$$

The standard deviation of an observation of unit weight[30] was 3.32. The weighting scheme was based on counting statistics and included a factor ($p = 0.005$) to downweight the intense reflections. Plots of $\Sigma w \, (|Fo| - |Fc|)^2$ versus $|Fo|$, reflection order in data collection, $\sin\theta/\lambda$ and various classes of indices showed no unusual trends. The maximum and minimum peaks on the final difference Fourier map corresponded to 0.68 and -0.40 $e^-/Å^3$, respectively.

Neutral atom scattering factors were taken from Cromer and Waber[31]. Anomalous dispersion effects were included in Fcalc[32]; the values for $\Delta f'$ and $\Delta f''$ were those of Creagh and McAuley[33]. The values for the mass attenuation coefficients are those of Creagh and Hubbel[34]. All calculations were performed using the teXsan[35] crystallographic software package of Molecular Structure Corporation.

Table 2.7 Atomic coordinates

atom	x	y	z
Ni(1)	0.13165(2)	0.20776(5)	0.05148(4)
Cl(1)	0.20477(4)	0.6045(1)	0.13286(8)
Cl(2)	0.05704(4)	-0.1480(1)	-0.04521(8)
N(1)	0.1783(1)	0.0958(4)	0.1436(2)
N(2)	0.1624(1)	0.1794(4)	-0.0405(2)
N(3)	0.1241(1)	0.3693(4)	-0.1547(2)
N(4)	0.0848(1)	0.3215(3)	-0.0437(2)
N(5)	0.1038(1)	0.2414(3)	0.1482(2)
N(6)	0.1431(1)	0.0591(4)	0.2672(2)
C(1)	0.2019(1)	0.0190(4)	0.0877(3)
C(2)	0.2073(1)	0.1242(5)	0.0162(3)
C(3)	0.1649(1)	0.3035(5)	-0.1029(3)
C(4)	0.1037(1)	0.4299(4)	-0.0919(3)
C(5)	0.0619(1)	0.3939(5)	0.0155(3)
C(6)	0.0584(1)	0.2892(5)	0.0895(3)
C(7)	0.1006(1)	0.1098(5)	0.2037(3)
C(8)	0.1673(1)	-0.0034(5)	0.2121(3)
C(9)	0.0921(2)	0.2919(5)	-0.2375(3)
C(10)	0.0672(1)	0.1818(5)	-0.2022(3)
C(11)	0.0502(1)	0.2442(4)	-0.1265(3)
C(12)	0.1258(1)	0.3511(5)	0.2249(3)
C(13)	0.1696(2)	0.3068(5)	0.2999(3)
C(14)	0.1670(2)	0.1640(5)	0.3432(3)

Table 2.8 Bond Lengths(Å)

atom	atom	distance	atom	atom	distance
Ni(1)	N(1)	1.940(3)	Ni(1)	N(2)	1.952(3)
Ni(1)	N(4)	1.971(3)	Ni(1)	N(5)	1.952(3)
N(1)	C(1)	1.495(5)	N(1)	C(8)	1.507(5)
N(2)	C(2)	1.491(5)	N(2)	C(3)	1.514(5)
N(3)	C(3)	1.414(5)	N(3)	C(4)	1.428(5)
N(3)	C(9)	1.470(5)	N(4)	C(4)	1.502(5)
N(4)	C(5)	1.496(5)	N(4)	C(11)	1.508(5)
N(5)	C(6)	1.485(5)	N(5)	C(7)	1.518(5)
N(5)	C(12)	1.507(5)	N(6)	C(7)	1.439(5)
N(6)	C(8)	1.441(5)	N(6)	C(14)	1.485(5)
C(1)	C(2)	1.500(6)	C(5)	C(6)	1.501(6)
C(9)	C(10)	1.529(6)	C(10)	C(11)	1.518(6)
C(12)	C(13)	1.507(6)	C(13)	C(14)	1.521(6)
O(9)	H(31)	0.65(10)			

Table 2.9 Bond Angles(°)

atom	atom	atom	angle	atom	atom	atom	angle
N(1)	Ni(1)	N(2)	85.6(1)	N(1)	Ni(1)	N(4)	179.0(1)
N(1)	Ni(1)	N(5)	93.0(1)	N(2)	Ni(1)	N(4)	93.4(1)
N(2)	Ni(1)	N(5)	176.9(1)	N(4)	Ni(1)	N(5)	88.0(1)
Ni(1)	N(1)	C(1)	109.3(2)	Ni(1)	N(1)	C(8)	119.0(3)
C(1)	N(1)	C(8)	109.6(3)	Ni(1)	N(2)	C(2)	108.6(2)
Ni(1)	N(2)	C(3)	116.6(3)	C(2)	N(2)	C(3)	110.6(3)
C(3)	N(3)	C(4)	114.2(3)	C(3)	N(3)	C(9)	117.2(4)

C(4)	N(3)	C(9)	111.6(3)	Ni(1)	N(4)	C(4)	111.3(2)
Ni(1)	N(4)	C(5)	106.1(2)	Ni(1)	N(4)	C(11)	116.6(2)
C(4)	N(4)	C(5)	108.6(3)	C(4)	N(4)	C(11)	106.6(3)
C(5)	N(4)	C(11)	107.3(3)	Ni(1)	N(5)	C(6)	105.5(2)
Ni(1)	N(5)	C(7)	112.4(2)	Ni(1)	N(5)	C(12)	114.9(3)
C(6)	N(5)	C(7)	108.3(3)	C(6)	N(5)	C(12)	108.3(3)
C(7)	N(5)	C(12)	107.3(3)	C(7)	N(6)	C(8)	112.4(3)
C(7)	N(6)	C(14)	111.6(4)	C(8)	N(6)	C(14)	116.4(4)
N(1)	C(1)	C(2)	104.7(3)	N(2)	C(2)	C(1)	106.3(3)
N(2)	C(3)	N(3)	115.0(3)	N(3)	C(4)	N(4)	112.2(3)
N(4)	C(5)	C(6)	106.3(3)	N(5)	C(6)	C(5)	107.2(3)
N(5)	C(7)	N(6)	112.5(3)	N(1)	C(8)	N(6)	114.3(3)
N(3)	C(9)	C(10)	112.4(3)	C(9)	C(10)	C(11)	110.3(4)
N(4)	C(11)	C(10)	113.7(3)	N(5)	C(12)	C(13)	114.0(4)
C(12)	C(13)	C(14)	111.7(4)	N(6)	C(14)	C(13)	113.4(3)

2.3.4 Crystal Structure Determination of *cis*-$[Ni(L_1)(en)](ClO_4)_2.en.H_2O$ (L = 3-hydroxyethyl-1,3,5,8,12-pentaazacyclotetradecane).

Two ORTEP views of $[Ni(L_1)(en)](ClO_4)_2$ are shown in Figure 2.17. Selected atomic coordinates, bond distances and bond angles are summarised in Tables 2.10 to 2.12 The Ni(II) ion is in an octahedral environment coordinated by the four secondary nitrogen donors of the macrocycle and the two primary nitrogen donors of 1,2-diaminoethane. N_1, N_2, N_3 and N_4 of the macrocycle are bonded to the Ni(II) ion with Ni-N bond distances in the range 2.099(7) to 2.129(7)Å, values which are typical for triplet ground state nickel(II). The Ni-N bond distances

to the 1,2-diaminoethane ligand are 2.168(7) and 2.161(7)Å. The macrocyclic ligand has the *trans* V stereochemistry with one set of diagonal *sec*-NH groups "up" and one set "down". The six-membered chelate rings have a chair conformation and the five-membered chelate rings are *gauche*, the square planar complex has the *trans* III configuration and the conversion to *trans* V is facilitated by the inversion of one of the macrocycle nitrogen donor atoms. This type of stereochemistry is normally observed in *cis*-complexes of cyclam. For example *cis*-$[Co(cyclam)Cl_2]^+$ has the *trans* V configuration of the *sec*-NH centres[26a]. The bite angles of the five membered rings are 83.3(3) and 82.3(3)° and the bite angles of the six membered rings are 88.9(3) and 90.2(3)°. The bite angle of the five membered ring with 1,2-diaminoethane is 78.9(3)°. These angles are smaller than for the square planar complex {87.0(1), 86.7(1) and 94.2(1), 92.1(1) respectively} and the bond angles are longer than for the square planar complex being in the range 2.099(7) to 2.129(7)Å compared to 1.930(3) to 1.938(3)Å[14, 26b]. These effects are expected given the increase in coordination number, the distortion of the macrocycle due to the folding and the inversion of one of the secondary nitrogen donors. The N-C bond lengths of the tertiary bridgehead nitrogen N_5 are 1.46(1) and 1.43(1)Å which are shorter than normal N-C single bonds. The bond angle of the bridgehead nitrogen C-N-C is 114.7(7)°. Similar shortening of the bond and flattening of this bond angle have been observed for other complexes and is attributed to a long range interaction between the nitrogen lone pair and the nickel centre. The macrocyclic elipsoids are large and this is probably due to the strain in the folded molecule, at room temperature the crystal looses the 1,2-diaminoethane of crystallisation and the integrity of the crystal breaks down, hence the data were collected at –79 °C.

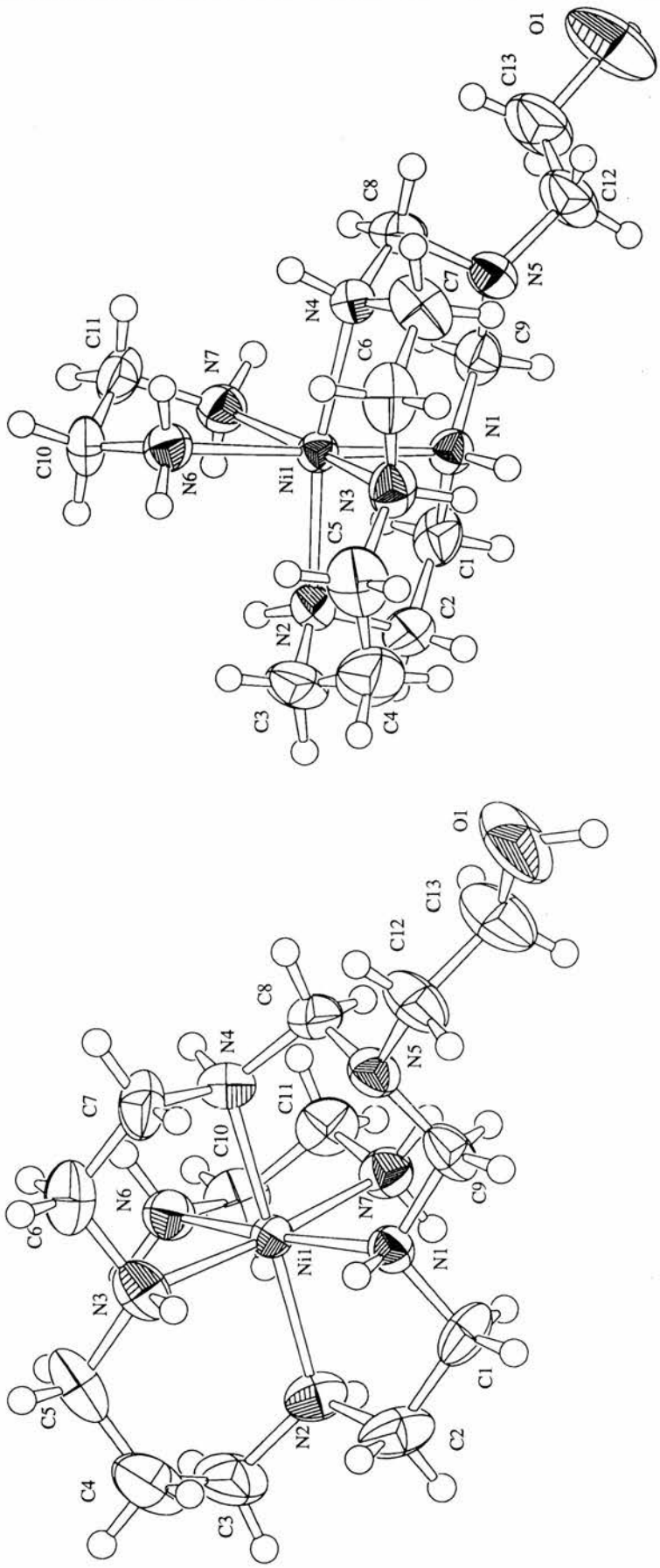

Figure 2.18: *Two ORTEP views of* cis-*[Ni(L$_1$)(en)](ClO$_4$)$_2$*

2.3.4.1 Data Collection

A purple block crystal of $C_{15}H_{45}N_9O_{10}Cl_2Ni$ having approximate dimensions of 0.35 x 0.20 x 0.15 mm was mounted on a glass fibre. All measurements were made on a Rigaku AFC7S diffractometer with graphite monochromated Mo-Kα radiation.

Cell constants and an orientation matrix for data collection, obtained from a least squares refinement using the setting angles of 20 carefully centred reflections in the range $6.42<2\theta<9.71°$ corresponded to a primitive monoclinic cell with dimensions:

$a = 12.21\ (1)$ Å

$b = 17.594(10)$ Å $\quad \beta = 91.76(7)°$

$c = 13.61(1)$ Å

$V = 2921(3)$ Å^3

For Z = 4 and F.W. = 641.18, the calculated density is 1.46 g/ cm^3. The systematic absences of:

$h0l: h+l \neq 2n$

$0k0: k \neq 2n$

uniquely determine the space group to be:

$P2_1/n$ (#14)

The data were collected at a temperature of -79 ± 1°C using the ω-2θ scan technique to a maximum 2θ value of 46.0°. Omega scans of several intense reflections, made prior to data

collection, had an average width at half height of 38° with a take-off angle of 6.0°. Scans of (1.73 + 0.35 tan θ)° were made at a speed of 16.0°/ min (in omega). The weak reflections (I < 15.0s(I)) were rescanned (maximum of 4 scans) and the counts were accumulated to ensure good counting statistics. Stationary background counts were recorded on each side of the reflection. The ratio of peak counting time to background counting time was 2:1. The diameter of the incident beam collimator was 1.0 mm and the crystal to detector distance was 235 mm. The computer-controlled slits were set to 9.0 mm (horizontal) and 13.0 mm (vertical).

2.3.4.2 Data Reduction

Of the 4319 reflections which were collected, 4093 were unique (R_{int} = 0.041). The intensities of three representative reflections were measured after every 150 reflections. No decay correction was applied.

The linear absorption coefficient, μ, for Mo-Kα radiation is 9.1 cm^{-1}. Azimuthal scans of several reflections indicated no need for an absorption correction. The data were corrected for Lorentz and polarisation effects.

2.3.4.3 Structure Solution and Refinement

The structure was solved by direct methods[27] and expanded using Fourier techniques[28]. The non-hydrogen atoms were refined anisotropically. The final cycle of full matrix least-squares refinement[29] was based on 2666 observed reflections (I > 3.00σ(I)) and 337 variable parameters and converged (largest parameter shift was 0.04 times its esd) with unweighted and weighted agreement factors of:

$$R = \Sigma||Fo| - |Fc||/\Sigma|Fo| = 0.065$$

$$R_\omega = \sqrt{(\Sigma\omega(|Fo| - |Fc|)^2/\Sigma\omega Fo^2)} = 0.052$$

The standard deviation of an observation of unit weight[30] was 3.82. The weighting scheme was based on counting statistics and included a factor (p = o.002) to downweight the intense reflections. Plots of $\Sigma\omega(|Fo| - |Fc|)^2$ versus $|Fo|$, reflection order in data collection, sin θ/λ and various classes of indices showed no unusual trends. The maximum and minimum peaks on the final difference Fourier map corresponded to 0.84 and –0.68 $e^-/Å^3$, respectively.

Neutral atom scattering factors were taken from Cromer and Waber[31]. Anomalous dispersion effects were included in Fcalc[32]; the values for $\Delta f'$ and $\Delta f''$ were those of Creagh and McAuley[33]. The values for the mass attenuation coefficients are those of Creagh and Hubbel[34]. All calculations were performed using the teXsan[35] crystallographic software package of Molecular Structure Corporation.

Table 2.10 Atomic Coordinates

Atom	x	y	z
Ni(1)	0.70333(8)	-0.00152(7)	0.25736
N(5)	0.8260(6)	-0.0415(4)	0.0448(5)
C(9)	0.8084(7)	-0.1075(6)	0.1068(6)
N(1)	0.8139(5)	-0.0844(4)	0.2108(5)
C(1)	0.7992(7)	-0.1494(5)	0.2769(7)
C(2)	0.8056(8)	-0.1201(6)	0.3828(7)
N(2)	0.7194(5)	-0.0596(4)	0.3927(5)

C(3)	0.7400(8)	-0.0160(6)	0.4838(6)
C(4)	0.8365(9)	0.0383(7)	0.4803(8)
C(12)	0.8815(8)	-0.0572(6)	-0.0463(6)
C(13)	0.8143(9)	-0.0988(7)	-0.1243(7)
O(1)	0.8713(8)	-0.0976(5)	-0.2131(5)

Table 2.11 Bond Lengths (Å)

Atom	Atom	Distance	Atom	Atom	Distance
Macrocycle					
Ni	N_1	2.099(7)	Ni	N_2	2.110(7)
Ni	N_3	2.109(7)	Ni	N_4	2.129(7)
1,2-diaminothane					
Ni	N_6	2.168(7)	Ni	N_7	2.161(7)

Table 2.12 Bond Angles (°)

Atom	Atom	Atom	Angle	Atom	Atom	Atom	Angle
Macrocycle							
N_1	Ni	N_2	83.3(3)	N_1	Ni	N_3	95.9(3)
N_1	Ni	N_4	88.9(3)	N_2	Ni	N_3	90.2(3)
N_2	Ni	N_4	168.6(3)	N_3	Ni	N_4	82.3(3)
1,2-diaminoethane							
N_6	**Ni**	**N_7**	**78.9(3)**	N_1	Ni	N_6	171.1(3)
N_2	Ni	N_6	96.3(3)	N_3	Ni	N_6	93.0(3)

N_4	Ni	N_6	92.6(3)	N_1	Ni	N_7	92.2(3)
N_2	Ni	N_7	92.7(3)	N_3	Ni	N_7	171.7(3)
N_4	Ni	N_7	95.9(3)				

2.4 Summary and Conclusions

The syntheses of a novel square planar hydroxyethyl pendant arm padlock macrocyclic Ni(II) complex and its octahedral *trans*-dichloro and *trans*-diisothiocyanato adducts have been described. In addition the folded octahedral *cis*-1,2-diaminoethane adduct has been prepared. X-ray crystal structures of all but the dichloro adduct, which was not isolated, were presented. In addition a benzyl pendant arm macrocycle, a hexaaza tricyclo macrocyclic complex and a dimeric macrocyclic complex were synthesised. The crystal structure of the *R,R,S,S*-hexaaza tricyclo macrocyclic complex was also presented. All the complexes were synthesised using the padlocking methodology. All except the hexaaza tricyclo macrocyclic complex were prepared using 1,9-diamino-3,7-diazanonane (2,3,2-tet) as the initial "wrap around" ligand followed by padlocking with the appropriate functionalised amine. This gave rise to complexes with a single functionalised pendant arm, except in the case of the dimeric macrocycle which was prepared using 1,4-diaminobutane as the padlocking amine and thus gave rise to a padlocked metal complex on both ends of the amine. The hexaaza tricyclo macrocyclic complex was prepared by initial complexation of the nickel(II) ion with N,N'-bis(3-aminopropyl)ethanediamine and 1,2-diaminoethane which, after padlocking, gave rise to the hexaaza tricyclo complex.

With the notable exception of the 1,2-diaminoethane adduct all the X-ray structures showed that the macrocycle is in the most stable *trans*-III configuration, with the pendant arm, on the non-coordinating nitrogen, in the axial position, as has been reported for padlock macrocycles incorporating alkyl pendant arms[36]. The probability elipsoids for the hydroxyl group on the hydroxyethyl pendant arm are large due to a significant amount of vibrational freedom and this has also been observed for other pendant arm padlock macrocycles[36]. There was no internal interaction between the nickel(II) centre and the pendant arm. They also showed the

characteristic flattening of the uncoordinated bridgehead nitrogen atoms. Ni-N bond distances were comparable in the square planar structures (1.930 – 1.938 Å) except the tricyclo structure which had longer bonds to the tertiary nitrogen atoms (1.940 – 1.971 Å). The bond lengths of the *trans*-diisothiocyanato adduct (2.053 – 2.076 Å, Ni-N macrocycle and 2.106 – 2.145 Å, Ni-N NCS) and the *cis*-1,2-diaminoethane adduct were typical for octahedral nickel(II) with the 1,2-diaminoethane adduct having slightly longer Ni-N bond distances due to the geometrical distortion of the macrocyclic folding (2.099 – 2.129 Å, Ni-N macrocycle; 2.168 – 2.161 Å, Ni-N en). The macrocyclic ligand has *trans* V stereochemistry with one set of diagonal *sec*- NH groups up and one set down. The six membered chelate rings have a chair conformation and the five membered rings are *gauche*.

In the following chapters a selection of these complexes, as well as another series of complexes, will be assessed for their electrocatalytic activity in the reduction of carbon dioxide and in the case of the hydroxyethyl pendant arm complex, the thermodynamics of its folding will be investigated.

2.5 Experimental

2.5.1 Physical Measurements

Visible spectra were determined with a Perkin Elmer Lambda 14P scanning spectrophotometer or a Phillips PU8720 scanning uv/vis spectrometer. Conductivities were measured with an AGB 1000 conductivity meter. NMR spectra were obtained using a 300MHz Varian Gemini spectrophotometer, X-Ray crystallography data were collected and determined as described in the previous section.

2.5.2 1,9-Diamino-3,7-diazanonane (2,3,2-tet) was prepared as described by Barefield *et al.*[4] and purified by vacuum distillation.

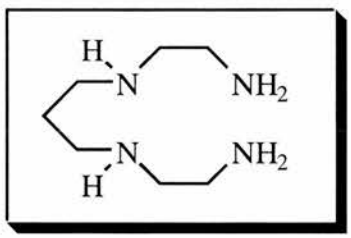

2.5.3 Synthesis of 3-(2-hydroxyethyl)-1,3,5,8,12-pentaazacyclotetradecane)nickel(II) perchlorate

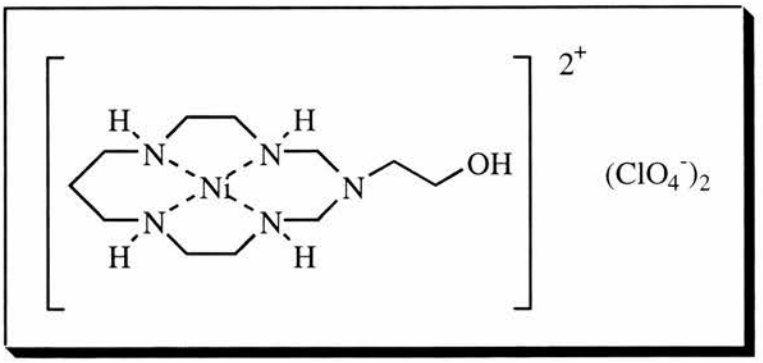

To a solution of $NiCl_2.6H_2O$ (5.75 g, 24 mmol) in ethanol (120 cm^3) was added dropwise 1,9-diamino-3,7-diazanonane (2,3,2-tet) (3.87 g, 24 mmol). A violet solution resulted to which triethylamine (6.6 cm^3, 48 mmol), aqueous ethanolamine (8.5 cm^3, 40 %) and formaldehyde (11 cm^3, 36 %) were slowly added. The solution was refluxed for 24 hr after which time the precipitate of $Ni(OH)_2$ was removed by filtration. A saturated solution of sodium perchlorate was added to the filtrate which on refrigeration gave orange crystals, which were filtered off and recrystallised from water-ethanol and then dried *in vacuo* over silica gel. A $1x10^{-3}$ mol dm^{-3} solution of the complex in water gave Λ_M = 237 S cm^{-2} mol^{-1} consistent with a 2:1 electrolyte. Suitable crystals for X-ray crystallography were obtained by slow recrystallisation from ethanol/ water the uv/vis spectrum obtained in H_2O which shows the characteristic band of square planar nickel(II) complexes at 453 nm, in nitromethane solution the complex has λ_{max} = 454 nm (ε = 60 dm^3 mol^{-1} cm^{-1}). 7.6 g, 63%. Found: C, 26.2; H, 5.3; N, 13.7. Calc. for $C_{11}H_{27}N_5NiCl_2O_9$: C, 26.3; H, 5.4; N, 13.9 %. I.R./cm^{-1} 3510(s) ν(OH); 3314(s), 3213(s), 3157(s), 3122(s) ν(NH); 2936(s), 2875(s) ν(CH); 1645(w) ν(NH); 1461(s), 1441(s), 1302(m), 1291(m) ν(CN); 1115(vs), 627(s) $\nu(ClO_4)$. δ_H (300 MHz, CD_3NO_2) 1.3 – 2.05 (2H, m, ($NHCH_2C\underline{H}_2CH_2NH$), 2.05 – 2.9

(12H, m, (NHC$\underline{H}_2$C$\underline{H}_2$NH, NC$\underline{H}_2$CH$_2$C$\underline{H}_2$N), 3.0 (2H, m, NC$\underline{H}_2$CH$_2$OH), 3.1 – 3.5 (4H, m, N$\underline{H}$), 3.5 – 3.8 (4H, m, (NC$\underline{H}_2$N), 3.9 (2H, m, NHCH$_2$C$\underline{H}_2$OH).

2.5.4 Synthesis of *trans*-dichloro3-(2-hydroxyethyl)-1,3,5,8,12pentaaza-cyclotetradecane)nickel(II)

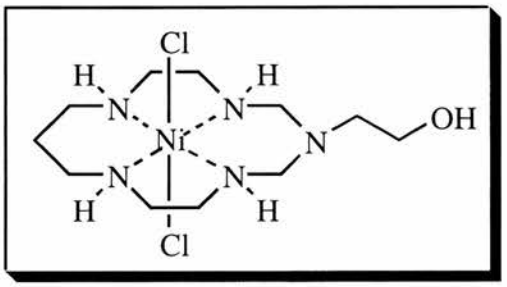

To a solution of the square planar $[NiL_1](ClO_4)_2$ in H_2O (25 cm^3) was added concentrated hydrochloric acid (3 cm^3) dropwise with stirring. The solution changed colour from orange to purple almost immediately and was left to stir for 10 min. The complex was not isolated but its visible spectrum was recorded and shows the characteristic bands for octahedral nickel(II) complexes at 515 and 672 nm.

2.5.5 Synthesis of *trans*-diisothiocyanato3-(2-hydroxyethyl)-1,3,5,8,12-pentaaza-cyclotetradecane)nickel(II)

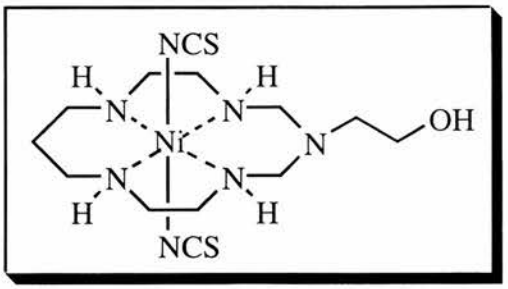

To a solution of the square planar $[NiL_1](ClO_4)_2$ (0.44 g, 1.87 mmol) in H_2O (25 cm^3) was added a saturated aqueous solution of KNCS (5 cm^3) dropwise with stirring. The pale pink/ lilac complex precipitated almost immediately from solution and was filtered off and washed with H_2O and dried *in vacuo*. Crystals suitable for diffraction studies were obtained by slow crystallisation from $MeNO_2$ over several days (296 mg, 80%). (Found: C, 37.2; H, 6.35; N, 23.35; $C_{13}H_{27}N_7ONiS_2$ calculated.: C, 37.2; H, 6.5; N 23.35%.) The uv/vis spectrum obtained in $MeNO_2$ which shows the characteristic bands of octahedral nickel(II) complexes, λ_{max} at 498 (ε = 12.7), 799 (ε = 6.7) and 923 nm (ε = 10.7 $dm^3\ mol^{-1}\ cm^{-1}$).

2.5.6 Synthesis of *cis*-1,2-diaminoethane3-(2-hydroxyethyl)-1,3,5,8,12-pentaaza-cyclotetradecane)nickel(II) perchlorate

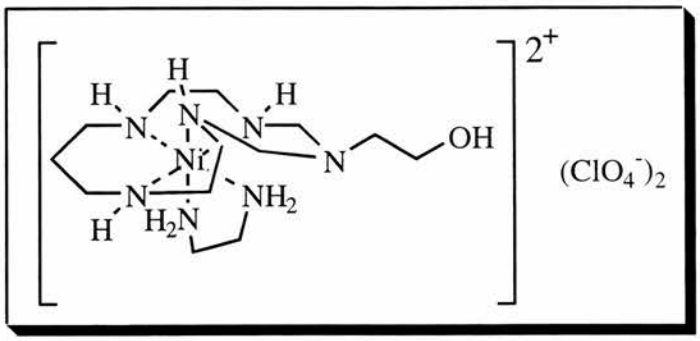

Preparation 1: to give crystals suitable for X-Ray crystallography which incorporate a 1,2-diaminoethane and a water molecule of crystallisation:

To a solution of the square planar $[NiL_1](ClO_4)_2$ in H_2O (25 cm^3) was added 1,2-diaminoethane (7 cm^3). The solution changed colour from orange to purple almost immediately. The solution was reduced to about one third volume and refrigerated for several weeks whereupon crystals suitable for X-Ray crystallography were obtained. The uv/vis spectrum obtained in H_2O shows the characteristic bands of nickel(II) octahedral complexes at 535 (ε = 8.8 dm^3 mol^{-1} cm-^{1}) and 806 nm (ε = 10.4 dm^3 mol^{-1} cm^{-1}) . Found: C, 28.4; H, 7.2; N, 19.95. Calc. for $C_{15}H_{45}N_9O_{10}Cl_2Ni$ ($[NiL(en)](ClO_4)_2.en.H_2O$): C, 28.1; H, 7.1; N, 19.7 %.

Preparation 2: to give pale pink crystals not suitable for X-Ray crystallography without the 1,2-diamoethane and water of crystallisation:

$[NiL_1](ClO4)2$ (2.11 g, 4.2 mmol) was dissolved in water (20 cm3) with stirring at room temperature. One molar equivalent of 1,2-diaminoethane (0.28 cm3, 4.2 mmol) was added and

the solution underwent a colour change from orange to pink. A further drop of 1,2-diaminoethane was added and the solution was refrigerated overnight. Small pale pink crystals precipitated which were filtered and dried *in vacuo* (1.04 g, 44%). Found: C, 27.9; H, 6.2; N, 17.4. Calc. for $C_{13}H_{35}N_7O_9Cl_2Ni$ ([NiL(en)]$(ClO_4)_2$): C, 27.7; H, 6.3; N, 17.4 %. I.R./cm^{-1} 3521(m), 3343(s), 3278(s) ν(NH); 2943(m), 2890(m) ν(CH); 1600(w) ν(NH); 1478(w), 1461(m), 1435(m) ν(CN); 1084(vs), 1030(vs), 623(s) ν(ClO_4).

2.5.7 Synthesis of (3-benzyl-1,3,5,8,12-pentaazacyclotetradecane)nickel(II) perchlorate

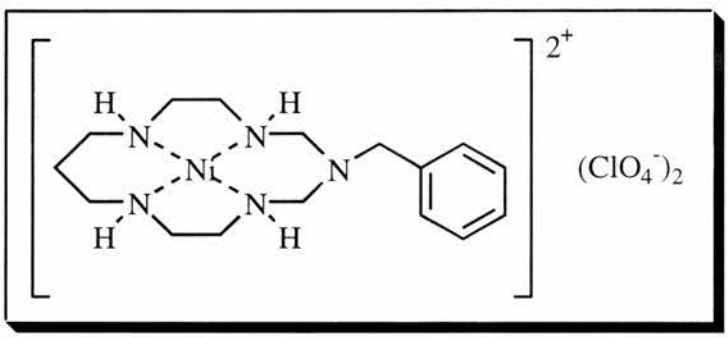

To a solution of $NiCl_2.6H_2O$ (3.13 g, 13.2 mmol) in ethanol (100 cm^3) was added dropwise 1,9-diamino-3,7-diazanonane (2,3,2-tet) (2.11 g, 13.2 mmol). A violet solution resulted to which triethylamine (4.04 cm^3, 29 mmol), benzylamine (1.44 cm^3, 13.2 mmol) and formaldehyde (5.5 cm^3, 36 %) were slowly added. The solution was refluxed for 24 hr after which time the precipitate of $Ni(OH)_2$ was removed by filtration. A saturated solution of sodium perchlorate was added to the filtrate which on refrigeration gave orange crystals, which were filtered off and recrystallised from water-ethanol and then dried *in vacuo* over silica gel (2.89 g, 40%). Found: C, 34.8; H, 5.3; N, 12.75. Calc. for $C_{16}H_{29}N_5NiCl_2O_8$: C, 35.0; H, 5.3; N, 12.75 %. The visible spectrum obtained in H_2O which shows the characteristic band of square planar nickel(II) complexes at 453 nm.

2.5.8 Synthesis of *R,R,S,S*-[(1,3,6,8,12,15-hexaazatricyclo[13.3.1.1]eicosane)nickel(II)] perchlorate

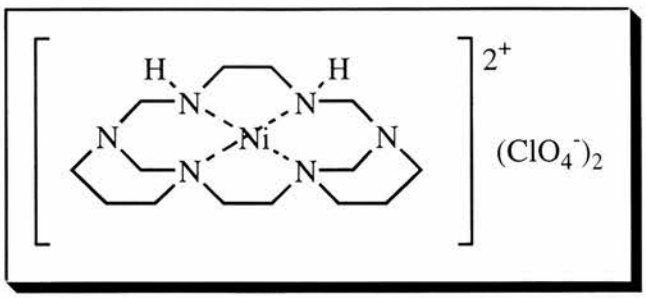

N,N'-bis(3-aminopropyl)ethanediamine (9.6 cm^3, 52.5 mmol) was added to a solution of $NiCl_2.6H_2O$ (11.9 g, 50.1 mmol) in methanol (100 cm^3). 7.5 g, 250 mmol of paraformaldehyde (an xs of 2.2) was added resulting in a pink suspension. 1,2-diaminoethane (3.4 cm^3, 51 mmol) was added, the mixture darkened and was stirred and heated under reflux for 4 hrs. The mixture was filtered and reduced to *ca.* ½ volume on a rotary evaporator. Addition of 3-5 cm^3 of concentrated perchloric acid followed by cooling overnight in the refrigerator yielded a pink precipitate which was filtered and washed with ether and methanol (20.83 g, 77%). Found: C, 30.65; H, 5.5; N, 15.2. Calc. for $C_{14}H_{30}N_6NiCl_2O_8$: C, 31.1; H, 5.6; N, 15.55 %. I.R./cm^{-1} 3545(s), 3492(s), 3237(s) ν(NH); 2947(m), 2897(m) ν(CH); 1644(m) ν(NH); 1471(s), 1428(m), 1415(m), 1287(m), 1265(m) ν(CN); 1091(vs), 1037(s), 621(s) ν(ClO_4).

2.5.9 Synthesis of (1,9-diamino-3,7-diazanonane)nickel(II) perchlorate, [Ni(2,3,2-tet)] $(ClO_4)_2$

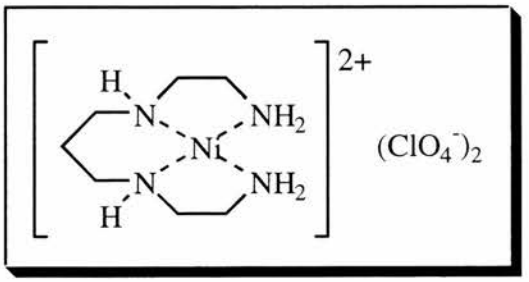

1,9-diamino-3,7-diazanonane (2.1 g, 13.1 mmol) was dissolved in methanol (100 cm^3) and $Ni(ClO_4)_2.6H_2O$ (4.34 g, 11.9 mmol) was added as the solid slowly. The mixture was gently warmed on a steam bath until the solid had dissolved and the resulting blue solution was reduced to half volume *in vacuo*. A few drops of perchloric acid (conc.) were added slowly and the pale blue precipitate was filtered, washed with ether and dried *in vacuo* (3.48 g, 64%). Found: C, 20.6; H, 4.9; N, 13.5. Calc. for $C_7H_{20}N_4NiCl_2O_8$: C, 20.1; H, 4.8; N, 13.4 %.

2.5.10 Synthesis of [1,1'-butyl bis(1,3,6,10,13-pentaazacyclotetradecane)] dinickel(II) perchlorate

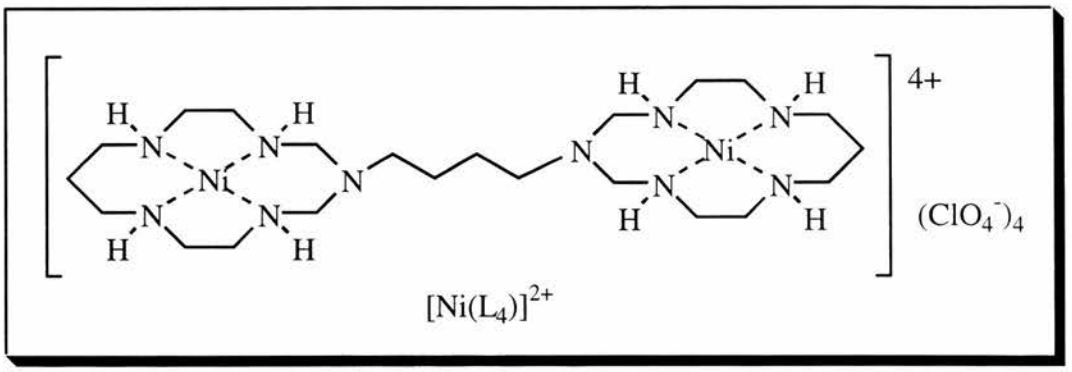

To a solution of $[Ni(2,3,2\text{-tet})](ClO_4)_2$ (1.52 g, 4.31 mmol) in methanol (120 cm^3) was added dropwise 1,4-diaminobutane (0.18 g, 2.15 mmol). A violet solution resulted to which formaldehyde (3 cm^3, 36 %) was slowly added. The solution was refluxed for 24 hr after which time the mixture was allowed to cool, a light brown precipitate of crude product formed on cooling which was filtered. The crude product was dissolved in acetone, filtered and fractionally recrystallised from acetone (335 mg, 8%). $[Ni(L_4)](ClO_4)_2$ was filtered and dried *in vacuo* over silica gel. Found: C, 27.4; H, 5.4; N, 14.4. Calc. for $C_{22}H_{52}N_{10}Ni_2Cl_4O_{16}$: C, 27.2; H, 5.4; N, 14.4 %. I.R./cm^{-1} 3455(m), 3203(m) ν(NH); 2945(m), 2875(m) ν(CH); 1634(w) ν(NH); 1466(w), 1433(w), 1391(w), 1290(w) ν(CN); 1143(s), 1091(vs), 1017(s), 627(s) $\nu(ClO_4)$.

2.6 References

1. U. Thewalt and J. Weiss, *Z. Anorg. Chem.*, 1966, **348**, 238.
2. R. W. Hay, J. M. Armstrong, M. M. Hassan, *Transition Met. Chem.*, 1992, **17**, 270.
3. F. G. Riddell and P. Murray-Rust, *J. Chem. Soc., Chem. Commun.*, 1970, 1075.
4. E. K. Barefield, F. Wagner, A. W. Herlinger and A. R. Dahl, *Inorg. Syn.*, 1976, **16**, 220.
5. M. P. Suh, W. Shin, H. Kim and C. H. Koo, *Inorg. Chem.*, 1987, **26**, 1846.
6. M. P. Suh and S. G. Kang, *Inorg. Chem.*, 1988, **27**, 2544.
7. M. P. Suh, S. G. Kang and S. K. Jung, *Bull. Korean Chem. Soc.*, 1989, **10**, 362.
8. R. W. Hay, M. J. Armstrong and M. Hassan, *Trans. Met. Chem.*, 1992, **17**, 270.
9. M. P. Suh, B. Y. Shim and T. S. Yoon, *Inorg. Chem.*, 1994, **33**, 5509.
10. M. Shakir, A. K. Mohamed, S. P. Varkey and Z. A. Siddiqi, *Trans. Met. Chem.*, 1996, **21**, 162.
11. M. P. Suh, S. Kim, B. Y. Kim, D. Hong and T. S. Yoon, *Inorg. Chem.*, 1996, **35**, 3595.
12. M. P. Suh, Y. E. Lee and B. Y. Shin, *Inorg. Chim. Acta*, 1998, **269**, 337.
13 L. Fabbrizzi, M. Licchelli, A. M. M. Lanfredi and O. Vassalli, *Inorg. Chem.*, 1996, **35**, 1582.
14 R. W. Hay, J. A. Crayston, T. J. Cromie, P. Lightfoot and D. C. L. de Alwis, *Polyhedron*, 1997, **16**, 3557.
15 R. W. Hay, T. J. Cromie and P. Lightfoot, *Trans. Met. Chem.*, 1997, **22**, 510.
16 C. de Alwis, J. A. Crayston, T. J. Cromie, T. Eisenblätter, R. W. Hay, Ya. D. Lampeka, L. V. Tsymbal, *Electrochimica Acta*, 2000, **45**, 2061.
17 S. G. Kang, S. K. Jung, *J. Sci. Edu. Taegue Univ.*, 1992, **5**, 87.
18. B. Fisher and R. Eisenberg, *J. Am. Chem. Soc.*, 1980, **102**, 7363.
19. M. Beley, J-P. Ruppert and J-P. Sauvage, *J. Chem. Soc., Chem. Commun.*, 1984, 1315.

21. M. Beley, J-P. Collin, J-P. Ruppert and J-P. Sauvage, *J. Am. Chem. Soc.*, 1986, **108**, 7461.

22. F.Abba, G. De Santis, L. Fabbrizzi, M. Licchelli, A. M.M. Lanfred, P. Pallavicini, A. Poggi and F. Ugozzoli, *Inorg. Chem.*, 1994, **33**, 1366.

23. T. J. Cromie, R. W. Hay, P. Lightfoot, D. T. Richens, J. A. Crayston, *Polyhedron*, 2001, **20**, 307.

24. D. Lee, M. P. Suh, J. W. Lee, *J. Chem. Soc., Dalton Trans.*, 1997, 577.

25. S. V. Rosokha, Ya. D. Lampeka, I. M. Maloshtan, *J. Chem. Soc., Dalton Trans.*, 1993, 631.

26 L. Fabbrizzi, M. Licchelli, A. Poggi, O. Vassalli, L. Ungaretti and W. Sardone, *Inorg. Chim. Acta.*, 1996, **246**, 379.

26a M. E. Sosa-Torres, R. A. Toscano, *Acta Crystallogr.*, 1997, **53**, 1585.

26b S. V. Rosokha, Y. D. Lampeka, *J. Chem. Soc., Chem. Commun.*, 1991, 1077.

27 SIR92: Altomare, A., Burla, M.C., Camalli, M., Cascarano, M., Giacovazzo, C., Guagliardi, A., Polidori, G. (1994). *J. Appl. Cryst.*

28 DIRDIF94: Beurskens, P.T., Admiraal, G., Beurskens, G., Bosman, W.P., de Gelder, R., Israel, R. and Smits, J.M.M/ (1994). The DIRDIF-94 program system, Technical Report of the Crystallography Laboratory, University of Nijmegen, The Netherlands.

29 Least-Squares:

Function minimised: $\Sigma\omega(|Fo| - |Fc|)^2$

Where $\omega = \frac{1}{\sigma^2(Fo)} = \frac{4Fo^2}{\sigma^2(Fo^2)}$

$\sigma^2(Fo^2) = \frac{S^2(C+R^2B)+(pFo^2)^2}{Lp^2}$

S = Scan rate, C = Total integrated peak count, R = Ratio of scan time to background counting time, B= Total background count, Lp = Lorentz-polarisation factor, p = p-factor.

30 Standard deviation of an observation of unit weight:

$$\sqrt{\Sigma\omega(|Fo| - |Fc|)^2/(No - Nv)}$$

where: No = number of observations

Nv = number of variables

31 Cromer, D.T & Waber, J.T.; "International Tables for X-ray Crystallography", Vol. IV, The Kynoch Press, Birmingham, England, Table 2.2 A (1974).

32 Ibers, J.A. & Hamilton, W.C.; *Acta Cryst.*, **17**, 781 (1964).

33 Creagh, D.C. & McAuley, W.J.; "International Tables for Crystallography", Vol C, (A.J.C. Wilson, ed.), Kluwer Academic Publishers, Boston, Table 4.2.6.8, pages 219-222 (1992).

34 Creagh, D.C. & Hubbell, J.H.; "International Tables for Crystallography", Vol C, (A.J.C. Wilson, ed.), Kluwer Academic Publishers, Boston, Table 4.2.4.3, pages 200-206 (1992).

35 teXsan: Crystal Structure Ananlysis Package, Molecular Structure Corporation (1985 & 1992).

36 R. W. Hay, A. Danby, P. Lightfoot, Ya. D. Lampeka, *Polyhedron*, 1997, **16**, 2777.

Chapter Three

Electrocatalytic Activity

3.1 Introduction

3.1.1 Carbon Dioxide

Carbon dioxide is a colourless gas, which was first identified in 1577 by Van Helmont who detected it in the products of both fermentation and charcoal burning[1]. It occurs in the products of combustion of all carbonaceous fuels and can be recovered from them in a variety of ways. CO_2 is also a product of animal metabolism and is important in the life cycles of both animals and plants. It is present in the atmosphere in small quantities (0.03%, by vol).

CO_2 is not very reactive at normal temperatures. It does however form carbonic acid, H_2CO_3 in aqueous solution. This will undergo the typical reactions of a weak acid to form salts and esters. A solid hydrate, $CO_2.8H_2O$ separates from aqueous solutions of CO_2 that are chilled at elevated pressures. This hydrate is very stable at normal temperatures but forms CO and O_2 when heated above 1700°C.

CO_2 can be reduced by several methods, the most common being its reaction with hydrogen. This is the reverse of the water gas shift reaction, commonly used in the production of hydrogen and ammonia. It can also be reduced with hydrocarbons and carbon at elevated temperatures. CO_2 will react with ammonia to form ammonium carbonate, which is used as the first stage of urea manufacture. CO_2 is a normal constituent of exhaled air but high concentrations of the gas are hazardous. 5% of CO_2 (vol) in air increases the breathing rate and prolonged exposure to volumes greater than 5% can cause unconsciousness and/or death.

3.1.2 Global Warming and the Greenhouse Effect

Over recent years increasing environmental awareness has identified the increase of carbon dioxide levels as a real threat and contributor to the phenomenon of global warming, known as the Greenhouse Effect. Since the industrial revolution levels of carbon dioxide in the atmosphere have increased by almost 1/3 from an estimated 275 µl/ l to 350 µl/ l. Carbon dioxide has been estimated to account for 85% of the total greenhouse gas emissions so this increase could be said to have had a major effect on the global temperature[2]. Estimates have put the temperature rise at 0.5 °C and whilst many argue that this is part of a natural cyclical fluctuation in global temperature it is clear that the interference of man in the natural cycle of carbon dioxide production (respiration etc.) and absorption (photosynthesis) is a serious concern.

Radiation from the sun, principally uv is absorbed by the Earth's crust and re-emitted as infra-red radiation. Various gases in the atmosphere absorb and re-emit this infra red light in all directions, including back to the Earth's surface, so that the balance of energy is such that less energy leaves the atmosphere than enters the atmosphere. Since the "leaving" energy is emitted as infra-red light the net effect is a warming of the atmosphere (Figure 1). Many gases with strong absorption in the infra-red region of the spectrum act as greenhouse gases including water vapour CO_2, N_2O and CH_4.

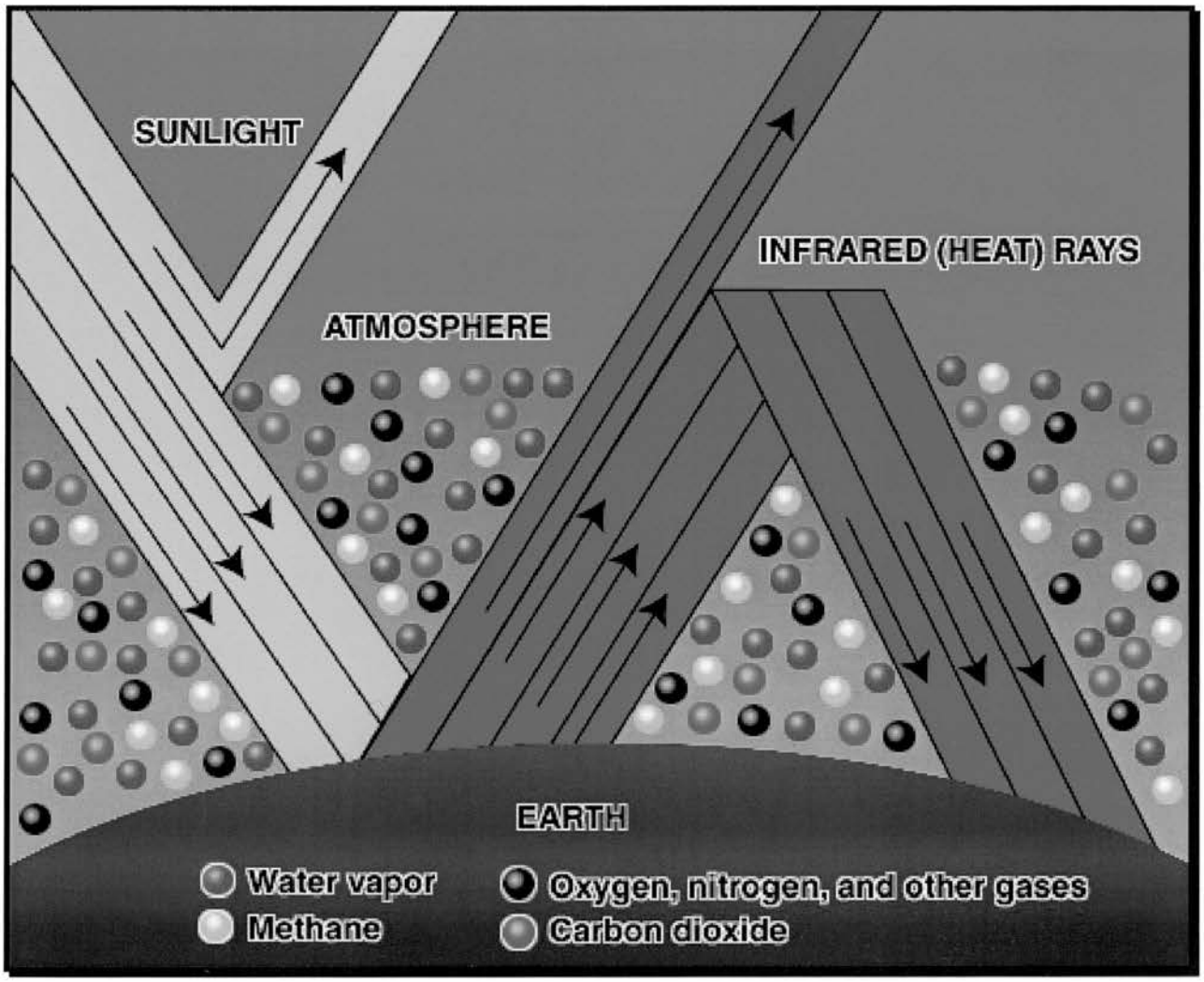

Figure 3.1: *Figure showing overall absorption of infra-red light by the Earth's surface*[3].

This warming effect is essential to life on the planet since without the protective insulation of the atmosphere and the greenhouse gases within it, the temperature on the Earth's surface would be approximately -73 ºC and even the oceans would be frozen at these temperatures. However, with Man's interference in the balance of greenhouse gases there is a fear of global warming and ultimately perhaps an unchecked greenhouse effect, as on Venus, where surface temperatures are as high as 500 ºC.

Owing to the rise in atmospheric carbon dioxide in particular, caused by modern industrial societies' widespread combustion of fossil fuels (coal, oil, and natural gas), the greenhouse effect

on Earth may be intensified and long-term climatic changes may result. An increase in atmospheric concentrations of other trace gases such as chlorofluorocarbons, nitrous oxide, and methane, due again largely to human activity, may also aggravate greenhouse conditions. The amount of carbon cycling from naturally occurring processes each year through the biosphere as CO_2 is estimated at 800 billion tonnes[4]. Ice cores and other climate data have shown, in general, a relatively stable global climate over the 10,000 years. Therefore, many scientists propose that the amount of CO_2 generated by natural processes is about equal to the amounts absorbed and sequestered by natural processes. Since the Industrial Revolution (ca. 1850) human activity, principally burning fossil fuels, is now generating somewhere in the region of an additional 24 billion tonnes of CO_2 per year[5]. Available evidence suggests that as much as half of this amount is absorbed by natural processes on the Earth's surface. Some groups of scientists believe that a large amount of CO_2 may be stored in northern latitude soils and in temperate and tropical forests, suggesting a greater importance of the role of natural resources management and land-use practices in these regions, including the burning of biomass and deforestation. Scientists estimate that anthropogenic emissions of CO_2 alone may account for as much as a 60% increase in global mean temperatures of 0.9 °C, since 1850[5].

Computer models of the Earth's climate (GCMs) have projected a globally averaged warming of 3 to 8 °C over the next 100 years, if greenhouse gas levels in the atmosphere continue to rise at the current rate. Such warming would shift temperature zones, rainfall patterns, agricultural belts and under certain scenarios cause sea levels to rise, these effects would be detrimental to some regions and advantageous to others.

Sceptics of global warming theory question the reliability of the computer climate models and also challenge assertions that, although recent episodic weather events may seem more extreme in nature, this is indicative of long-term climate change[5].

Evidence of the natural variability of the climate is plentiful enough that even the record-setting warmth at the end of the 20th century does not entirely confirm that the weather extremes experienced over the last two decades are attributable to global warming. However, the warming trend at the surface appears to continue. Relationships between seasonal and annual climate changes and present-day severe weather events are beginning to be recognised and predicted because of an improved ability to observe the El Nino and La Nina phenomena. Also singular extreme weather events have focused public attention on the possible consequences of long-term climate change and a need for a better understanding of regional climates on a longer time scale.

National Oceanic and Atmospheric Administration's (NOAA) researchers reported that the 12 warmest years since records began have occurred in the past two decades, 1990 and 1998 among the warmest[6]. At least some of this warming, they concluded, is human induced. Alternatively, satellite measurements, which measure indirectly average temperatures of the atmosphere in a deep column above the surface, for the last 20 years cannot demonstrate any definitive positive trends.

A growing number of scientists have predicted that significant alterations in climate patterns will be seen by the turn of the century. They estimate that global average temperatures could increase by as much as 5° C by the middle of the 21st century[7]. Such global warming would cause the polar ice caps and mountain glaciers to melt rapidly and result in appreciably higher coastal waters. The rise in global temperature would also produce new patterns and extremes of drought and rainfall, seriously disrupting food production in certain regions. Other scientists involved in climatic research maintain that such predictions are overstated, however. The arguments for and against global warming are obviously contradictory and confusing it has also become something of a political issue which has had the effect of making the issue even less clear.

3.1.3 Occurrence of Carbon Dioxide (The Carbon cycle)

The total amount of CO_2 in the atmosphere is estimated at 720 x 10^9 tonnes[3]. In the hydrosphere and lithosphere the occurrence of carbon in carbon dioxide, carbonate or bicarbonate form is estimated at between 10^{14} and 10^{16} tonnes of carbon[3]. These values vary with the natural cycle of carbon and with man's interference. During photosynthesis in plants the chloroplasts react with gaseous carbon dioxide and water to produce carbohydrates and oxygen.

$$nCO_2 + nH_2O \rightarrow (CH_2O)_n + nO_2 \qquad \text{(eqn. 3.1)}$$

Respiration of animals and the degradation of organic matter returns a similar amount of carbon dioxide to the atmosphere. This global equilibrium has been upset by Man's interference with the increase in carbon dioxide emissions and deforestation.

3.1.4 Commercial Uses of Carbon Dioxide

Due to its relative inertness carbon dioxide is widely used as a protective gas in the food and beverage industry and in heavy industries. It is also used as a coolant (dry ice), a propellant gas and as a fire extinguishing agent. More recently carbon dioxide has been used to supplement greenhouse atmospheres and CO_2 lasers have been developed which are used in welding and metal working. In chemistry research supercritical carbon dioxide is being used in reactions and extractions.

Some industrial processes use carbon dioxide as a raw material but not many due to its thermodynamic stability.

3.1.5 Stability of Carbon Dioxide

Carbon dioxide is the ultimate oxidation product of carbon and is extremely thermodynamically stable (ΔG = -394 kJ mol^{-1}, carbon monoxide having a ΔG = -137 kJ mol^{-1}). The C-O bond in carbon monoxide is the strongest known bond at D = 1076 kJ mol^{-1} and in carbon dioxide the CO bond strength is D = 532 kJ mol^{-1} [8].

Carbon dioxide is a linear molecule for which the following canonical structures can be drawn:

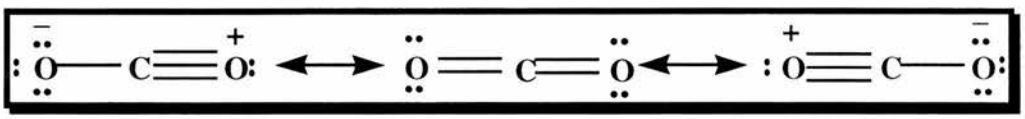

Figure 3.2: *The Canonical structures of Carbon Dioxide.*

Despite the linear symmetry and overall nonpolar nature of the molecule, some chemical reactivity might be anticipated associated either with the presence of the π-electron density of the double bonds and the lone pairs of electrons on the oxygen atoms, or with the electrophilic carbon atom. The qualitative MO energy level diagram is given in Figure 3.3, and the estimation of the level of the lowest unoccupied antibonding orbital (ca. 3.8 eV) indicates a high electron affinity associated with the central carbon atom[8]. On the other hand, the first ionisation potential is high (13.7 eV) so that the electrophilicity of the central carbon atom might be anticipated as the site of predominant reactivity.

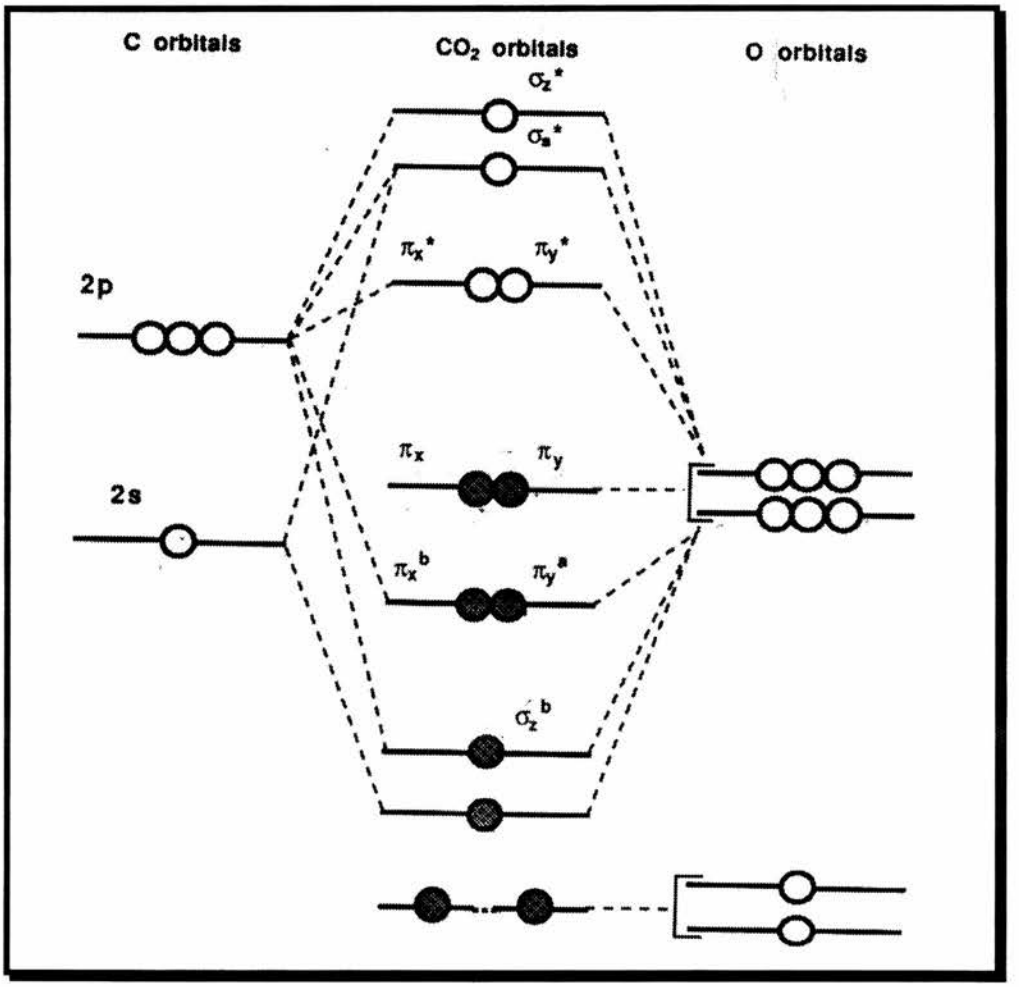

Figure 3.3: *MO Energy Level Diagram for Carbon Dioxide.*

3.2.1 Electrochemical Reduction of Carbon Dioxide

In order to convert the thermodynamically stable and relatively unreactive CO_2 molecule into the desired products in an efficient manner, suitable reaction conditions and activation mechanisms must be found. Among the various possible approaches for activation of this molecule, electrochemical reduction seems to be quite promising. One particular reason for this is that, assuming all reactions are kinetically facile at the electrode being used, the reaction can be controlled by varying the applied potential (Scheme 3.1)[9].

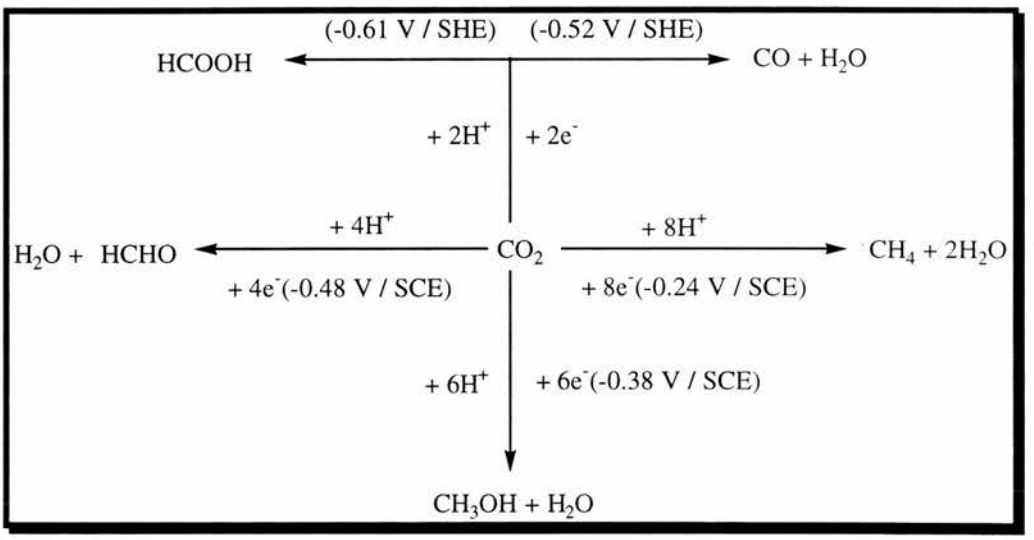

Scheme 3.1: *Thermodynamics of CO_2 Reduction at pH 0.*

However, due to kinetic restrictions direct electrochemical reduction on most metallic electrodes requires highly negative potentials and results in a variety of products. The distribution of these products critically depends on reaction conditions such as the kind of electrode material and its pre-treatment, solvent systems and other operational parameters like the supporting electrolyte, pH, temperature and pressure[10-16]. In water, the main product is formic acid, whereas in solvents with lower proton availability (such as dimethylformamide, dimethyl sulfoxide or propylene carbonate) oxalic acid and carbon monoxide are formed[11,17-19]. The addition of small amounts of

water (or the presence of adventitious water) in such dipolar aprotic solvents favours the formation of formic acid and promotes the further reduction of oxalic acid to glycolic acid, $HOCH_2$-CO_2H[20]. The relative amounts of oxalate and carbon monoxide depend upon current density and CO_2 concentration[21].

The product distribution found in DMF at inert electrodes such as Hg and Pb and its variations with current density and CO_2 concentration suggested the mechanism depicted in Scheme 3.2[21]. Oxalate is considered to be formed from the coupling of two radical anions (eqn.3.2) while the production of CO and an equimolar amount of carbonate involves, as intermediate, an adduct between CO_2 and its radical anion where the C-O bond formed results from the donation of an electron pair from latter to the former (eqn.3.3). The secondary radical anion thus produced may successively undergo electron transfer from the electrode or from the primary radical anion accompanied by the breaking of one of the C-O bonds of the primary radical anion to yield CO and carbonate (eqns. 3.4, 3.5). The production of formate involves the water that is present which may protonate $CO_2^{\cdot-}$ leading to a neutral radical (eqn. 3.6) from which formate is derived after an additional electron transfer step (eqns.3.7, 3.8). Besides formate, CO, and oxalate, other products such as formaldehyde, methanol and methane can be formed[22-29].

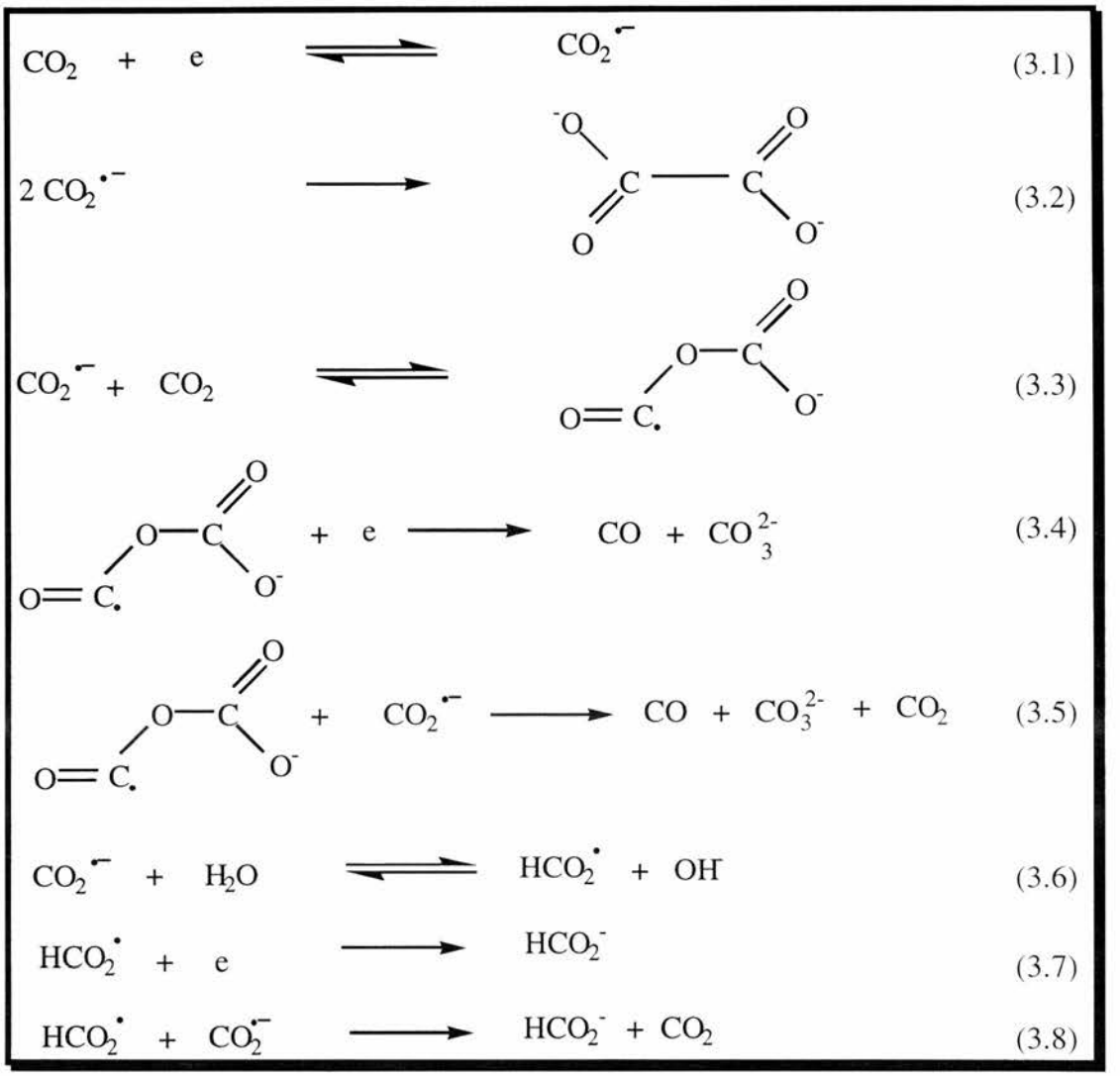

Scheme 3.2: *The product distribution at inert electrodes in non-aqueous solvents[21]. Note that the dimeric species in (3.3)-(3.5) are unstable and not isolable.*

The electrochemical reduction of CO_2 at metal cathodes generally occurs at highly negative potentials, up to -2.24V vs SCE[8]. This has prompted the search for suitable catalytic systems capable of mediating the electroreduction. Use of catalysts in the electrocatalytic activation of CO_2 offer some advantages both in reducing energy consumption and in product selectivity optimisation. The presence of transition metal species substantially decreases the reduction potential.

3.2.2 Electrocatalytic Reduction of Carbon Dioxide using [Ni(cyclam)]2^+ as a Catalyst

Cyclam, 1,4,8,11-tetraazacyclotetradecane(L_1), is one of the most popular macrocyclic ligands in metal complex catalysts for the electrocatalytic reduction of carbon dioxide. Among the variety of transition metals nickel cyclam(L_2) has displayed the highest efficiency towards the CO_2 reduction. This was first demonstrated by Fisher and Eisenberg using Me_6[14]aneN_4(L_3) complexes of Ni(II) and Co(II) (Figure 3.4)[30]. Bulk electrolysis on a mercury pool electrode at −1.6 V (Vs SCE) in a 2:1 H_2O-CH_3CN solution produced CO and H_2 as the gaseous products in 2:1 ratio with a faradaic yield(η) of 98 % in the case of Ni(II) whereas CO : H_2 was 1:1(η = 93 %) in the case of Co(II). Sauvage *et al.* reported the exceptional selectivity of $[Ni(cyclam)]^{2+}$ for CO_2 reduction over hydrogen evolution in purely aqueous medium. Only CO was formed as the reduction product with a faradaic yield of 99 % even at pH = 4.1[31,32].

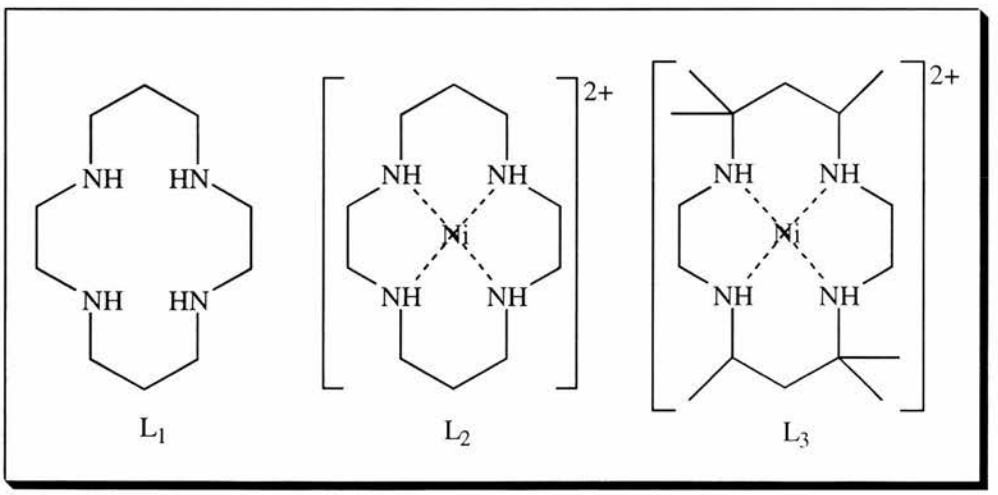

Figure 3.4: *Cyclam (L_1) and the complexes first used to assess their efficiency in reducing carbon dioxide.*

The mechanism proposed by Sauvage *et al.* for the electrocatalytic reduction of CO_2 is given in Scheme 3.3. They assumed that the active form of the catalyst was the Hg-adsorbed complex.

This assumption was based on the observation of a weak dependence of the catalytic current on the bulk concentration of the catalyst, and later justified by the adsorption studies which they reported[33]. Sauvage *et al.* proposed that the reduction of CO_2 occurs via an Ni(III)-CO_2^+ intermediate but subsequent authors identified Ni(I)-$CO_2^+{}_{ads}$ as the key intermediate, as given in Scheme 3.4[9,33,34]. A reasonable explanation for the fact that the adsorbed Ni(I) complex $[Ni(cyclam)]^+{}_{ads}$, but not the same complex in solution, is catalytically active towards the reduction of CO_2 has been provided on the basis of theoretical calculations. Sakaki *et al.* reported SCF *ab initio* calculations for $[NiF(NH_3)_4]^+$ as the model of $[Ni(cyclam)]^+$ adsorbed onto Hg, and proposed a Ni(I)-η-CO_2 as the active species for CO_2 reduction[35]. The *ab initio* calculations of several Ni(I)- and Ni(II)-CO_2 complexes indicate that CO_2 can coordinate to $[Ni(I)F(NH_3)_4]$, yielding a stable Ni-CO_2 complex but not to $[Ni(II)F(NH_3)_4]^+$, $[Ni(I)(NH_3)_4]^+$ or $[Ni(I)(NH_3)_5]^+$. The HOMO of $[Ni(I)F(NH_3)_4(\eta^1\text{-}CO_2)]$ is largely the oxygen pπ orbital and lies at a higher energy than the HOMO (non bonding π orbital) of the uncomplexed CO_2. In addition, the electron density increases around the oxygen atom upon CO_2 coordination. As a result, the coordinated CO_2 in $[Ni(I)F(NH_3)_4(\eta^1\text{-}CO_2)]$ is activated with regard to electrophilic attack and is expected to undergo facile protonation. MO calculations also show that the second one-electron reduction can easily occur in the protonated species $[Ni(I)F(NH_3)_4(CO_2H)]^+$, yielding the triplet state $[Ni(NH_3)_4(CO_2H)]$, but cannot occur in the unprotonated species $[Ni(I)F(NH_3)_4(CO_2)]$. The second reduction significantly weakens the C-OH bond, which suggest that OH^- easily dissociates from $[Ni(NH_3)_4(CO_2H)$, yielding the triplet state of $[Ni(II)F(NH_3)_4(CO)]^+$. The CO bond to Ni(II) is calculated to be weak, which suggests that CO easily dissociates from Ni(II). All these results support a reaction mechanism proposed previously for the reduction of CO_2 electrocatalyzed by $[Ni(cyclam)]^{2+}$. Although none of the Ni-CO_2, -C(O)OH or –CO species have been isolated, there is sufficient *in situ* UV-Vis and IR spectroscopic evidence for the existence of such intermediates[36,37]. Note that scheme 3.3 does not include a hydride

intermediate. However, this cannot yet be ruled out given the necessity of a proton source and the fact that hydride species have been detected in pulse radiolysis studies[38].

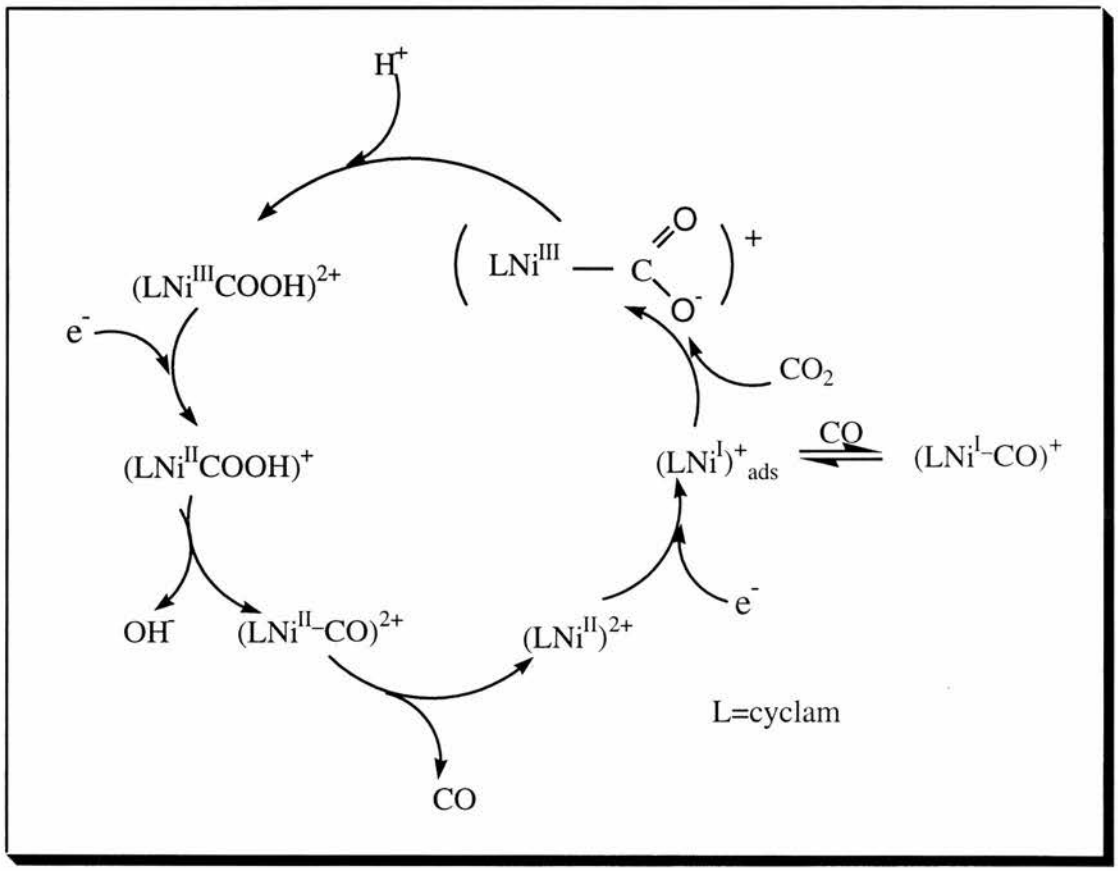

Scheme 3.3: *Mechanistic cycle involving Ni(III) for the electrocatalytic reduction of CO_2 into CO by $[Ni(cyclam)]^{2+}$ in water at Hg proposed by Sauvage* et al.[32].

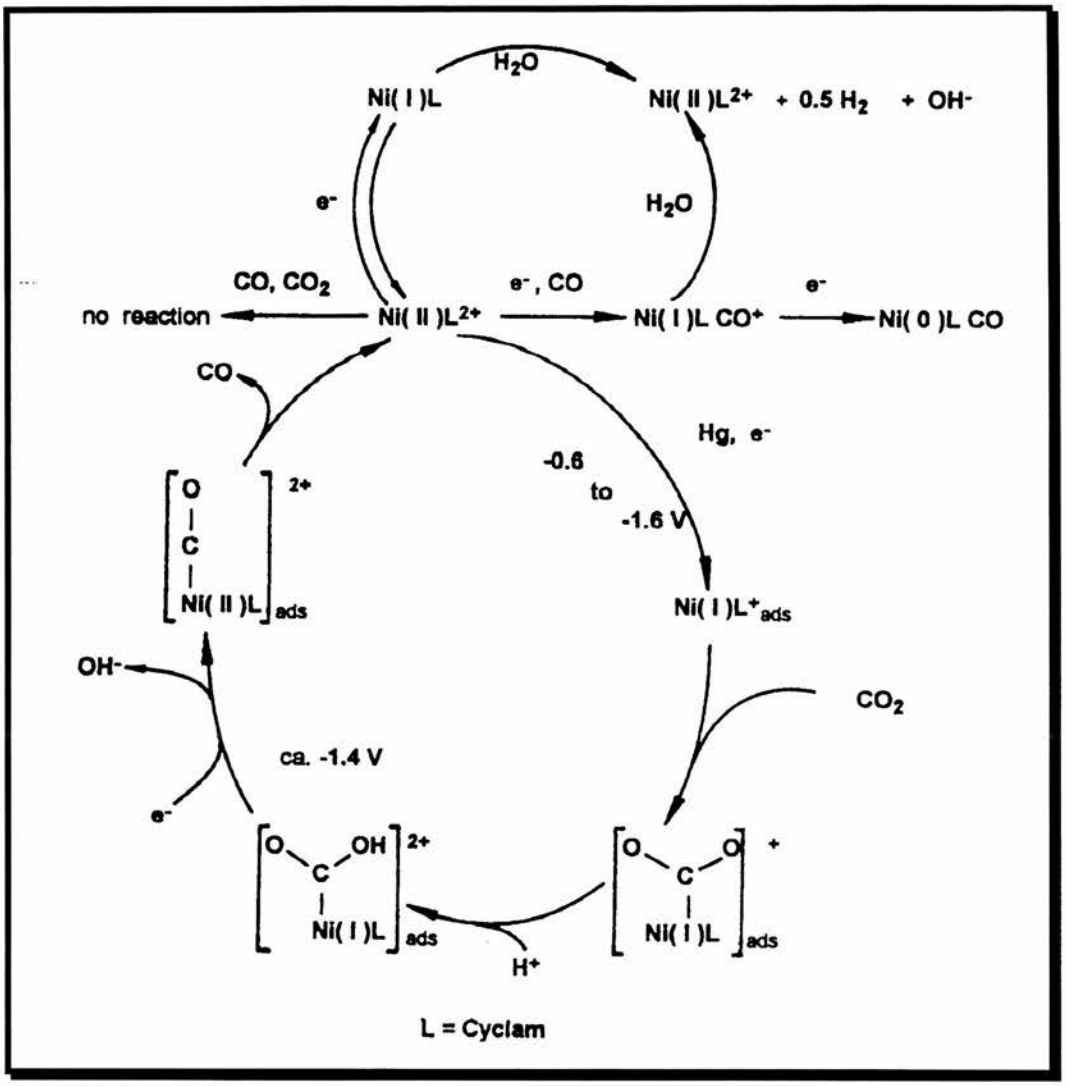

Scheme 3.4: *Mechanism not involving Ni(III) for the electrocatalytic reduction of CO_2 by Ni[(cyclam)]$^{2+}$ at Hg proposed by Costamagna* et al.[9].

Studies of the stereochemical effect of substituents on the electrocatalytic reduction of CO_2 have shown that the RRSS(*trans* III)(L_4) isomer is more active than cyclam, whereas RSRS(trans I)(L_5) is not as active as cyclam (Figure 3.5)[39].

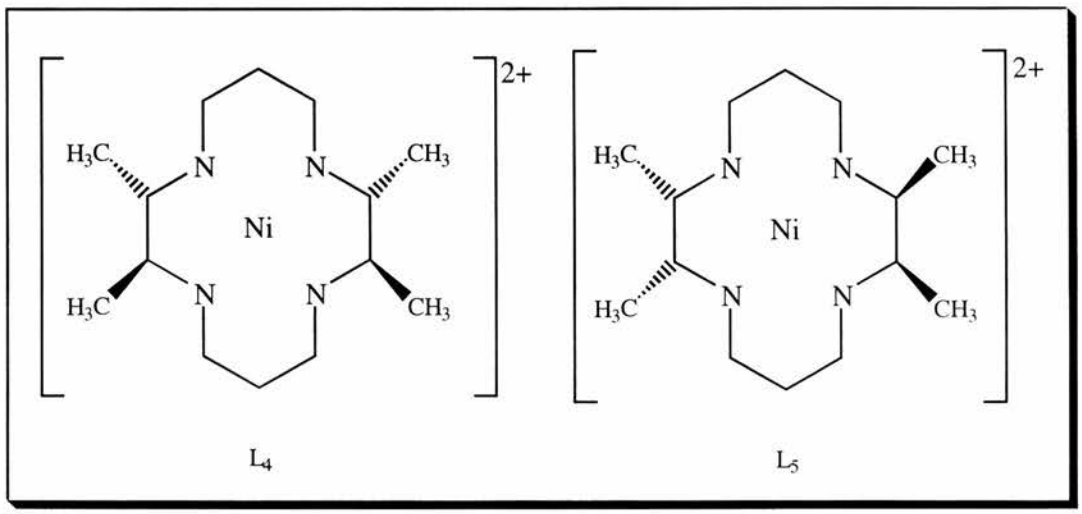

Figure 3.5: RRSS-*(trans III)*(L_4) *and* RSRS-*(trans I)*(L_5).

Interestingly, the arrangement of the chelating rings in the macrocycle also influences the catalytic activity. The geometrical isomer of $[Ni(cyclam)]^{2+}$, $[Ni(isocyclam)]^{2+}$(L_6) (Figure 3.6) reduces the CO_2 reduction potential by 160 mV although the catalytic current is less than that for $[Ni(cyclam)]^{2+}$ [40]. These isomers of cyclam and the tetramethylated cyclams are poor because their ring structure is not as flat as for cyclam and therefore, do not adsorb as well onto the electrode surface.

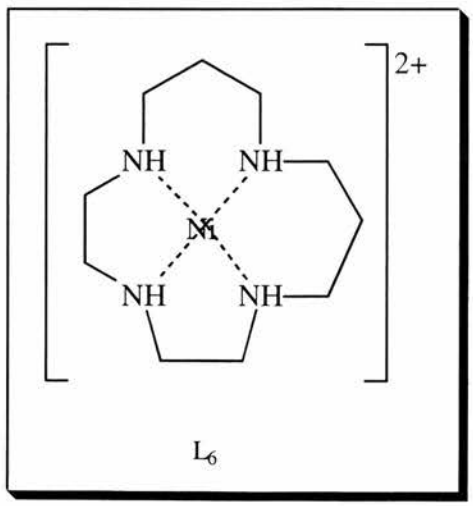

Figure 3.6: *[Ni(isocyclam)]*$^{2+}$

3.2.3 The Mechanism of $[Ni(Cyclam)]^{2+}$ Catalysed CO_2 Reduction at Mercury

Taking into consideration both the experimental observations described earlier and literature data, the following reaction scheme (Scheme 3.5) is proposed for the electrocatalytic reduction of CO_2 at mercury electrode. The main catalytic cycle is similar to that proposed by Anson *et al.*[34]. The principal difference between this mechanism and those of schemes 3.3 and 3.4 is that a Ni(I) rather than a Ni(II) carbonyl complex is involved in the cycle. This was proposed because the carbonyl intermediate was shown to be oxidizable by one electron and this was believed to be the Ni(I)/ Ni(II) oxidation. Therefore, the nickel oxidation state is +1 during the entire catalytic cycle.

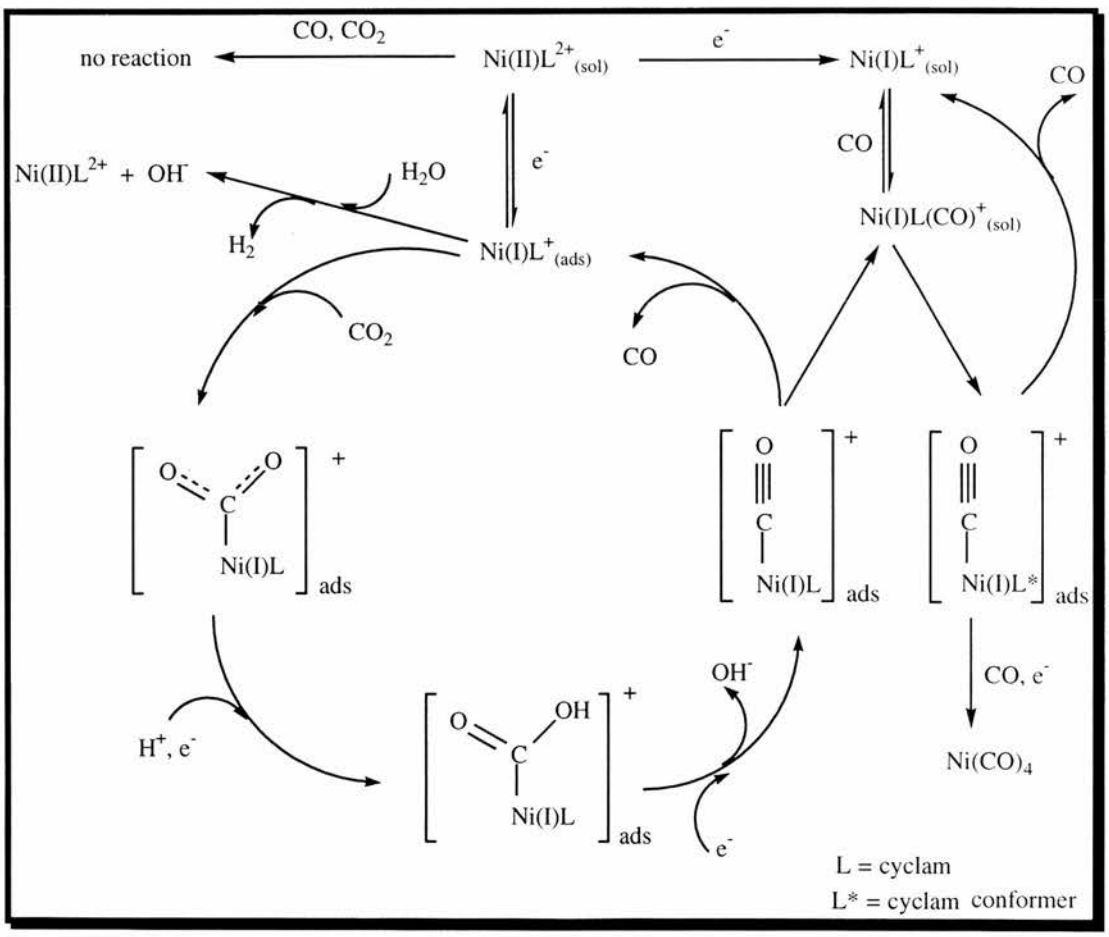

Scheme 3.5: *Proposed mechanism for the electrocatalytic reduction of CO_2 at mercury electrode.*

As shown in the Scheme 3.5 the catalytically active species towards CO_2 reduction is Ni(I) adsorbed onto Hg. The overall process for the transformation of CO_2 into CO involves an inner-sphere reorganisation. The adsorbed Ni(I) forms a nickel-carbon dioxide complex which transforms into a carbonyl complex in the presence of water. The potential at which the electrocatalyzed reduction of CO_2 proceeds is determined by the potential at which the adsorbed $[Ni(I)L\text{-}CO_2H]^+$ intermediate accepts electrons from the electrode.

The major disadvantage of this catalytic system is that the product, CO can irreversibly bind to $Ni(I)_{ads}$ or $Ni(I)_{sol}$. The reaction with $Ni(I)_{sol}$ removes the catalyst from the catalytic cycle while $[Ni(I)LCO]^+_{ads}$ causes passivation of the electrode surface. $Ni(CO)_4$ is also a minor by product which can be expected as a result of stepwise carbonylation of $[Ni(I)L]^+$. Incidentally, it is these products which represent the difference between our scheme and that of Anson et. al , who proposed neutral $[NiLCO]^0$ as the poison and did not detect $Ni(CO)_4$[34].

H_2 production is another important side reaction which takes place parallel to the CO_2 reduction.

3.3 Results and Discussion

3.3.1 Electrochemistry of Pendant Arm Pentaaza Macrocycles

The electrochemistry of the various complexes synthesised (Figure 3.7) was studied to compare their activity with that of $[Ni(cyclam)]^{2+}$ in the electrocatalytic reduction of CO_2 to CO. $[Ni(cyclam)]^{2+}$ is a well known catalyst for this reaction and has been studied in depth as discussed in Section 3.2.2.

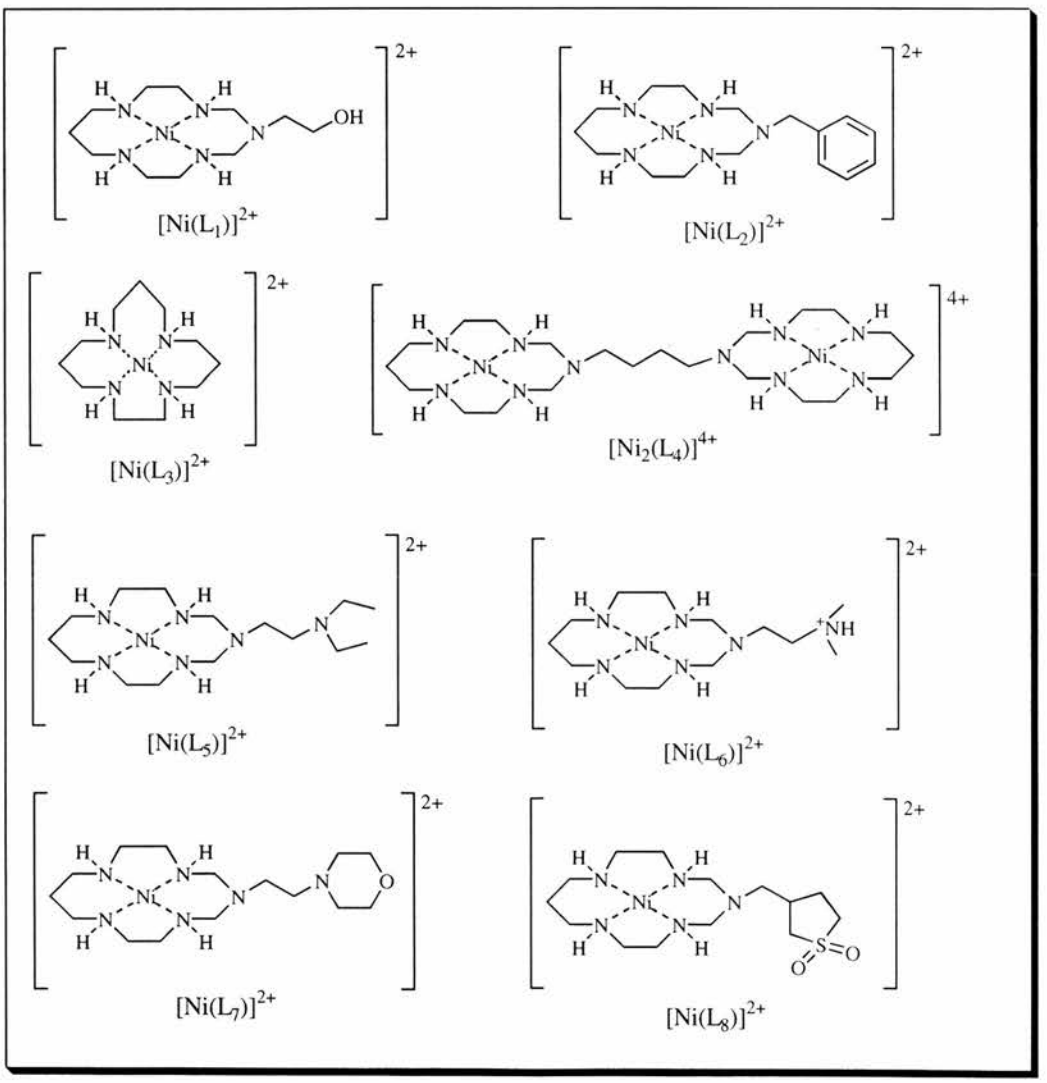

Figure 3.7: *The Ni(II) complexes tested for their catalytic activity in the reduction of carbon dioxide.*

Complexes $[Ni(L_{1-4})]^{2+}$ were prepared by us and complexes $[Ni(L_{5-8})]^{2+}$ were supplied to us by Ya. D. Lampeka as part of our collaborative project and were tested as supplied.

3.3.2 The Electrochemistry of $[NiL_1(ClO_4)_2]$

Our initial results showed that $[Ni(L_1)]^{2+}$ was more efficient at the electrocatalytic reduction of CO_2 than $[Ni(cyclam)]^{2+}$ in 0.1M NaOAc. This was an exciting result and prompted further work on the pendant arm complexes, hence the range of complexes tested.

3.3.2.1 Initial Experiments Comparing Catalytic Activity with $[Ni(cyclam)]^{2+}$

The electrochemistry of the complex $[Ni(L_1)]^{2+}$ was studied to compare its activity with that of $[Ni(cyclam)]^{2+}$ in the electrocatalytic reduction of CO_2 to CO. The $Ni^{III/II}$ and $Ni^{II/I}$ redox processes were studied in acetonitrile as solvent prior to the electrocatalysis measurements. Cyclic voltammetric measurements are summarised in Table 1. Both complexes display $Ni^{III/II}$ waves close to +1.0 V. The $Ni^{II/I}$ couple for $[NiL_1]^{2+}$ occurs at -1.416 V on carbon similar to that of $[Ni(cyclam)]^{2+}$ on Pt. However, the reduction behaviour of both complexes depended strongly on the type of electrode employed, indicating the occurrence of adsorption effects. Both complexes showed an additional broad cathodic wave at -0.7 to-0.8 V which appeared to be associated with adsorption of the complex and caused broadening, splitting and shifts of the $Ni^{II/I}$ waves at solid electrodes, or lack of a $Ni^{II/I}$ wave as was observed with $[Ni(cyclam)]^{2+}$ at a mercury electrode (Figure 3.8). These effects were greatest for $[Ni(cyclam)]^{2+}$ on carbon and were removed when 1 mmol dm^{-3} water was present leading to a positive shift in the $Ni^{II/I}$ redox potential.

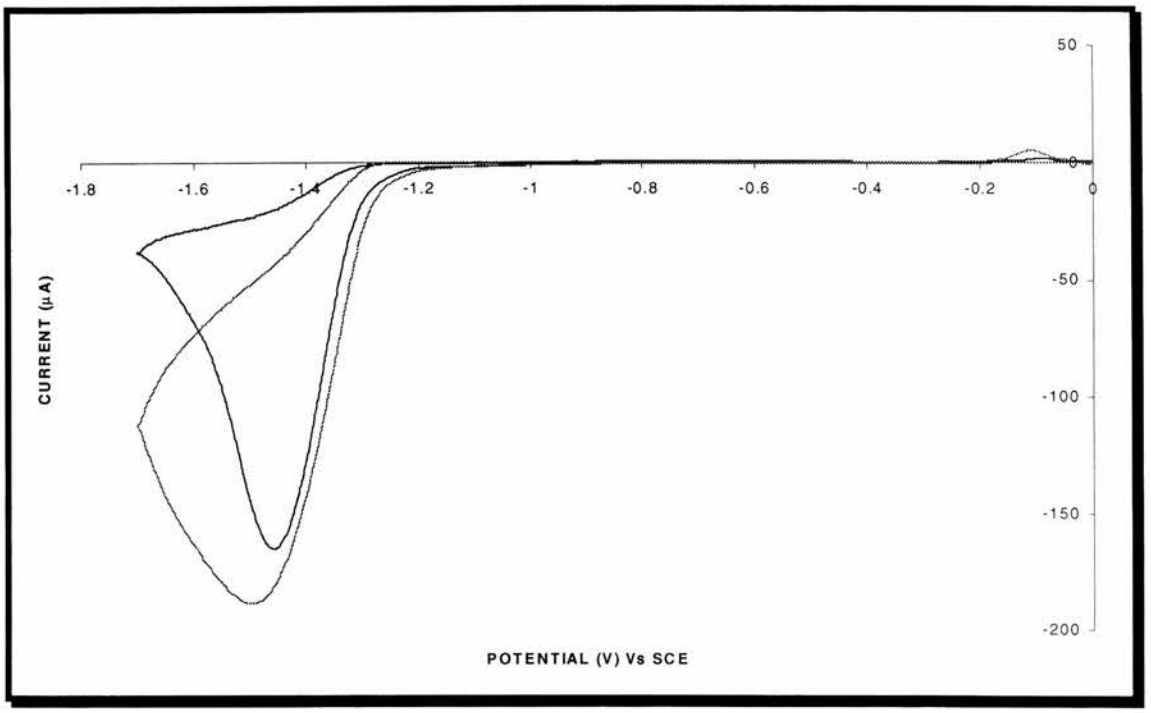

Figure 3.8: *Cyclic voltammograms of 1mM solution of (---) $[Ni(cyclam)]^{2+}$ (---) $[NiL_1]^{2+}$ in 0.1 M $KClO_4$(aq) under CO_2 at a mercury plated Ag electrode*

In aqueous media under argon the cyclic voltammetry of the complexes at a hanging drop mercury electrode showed broad waves for the $Ni^{II/I}$ reduction which were comparable in potential. On the return scan there is a small sharp peak at *ca.* -0.2 V which has previously been assigned to a carbonyl adduct of the nickel complexes. This result suggests that there is some residual CO_2 or carbonate reduction in carbonate media even in the absence of externally introduced CO_2. When CO_2 is bubbled into the bicarbonate buffer solution (pH = 6.2 - 6.8) the catalytic current measured with $[Ni(L_1)]^{2+}$ is about one third of that of the cyclam complex under the same conditions. The cathodic peak was also 50 mV more negative. The $[Ni(L_1)]^{2+}$ complex does not give as much catalytic current under cyclic voltammetric conditions as $[Ni(cyclam)]^{2+}$ Table 2.

The data indicate that $[Ni(L_1)]^{2+}$ is less active for hydrogen evolution in an acetate electrolyte than the cyclam complex and thus appeared to be more active than the cyclam complex for CO_2

reduction under these conditions. A further observation is that prolonged (30 min) CO_2 bubbling in 0.1 mol dm^{-3} $KHCO_3$ leads to loss of the catalytic current for $[Ni(cyclam)]^{2+}$ and decolourisation of the solution. Under the same conditions, the complex $[Ni(L_1)]^{2+}$ is more resistant to this effect.

Complex	Electrode	$Ni^{III/II}$		$Ni^{II/I}$	
		$E_{1/2}$ (V)	ΔE_P (mV)	$E_{1/2}$ (V)	ΔE_P (mV)
$[Ni(L_1)](ClO_4)_2$	Pt	+1.013	82	-1.536[a]	184[a]
	C	+1.000	92	-1.416	84
	Hg	-	-	-1.541	502
[Ni(cyclam)] $(ClO_4)_2$	Pt	+1.032	96	-1.420	108
	C	+0.993	98	-1.644	172

Table 3.1: *Electrochemical data for the complexes $[Ni(L_1)]^{2+}$ and $[Ni(cyclam)]^{2+}$ in acetonitrile with 0.1 mol dm^{-3} tetra-n-butylammonium hexafluorophosphate as the supporting electrolyte. $E_{1/2} = (E_P^a + E_P^c)/2$. [a] Ni(II)/ Ni(I) has a prewave at - 1.38 V.*

Complex	Electrolyte	$E_{1/2}$ ($Ni^{II/I}$) (V)	ΔE_P (mV)	E_P^c (V)	i_P^c (mA cm^{-2})
$[Ni(L_1)](ClO_4)_2$	0.1M $KHCO_3$	- 1.4[a]	-	- 1.41	3.79
	0.1M NaOAc	**- 1.53**	**60**	**- 1.46**	**7.13**
[Ni(cyclam)]	0.1M $KHCO_3$	- 1.4	-	- 1.36	10.6
	0.1M NaOAc	**- 1.43[b]**	**60**	**- 1.80**	**3.45**

Table 3.2: *Electrochemical data for the electrochemical reduction of CO_2 in aqueous media. $E_{1/2} = (E_P^a + E_P^c)/2$. [a] The CO_2 concentration was ca. 0.032 mol dm^{-3}. The 0.1 mol dm^{-3} solution of $KHCO_3$ had a pH = 6.2 - 6.8 and the 0.1 mol dm^{-3} solution of NaOAc had a pH = 7.38 which fell to 5.8 after bubbling with CO_2.*

3.3.2.2 Importance of pH Control: Catalytic Current *vs* pH

Further work revealed that the other pendant arm complexes were not more efficient than $[Ni(cyclam)]^{2+}$. It was clear that our results were a little misleading because of the pH effect on the catalytic current. Over a small pH range (5.5-7) there is a very steep dependence of catalytic current on pH (Figures 3.9 and 3.10) and that this is largely affected by hydrogen evolution and the electrolyte employed. Therefore, whilst the hydroxyethyl complex is comparable to cyclam under certain conditions, the earlier result that $[Ni(L_1)]^{2+}$ was better than $[Ni(cyclam)]^{2+}$ is probably an artifact of this steep variation.

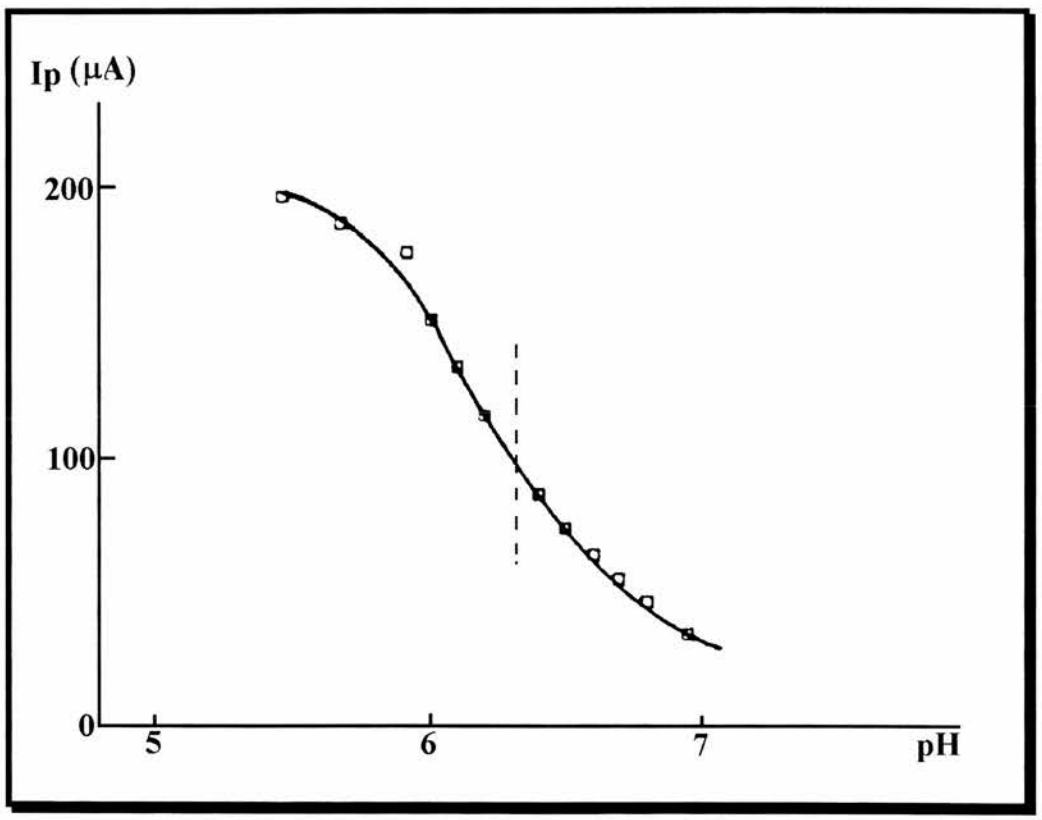

Figure 3.9: *Dependence of the catalytic current on the pH measured at a hanging mercury drop electrode (area = 0.0087 cm^2, scan rate = 100 mV s^{-1}) for 1 mM solution of $[Ni(cyclam)](ClO_4)_2$.*

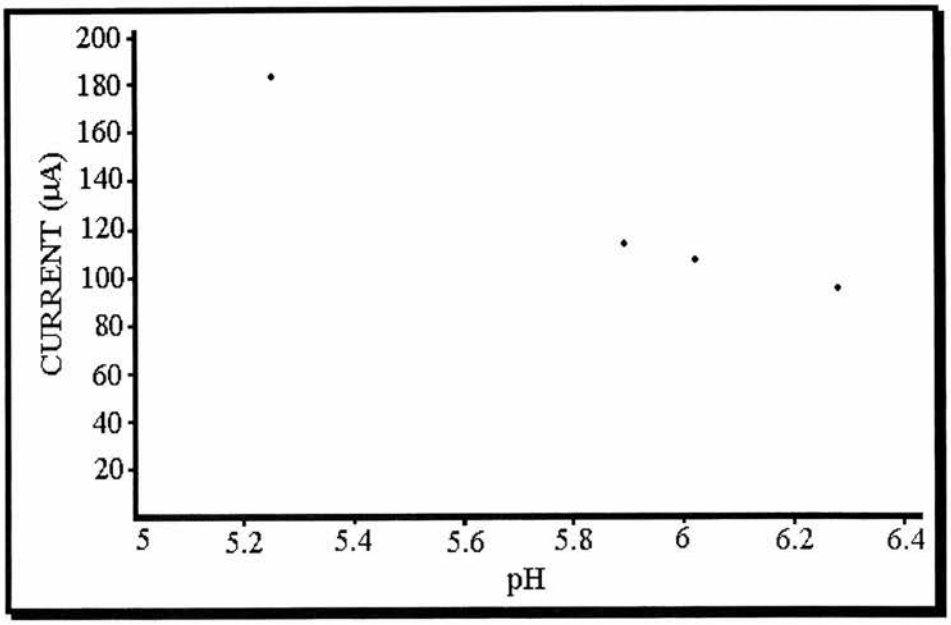

Figure 3.10: *Dependence of the catalytic current on the pH reported by Beley* et al.[40a].

Explanations of the poorer performance of the pentaaza macrocycles will be discussed in a later section.

3.3.3 Comparative Electrochemistry of $[Ni(L_{1\text{-}8})]^{2+}$

The redox potentials of all the complexes were measured at a glassy carbon electrode.

Complex	Under Argon			
	$Ni^{II/I}$ (V)	ΔE_p (mV)	$Ni^{III/II}$ (V)	ΔE_p (mV)
$[Ni(L_1)](ClO_4)_2$	-1.42	84	+1.00	92
$[Ni(L_2)](ClO_4)_2$	-1.41	88	+1.09	92
$[Ni(L_3)](ClO_4)_2$	-1.42	72	+1.01	78
$[Ni_2(L_4)](ClO_4)_4$	-1.43	86	+1.00	92
$[Ni(L_5)](ClO_4)_2$	-1.44	128	+1.045	90

$[Ni(L_6)](ClO_4)_2$	-1.43	90	+1.05	95
$[Ni(L_7)](ClO_4)_2$	-1.45	108	+1.048	119
$[Ni(L_8)](ClO_4)_2$	-1.41	73	+1.03	87

Table 3.3: *Redox data at glassy carbon electrode in acetonitrile/ 10% H_2O with 0.1 mol dm^{-3} tetra-n-butylammonium hexafluorphosphate as the supporting electrolyte.*

The first point to note in Table 3.3 is that all the $Ni^{II/I}$ potentials are all similar at approx. -1.4 V. The $Ni^{III/II}$ potentials are also very similar (approx. +1 V) with the exception of L_2 which is slightly more positive at +1.09 V. Ni^{III} species are often strongly stabilised by solvent or anion binding, while this is less important for Ni^{II}. However, the large electron rich benzene ring only one methylene group from the macrocyclic ring itself may partially block solvent axially binding and, therefore, shift the potential to a more positive value, than for Ni^{III} species with axially bound solvent, because of the destabilising effect on Ni^{III}. The peak separations ΔE_P are all fairly similar also except for L_5 and L_7 which are both approximately 30% larger than for the other complexes (~85 *vs* ~110 mV). Interestingly L_5 and L_7 are both unprotonated tertiary amines and tertiary amines are known to adsorb strongly onto the electrode surface. With the pendant tertiary amine adsorbed onto the electrode surface the electron required to reduce the metal centre has further to tunnel and, therefore, the redox reaction takes longer. The non pendant arm complex L_3 has the smallest ΔE_P (72 and 78 mV) and this is probably because there is nothing disrupting the macrocycle adsorbing onto the electrode via the nickel centre.

The electrochemical kinetics for the $Ni^{III/II}$ reaction of $[Ni(L_5)]^{2+}$ are interesting with ΔE_P = 90 mV more closely resembling that for the protonated tertiary amine L_6 (ΔE_P = 95 mV), than the other unprotonated tertiary amine L_7 (ΔE_P = 119 mV). One explanation of this is that at the more positive potential the amine is oxidised or protonated so becoming more like the protonated

tertiary amine L_6 and, therefore, desorbing from the electrode. This favours direct nickel adsorption and hence the kinetics of the oxidation speed up. As to why this does not happen to $[Ni(L_7)]^{2+}$ is unclear although the nitrogen of the morpholine ring is in a very different environment electrically than the alkyl tertiary amine and has a lower pK_a (10.7 for triethylamine *vs* 7.70 for N-ethyl morpholine).

3.3.4 Comparative Electrocatalytic Data for $[Ni(L_{1\text{-}8})]^{2+}$

Complex	Under Ar		Under CO_2	
	$Ni^{II/I}$ (V)	ΔE_p (mV)	i_c (mA cm^{-2})	E_p^c (V)
$[NiL_1](ClO_4)_2$	-1.45	79	23.6	-1.91
$[NiL_2](ClO_4)_2$	-1.51	280	3.25	-1.84
$[NiL_3](ClO_4)_2$	-1.40	160	3.17[a]	-1.7[a]
$[Ni_2L_4](ClO_4)_4$	-1.45	246	2.52	-1.55
$[NiL_5](ClO_4)_2$	-1.46	162	25.9	-1.95
$[NiL_6](ClO_4)_2$	-1.45	73	26.4	-1.92
$[NiL_7](ClO_4)_2$	-1.53	88	21.9	-1.85
$[NiL_8](ClO_4)_2$	-1.43	84	17.5	-1.81

Table 3.4: *Electrochemical data at a mercury plated Ag electrode(area = 0.0314 cm^2) for the electrocatalytic reduction of CO_2 in acetonitrile with 10% H_2O. [a] measured at a hanging mercury drop electrode.*

The electrochemical data in Table 3.4 were measured using a mercury plated silver electrode. This change of electrode has affected the ΔE_P values of the $Ni^{II/I}$ reduction significantly whilst the potentials remain largely unchanged.

$[Ni(L_1)]^{2+}$ was unaffected by the change of electrode but $[Ni(L_2)]^{2+}$ shows a large change in both potential (-1.41 *vs* –1.51 V) and peak separation (ΔE_P) (88 *vs* 280 mV) and this is probably an electrode specific affect such that the aromatic ring side arm adsorbs strongly onto mercury. Such adsorption of aromatic rings on to electrode surfaces has been described before[41]. The L_3 complex also experiences a large increase in ΔE_P (72 *vs* 160 mV) and again this is probably an electrode specific effect. The $Ni^{II/I}$ potential of the binuclear L_4 complex is unaffected but the ΔE_P has almost tripled (86 vs 246 mV). The complex has two metal centres and two macrocyclic rings and it may be that both rings are not adsorbing on to the electrode simultaneously. If one ring adsorbs and the other ring does not then the second electron has to tunnel some distance which would give rise to such a large peak separation and we have observed this in the other binuclear systems that we have studied[42]. $[Ni(L_5)]^{2+}$, the unprotonated tertiary amine, is not greatly affected; the ΔE_P suggests the reduction reaction is slightly slower on this electrode. Conversely the protonated tertiary amine L_6 is reduced slightly faster on this electrode. The morpholine pendant arm complex L_7 has a significantly more negative potential for the $Ni^{II/I}$ reduction on mercury for reasons which are unclear, however, the reaction does go faster (108 *vs* 88 mV). Finally, complex L_8 does not show any significant difference between the two electrodes.

3.3.4.1 Relationship Between Catalytic Current and the Peak Separation

Turning now to the data for the catalytic current for CO_2 reduction in Table 3.4 we first notice that a very wide range of catalytic current is observed. Surprisingly, there existed a relationship between the catalytic current and ΔE_P (peak separation) emerged that was unexpected and is illustrated in Figure 3.11. The one point which does not appear to fit is the unprotonated tertiary amine $[Ni(L_5)]^{2+}$ and this will be discussed later in detail.

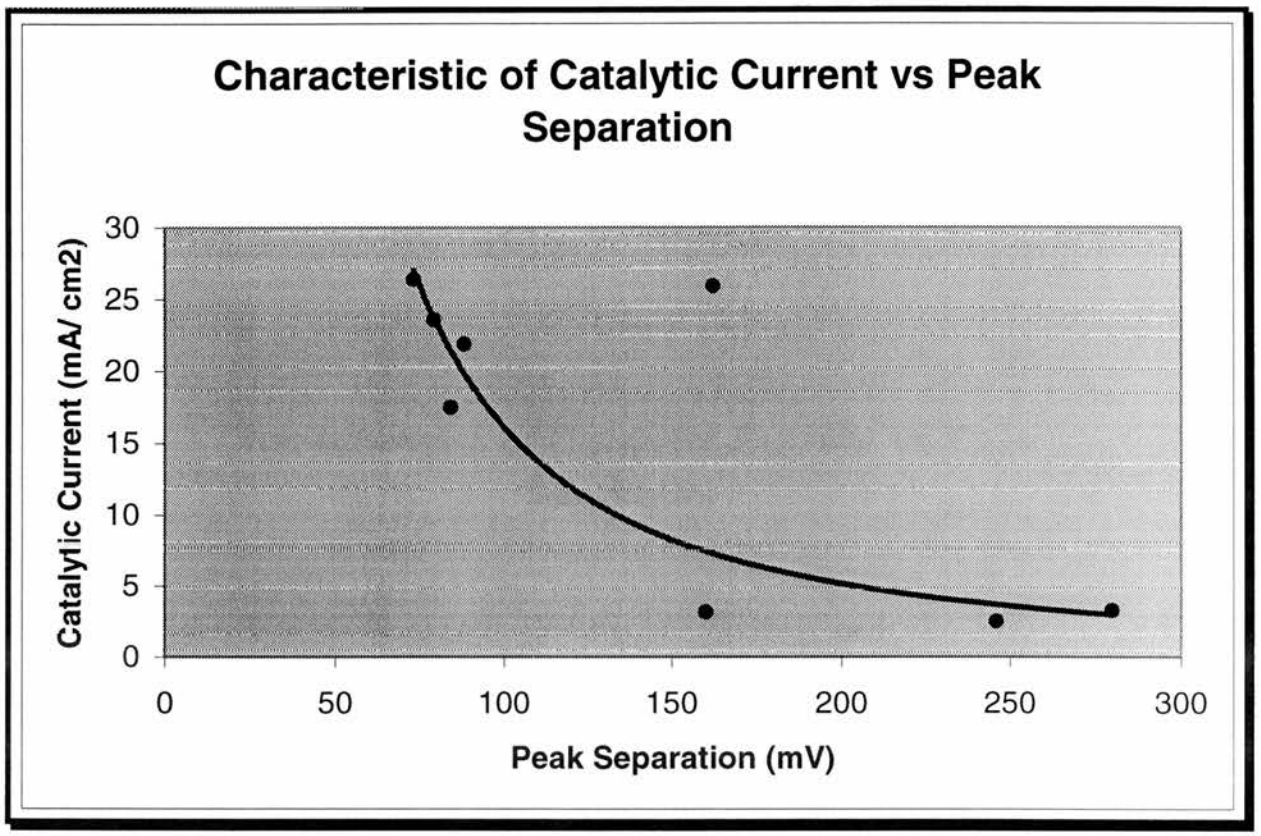

Figure 3.11: *Characteristic showing the relationship between catalytic current and ΔE_P for the complexes L_1-L_8.*

The reason for this dependence is not clear at present, though follow-up reaction current peaks and catalytic current peaks for solution species are known to exhibit a shifting of the wave to potentials in advance of the redox potential and so the electrochemical kinetics of the catalyst (here the $Ni^{II/I}$ process) influence the observed current[43]. In the case of a surface catalytic wave the theory is less well advanced. The maximum catalytic current possible at large overpotentials is governed by the diffusion current of CO_2 to the electrode. For the present case, the solubility of CO_2 in $CH_3CN/10\%$ H_2O is approximately 225 mmol dm^{-3} and so using a diffusion coefficient of 1 x 10^{-6} cm^2s^{-1} and for a 2e reduction we calculate from the Randles-Sevcik equation $I_p^{cat,max} = 2.69 \times 10^5 n^{3/2} c D^{1/2} v^{1/2} = 54$ mA cm^2 [38]. This is the maximum current possible:

the observed maximum could be less if the coverage of catalyst is low or the rate of catalyst turnover is lower. Up until now these factors have been used to explain variations in catalyst performance. However, the catalytic wave shape (and therefore observed peak maximum) is influenced by two other factors: firstly, the current decays very rapidly at high overpotentials, due to an unknown process, possibly desorption of the catalyst or catalyst poisoning by the CO product. The latter is at present the favoured explanation as explained in the introduction to this chapter. Secondly, the rising part of the wave (low overpotentials) is influenced by the electrochemical kinetics of the one-electron transfer to the Ni catalyst, as in the expression $I = nFAkc$, where $k = k^0\exp(-\alpha nF/RT)$ in which k^0 is the standard heterogeneous rate constant for charge transfer and α is the transfer coefficient . So far it is this aspect which has not been explored.

The cyclic voltammetry peak separation, ΔE_p, for the $Ni^{II/I}$ process on Hg is related to the heterogeneous rate constant, k^0, in a complex manner which has been solved numerically, and expressed in the graph of ΔE_p vs $\log_{10}\Psi$, where $\Psi = (RT/nFD\pi\nu)^{1/2}k^0$, where D is the diffusion coefficient and ν is the scan rate (Figure 3.12)[44,45]. There are a few caveats to using ΔE_p values to calculate k^0. The data should probably be calculated at a variety of sweep rates and also the effects of uncompensated resistance are identical to the effects of slow electrode kinetics. Nevertheless, if one uses this graph to determine k^0 from the data in Table 3.4 and then plots the catalytic current peak maximum, i_{cat}, vs k^0 the plot in Figure 3.13 is obtained. The linearity of the plot is quite remarkable given that we are making the large approximation that all the overpotentials at the peak maxima are identical, and we are also assuming that the transfer coefficients, α, are identical. The linearity of the plot seems to suggest therefore that the variation in the peak maximum amongst the different complexes is influenced largely by the

electrochemical kinetics, specifically the rate of heterogeneous charge transfer, k^0, of the $Ni^{II/I}$ process on Hg.

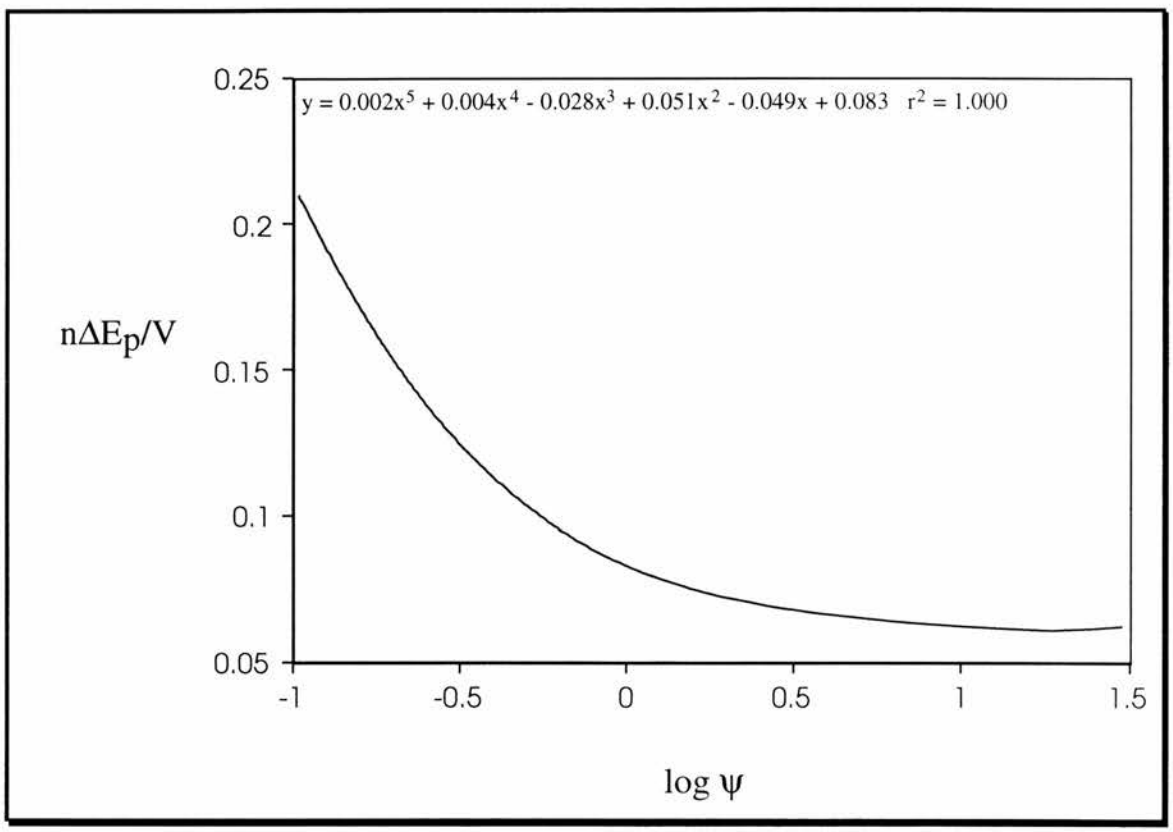

Figure 3.12: *Calculated dependence of the peak separation ΔE_p vs $log_{10}\Psi$, where $\Psi = (RT/nFD\pi v)^{1/2}k^0$, where D is the diffusion coefficient and v is the scan rate*[43].

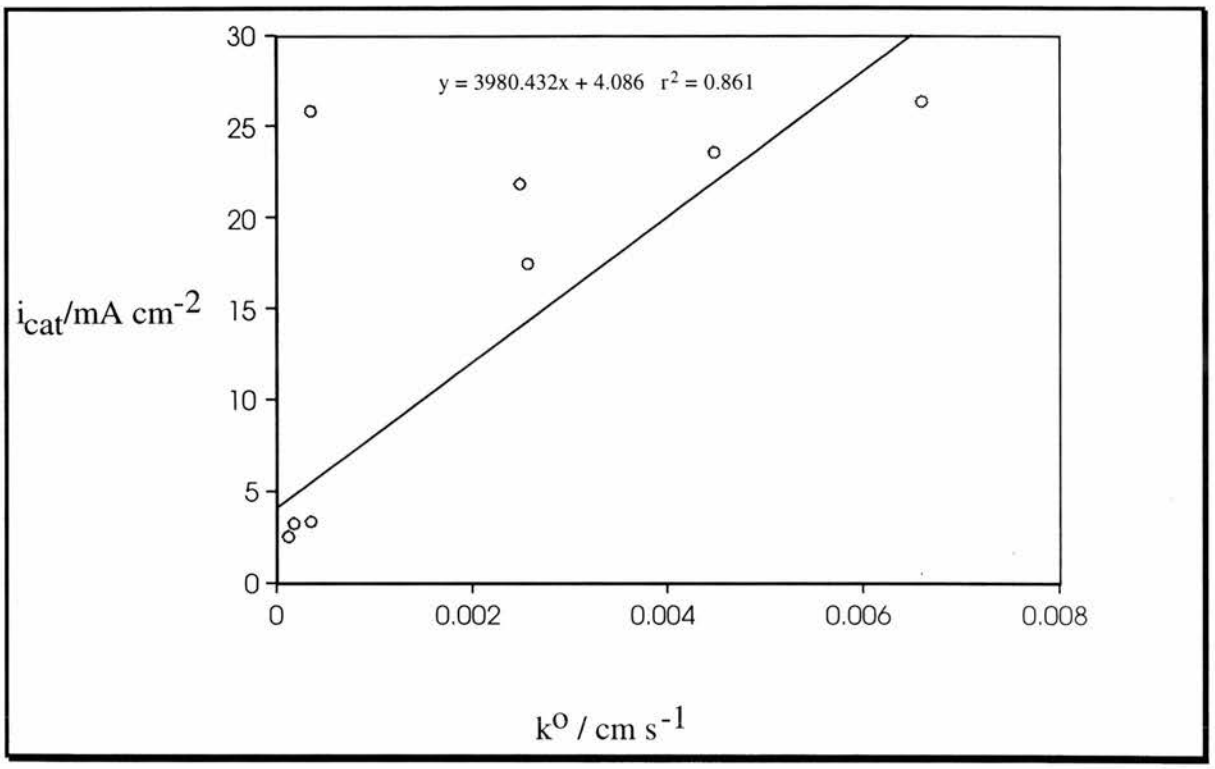

Figure 3.13: *Plot of the peak maximum of the catalytic current density , i_{cat}, vs k^0, the heterogeneous rate constant for the $Ni^{II/I}$ charge transfer on Hg.*

3.3.4.2 Peak Separation, Catalytic Efficiency and Macrocycle Structure

The ideal configuration for catalysis is shown below where one face of the macrocycle adsorbs onto the electrode surface presenting one face with an activated metal centre for carbon dioxide binding (Figure 3.14). $[Ni(cyclam)]^{2+}$ is probably so good at this because it is a very flat molecule.

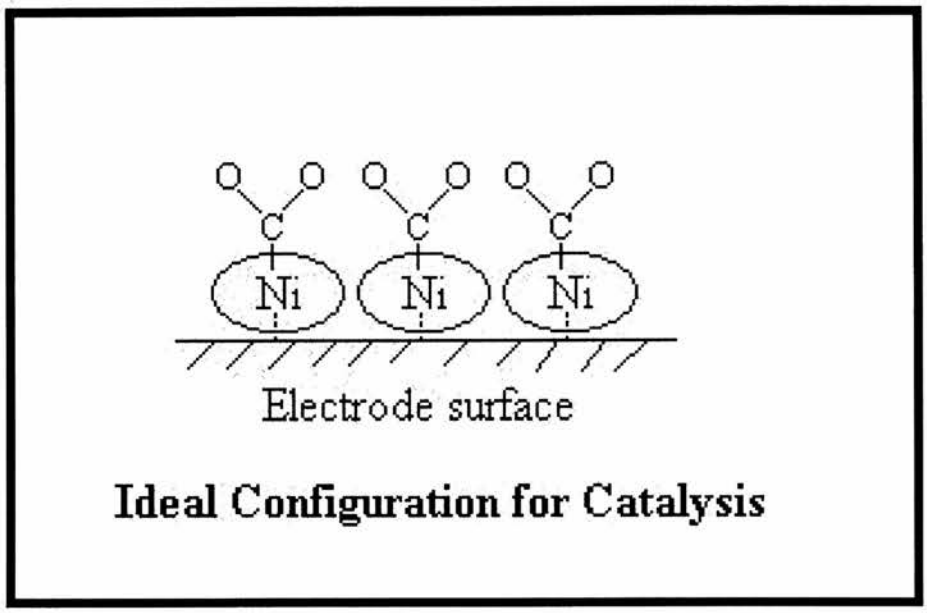

Figure 3.14: *Cartoon describing the ideal conditions for catalysis.*

We believe that there are two possible explanations for the poorer performance of the pendant arms macrocycles. Firstly, the side arm binds to the electrode surface (Figure 3.15, Type 1). Alternatively, the macrocycle binds to the electrode surface and the side arm is taking the space that would have been occupied by another macrocycle (Figure 3.15, Type2).

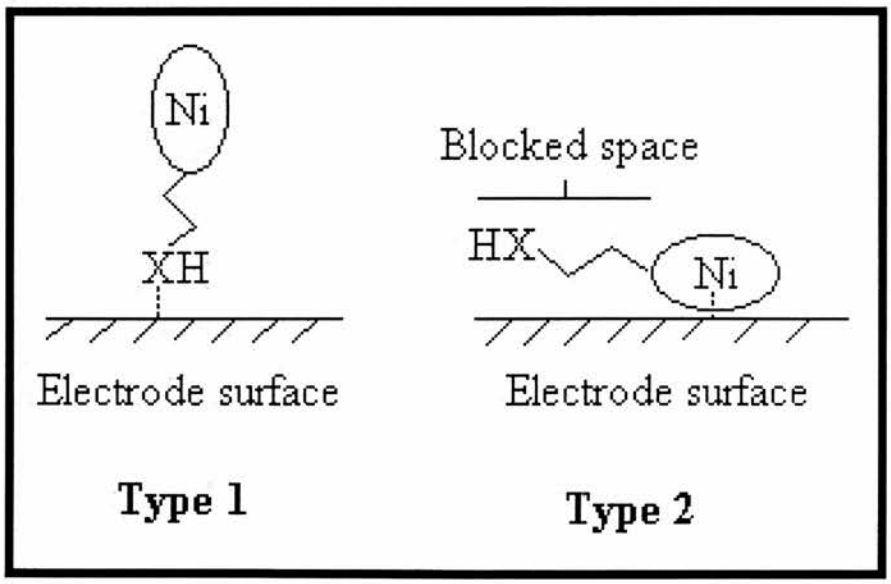

Figure 3.15: *Cartoon describing two binding orientations giving rise to poor catalytic efficiency.*

Both of these binding patterns would account for a reduction in catalytic current. We believe that for side arms such as the thioethyl pentaaza macrocycle investigated by de Alwis that the side arm is binding to the electrode (Figure 3.15, Type 1)[38]. As previously mentioned this Type 1 behaviour is also true for the aromatic ring side arm of $[Ni(L_2)]^{2+}$ and its catalytic current is much smaller than for $[Ni(L_1)]^{2+}$ (3.25 *vs* 23.6 mA cm^{-2}). Surprisingly, $[Ni(L_3)]^{2+}$ performs very poorly also (3.17 mA cm^{-2}) and this may be due to a poor interaction with the electrode as the ΔE_P value of 160 mV would suggest. This poor interaction with the electrode could be due to the structure of $[Ni(L_3)]^{2+}$ which, whilst similar to cyclam, is not as planar a molecule and as discussed earlier (*re:* isocyclam) small structural differences can have large effects on the catalytic current.

The binuclear bis-macrocyclic complex $[Ni_2(L_4)]^{4+}$ has a very large ΔE_P and a correspondingly poor i_{cat}. This was not a surprising result as we had observed this in a series of similar binuclear complexes. An explanation for this behaviour is that the rate of charge transfer to these types of molecules is slower because a greater degree of macrocycle strain is necessary prior to electron transfer and/or because one nickel centre is strongly adsorbed on the electrode, blocking fast electron transfer to the other nickel centre.

The three tertiary amine pendant arm complexes $[Ni(L_5\text{-}L_7)]^{2+}$ are interesting in their electrochemical and electrocatalytic behaviour. Under argon $[Ni(L_5)]^{2+}$ has a ΔE_P of 128 mV for the $Ni^{II/I}$ reaction on mercury whereas the $[Ni(L_5)]^{2+}$ is much lower at 90 mV. However, at the positive potential required for the $Ni^{III/II}$ reaction the ΔE_P's are very similar (90, 95 mV). Tertiary amines adsorb strongly on to the electrode surface resulting in poorer catalysis and a larger ΔE_P. However, $[Ni(L_6)]^{2+}$ is protonated at the tertiary amine and, therefore, does not interact with the electrode and consequently a lower ΔE_P is observed, 90mV. For the $Ni^{III/II}$ reaction at a positive

potential the unprotonated tertiary amine $[Ni(L_5)]^{2+}$ either loses an electron or becomes protonated thereby coming off the electrode surface and lowering the ΔE_P to a value similar to that of $[Ni(L_6)]^{2+}$, 90 and 95 mV respectively. This is clearly Type 1 behaviour. However, for $[Ni(L_7)]^{2+}$ this type of behaviour is not observed and the ΔE_P is actually slightly larger at the positive potential, 108 and 119 mV for $Ni^{II/I}$ and $Ni^{III/II}$ respectively. Whilst the pendant side arm contains a tertiary nitrogen it is part of the morpholine ring, the tertiary nitrogen has a pK_a of ~7.70, which is lower than that of triethylamine (10.7).

The behaviour of $[Ni(L_7)]^{2+}$ may be due to Type 2 activity. The same is probably true of $[Ni(L_8)]^{2+}$, which has a sulphoxide side arm. It has a low ΔE_P, 84 mV, and a slightly lower catalytic current than $[Ni(L_1)]^{2+}$ at 17.5 *cf.* 23.6 mA cm^{-2}.

In the same way that $[Ni(L_5)]^{2+}$ becomes protonated or oxidised in the $Ni^{III/II}$ reaction then in the catalytic reaction as CO_2 is bubbled through the reaction mixture the pH drops and the tertiary amine is oxidised, therefore, coming away from the electrode and catalysing at a similar rate to $[Ni(L_6)]^{2+}$. So $[Ni(L_5)]^{2+}$ starts as Type 1 and becomes Type 2 after the CO_2 lowers the pH and protonates then pendant amino group.

3.4 Summary and Conclusions

The reduction of carbon dioxide to carbon monoxide using nickel(II) macrocyclic complexes as electrocatalysts has been described. The catalytic currents for the complexes in the electrocatalytic reduction ranged from 3.17 – 26.4 mA cm^{-2} and had peak separations (ΔE_P) in the range 73 – 280 mV. The electrocatalytic activity of the various complexes appeared to fall into two categories termed Type 1 and Type 2.

Type 1 behaviour occurs when the pendant arm of the macrocycle binds to the electrode surface thus preventing or greatly impeding catalysis. Type 2 behaviour occurs when the macrocycle binds to the electrode surface and the pendant arm lies across the surface of the electrode occupying space that would otherwise have been taken up by another macrocycle and thus reducing catalytic activity.

The Type 2 complexes, $[Ni(L_1)]^{2+}$, $[Ni(L_6)]^{2+}$, $[Ni(L_7)]^{2+}$ and $[Ni(L_8)]^{2+}$ all showed low ΔE_P's (73-88 mV) for $Ni^{II/I}$ and reasonable catalytic currents for the reduction of carbon dioxide (17.5-26.4 mA cm^{-2}). $[Ni(L_5)]^{2+}$ started as Type 1 with a high ΔE_P and became a Type 2 species under reaction conditions as the pH dropped to catalyse at a similar rate to Type 2 species.

Of the other complexes tested, $[Ni(L_2)]^{2+}$ with the aromatic ring side arm is strongly Type 1 and had a high ΔE_P and a very low i_{cat}. Complex $[Ni(L_3)]^{2+}$ is not a pentaaza pendant side arm macrocycle and does not come under the Type 1 and 2 definitions but was poor for structural reasons: the six membered rings and the five membered ring do not sit well or adsorb well on to the electrode as we saw previously for isocyclam. The binuclear, dimeric complex $[Ni_2(L_4)]^{4+}$ is not a pendant arm macrocycle either and was a poor catalyst possibly due to a greater degree of

macrocycle strain prior to electron transfer or because one of the rings is strongly adsorbed onto the electrode, blocking efficient electron transfer to the other ring.

A wide range of nickel(II) macrocycles were tested in this study and a relationship emerged that was quite unexpected and had probably not been observed before due to the fact that most studies of this type concentrate on, structurally, closely related compounds. It became apparent that there existed a relationship between the catalytic current and peak separation. The reasons are unclear at present although follow-up reaction current peaks and catalytic current peaks for solution species are known to exhibit a shifting of the wave to potentials in advance of the redox potential, therefore, the electrochemical kinetics of the catalyst has exerted some influence on the observed current. When we plot the catalytic current against the heterogeneous rate constant, k^0, a linear plot results which suggest that the variations in the peak maxima are influenced largely by the rate of heterogeneous charge transfer.

This was a particularly interesting study and further work will concentrate on the observed relationship as well as further investigations of macrocycle structure on electrocatalytic activity.

3.5 Experimental

3.5.1 Electrochemistry

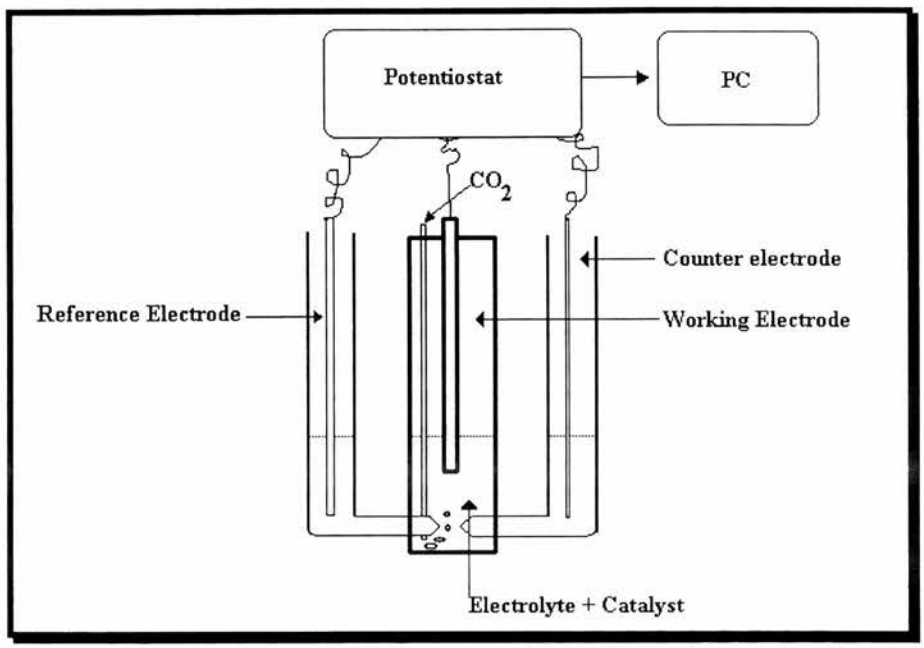

Figure 3.16: *Schematic diagram of the electrochemical cell.*

Cyclic voltammograms were recorded using an EG and G PARC 273A potentiostat/galvanostat controlled by version 4.11 of the Electrochemistry Research software running on a PC. The measurements were carried out using a three-necked glass cell using a saturated calomel electrode (SCE) as the reference with a Luggin capillary and a Pt wire as the counter (auxiliary) electrode (Figure 3.16). The working electrode was either a hanging mercury drop electrode (Metrohm, area = 0.0087 cm^2 and 0.0284 cm^2) or a mercury-plated silver disk electrode (0.0314 cm^2) The drop area of HMDE was determined by weighing the average of 10 drops[38]. The mercury-plated silver disk electrode was prepared by dipping the freshly-polished silver electrode into triply-distilled mercury for 10 min. Periodically, the hydrogen evolution background current in pH 7 buffer was checked to be less than 10 μA at -1.8 V, and re-dipped if necessary. A Pt micro-disc electrode (radius 68 μm) was used in chronoamperometry

measurements. The solution was purged with argon for 20 mins before each measurement and no IR compensation was used. A peak separation of 66 mV was observed for ferrocene under the same conditions. Unless stated all the measurements were done at room temperature (25 ^{0}C). The catalytic currents were recorded in saturated solutions of CO_2.

The water employed was triply distilled and acetonitrile (Aldrich HPLC grade) was used as the solvent. Acetonitrile was distilled from P_2O_5 in all-glass apparatus. The distillate was reflux over CaH_2 for an hour and then slowly distilled discarding the first 5 and last 10% of the distillate. Tetra-*n*-butylammonium hexafluorophosphate (TBAH, Fluka, electrochemical grade) as the supporting electrolyte.

3.5.2 Bulk Electrolysis

Bulk electrolysis was carried out in a specially designed air-tight cell with separated compartments for counter and reference electrodes. A mercury pool was used as a working electrode with 20 cm^3 exposed area. The cell volume was 125 cm^3 of which 90 cm^3 was occupied by gaseous products.

3.5.3 UV-Vis spectroscopy

Electronic absorption spectra were recorded on Perkin-Elmer spectrometer controlled by PE UV Winlab Lambda software.

3.5.4 Synthesis of the Complexes

3.5.4.1 Synthesis of $[Ni(L_{1,2,4})]^{n+}$

The synthesis of these complexes was discussed in Chapter 2.

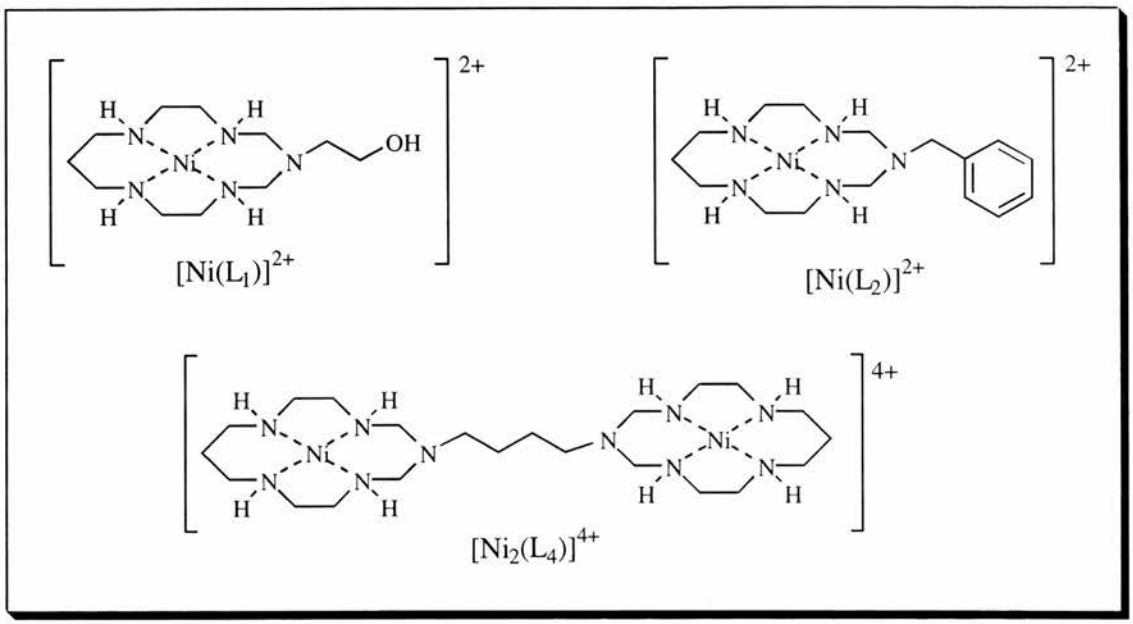

3.5.4.2 Synthesis of (1,4,8,12-tetraazacyclopentadecane)nickel(II) perchlorate;

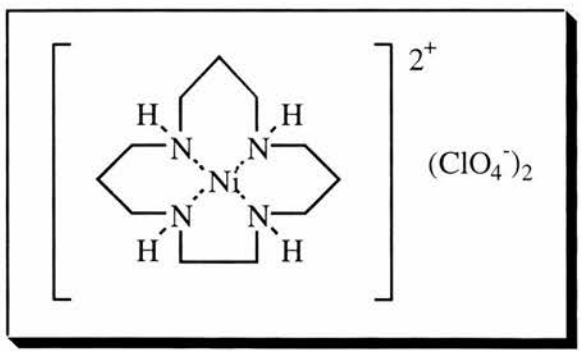

To a solution of 1,4,8,12-tetraazacyclopentadecane (0.2 g, 0.93 mmol) in ethanol (10 cm^3) was added a solution of $NiCl_2.6H_2O$ (0.24 g, mmol) in ethanol (10 cm^3). The solution was heated on

a steam bath for 10 minutes. 3 drops of perchloric acid (conc.) were added slowly and the mixture was heated for a further 10 minutes, an orange/ brown suspension resulted. The mixture was left to stand at room temperature overnight. The mixture was filtered and the resulting orange powder was washed with ether and dried *in vacuo* (0.37 g, 85%). Found: C, 28.05; H, 5.3; N, 11.7. Calc. for $C_{11}H_{26}N_4NiCl_2O_8$: C, 28.0; H, 5.55; N, 11.85 %. I.R./cm^{-1} 3220(m) ν(NH); 2929(m), 2865(m) ν(CH); 1634(w) ν(NH); 1454(m), 1437(m) ν(CN); 1144(s), 1091(s), 627(s) ν(ClO_4).

3.5.4.3 Synthesis of $[Ni(L_{5\text{-}8})](ClO_4)_2$

The complexes $[Ni(L_{5\text{-}8})](ClO_4)_2$ were supplied by Lampeka and Ludmilla, they were analytically pure and were used as received;

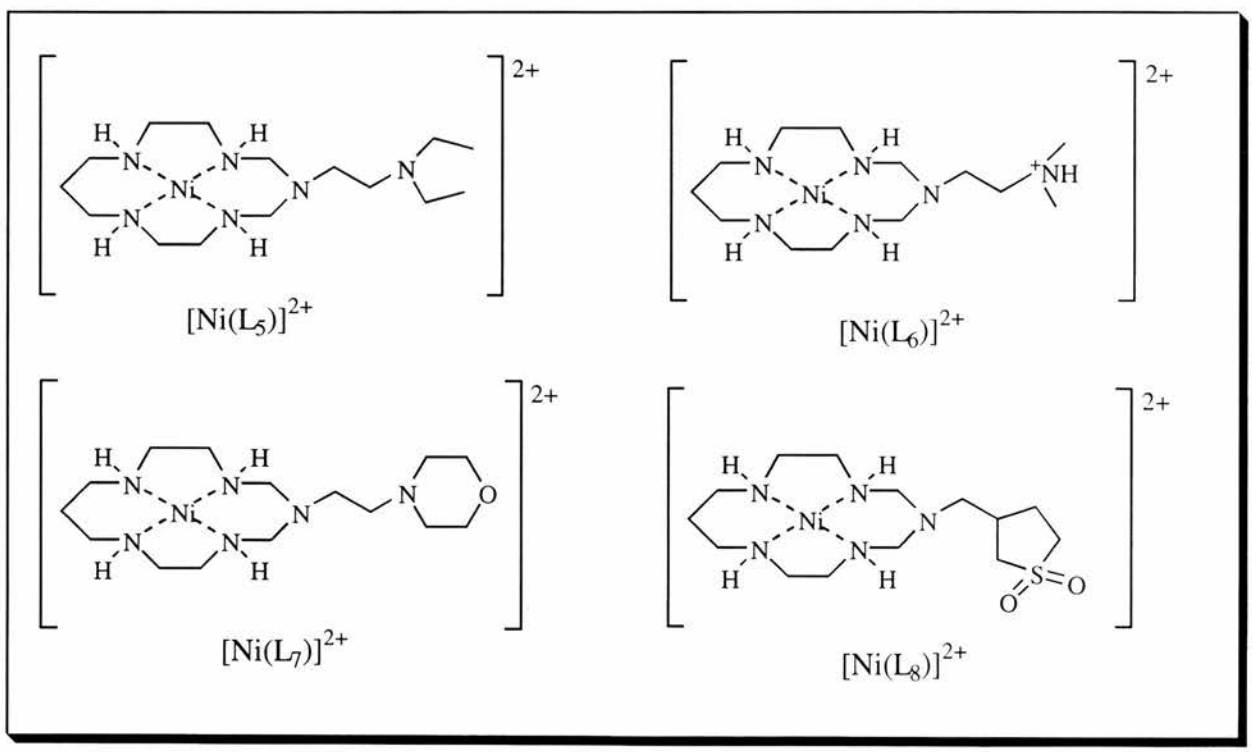

3.6 References

1. Source: IEA Greenhouse Gas R&D Programme, http://www.ieagreen.org.uk/index.htm
2. *Chem. Eng. News*, 1993, Oct 5, p4.
3. Source: Windows to the Universe, http://www.windows.ucar.edu/ at the University Corporation for Atmospheric Research (UCAR).
4. W. Leitner, *Angew. Chem. Int. Ed. Engl.*, 1995, **34**, 2207.
5. J. R. Justus and S. R. Fletcher, *The National Council for Science and the Environment*, 2001, April 11.
6. A.Irvine, *Electronic Telegraph*, 1999, March 5.
7. The Intergovernmental Panel on Climate Change (IPCC), Second Assessment, 1996.
8. B.P.Sullivan, K.Krist and H.E.Guard, "Electrochemical and Electrocatalytic Reduction of Carbon Dioxide", Elsevier, New York, 1993.
9. J. Costamagna, G. Ferraudi, J. Canales and J. Vargas, *Coord. Chem. Rev.*, 1996, **148**, 221.
10. Y. Hori, A. Murata and R. Takahashi, *J. Chem. Soc., Faraday Trans.*, 1989, **85**, 2309.
11. K. Ito, M. Yoshida and S. Ikeda, *Bull. Chem. Soc. Jpn.*,1985, **58**, 1353.
12. J. Fisher, T. Lehmann and E. Heitz, *J. Appl. Electrochem.*, 1981, **11**, 743.
13. S. Ikeda, T. Takagi and K. Ito, *Bull. Chem. Soc. Jpn.*, 1987, **60**, 2517.
14. K. Hara, A. Suneto, A. Kudo and T Sakata, *J. Electrochem. Soc.*, 1994, **141**, 2097.
15. Y. Hori, A. Murata, R. Takashi and S. Suzuky, *J. Chem. Soc., Chem.Commun.*, 1988, 17.
16. G. Z. Kyriacou and A. K. Anagnostopoulos, *J. Appl. Electrochem.*, 1993, **23**, 483.
17. P. G. Russel, N. Novac, S. Sirinivasan and M. Steinberg, *J. Electrochem. Soc.*, 1977, **124**, 1329.

18. H. Noda, S. Ikeda, Y. Oda, K. Imai, M. Maeda and K. Ito, *Bull. Chem. Soc. Jpn.*, 1990, **63**, 2459.

19. K. Ito, S. Ikeda, N. Yamauchi, T. Ikeda and T. Takagi, *Bull. Chem. Soc. Jpn.*, 1985, **58**, 3027.

20. B. R. Eggins, E. M. Benett and E. A. McMullan, *J. Electroanal. Chem.*,1996, **408**, 165.

21. A. Gennaro, A. A. Isse, M. G. Severin, E.Vianello, I. Bhugun and J-M. Saveant, *J. Chem. Soc. Faraday Trans.*, 1996, **92**, 3963

22. N. V. Ostrova, Y. V. Vasiliev, V. S. Bagotskii, R .G. Sadkova and A.F.Cherashev, A. P. Khrushch , *Elektrokhimiya*, 1984, **20**, 286.

23. D. P. Summers, S. Leach and K. W. Frese, *J. Electroanal. Chem.*, 1986, **205**, 219.

24. K. W. Frese and S. Leach, *J. Electrochem. Soc.*, 1985, **132**, 259.

25. Y. Hori, K. Kikuchi and S. Suzuki, *Chem. Lett.*, 1985, 1695.

26. Y. Hori, K. Kikuchi A. Murata and S. Suzuki, *Chem. Lett.*, 1986, 897.

27. R. L. Cook, R. C. Macduff and A. F. Sammells, *J. Electrochem. Soc.*, 1987, **134**, 2375.

28. R .L. Cook, R. C. Macduff and A. F. Sammells, *J. Electrochem.Soc.*, 1988, **135**, 1320.

29. J.J.Kim,D.P.Summers and K.W.Frese, *J. Electroanal. Chem.*, 1988, **245**, 223.

30. B. Fisher and R. Eisenberg, *J. Am. Chem. Soc.*, 1980, **102**, 7363.

31. M. Beley, J-P. Ruppert and J-P. Sauvage, *J. Chem. Soc., Chem. Commun.*, 1984, 1315.

32. M. Beley, J-P. Collin, J-P. Ruppert and J-P. Sauvage, *J. Am.Chem. Soc.*, 1986, **108**, 7461.

33. G. B. Balazs and F. C. Anson, *J. Electroanal. Chem.*, 1992, **322**, 325.

34. G. B. Balazs and F. C. Anson, *J. Electroanal. Chem.*, 1993, **361**, 149.

35. S. Sakaki, *J. Am. Chem. Soc.*, 1990, **112**, 2055.

36. D. J. Szalda, E. Fujita. R. Sanzenbacher, H. Paulus and H. Elias, *Inorg. Chem.*,1994, **33**, 5855.

37. R. R. Gagne and D. M. Ingle, *Inorg. Chem.*, 1981, **20**, 420.

38. D. C. L. de Alwis, Ph.D. Thesis, University of St Andrews. 1999

39. E. Fujita, J. Haff, R. Sanzenbacher and H. Elias, *Inorg. Chem.*, 1994, **33**, 4627.

40. C. I. Smith, J. A. Crayston and R. W. Hay, *J. Chem. Soc., Dalton Trans.*, 1993, 3267.

40a M. Beley, J-P Collin, R. Ruppert and J-P Sauvage, *J. Am. Chem. Soc.*, 1986, **108**, 7461.

41. A. J. Bard & L. R. Faulkner, Electrochemical Methods, Wiley, New York, 2001.

42. D. C. L. de Alwis, J. A. Crayston, T. J. Cromie, T. Eisenblätter, R. W. Hay, Ya. D. Lampeka and L. V. Tsymbal, *Electrochimica Acta*, 2000, **45**, 2061.

43. A. J. Bard and L. R. Faulkner, Electrochemical Methods, Wiley, New York, 1980.

44. R. S. Nicholson, *Anal. Chem.*, 1965, **37**, 1351.

45. Instrumental Methods in Electrochemistry, Southampton Electrochemistry Group, Ellis Horwood, 1985.

Chapter Four

Nickel(II) Pentaaza Macrocyclic Folding

4.1 Introduction

In the previous chapters we have discussed the synthesis and some of the chemical and electrochemical properties of a range of new and existing padlock macrocycles[1-4]. In this chapter we study the "folding" of such macrocycles by uv/vis spectrophotometry, paying particular attention to $[Ni(L_1)](ClO_4)_2$ where L_1 = 3-(2-hydroxyethyl)-1,3,5,8,12-penta-azacyclotetradecane Figure 4.1[5,6].

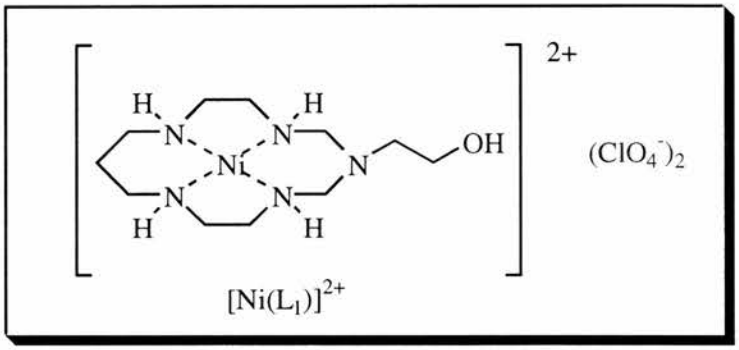

Figure 4.1

The pentaaza macrocycles previously discussed are all square planar about the nickel(II) centre and any additional ligands tend to add axially, e.g. the *trans*-dichloro and *trans*-diisothiocyanato complexes in Figure 4.2[5,6]:

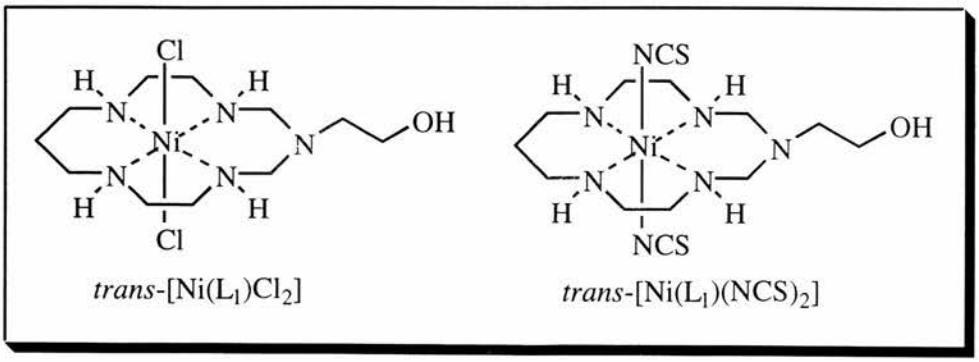

Figure 4.2

Coordinating solvents also add axially to square planar nickel(II) complexes to give *trans*-octahedral complexes. NMR spectra of square planar nickel(II) complexes must be carried out using non-coordinating solvents such as deuterated nitromethane. Coordinating NMR solvents such as D_2O, CD_3OD etc. add axially to form octahedral complexes nickel(II) complexes which are paramagnetic due to the unpaired electrons (see effect on NMR spectra in Chapter 2)[5,6].

In aqueous solution an equilibrium is established between the square planar nickel(II) complex and the octahedral nickel(II) complex, with water adding axially. This equilibrium for $[Ni(L_1)](ClO_4)_2$ was studied in detail (Scheme 4.1):

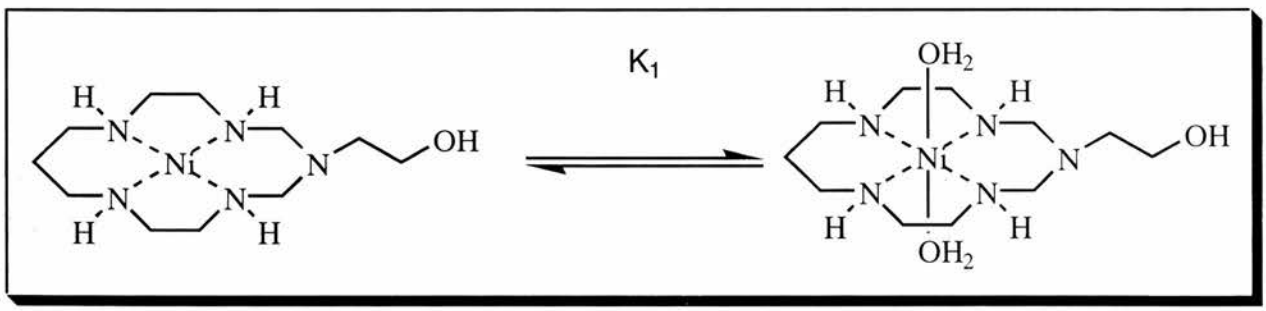

Scheme 4.1: *The square planar/*trans*-octahedral diaqua equilibrium of* $[Ni(L_1)]^{2+}$ *in water.*

This type of *trans* axial addition is not possible with chelating bidentate ligands such as 1,2-diaminoethane which will only bind in a *cis* manner forcing the planar macrocycle to "fold" out of the plane[7-9]. Billo and Margerum *et al.* have studied the kinetics of the reaction of $[Ni(cyclam)]^{2+}$ with a number of chelating bidentate ligands (1,2-diaminoethane, glycinate, oxalate) in detail. Billo suggests a reaction mechanism that goes through the *trans* diaqua complex followed by either: (i) displacement of one of the water molecules by the bidentate ligand and then folding; or, (ii) the diaqua complex folds spontaneously followed by displacement of the water molecules by the bidentate ligand (Scheme 4.2)[8,9].

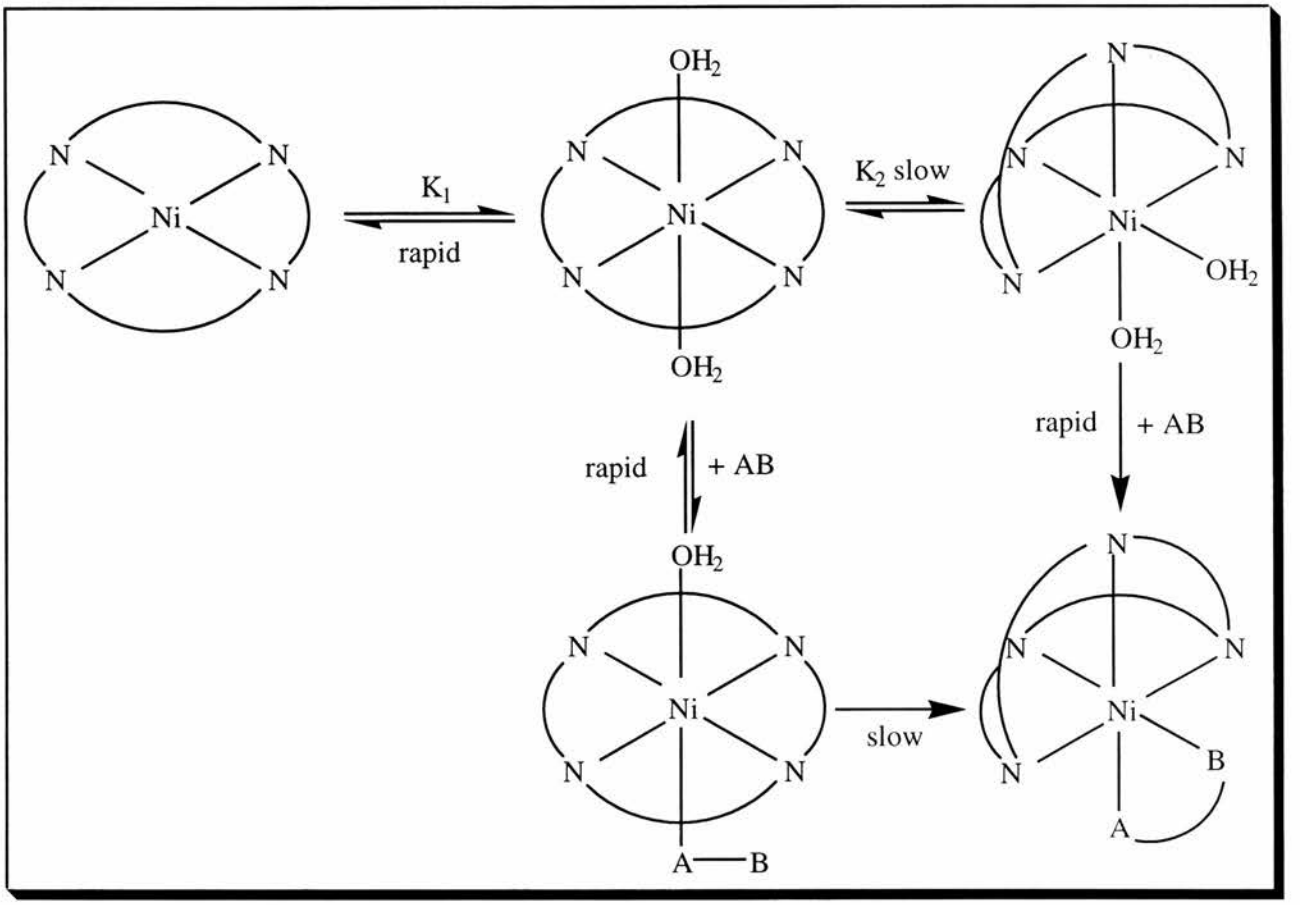

Scheme 4.2: *Reaction scheme proposed by Billo* et al. *for the folding of* $[Ni(cyclam)]^{2+}$ *with chelating bidentate ligands*[8].

We have studied the solution chemistry of the reaction shown in Scheme 4.3 between $[Ni(L_1)]^{2+}$ and 1,2-diaminoethane. As can be seen from the pictorial representation in Scheme 4.3 of $[Ni(L_1)(en)]^{2+}$ and in particular from the crystal structure (see Chapter 2) the macrocycle has been puckered out of the plane and out of shape[7]. This is clearly a rearrangement requiring significant amounts of energy. For this reason we propose an alternative mechanism (Scheme 4.4) to folding of this type which is driven by the chelating ligand and does not go through a *trans*-diaqua octahedral intermediate; indeed the square planar ⇌ *trans*-diaqua equilibrium competes with the chelation equilibrium.

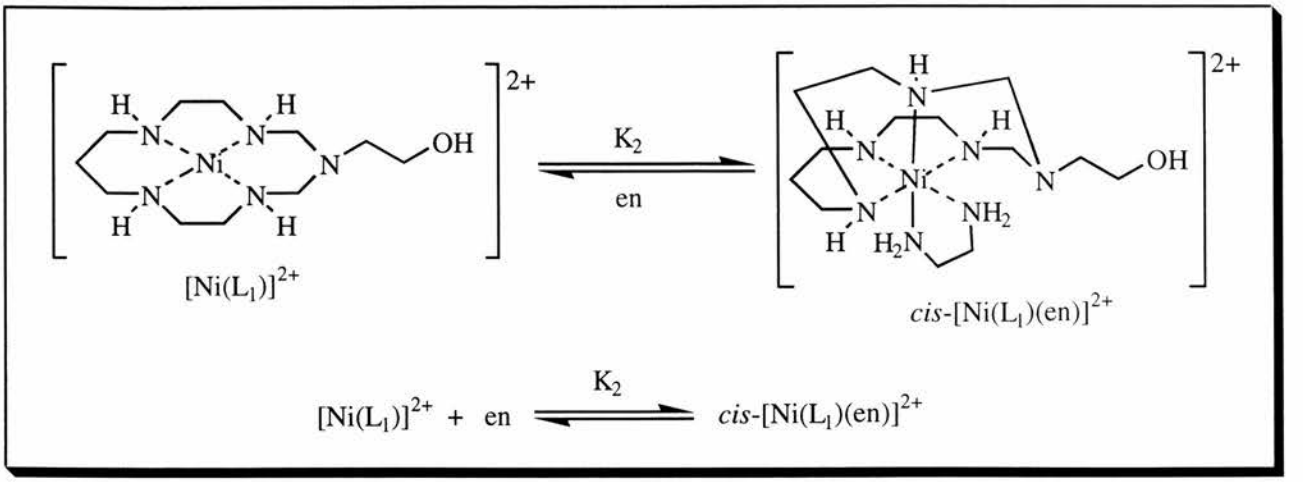

Scheme 4.3: *Showing the reaction of* $[Ni(L_1)]^{2+}$ *with 1,2-diaminoethane.*

The equilibrium between square planar and *trans*-diaqua octahedral lies very much to the left (87.1% square planar $[Ni(L_1)]^{2+}$, at 31 °C).

$$[Ni(L_1)]^{2+} + 2\,H_2O \rightleftharpoons [Ni(L_1)(OH_2)_2]^{2+} \qquad \text{(eqn4.1)}$$

Our initial data supports this mechanism in that our initial measurements of the folding process in solution were confusing until we took into consideration the competing *trans*-diaqua equilibrium. The reaction scheme we propose (Scheme 4.4) is based on this observation. This scheme suggests that the chelating ligand binds directly to the square planar nickel(II) centre and does not attack the *trans*-diaqua species in a displacement reaction of the type Billo suggests[8].

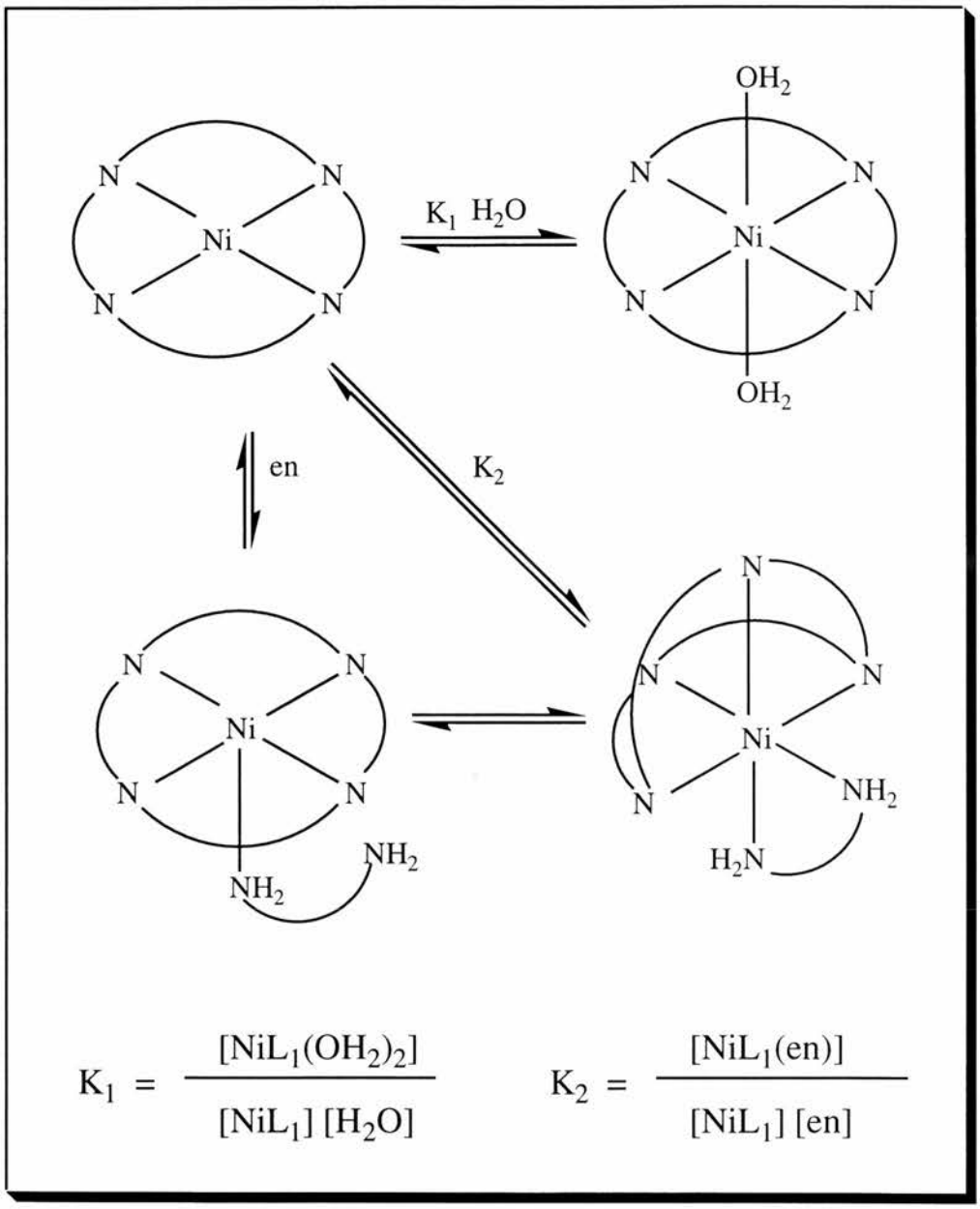

Scheme 4.4: *Showing the two competing equilibria set up in an aqueous solution of* $[Ni(L_1)]^{2+}$ *on addition of 1,2-diaminoethane.*

4.2.1 Results and Discussion

The square-planar to *trans*-diaqua octahedral equilibrium and the folding equilibrium in the presence of 1,2-diaminoethane were studied by visible spectrophotometric methods. Measurements were made using a Perkin Elmer Lambda 14 fitted with a Peltier cell or with a Phillips PU 8720 spectrophotometer which was thermostatted by circulating water.

4.2.2 The Square Planar - *Trans*-Diaqua Octahedral Equilibrium

The proportion of *cis*-$[Ni(L_1)(en)]^{2+}$ (λ_{max} = 535 nm, ε = 8.8 $dm^3\ mol^{-1}\ cm^{-1}$) (Figure 4.3) can be determined easily against known quantities of the square planar $[Ni(L_1)]^{2+}$ complex (λ_{max} = 460 nm, ε = 60 $dm^3\ mol^{-1}\ cm^{-1}$, in nitromethane) and 1,2-diaminoethane over a range of concentrations[6,9]. Since the reaction is performed in water, allowance must be made for the competing square planar $\rightleftharpoons$ *trans*-diaqua octahedral equilibrium. This extinction coefficient was measured in nitromethane in which the square planar form dominates and it can be assumed that no octahedral species are present since nitromethane is a noncoordinating solvent (Figure 4.3).

Knowing the total concentration of the aqueous $[Ni(L_1)]^{2+}$ solution and the extinction coefficient of planar Ni^{2+}, the proportion of square planar $[Ni(L_1)]^{2+}$ in solution can be calculated. Performing these experiments over a range of temperatures allows the values of K_1, $\Delta H°$ and $\Delta S°$ for the reaction to be determined.

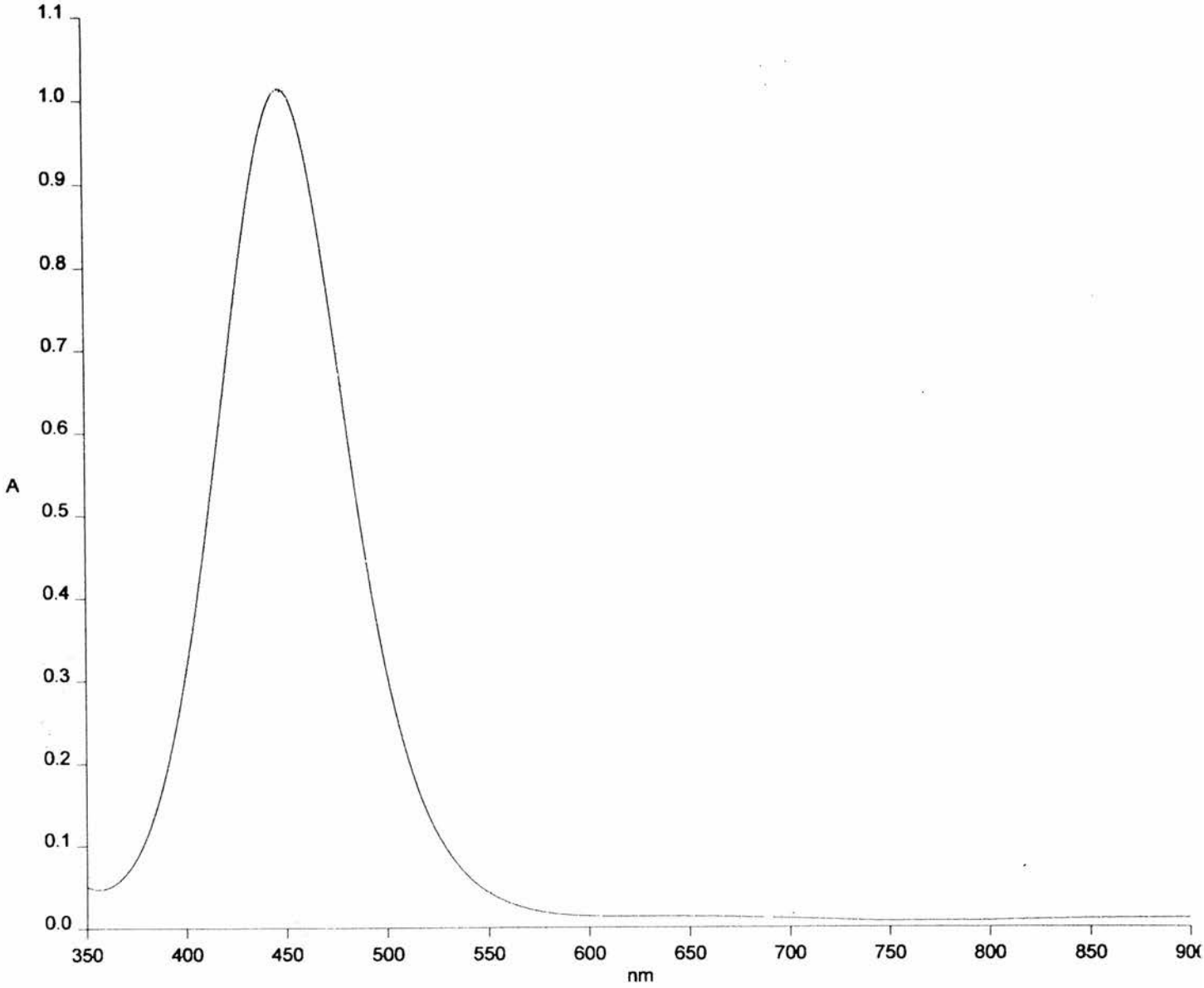

Figure 4.3: *Uv/vis spectrum of* $[Ni(L_1)](ClO_4)_2$ *in nitromethane,*

$\lambda_{max} = 460\ nm,\ \varepsilon = 60\ dm^3\ mol^{-1}\ cm^{-1}.$

4.2.2.1 Beer-Lambert's Law

According to Beer's Law the absorbance of a species is directly proportional to the concentration of that species:

$$\mathbf{A = \varepsilon c l} \qquad \text{(eqn 4.2)}$$

Where, A = absorbance

ε = extinction coefficient ($dm^3\ mol^{-1}\ cm^{-1}$)

c = concentration (mol dm^{-3})

l = cell path length (cm)

Using this relationship we can directly measure the concentration of square planar $[Ni(L_1)]^{2+}$ by uv/vis spectroscopy, starting with a solution of known concentration (1.93×10^{-2} mol dm^{-3}) and thereby calculate the proportion of *trans*-$[Ni(L_1)(OH_2)_2]^{2+}$ present.

Accordingly, K_1 was calculated for a range of temperatures, Table 4.1, and from these data $\Delta H°$ and $\Delta S°$ were determined using the Van't Hoff equation and plotting ln K *vs* 1/T. From the Gibbs equations we can derive thermodynamic information from physical measurements:

$$\Delta G = \Delta H - T\Delta S \qquad \text{(eqn 4.3)}$$

$$\Delta G = -RT\ln K \qquad \text{(eqn 4.4)}$$

so:

$$-RT\ln K = \Delta H - T\Delta S \qquad \text{(eqn 4.5)}$$

Therefore:

$$\ln K = \Delta S/R - \Delta H/RT \qquad \text{(eqn 4.6)}$$

Where lnK is the natural log of the equilibrium constant, R is the constant 8.314 J mol^{-1} K^{-1} and T is the temperature in Kelvin. A plot of lnK *vs* 1/T gives $\Delta S/R$ as the intercept and $-\Delta H/R$ as the gradient.

The data from these experiments are given in Table 4.1 and are plotted in Figure 4.4.

Table 4.1: *Temperature dependence of the equilibrium constant for the planar ⇌ octahedral equilibrium:* $[NiL_1]^{2+} + 2H_2O \rightleftharpoons [NiL_1(OH_2)_2]^{2+}$ *(eqn 4.1).*

Temp (°C)	Absorbance	% Planar	% Octahedral	K_1 (dm^3 mol^{-1})
31	1.01	87.1	12.9	0.149
36	1.06	91.0	9.0	0.100
53	1.12	96.6	3.4	0.036

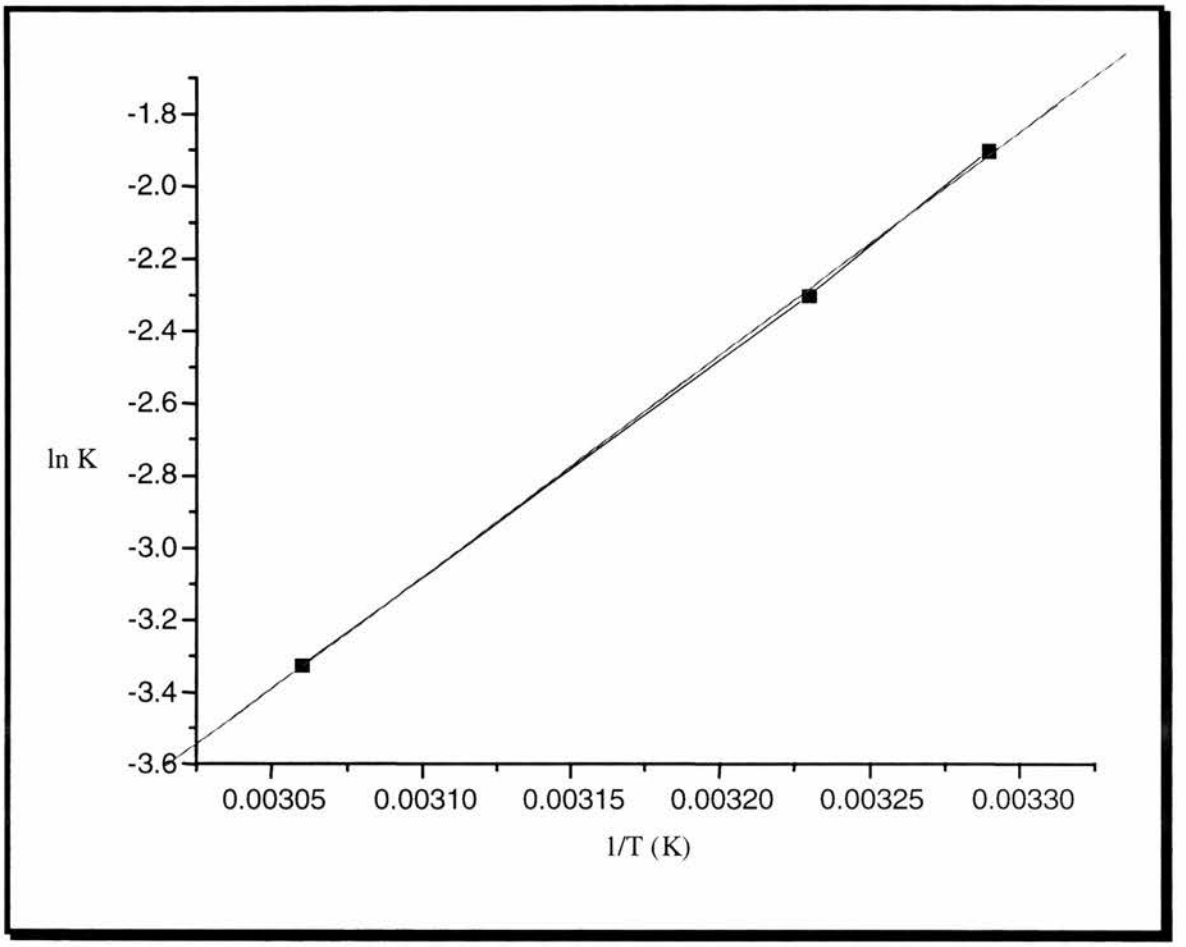

Figure 4.4: *Plot of lnK* vs *1/T for the trans-diaqua equilibrium.*

The line is fit with correlation factor of 0.99976 and the graph gives, ΔH = -55 kJ mol^{-1} and ΔS = -198 J K^{-1} mol^{-1}, Table 4.2.

The exothermic nature of the process (ΔH = -55 kJ mol^{-1}) reflects the increase in coordination number and the making of two new axial bonds. Similarly the negative ΔS of –198 J K^{-1} mol^{-1} reflects the increase in order as a result of the take up of two water molecules.

Table 4.2: *Thermodynamic data from the equilibrium:* $[Ni(L_1)]^{2+} + 2\ H_2O \Leftrightarrow [Ni(L_1)(H_2O)]^{2+}$

K_1 ($dm^3\ mol^{-1}$)(at 25 °C)	$\Delta H°$ (kJ mol^{-1})	$\Delta S°$ (J $K\ mol^{-1}$)
0.167	-55 ± 3	-198 ± 30

4.2.3 The Square Planar ⇌ *Cis*-1,2-Diaminoethano Octahedral Equilibrium in H_2O

Having determined the proportion of $[Ni(L_1)]^{2+}$ that is in the square planar form at various temperatures we were able to calculate the amount of the complex available for the *cis* folding reaction and thereby determine the thermodynamic data:

$$[Ni(L_1)]^{2+} + en \rightleftharpoons cis\text{-}[Ni(L_1)(en)]^{2+} \qquad \text{(eqn. 4.7)}$$

The experiments were run at 5 different temperatures and at each temperature 5 spectra were recorded for 5 different concentrations of 1,2-diaminoethane, starting at zero concentration of 1,2-diaminoethane and working up to 4 equivalents of the chelating ligand. This allowed us to determine an average equilibrium constant at each temperature and from those data to determine the thermodynamic parameters exactly as for the *trans*-diaqua equilibrium. The starting concentration of $[Ni(L_1)]^{2+}$ was 1.93×10^{-2} mol dm^{-3} for all the experiments and corresponds to an absorbance of 1.16. An example is given the next section of the experiments run at 42 °C.

4.2.3.1 The *Cis*-Folding Equilibrium at 42 °C

$[Ni(L_1)]^{2+} = 1.93 \times 10^{-2}$ mol dm^{-3}, from Beer's Law if pure planar then A = 1.16.

Observed starting A = 1.11, hence 95.69 % is present as square planar $Ni^{2+} = 1.847 \times 10^{-2}$ mol dm^{-3}.

Uv/vis spectra recorded at 42 °C are shown in Figure 4.5.

Table 4.3: *Spectroscopic and concentration data for the cis-folding experiment at 42 °C*

A	$[Ni(L_1)]^{2+}_{pl}$ ($x10^{-2}$)	$[Ni(L_1)(en)]^{2+}$ ($x\ 10^{-2}$)	[en]eqm ($x10^{-2}$)
1.11	1.847	0	0
0.468	0.777	1.12	0.81
0.235	0.39	1.52	2.34
0.128	0.212	1.71	4.08
0.091	0.151	1.77	5.95

The equilibrium at each concentration of 1,2-diaminoethane was calculated for the reaction:

$$K_2 = \frac{[NiL(en)]}{[NiL]\,[en]}$$

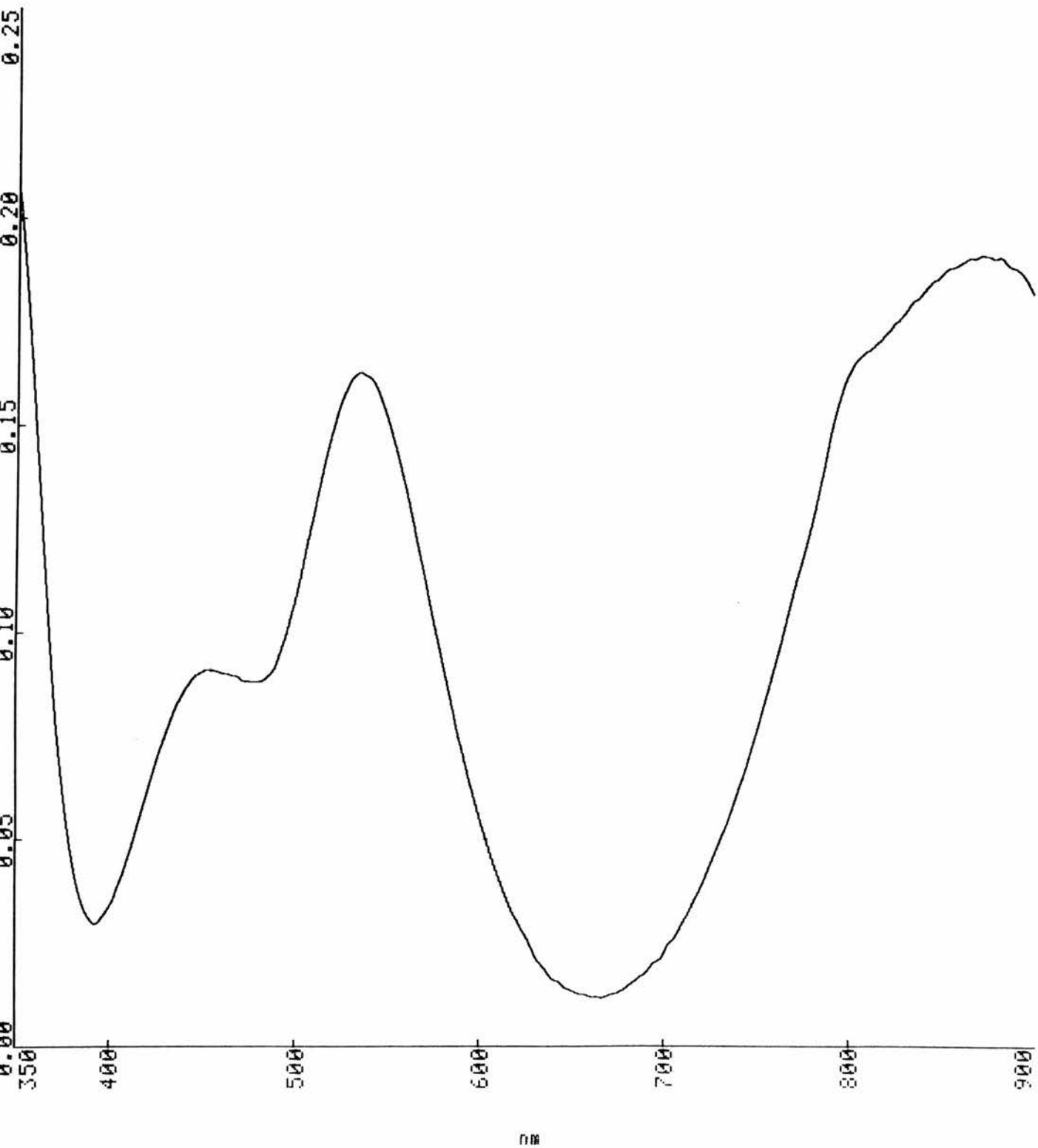

Figure 4.5: *Uv/vis spectrum of* $[Ni(L_1)](ClO_4)_2$ *+ 4 en in* H_2O *at 42 °C*

Table 4.4: *Equilibrium Constant Data for Added Equivalents of en*

Equivalents of en	Equilibrium Constant K_2 ($x10^2$ dm^3 mol^{-1})
1	1.78
2	1.67
3	1.98
4	1.97

The average for K_2 at 42 °C = 1.85 $x10^2$ dm^3 mol^{-1}

4.2.3.2 Results and Discussion of the Square Planar ⇌ *Cis*-1,2-Diaminoethano Octahedral Equilibrium in H_2O

The data calculated for all the temperatures measured are given in Table 4.5 and plotted in Figure 4.6:

Table 4.5: *Temperature dependence of the equilibrium constant for the planar ⇌ cis-octahedral equilibrium;* $[Ni(L_1)]^{2+} + en \rightleftharpoons [Ni(L_1)(en)]^{2+}$.

T (°C)	K_2 (dm^3 mol^{-1})
31	289
36	258
42	185
53	106
61	79

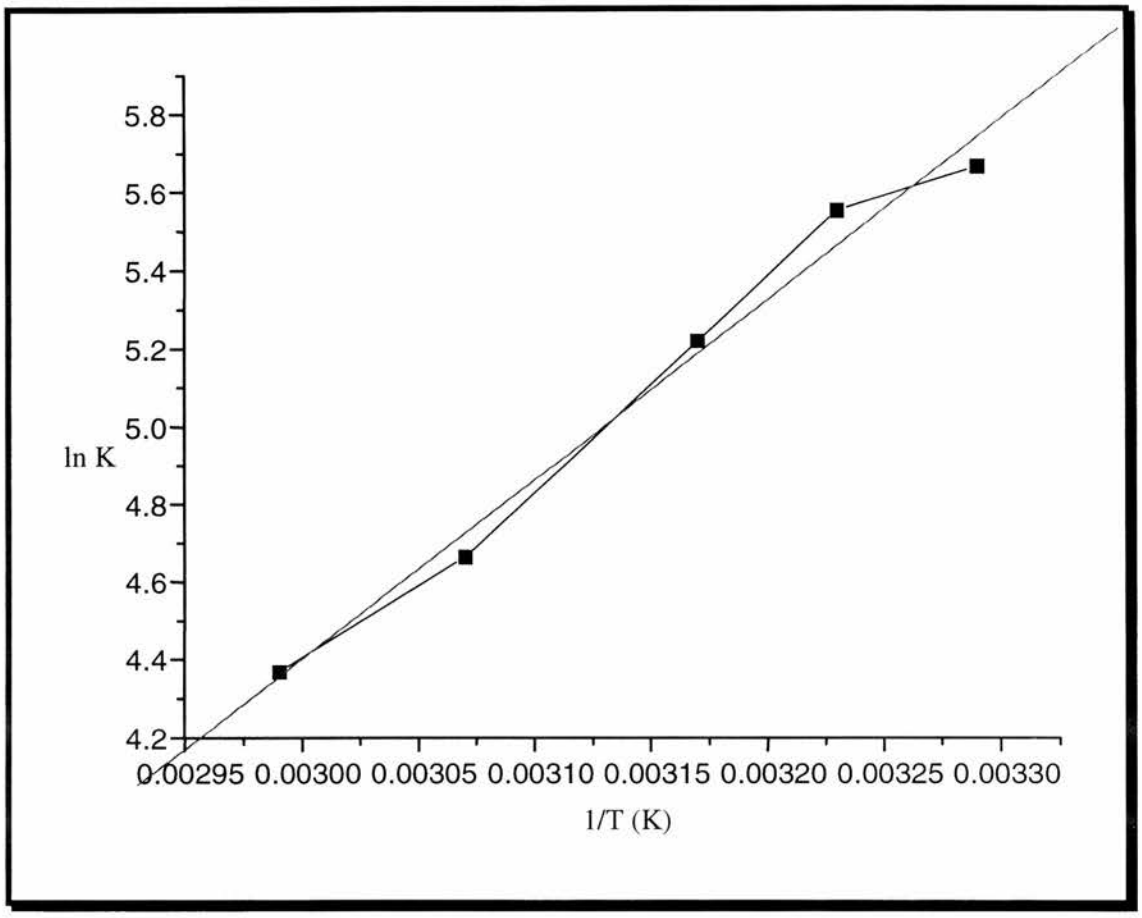

Figure 4.6: *Plot of lnK* vs *1/T for the* cis*-folding equilibrium.*

The planar ⇌ folded equilibrium is governed by K_2 (25 °C, Calc.) = 41.7 x 10^2 dm^3 mol^{-1}, $\Delta H°$ = -38.5 ± 2 kJ mol^{-1} and $\Delta S°$ = -79 ± 5 J K^{-1} mol^{-1}. The value of log K_2 at 25 °C (2.62) can be compared with the values reported previously by Billo (log K = 2.56) and by Margerum et al. (log K = 2.6) for the corresponding equilibrium involving the planar form of $[Ni(cyclam)]^{2+}$ with 1,2-diaminoethane[7,8]. Our results show that the presence of the pendant 2-hydroxyethyl group on the basic tetraazamacrocycle framework does not appear to have a significant influence on the position of the planar-folded equilibrium with such bidentate chelating ligands.

The $\Delta H°$ value of –38.5 kJ mol^{-1} is more endothermic than that found for the competing planar – *trans*-diaqua octahedral equilibrium which probably reflects the contribution from bond breaking

(since inversion occurs at one of the macrocycle N atoms accompanying the folding of the macrocycle) along with the making of two new Ni-N(en) bonds. The $\Delta S°$ for this process (-79 J K^{-1} mol^{-1}) is again negative, reflecting the decrease in order as a result of take up of the 1,2-diaminoethane ligand. But it is significantly less negative than that for the planar $\rightleftharpoons$ *trans*-diaqua octahedral process. This may be largely a result of a change from only two reacting species to one in this equilibrium but may also be due in part to solvation effects. The amino groups on 1,2-diaminoethane are highly solvated in free solution, therefore, the loss of solvation of 1,2-diaminoethane when it coordinates to the macrocycle may lead to greater disorder and, therefore, a less negative $\Delta S°$. The mechanism proposed by Billo was based on a kinetic study and the observation that the rate of the forward reaction was independent of bidentate ligand concentration, see Scheme 4.2[7]. Our thermodynamic study can neither confirm nor disprove Billo's mechanism since the Ni-N bond breaking with the macrocycle which is proposed as contributing to the more endothermic $\Delta H°$ value for the folding process compared with the competing planar $\rightleftharpoons$ *trans*-diaqua octahedral process could in principle be explained by folding of the Ni(II) macrocyclic complex either before or after complexation by the bidentate chelate ligand.

4.3 Test-tube Screening of Folding of Other Azamacrocycles

The following range of macrocycles were all assessed for folding in small test-tube reactions:

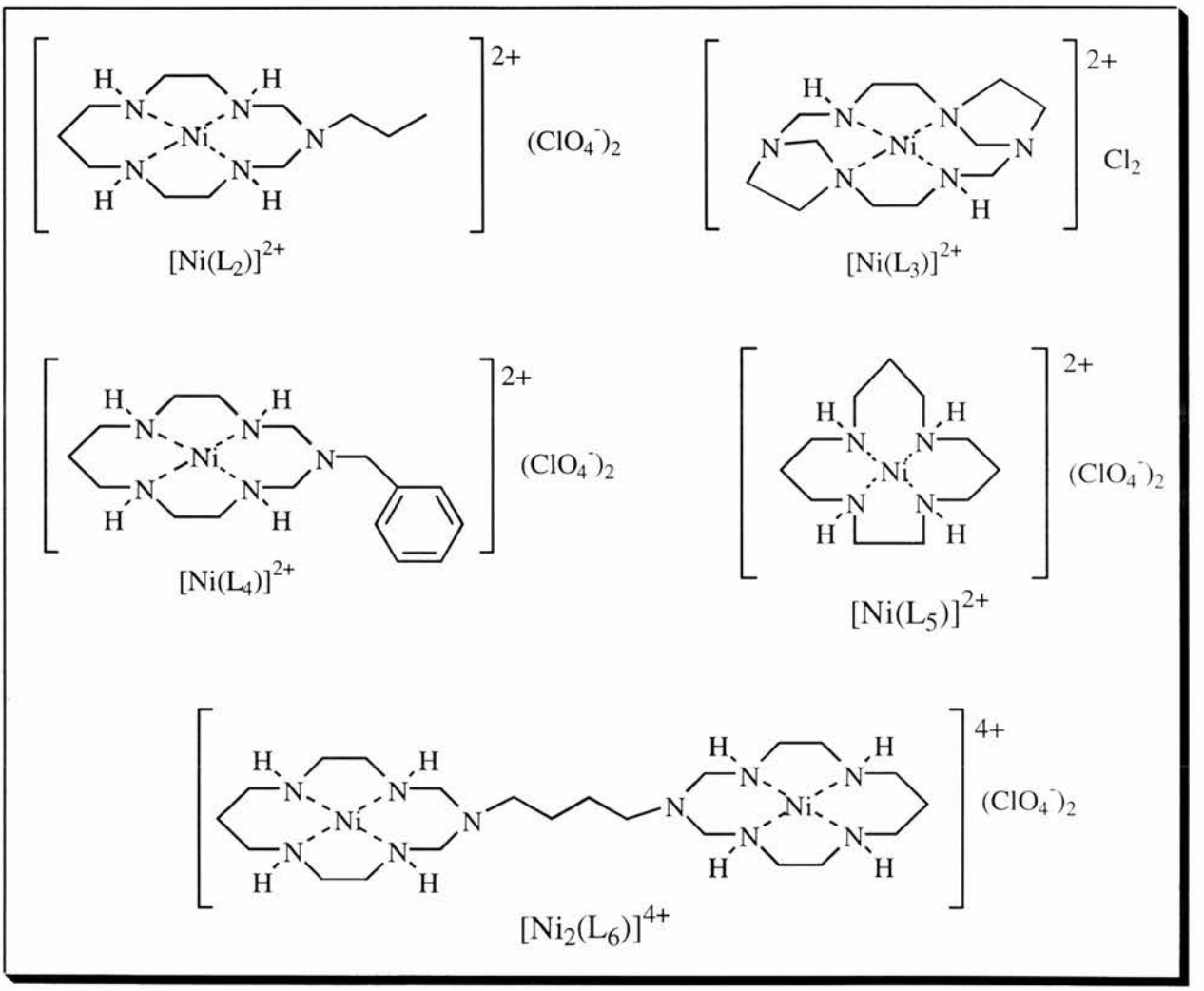

Figure 4.7: *The other azamacrocycles assessed for 1,2-diaminoethane folding.*

All the macrocycles tested gave orange aqueous solutions of the square planar nickel(II). On the addition of a few drops of 1,2-diaminoethane all of the solutions underwent a colour change to blue/purple except $[Ni(L_3)]^{2+}$ which changed to a pale pink colour, the uv/vis spectrum is shown in Figure 4.8.

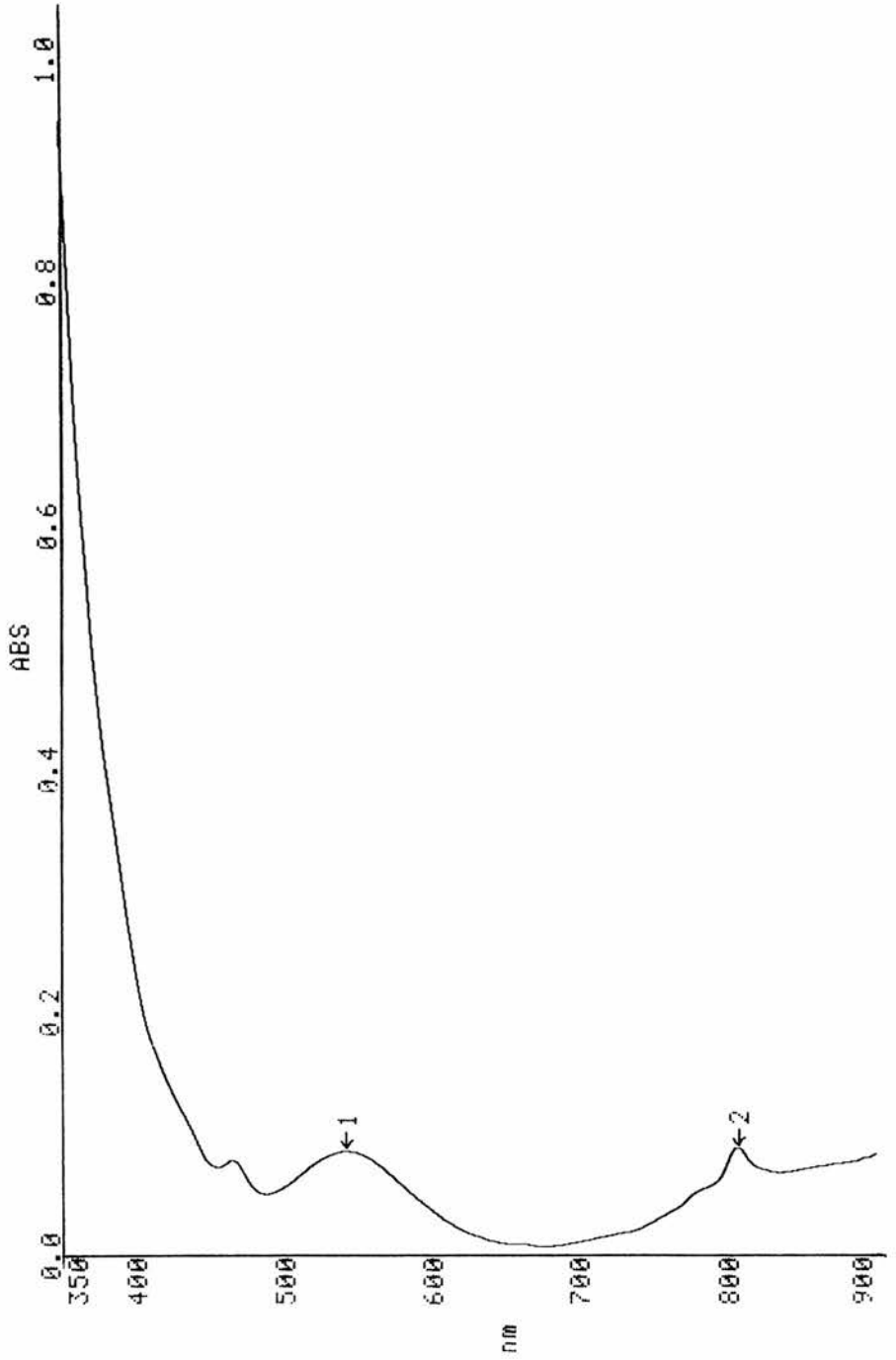

Figure 4.8: *Uv/vis spectrum of [Ni(L_3)en] showing the octahedral bands at 540 and 806 nm.*

This complex did not fold instantaneously as the others did, but required shaking and this was probably due to the steric effects of the two five membered rings of the tertiary nitrogens. After several seconds the solution of the complex did change colour to pale pink which is probably indicative of the weak ligand field surrounding the metal centre due to the strain of the steric restrictions. These systems will be studied in greater detail.

4.4 Conclusions and Future Work

The thermodynamics of the folding of [nickel(II)(3-hydroxyethyl-1,3,5,8,12-penta-azacyclotetradecane)] perchlorate, $[Ni(L_1)](ClO_4)_2$, by *cis*- chelation of 1,2-diaminothane have been described. The result of the folding is an octahedral complex of the ligand and bidentate 1,2-diaminoethane. One of the secondary nitrogens bound to the metal centre has had to invert to facilitate the folding which is quite an energetic process. The competing equilibrium of axially adding water has also been studied at a range of temperatures. The planar-*trans*-octahedral equilibrium is governed by: $K_1 = 0.167$, $\Delta H° = -55 \pm 3$ kJ mol^{-1} and $\Delta S° = -198 \pm 30$ J K^{-1} mol^{-1} and the planar-*cis*-folded equilibrium is governed by: $K_2 = 417$, $\Delta H° = -38.5 \pm 2$ kJ mol^{-1} and $\Delta S° = -79 \pm 5$ J K^{-1} mol^{-1}. The log of the equilibrium constant for the *cis*-folded process (2.62) compares favourably with that reported by Billo for a similar process studying the kinetics of cyclam folding in the presence of water (2.56), showing that the presence of the pendant arm did not significantly influence the position of the equilibrium.

A kinetic investigation of this process by stopped-flow over a range of *cis*- chelating ligands will be carried out. Further thermodynamic studies with a range of *cis*- chelating ligands will also be carried out, *cis*- chelating ligands such as: 2,2'-dipyridyl, 1,10-phenanthroline and acetylacetonate will be investigated.

This was an interesting study revealing some of the internal processes and energy requirements for the system. The crystal structure of the folded complex was described in chapter 2 and at the time this was the first example of an X-Ray crystal structure of this type.

4.5 Experimental

Measurements were made 1 cm quartz cuvettes using a Perkin Elmer Lambda 14 fitted with a Peltier cell or with a Phillips PU 8720 spectrophotometer which was thermostatted by circulating water.

The nickel(II) complexes $[Ni(L_1)](ClO_4)_2$ and $[Ni(L_{4\text{-}6})]^{2+}$ were prepared as described in Chapter 2. The complexes $[Ni(L_{2+3})]^{2+}$ were supplied by A. M. Danby.

4.6 References

1. L. Fabrizzi, A. M. Lanfredi, P. Pelavicini, A. Perotti, A Taglietti and F. Ugozzoli, *J. Chem. Soc. Dalton Trans.*, 1991, 3263.
2. R. W. Hay, A. Danby, P. Lightfoot and Y. D. Lampeka, *Polyhedron*, 1997, **16**, 2777.
3. I. M. Maloshtan, S. V. Rosokha and Y. D. Lampeka, *Zh. Neorg. Khim.*, 1994, **39**, 792.
4. S. V. Rosokha and Y. D. Lampeka, *J. Chem. Soc. Chem. Commun.*, 1991, 1077.
5. R. W. Hay, T. J. Cromie and P. Lightfoot, *Transition Met. Chem.*, 1997, **22**, 510.
6. R. W. Hay, J. A. Crayston, T. J. Cromie, P. Lightfoot and D. C. L. de Alwis, *Polyhedron*, 1997, **16**, 3557.
7. T. J. Cromie, R. W. Hay, P. Lightfoot, D. T. Richens and J. A. Crayston, *Polyhedron*, 2001, **20**, 307.
8. E. J. Billo, *Inorg. Chem.*, 1984, **23**, 2223.
9. D. W. Margerum, D. C. Weatherburn, G. Cayley, G. K. Pagenkopf, *ACS Monogr.* 1978, **No. 174**.

Chapter Five

Miscellaneous Syntheses

5.1 Introduction

This chapter describes other ligands and metal complexes which do not come under the umbrella of nickel(II) padlock macrocycles. During the course of the major project of the thesis, several exploratory projects were begun and the preliminary syntheses are described in this chapter.

The projects fall into four main areas:

i) *Trans*-dioxocyclam based ligands and complexes (Section 5.2).

ii) "Big Macs" (Section 5.5).

iii) Synthesis of dipeptides for the study of metal promoted peptide ester hydrolysis (Section 5.6).

iv) Copper cyclen complexes (Section 5.7).

Rather than explain each project in this section, it is more convenient to present the background, introduction and aims of each project in the appropriate sections.

During the course of the chapter X-ray crystal structures are presented for *trans*-dioxocyclam (1,4,8,11-tetraazacyclotetradecane-5,12-dione) dihydrate, nickel(II) trans-dioxocylam perchlorate and the copper(II) cyclen bromo cation. Characterisation data are presented where appropriate and discussions of the future and direction of the project are also presented.

5.2 *Trans*-dioxocyclam based ligands and complexes.

The dioxocyclams have been the subject of a great deal of research in recent years largely due to their thermodynamic and kinetic stability to metal ion dissociation which derives from the amide properties of the secondary nitrogen adjacent to the carbonyl and its effect on metal binding[1,2,3]. In addition the amide proton may be removed to give a ligand which is useful for stabilising high oxidation states. The dioxocyclams come in various isomeric forms, three of which are shown in Figure 5.1 and are non-systematically named *gem- cis-* and *trans-*[3].

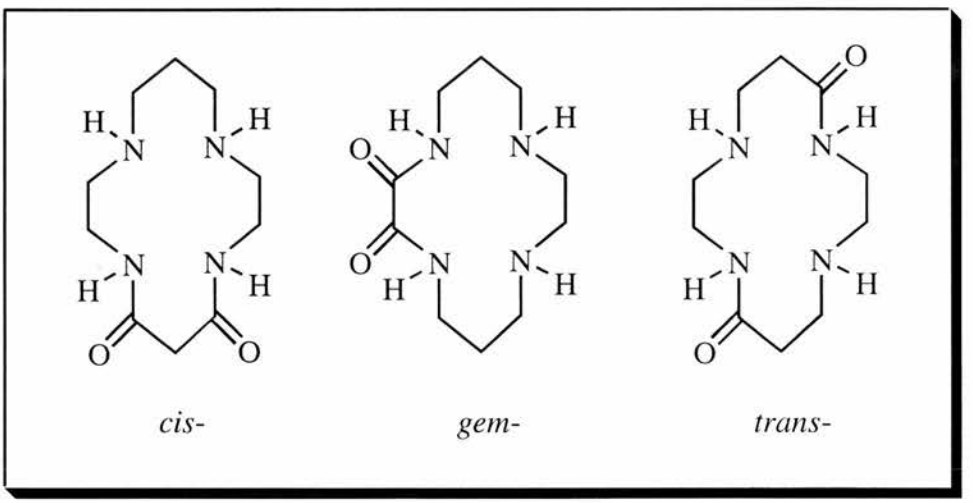

Figure 5.1

Our work concerned the much less well studied *trans*-dioxocyclam (1,4,8,11-tetraazacyclotetradecane-5,12-dione) ligand and the functionalisation of the secondary amines to provide additional binding sites on the macrocycle through pendant arms[1,2,4,5]. During the synthesis of the ligand we obtained crystals which were suitable for X-Ray crystallography. The structure of the nickel(II) complex of this ligand showed evidence for the characteristic deprotonation of the amide nitrogens on metal ion complexation[3] and crystals suitable for X-Ray diffraction were also obtained. At the time this work was carried out this was the first structure

determination of this ligand. In addition, the secondary amines were functionalised in a simple one-pot procedure with acrylonitrile to produce two cyanoethyl pendant arms. This reaction has been used successfully on cyclam previously[4].

5.2.1 Preparation of *trans*-dioxocyclam, 1,4,8,11-tetraazacyclotetradecane-5,12-dione dihydrate

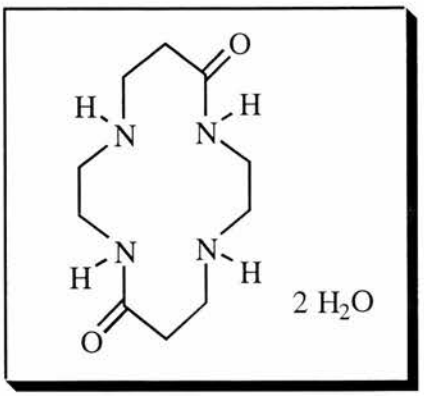

Figure 5.2

Methyl acrylate (9.18 cm^3, 102 mmol) was added dropwise with stirring to ethylene diamine (6.8 cm^3, 102 mmol) cooled in an ice bath over 1 hr. The resulting solution was stirred for several days after which time no discernible odour remained. The solution had become viscous and was heated on a water bath at *ca.* 70 °C. The solution became more viscous and was dissolved in water (*ca.* 20 cm^3) with difficulty. The water was removed under reduced pressure and the resulting oil left to stand for several days after which time clear, colourless crystals were obtained. The crystals were filtered, washed with ethanol and ether and dried *in vacuo*, the crystals were suitable for X-Ray crystallography (1.26 g, 4.7%). Found: C, 45.5; H, 9.2; N, 21.15. Calc. for $C_{10}H_{24}N_4O_4$: C, 45.4; H, 9.15; N, 21.2.

5.2.2 Preparation of nickel(II) *trans*-dioxocyclam dihydrate

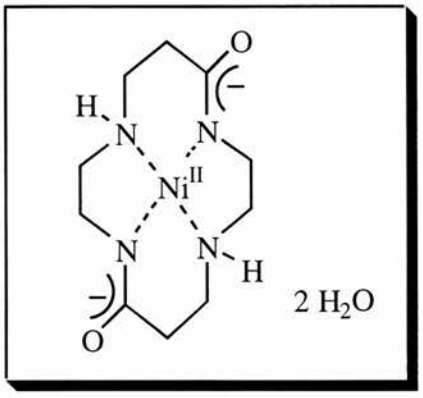

Figure 5.3

Trans-dioxocyclam (250 mg, 1.02 mmol) was dissolved in water (5 cm^3) and added to an aqueous solution of nickel perchlorate hexahydrate (0.373 g, 1.02 mmol). The resulting solution was warmed gently on a water bath until the solution turned orange. It was then left to stand at room temperature. After several days small orange crystals were obtained. These were filtered, washed with ethanol and ether and dried *in vacuo* and were suitable for X-Ray crystallography (261 mg, 79%). Found: C, 37.3; H, 6.95; N, 17.25. Calc. for $C_{10}H_{22}N_4O_4Ni$: C, 37.4; H, 6.9; N, 17.45.

5.2.3 Preparation of *trans*-dioxocyclam cyano pendant arm ligand

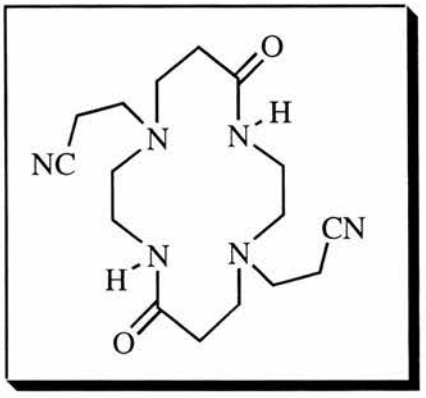

Figure 5.4

Trans-dioxocyclam (250 mg, 0.95 mmol) was dissolved in acrylonitrile (50 cm^3) and refluxed for 2 hrs. On cooling the solution was reduced in volume *in vacuo* and allowed to stand in the refrigerator for several days after which time a white precipitate formed. The precipitate was filtered, washed with ether and dried *in vacuo*. The yield was less than 100 mg.

Found: C, 58.15; H, 7.95; N, 25.5. Calc. for $C_{16}H_{24}N_6O_4$: C, 57.45; H, 7.85; N, 25.15.

5.3 Crystal Structure Determinations using X-ray Diffraction

5.3.1 Crystal Structure Determination of *trans*-dioxocyclam, 1,4,8,11-tetraazacyclotetradecane-5,12-dione

The ORTEP view, with the ring numbering system, of the free ligand *trans*-dioxocyclam dihydrate looking down the axial axis of the ligand is shown in Figure 5.5. Tables 1 to 3 summarise the atomic coordinates, bond distances and bond angles.

Suitable crystals for X-Ray diffraction studies were obtained by slow crystallisation of the ligand from reaction mixture. This structure was determined by the School's crystallography service in 1997. Structural parameters are very similar to the very recently reported data[5]. All the C-C bond lengths are in the range 1.522(7)Å to 1.531(7)Å which are a little shorter than the standard C-C bond length of 1.544Å in diamond. This is due to the nature of the ring containing two secondary nitrogens and two amides which has the affect of shortening the C-C bonds. The shortest bond is the C(4)-C(5) (1.522Å) bond and this is to be expected as C(4) is bound to N(2), a secondary amine and C(5) is bound to N(1) an amide. The C-N bond lengths for the amines are: C(4)-N(2) 1.448(6)Å and C(3)-N(2) 1.469(6)Å the C(4)-N(2) is a little short than that expected and is due to the proximity to the amide. The C-N bonds lengths are: C(1)-N(1) 1.354(6)Å and C(5)-N(1) 1.470(6)Å, the shortness of the C(1)-N(1) bond indicates a significant amount of the tautomeric form of the amide as this bond length is closer to the C=N bond length of *ca* 1.322Å. The C(5)-N(1) bond length is much closer to the typical length for a C-N single bond of 1.479Å.

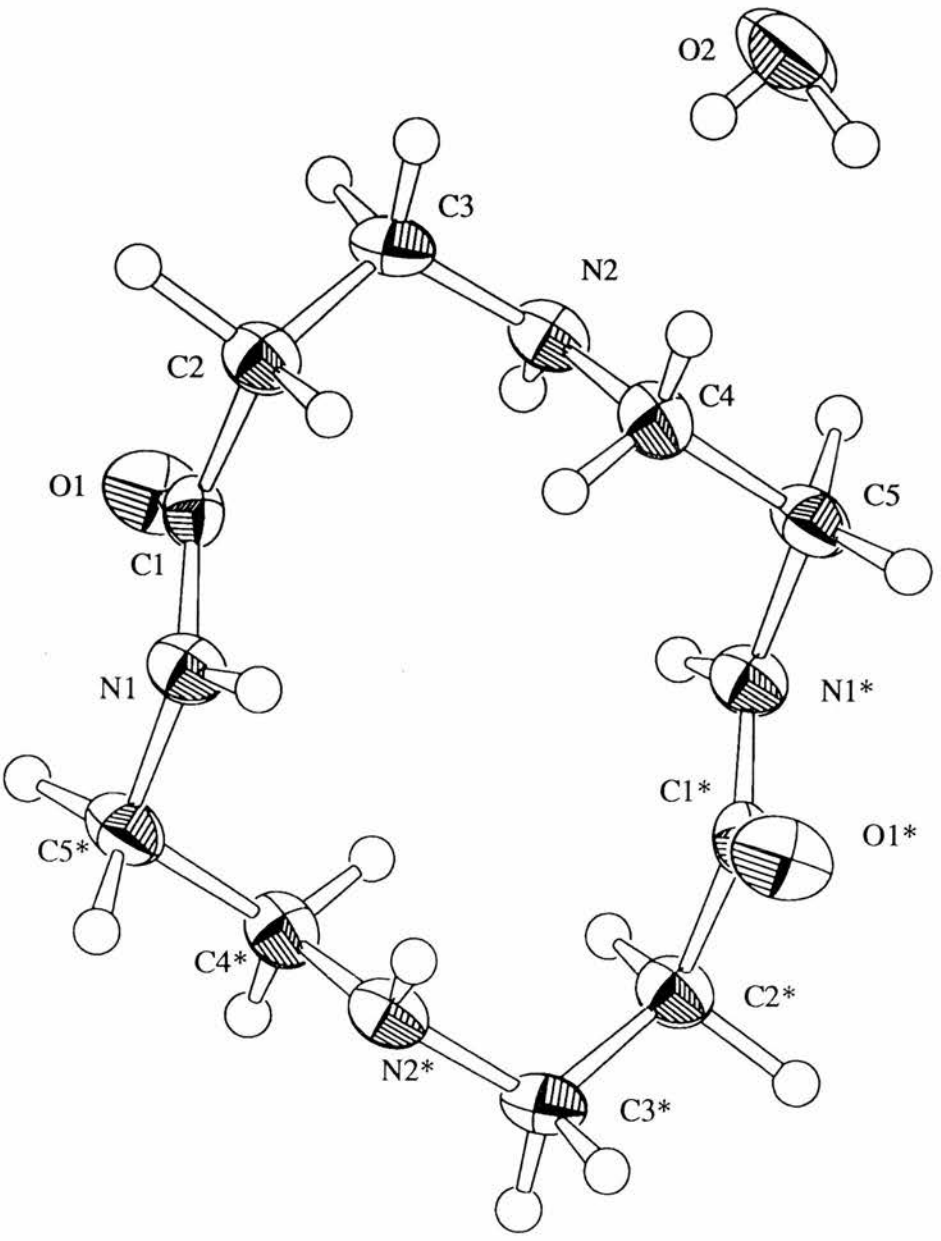

Figure 5.5: *ORTEP view of* trans-*dioxocyclam*

5.3.2 Data Collection

A colourless needle crystal of $C_{10}H_{24}N_4O_4$ having approximate dimensions of 0.45 x 0.2 x 0.20 mm was mounted on a glass fibre. All measurements were made on a Rigaku AFC7S diffractometer with graphite monochromated Mo-Kα radiation.

Cell constants and an orientation matrix for data collection, obtained from a least-squares refinement using the setting angles of 25 carefully centred reflections in the range $22.87 < 2\theta < 24.94°$ corresponded to a C-centred monoclinic cell with dimensions:

a = 7.571(1)Å	$\alpha = 91.35(3)°$
b = 9.193(2)Å	$\beta = 100.26(3)°$
c = 4.886(4)Å	$\gamma = 82.77(1)°$
V = 332.0(3)Å^3	

For Z = 1 and F.W. = 264.32, the calculated density is 1.32 g/cm^3. Based on the systematic absences of:

$P\bar{1}$ (#2)

The data were collected at a temperature of 20 ± 1 °C using the ω-2θ scan technique to a maximum 2θ value of 50.0°.Omega scans of several intense reflections, made prior to data collection, had an average width at half-height of 0.32° with a take-off angle of 6.0°. Scans of $(1.26 + 0.35 \tan \theta)°$ were made at a speed of 16.0° /min (in omega). The weak reflections (I <

15.0σ(I)) were rescanned (maximum of 4 scans) and the counts were accumulated to ensure good counting statistics. Stationary background counts were recorded on each side of the reflection. The ratio of peak counting time to background counting time was 2:1. The diameter of the incident beam collimator was 1.0 mm and the crystal to detector distance was 235 mm, The computer-controlled slits were set to 9.0 mm (horizontal) and 13.0 mm (vertical).

5.3.3 Data Reduction

Of the 1259 reflections which were collected, 1163 were unique (R_{int} = 0.028). The intensities of three representative reflection were measured after every 150 reflections. No decay correction was applied.

The linear absorption coefficient, μ, for Mo-Kα radiation is 1.0 cm^{-1}. Azimuthal scans of several reflections indicated no need for an absorption correction. The data were corrected for Lorentz and polarization effects.

5.3.4 Structure Solution and Refinement

For the relevant references please refer to Chapter 2 references 27 – 35.

The structure was solved by direct methods and expanded using Fourier techniques. The non-hydrogen atoms were refined anisotropically. The final cycle of full-matrix least-squares refinement was based on 969 observed reflections (I > 3.00σ(I)) and 131 variable parameters and converged (largest parameter shift was 0.42 times its esd) with unweighted and weighted agreement factors of:

$$R = \Sigma \, ||Fo| - |Fc|| \, / \, \Sigma \, |Fo| = 0.077$$

$$R_w = \sqrt{(\Sigma\omega(|Fo| - |Fc|)^2/\Sigma\omega Fo^2)} = 0.084$$

The standard deviation of an observation of unit weight was 6.56. The weighting scheme was based on counting statistics and included a factor (p = 0.003) to downweight the intense reflections. Plots of $\Sigma w \, (|Fo| - |Fc|)^2$ versus $|Fo|$, reflection order in data collection, sin θ/λ and various classes of indices showed no unusual trends. The maximum and minimum peaks on the final difference Fourier map corresponded to 0.30 and -0.39 $e^-/ Å^3$, respectively.

Neutral atom scattering factors were taken from Cromer and Waber. Anomalous dispersion effects were included in Fcalc; the values for $\Delta f'$ and $\Delta f''$ were those of Creagh and McAuley. The values for the mass attenuation coefficients are those of Creagh and Hubbel. All calculations were performed using the teXsan crystallographic software package of Molecular Structure Corporation.

Table 1 Atomic coordinates

atom	x	y	z
O(1)	0.2328(5)	0.5556(4)	1.0401(7)
O(2)	-0.4085(6)	0.9847(5)	0.775(1)
N(1)	0.3019(5)	0.4899(4)	0.6168(8)
N(2)	-0.1258(6)	0.7574(5)	0.6992(9)
C(1)	0.2517(6)	0.5882(5)	0.8079(9)
C(2)	0.2140(7)	0.7470(5)	0.706(1)

C(3)	0.0412(7)	0.8239(5)	0.793(1)
C(4)	-0.1742(7)	0.7446(6)	0.400(1)
C(5)	-0.3417(7)	0.6670(5)	0.314(1)

Table 2 Bond Lengths(Å)

Atom	atom	Distance	atom	atom	distance
O(1)	C(1)	1.218(5)	N(1)	C(1)	1.354(6)
N(1)	C(5)	1.470(6)	N(2)	C(3)	1.469(6)
N(2)	C(4)	1.448(6)	C(1)	C(2)	1.529(6)
C(2)	C(3)	1.531(7)	C(4)	C(5)	1.522(7)

Table 3 Bond Angles(°)

Atom	atom	atom	angle	atom	atom	atom	angle
C(1)	N(1)	C(5)	120.3(4)	C(3)	N(2)	C(4)	114.2(4)
O(1)	C(1)	N(1)	124.1(4)	O(1)	C(1)	C(2)	121.6(4)
N(1)	C(1)	C(2)	114.3(4)	C(1)	C(2)	C(3)	110.7(4)
N(2)	C(3)	C(2)	116.9(4)	N(2)	C(4)	C(5)	112.1(4)
N(1)	C(5)	C(4)	110.9(4)				

5.4 Crystal Structure Determination of nickel(II) *trans*-dioxocyclam dihydrate

Note: All the previously reported X-Ray crystal structures were determined by Dr. P. Lightfoot who ran the departmental service at the time. The current departmental service is run by Dr. A. Slawin and the following structures were determined by her using a different presentation format and a different graphics package. The structures are, therefore, presented as received.

The ORTEP view of the cation for nickel(II) *trans*-dioxocyclam dihydrate looking down the axial axis of the complex is shown in Figure 5.6. Tables 4 to 7 summarise the experimental parameters, atomic coordinates, bond distances and bond angles. The structure is very similar to that of nickel(II) cyclam as would be expected. The Ni-N(amide) bond lengths 1.879(3)Å are shorter than the Ni-N(amine) bond lengths of 1.898(2)Å which is to be expected given that the amide nitrogens are deprotonated and are therefore more basic and better sigma donors. As in the free ligand the C-N(amide) bond lengths are shorter than expected at 1.329(4)Å indicative of the tautomer. A recent paper presented the X-Ray crystal structure of nickel(II) *cis*-dioxocyclam in which the C-N(amide) bond lengths were even shorter at 1.311Å which is probably due to a greater extent of conjugation[6]. The Ni-N bond lengths were also different in the *cis*- isomer in that the metal sits much closer to the two deprotonated amide nitrogens (1.855Å) than the two amines (1.940Å).

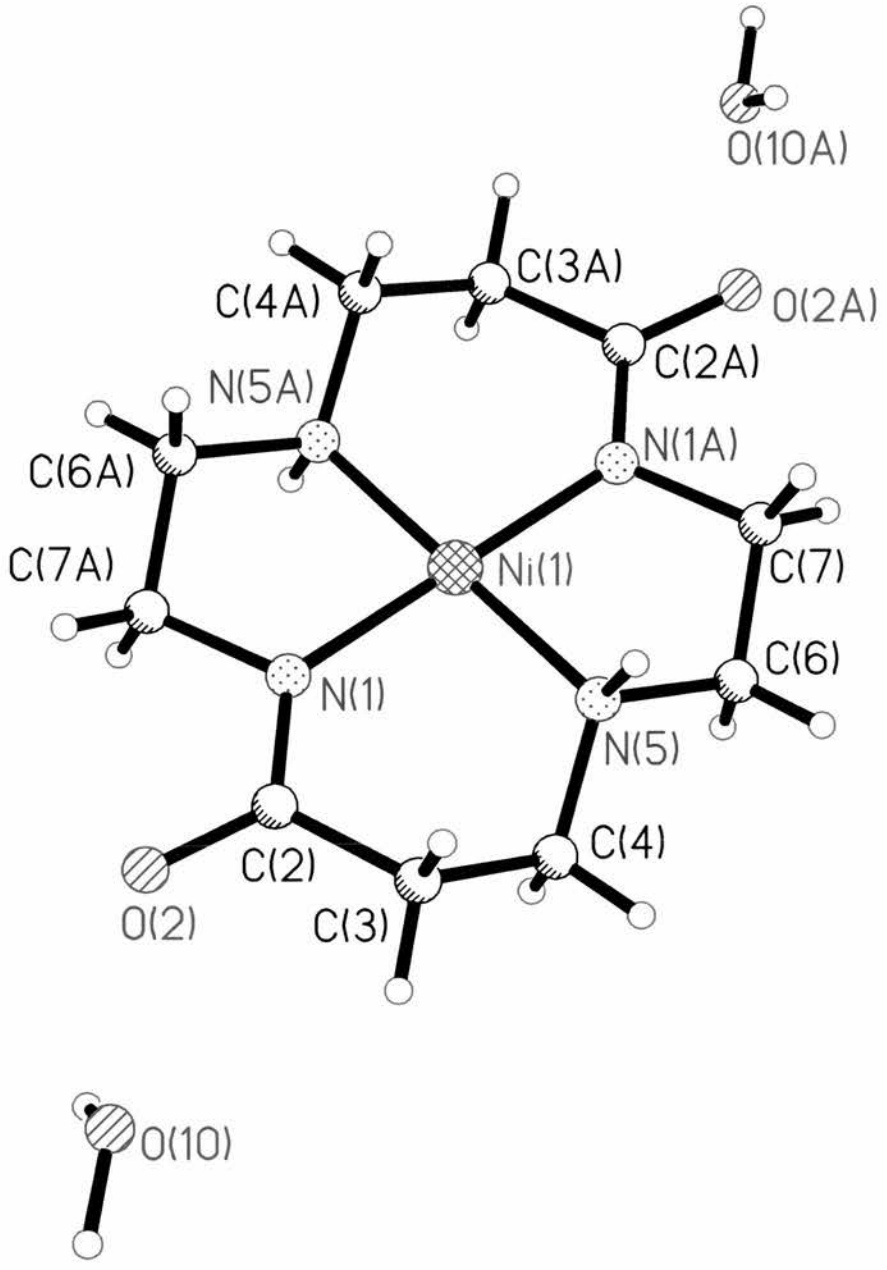

Figure 5.6: *ORTEP view of nickel(II)* trans-*dioxocyclam dihydrate*

Table 4: Experimental Parameters

Parameter	Value (units)	
Empirical formula	$C_{10}H_{22}N_4NiO_4$	
Formula weight	321.03	
Temperature	293(2) K	
Wavelength	0.71073 Å	
Crystal system	Monoclinic	
Space group	C2/c	
Unit cell dimensions	a = 20.834(10) Å	α= 90°.
	b = 7.359(4) Å	β = 112.358(6)°.
	c = 9.551(5) Å	γ = 90°.
Volume	1354.3(11) $Å^3$	
Z	4	
Density (calculated)	1.574 Mg/m^3	
Absorption coefficient	1.449 mm^{-1}	
F(000)	680	
Crystal size	.1 x .1 x .03 mm^3	
Theta range for data collection	2.11 to 23.37°.	
Index ranges	-23<=h<=23, -8<=k<=8, -10<=l<=10	
Reflections collected	3114	
Independent reflections	915 [R(int) = 0.1844]	
Completeness to theta = 23.37°	92.6 %	
Absorption correction	Sadabs	
Max. and min. transmission	1.00000 and 0.473748	

Refinement method	Full-matrix least-squares on F^2
Data / restraints / parameters	915 / 3 / 101
Goodness-of-fit on F^2	0.838
Final R indices [I>2sigma(I)]	R1 = 0.0616, wR2 = 0.1367
R indices (all data)	R1 = 0.1037, wR2 = 0.1596
Extinction coefficient	0.0027(6)
Largest diff. peak and hole	0.400 and -0.676 e.$Å^{-3}$

Table 5 Atomic coordinates

atom	x	y	z
Ni(1)	2500	-7500	5000
N(1)	2138(1)	-9606(4)	5539(3)
C(2)	1497(2)	-10271(5)	5057(4)
O(2)	1343(1)	-11710(4)	5592(3)
C(3)	944(2)	-9349(5)	3777(5)
C(4)	1004(2)	-7342(5)	3709(4)
N(5)	1636(1)	-6791(4)	3502(2)
C(6)	1659(2)	-4793(5)	3286(4)
C(7)	2340(2)	-4356(5)	3222(4)
O(10)	86(1)	-13480(3)	4087(3)

Table 6 Bond Lengths(Å)

Atom	atom	Distance	atom	atom	distance
Ni(1)	N(1)	1.879(3)	Ni(1)	N(1)(A)	1.879(3)

Ni(1)	N(5)	1.898(2)	Ni(1)	N(5)(A)	1.898(2)
N(1)	C(2)	1.329(4)	N(1)	C(7)(A)	1.478(4)
C(2)	O(2)	1.269(4)	C(2)	C(3)	1.488(5)
C(3)	C(4)	1.486(5)	C(4)	N(5)	1.461(5)
N(5)	C(6)	1.488(4)	C(6)	C(7)	1.480(5)
C(7)	N(1)(A)	1.479(4)			

Table 7 Bond Angles(°)

atom	atom	atom	angle	atom	atom	atom	angle
N(1)	Ni	N(1)(A)	179.999(1)	N(1)	Ni(1)	N(5)	93.93(11)
N(1)(A)	Ni(1)	N(5)	86.07(11)	N(1)	Ni(1)	N(5)(A)	86.07(11)
N(1)(A)	Ni(1)	N(5)(A)	93.93(11)	N(5)	Ni(1)	N(5)(A)	180.00(15)
C(2)	N(1)	C(7)(A)	115.0(3)	C(2)	N(1)	Ni(1)	131.6(2)
C(7)(A)	N(1)	Ni(1)	113.3(2)	O(2)	C(2)	N(1)	122.9(3)
O(2)	C(2)	C(3)	118.4(3)	N(1)	C(2)	C(3)	118.7(3)
C(2)	C(3)	C(4)	115.9(3)	N(5)	C(4)	C(3)	112.2(3)
C(4)	N(5)	C(6)	111.8(3)	C(4)	N(5)	Ni(1)	117.9(2)
C(6)	N(5)	Ni(1)	107.75(17)	C(7)	C(6)	N(5)	107.6(3)
N(1)(A)	C(7)	C(6)	106.2(3)				

5.5 "Big Macs"

Large macrocycles capable of binding two or more transition metals have attracted considerable interest over the last two decades[8,9]. This interest has been two-fold, firstly as biomolecule mimics and secondly as sensors. Binuclear sites are found widely in enzymes and biomolecules, most of which incorporate a bridging small molecule between the two metals, linking them electronically. The precise role of these binucleating ligands is unclear although it may be that the complexation of the small molecule leads to its activation and subsequent reaction at a physiologically important level, Figure 7[9,10].

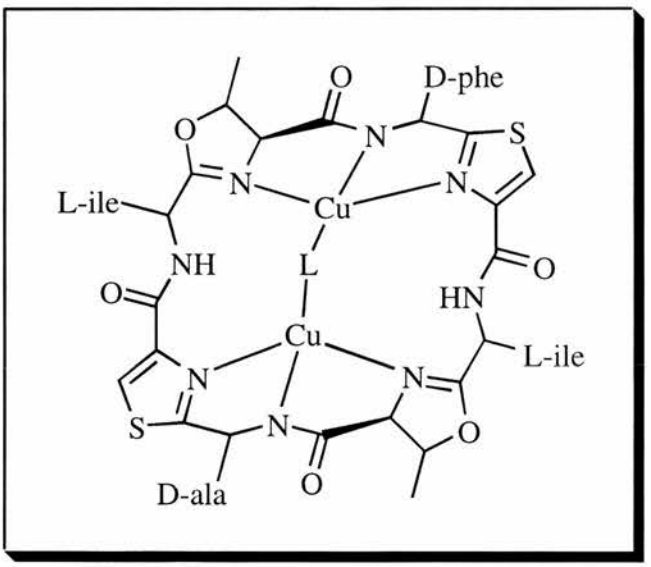

Figure 5.7

One of the difficulties in their synthesis had been removal of the templating cation from the "Big Mac", however, Schiff base [2 + 2] condensations in the absence of a templating metal have proved very successful and result, usually, in high yields[10,11,12]. The Schiff bases are then reduced to give the large macrocycles with two or more binding sites. Following work already

carried out in this group two of these Schiff bases, by the reaction of terephthaldehyde with bis(3-aminopropyl)amine and N,N'-bis(2-aminopropyl)-1,2-diaminoethane, have been prepared.

The borohydride reduction of Schiff bases **(1)** and **(2)** gives large hexaazamacrocycles capable of binding two metal centres, **(3)** and **(4)** respectively, Figure 5.8[12].

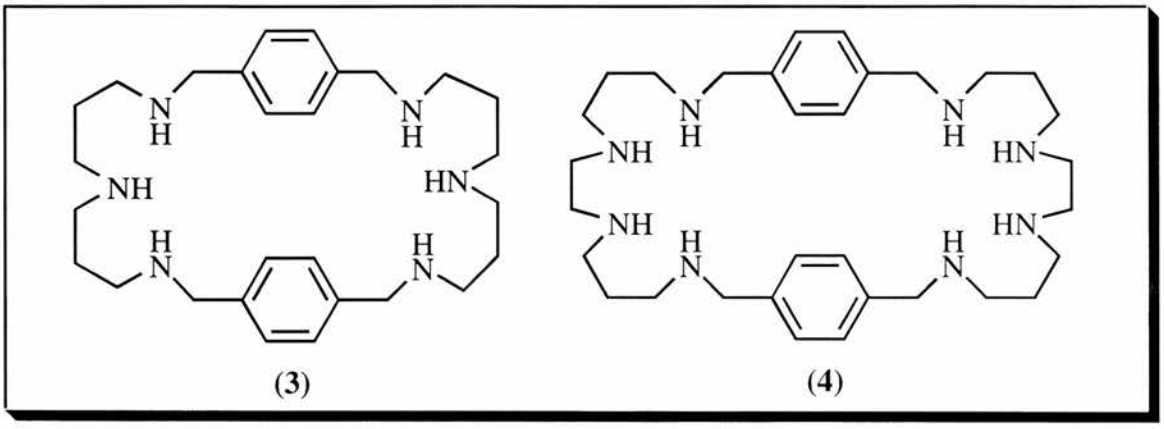

(3) **(4)**

Figure 5.8

The aim of this project had been to synthesise the two "Big Macs" shown in Figure 5.8 and then form the nickel(II) complexes and assess their electrocatalytic activity for the reduction of carbon dioxide.

5.5.1 Preparation of Schiff Base 1

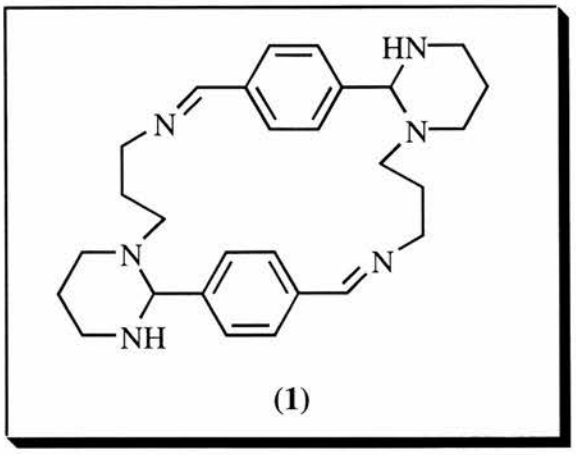

(1)

Figure 5.9: *Schiff base1*

Terephthaldehyde (5.2 g, 0.04 mol) was dissolved in THF (100 cm^3) with stirring in an ice bath and bis(3-aminopropyl)amine (5.4 g, 0.04 mol) dissolved in THF (100 cm^3) was added dropwise. A white precipitate formed after 20 min. and the mixture was stirred at 0 °C overnight then refrigerated for a further 24 hrs. The precipitate was filtered, washed with dry THF and dried *in vacuo*, m.p. 167 °C (15.2 g, 83%). Found: C, 72.9; H, 8.55; N, 18.4. Calc. for $C_{28}H_{38}N_6$: C, 73.3; H, 8.35; N, 18.3. I.R./cm^{-1} 3298(s) ν(NH); 2945(s) ν(CH); 1653 ν(C=N); 1450(m) ν(aromatic C-C); 900 ν(*p*-substituted aromatic C-C). δ_H (300 MHz; $CDCl_3$) 1.4 – 4.1 (28H, m), 7.35 (8H, m, aromatic), 8.1 (2H, s, C<u>H</u>=N).

5.5.2 Preparation of Schiff Base 2

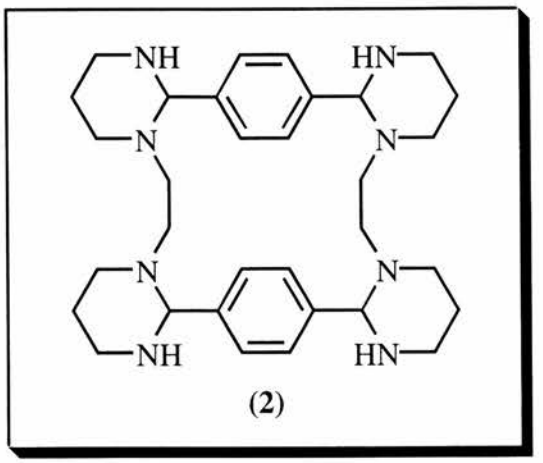

(2)

Figure 5.10: *Schiff base 2*

Terephthaldehyde (13.4 g, 0.1 mol) was dissolved in THF (200 cm^3) with stirring at room temperature and N,N'-bis(2-aminopropyl)-1,2-diaminoethane (17.4 g, 0.1 mol) was added with stirring. A white precipitate formed after 20 min. and the mixture was stirred at room temperature overnight. The precipitate was filtered, washed with dry THF and dried *in vacuo*, m.p. 128 °C (51.68 g, 95%). Found: C, 61.4; H, 8.6; N, 18.3. Calc. for $C_{32}H_{48}N_8$: C, 70.55; H, 8.9; N, 20.6.

5.5.3 Results and Discussion

The second Schiff base preparation differed from that of the first in that it was not cooled and the amine was not added dropwise to the terephthaldehyde solution. This probably resulted in some polymer formation as reflected in the low C and N in the microanalysis. Further purification and characterisation of Schiff base 2 was not attempted. High dilution methods and cooling would probably have avoided polymer formation and previously reported large hexaazamacrocycles of

this type are all prepared by dilution methods[11,12]. Neither Schiff base was pursued further because of the purification difficulties.

5.6 Synthesis of dipeptides for the study of metal Ion Promoted Peptide Ester Hydrolysis

5.6.1 Introduction

The copper(II) and palladium(II) promoted hydrolysis of a variety of amino acid and peptide esters has been studied. Rate accelerations of *ca.* 10^3 and 10^5 for the co-ordinated ligands have been reported for copper(II) and palladium(II) respectively[13,14].

The copper(II) promoted hydrolysis of the methyl esters of glycylglycine and glycylsarcosine was studied by Nakon and Angelici[15]. At low pH the peptide ligands bind to the metal *via* the terminal amino group, the deprotonated amide nitrogen and there is probably a weak interaction between the carbonyl oxygen of the ester and the metal ion. The peptide bond is not susceptible to hydrolysis in the deprotonated complex; indeed this bond is stabilised by co-ordination of the nitrogen atom to the copper ion as shown in Figure 5.11. The only other group, therefore, at which hydrolysis can occur is the ester group. Hay and Nolan studied the copper(II) promoted hydrolysis of the methyl esters of glycyl-(*2S*)-alanine, glycyl-(*2S*)-valine and glycyl-(*2S*)-leucine compared to the base hydrolysis of these esters[13]. This series of three dipeptides was chosen to complete the series already investigated by this group and to assess possible steric hindrance by the lengthening and branching of the alkyl chain.

The rate acceleration of the copper(II) promoted hydrolysis of ethyl glycylglycinate compared to base hydrolysis was *ca.* 4.6×10^3, this increase in rate indicates a degree of metal-ester carbonyl bonding. For the (*2S*)-alanine derivative the rate acceleration was 2×10^3 which is not significantly different for the glycine derivative. The rate acceleration for the hydroxo-copper complex of the (*2S*)-leucine derivative was *ca.* 9.2×10^2. It is clear that the copper(II) exerts a

significant effect on the hydrolysis of dipeptide esters, the rate acceleration being of the order 10^3. In cobalt(III) systems in which the carbonyl group of the ester is known to be bonded directly to the metal ion, rate accelerations of the order of 10^6 have been observed. It is clear, therefore, that in the copper(II) systems the ester-metal interactions are somewhat weaker.

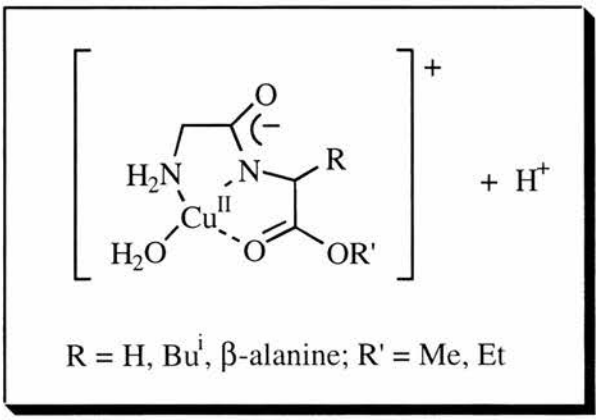

Figure 5.11

The palladium(II) promoted hydrolysis of methyl glycylglycinate and isopropyl glycylglycinate has also been studied by Hay *et al.* as expected the analogous complex of metal-dipeptide is formed, Figure 5.12[14].

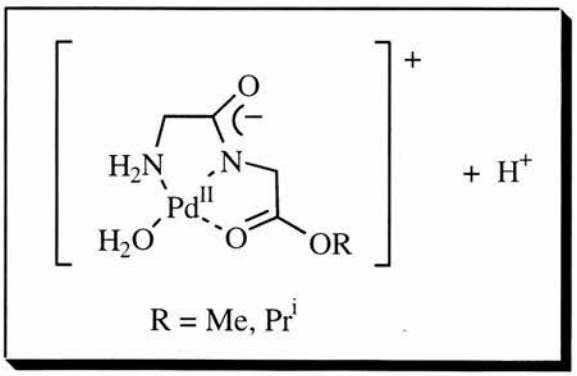

Figure 5.12

As with the copper(II) complexes in the Pd(II) centered complexes the dipeptide binds the metal *via* the terminal amine, the deprotonated amide nitrogen and the ester carbonyl oxygen. The rate accelerations observed for the palladium(II) promoted hydrolysis of co-ordinated peptide esters compared to that for uncoordinated peptide esters is of the order of *ca.* 10^5. This provides good evidence for the formation of a complex such as shown in Figure 10 where there is direct interaction between the ester carbonyl group and the metal as in the cobalt(III) complexes as opposed to the weak interaction in the copper(II) complexes. In such systems it has been found that the direct polarisation mechanism involving attack of a nucleophile such as water or hydroxide ion on a co-ordinated carbonyl group leads to rate accelerations of 10^5-10^6 for all substrates, independent of the leaving group. One implication of this is that the hydrolysis of sterically hindered peptide esters may be done effectively under mild conditions.

A similar set of rate accelerations are expected for both the copper(II) complexes and the palladium(II) complexes of these dipeptides under the same set of conditions as for the previous study. For this work it was decided to prepare the dipeptide esters from their correspondent protected amino acids. There are many methods for coupling two protected amino acids to form dipeptides, the N,N'-dicyclohexylcarbodiimide (DCC) method was chosen for these preparations[16,17]. This method was chosen for its simplicity. Where the salt of the amino acid ester is used, 1 equivalent of a tertiary base is added, the reaction is carried out at room temperature and is generally completed after *ca.* 4 hr. The product is readily obtained by removal of the insoluble urea and washing with dilute acid followed by dilute base and recrystallisation.

In addition it was postulated that it may be possible to use these systems to couple a further monoprotected amino acid to the dipeptide co-ordinated to the metal forming a tripeptide. The ease of hydrolysis of the C-terminal ester group using water or hydroxide as the nucleophile

suggests that the free amino group on the N-terminus of a further amino acid ester should be nucleophilic enough to effect the hydrolysis of the ester group bound to the metal thus forming a tripeptide *in situ.*, Figure 5.13 and this aspect was one of the original aims of the project.

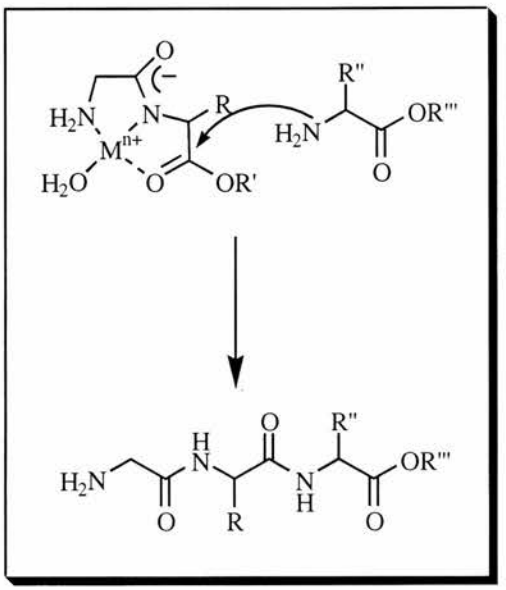

Figure 5.13

5.6.2 Results and Discussion

Although the DCC method for coupling amino acids and/or peptides is simple, the three dipeptides prepared by this method showed significant dicyclohexylurea contamination, several recrystallisations were attempted but were unsuccessful in removing this impurity.

All three dipeptides showed significant DCC contamination in their microanalyses and nmr spectra. Contrary to the literature method for preparing peptides in this way, removal of dicyclohexylurea is difficult and lengthy, requiring repeated recrystallisations and/or silica gel chromatography. On balance the mixed anhydride method of coupling amino acids and/or peptides is recommended[15].

The apparatus used for these experiments was calibrated using ethyl glycinate as substrate, a palladium(II) catalyst and a standardised NaOH solution. The experiments were carried out using automated titration equipment on which the results were processed. This calibration took several weeks and coupled with the problems encountered with the dipeptide purification meant that this project was not pursued.

5.6.3 Experimental

5.6.3.1 Preparation of methyl carboxybenzyl glycyl-(2*S*)-alaninate

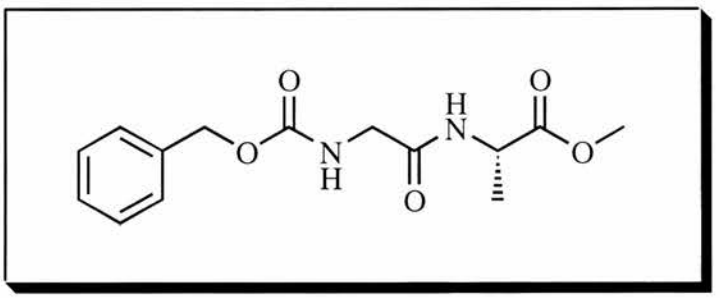

Figure 5.14

To a solution of carboxybenzyl glycine (1.00 g, 4.78 mmol), methyl-(2*S*)-alaninate hydrochloride (0.67 g, 4.78 mmol) and triethylamine (0.67 cm^3) in THF (150 cm^3) was added N,N'-dicyclohexylcarbodiimide (0.99 g, 4.78 mmol) with stirring at room temperature. The mixture was allowed to stir at room temperature for 4 hr whereupon acetic acid (1.00 cm^3) was added. The precipitated dicyclohexylurea was removed by filtration and the filtrate washed successively with water, hydrochloric acid (1 mol dm^{-3}), water, sodium bicarbonate (5%) and water and dried over anhydrous sodium sulphate. The solvent was removed under reduced pressure to give crude product as a off white solid which was recrystallised from methanol/ water to give methyl carboxybenzyl glycyl-(2*S*)-alaninate as a white solid. After two

recrystallisations: m.p. 145-147 °C. Found: C, 68.0; H, 9.35; N, 10.70. Calc. for $C_{14}H_{18}N_2O_5$: C, 57.1; H, 6.2; N, 9.5. δ_H (300 MHz; $CDCl_3$) 0.95-1.95 (C<u>H</u>, m, dicyclohexylurea contamination), 3.43 (3H, br s, OC<u>H</u>$_3$), 3.6 (N<u>H</u>, m, dicyclohexylurea contamination), 3.79 (1H, m, NHC<u>H</u>CH$_3$), 4.0 (2H, d, NHC<u>H</u>$_2$CO), 5.05 (2H, s, $C_6H_5C\underline{H}_2O$), 5.51 (1H, br s, OCON<u>H</u>CH$_2$), 7.1 (1H, br s, OCN<u>H</u>CHCH$_3$), 7.3 (5H, s, $C_6\underline{H}_5$-).

5.6.3.2 Preparation of methyl carboxybenzyl glycyl-(2*S*)-valinate

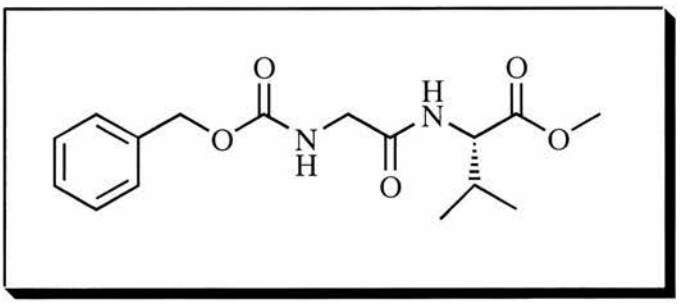

Figure 5.15

To a solution of carboxybenzyl glycine (2.00 g, 9.60 mmol), methyl-(2*S*)-valinate hydrochloride (1.61 g, 9.60 mmol) and triethylamine (1.34 cm^3) in dichloromethane (200 cm^3) was added N,N'-dicyclohexylcarbodiimide (2.06 g, 9.60 mmol) with stirring at room temperature. The mixture was allowed to stir at room temperature for 4 hr whereupon acetic acid (2.00 cm^3) was added. The precipitated dicyclohexylurea was removed by filtration and the filtrate washed successively with water, hydrochloric acid (1 mol dm^{-3}), water, sodium bicarbonate (5%) and water and dried over anhydrous sodium sulphate. The solvent was removed under reduced pressure to give crude product as a yellow white solid which was recrystallised from methanol/ water to give methyl carboxybenzyl glycyl-(2*S*)-valinate as a white solid. m.p. 144 °C. Found: C, 66.5; H, 8.3; N, 10.4. Calc. for $C_{16}H_{22}N_2O_5$: C, 59.6; H, 6.9; N, 8.7. δ_H (300 MHz; $CDCl_3$) 0.95-1.95 (C<u>H</u>, m,

dicyclohexylurea contamination), 1.61 (6H, s, $CH(C\underline{H}_3)_2$), 3.53 (3H, br s, $OC\underline{H}_3$), 3.68 ($N\underline{H}$, m, dicyclohexylurea contamination), 3.85 (1H, m, $NHC\underline{H}CH(CH_3)_2$), 4.08 (2H, d, $NHC\underline{H}_2CO$), 5.13 (2H, s, $C_6H_5C\underline{H}_2O$), 5.58 (1H, br s, $OCON\underline{H}CH_2$), 7.19 (1H, br s, $OCN\underline{H}CHCH(CH_3)_2$), 7.35 (5H, s, $C_6\underline{H}_5$-).

5.6.3.3 Preparation of methyl carboxybenzyl glycyl-(2*S*)-leucinate

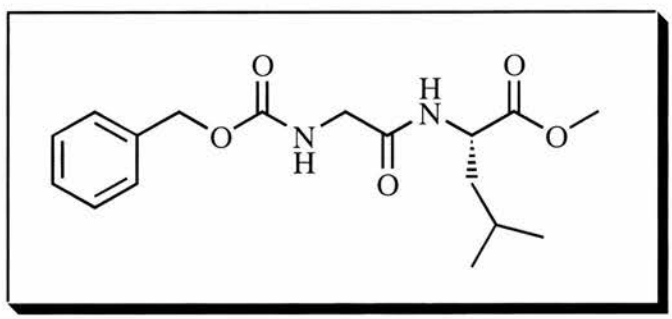

Figure 5.16

To a solution of carboxybenzyl glycine (2.00 g, 9.60 mmol), methyl-(2*S*)-leucinate hydrochloride (1.74 g, 9.60 mmol) and triethylamine (1.34 cm^3) in dichloromethane (200 cm^3) was added N,N'-dicyclohexylcarbodiimide (2.06 g, 9.60 mmol) with stirring at room temperature. The mixture was allowed to stir at room temperature for 4 hr whereupon acetic acid (2.00 cm^3) was added. The precipitated dicyclohexylurea was removed by filtration and the filtrate washed successively with water, hydrochloric acid (1 mol dm^{-3}), water, sodium bicarbonate (5%) and water and dried over anhydrous sodium sulphate. The solvent was removed under reduced pressure to give crude product as a yellow white solid which was recrystallised from methanol/ water to give methyl carboxybenzyl glycyl-(2*S*)-leucinate as a white solid. m.p. 141-2 °C. Found: C, 66.9; H, 8.7; N, 10.6. Calc. for $C_{17}H_{24}N_2O_5$: C, 60.7; H, 7.2; N, 8.3. δ_H (300 MHz; $CDCl_3$) 0.95-1.95 ($C\underline{H}$, m, dicyclohexylurea contamination), 3.45

(3H, br s, $OC\underline{H}_3$), 3.65 ($N\underline{H}$, m, dicyclohexylurea contamination), 3.85 (1H, m, $NHC\underline{H}CO$), 4.07 (2H, d, $NHC\underline{H}_2CO$), 5.15 (2H, s, $C_6H_5C\underline{H}_2O$), 5.61 (1H, br s, $OCON\underline{H}CH_2$), 7.2 (1H, br s, $N\underline{H}CHCO$), 7.34 (5H, s, $C_6\underline{H}_5$-).

5.7 Copper(II) cyclen complexes

As for the cyclam based tetraaza ligands [14aneN$_4$] cyclen tetraaza ligands [12aneN$_4$] have been known for several decades and their metal ion complexation with a variety of metal ions has been studied extensively[19,20,21]. These ligands lead to complexes with enhanced thermodynamic and kinetic properties for metal ion dissociation compared to their open chain analogues (the macrocyclic effect). However, the 12-membered ring macrocyclic ligands such as cyclen dissociate much more rapidly than cyclam ($x10^4$)[22]. This is thought to be due to the copper sitting "atop" the plane of the for donor nitrogen atoms of the cyclen ring. This geometry has been observed in the crystal structure of the [Cu(cyclen)(ONO_2)]$^+$ cation in which the copper lies 0.5Å above the plane[23]. In addition, functionalised cyclen complexes have been used as sensors for lanthanides and gadolinium complexes of functionalised cyclens are being used as contrast agents in magnetic resonance imaging, MRI[24,25]. Our group had already looked at functionalising one or more of the secondary amines starting with the molybdenum complex, here the synthesis of two copper(II) complexes is presented. The cyclen was used as received from Professor Parker. The X-Ray crystal structure of the [Cu(cyclen)Br]$^+$ cation is presented. Structurally accurate data on simple macrocycles has become increasingly important in recent years for the testing of molecular mechanics and Density Functional Theory (DFT) calculations[26,27].

5.7.1 Preparation of $[Cu(cyclen)ClO_4](ClO_4)$.

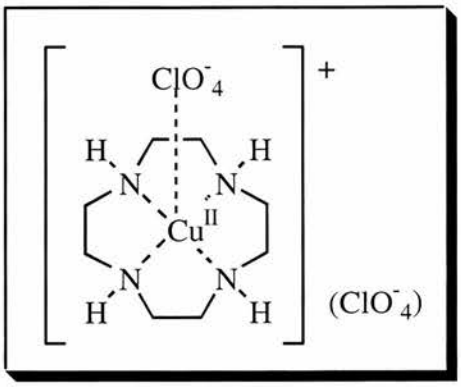

Figure 5.17

$Cu(ClO_4)_2.6H_2O$ (0.43 g, 1.16 mmol) was dissolved in the minimum volume of ethanol and cyclen (0.19 g, 1.16 mmol) was dissolved in the minimum volume of ethanol. The two solutions were added together and warmed on a water bath (45°C) for 20 min. and allowed to cool to room temperature. On standing large dark blue crystals precipitated. These were filtered and dried *in vacuo* (612 mg, 88%). Found: C, 22.0; H, 4.5; N, 12.5. Calc. for $C_8H_{20}N_4Cl_2O_8Cu$: C, 22.1; H, 4.65; N, 13.0.

5.7.2 Preparation of $[Cu(cyclen)Br]ClO_4.NaClO_4.H_2O$

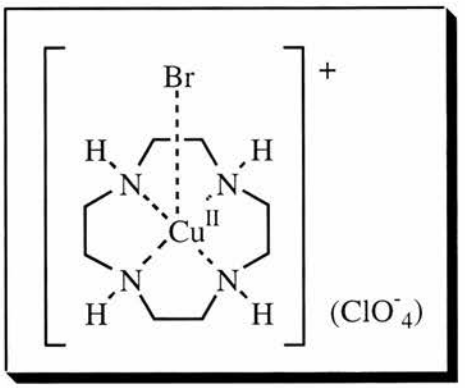

Figure 5.18

$CuBr_2$ (0.256 g, 1.16 mmol) was dissolved in the minimum volume of ethanol and cyclen (0.19 g, 1.16 mmol) was dissolved in the minimum volume of ethanol. The two solutions were added together and warmed on a water bath (45 °C) for 20 min. and allowed to cool to room temperature. A saturated solution of $NaClO_4$ was added to the reaction mixture to facilitate precipitation. On standing large dark blue crystals precipitated which were filtered and dried *in vacuo* (532 mg, 83%). The crystals were suitable for X-Ray crystallography and the structure showed that perchlorate had crystallised as the counter ion. Found: C, 17.2; H, 3.7; N, 9.85. Calc. for $C_8H_{20}N_4BrCuClO_4.NaClO_4.H_2O$: C, 17.35; H, 4.0; N, 10.1.

5.8 Crystal Structure Determination of $[Cu(cyclen)Br]ClO_4.NaClO_4.H_2O$

Crystals suitable for X-Ray diffraction were prepared as described and showed an interesting system in which the salt added to facilitate crystallisation has crystallised with the complex and the expected bromide counter ion has been replaced by a perchlorate counter ion.

The cation crystallised as expected with a bromide occupying the fifth coordination site on the copper(II) centre also incorporated were a sodium perchlorate and a water of crystallisation, the overall formulation is thus: $[Cu(cyclen)Br]ClO_4.NaClO_4.H_2O$, to our knowledge, of the cyclen complexes which have been solved to date this is the first example incorporating a bromide. The ORTEP views of $[Cu(cyclen)Br]ClO_4.NaClO_4.H_2O$ looking down the axial axis of the complex and from the side are shown in Figure 5.19. Tables 8 to 11 summarise the experimental parameters, atomic coordinates, bond distances and bond angles. The geometry is clearly purely square pyramidal, rather than trigonal bipyramidal with Br occupying the apical position. The bond angles N(7)-Cu-N(1) and N(4)-Cu-N(10) are both close to 146° indicating significant raising of the copper above the N_4 plane. It is clear from the lower ORTEP diagram that the copper does indeed lie above the plane and the distance is calculated to be 0.53Å which is similar to 0.5Å found for the nitrate complex[23]. All the hydrogens on the amines point axially, as the macrocycle folds down to incorporate the metal. The Cu-Br bond length is 2.57Å, compared to 2.42Å in the copper complex of an adamazane ligand and 2.515Å in $[Cu(13aneN_3O)Br]Br$[28,29]. The long bond length may be explained by a Jahn Teller effect or hydrogen bonding between the axial bromide and an NH group of a neighbouring cyclen[27]. The N(7)-H(7)-Br' is 2.68Å indicating that there is a hydrogen bond formed. Another hydrogen bond of note is that between N(10)-H(10) and a perchlorate oxygen O(4)', this as rather shorter than the bromide hydrogen bond at 2.28Å. An effect of this hydrogen bond is that the Cu-N(10) bond is shorter than the other Cu-N bonds at 1.974(4)Å and this is due to the extent of the hydrogen atom "leaving" the amine and allowing more electron density to become associated with the dipositive metal centre and hence the bond shortens.

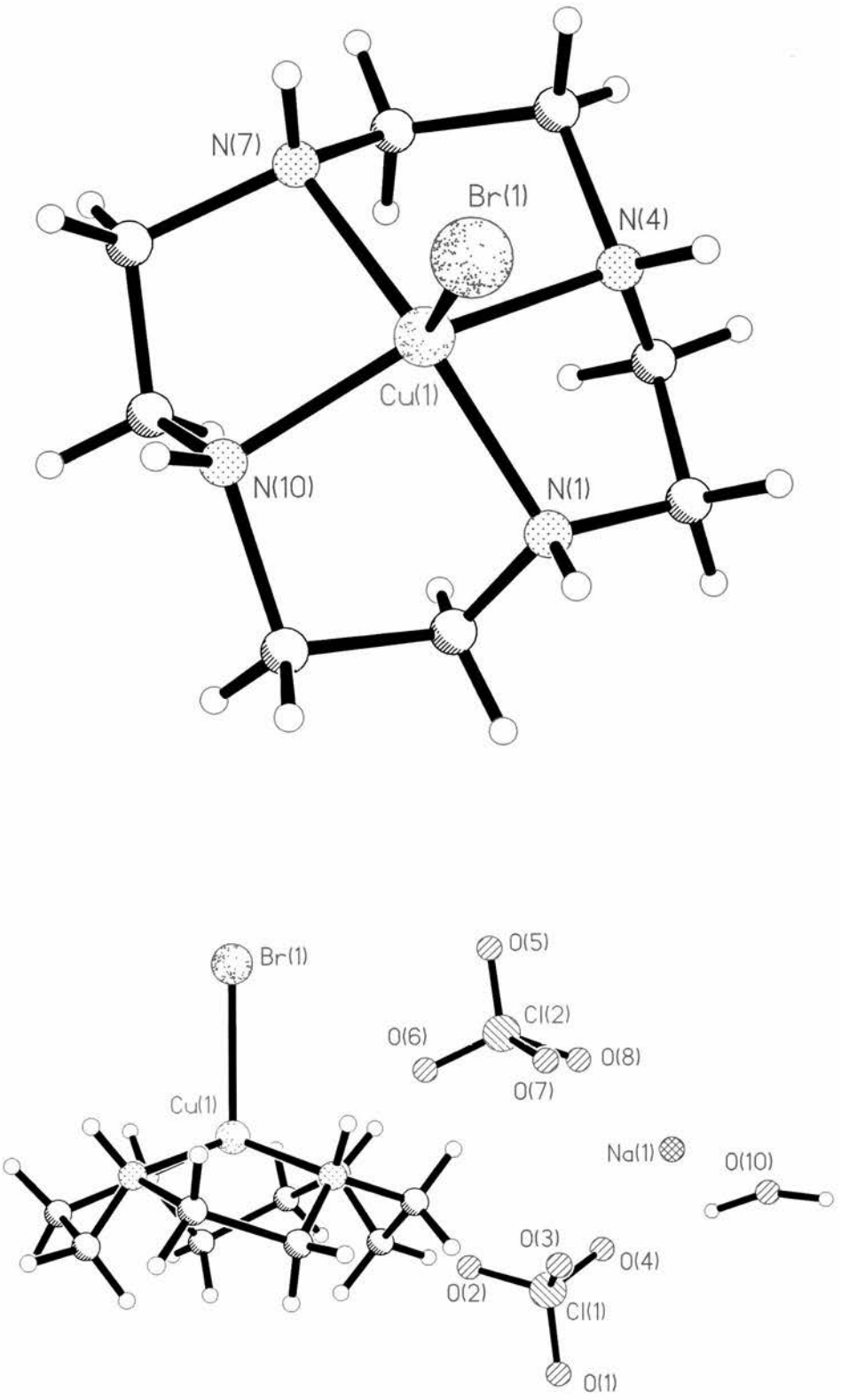

Figure 5.19: *ORTEP views of [Cu(cyclen)Br]ClO_4.$NaClO_4$*

Table 8: Experimental Parameters

Parameter	Value (units)
Empirical formula	$C_8H_{20}N_4Cl_2O_8Cu.NaClO_4$
Formula weight	370.42
Temperature	293(2) K
Wavelength	0.71073 Å
Crystal system	Orthorhombic
Space group	Pca2(1)
Unit cell dimensions	a = 17.4477(4) Å α= 90°.
	b = 12.0458(3) Å β = 90°.
	c = 9.6247(3) Å γ = 90°.
Volume	2022.84(9) $Å^3$
Z	6
Density (calculated)	1.824 Mg/m^3
Absorption coefficient	3.387 mm^{-1}
F(000)	1116
Crystal size	.1 x .1 x .02 mm^3
Theta range for data collection	2.88 to 23.26°.
Index ranges	-19<=h<=19, -13<=k<=10, -10<=l<=10
Reflections collected	9584
Independent reflections	2837 [R(int) = 0.0394]
Completeness to theta = 23.37°	98.5 %
Absorption correction	Sadabs
Max. and min. transmission	1.00000 and 0.728319

Refinement method	Full-matrix least-squares on F^2
Data / restraints / parameters	2837 / 3 / 240
Goodness-of-fit on F^2	0.965
Final R indices [I>2sigma(I)]	R1 = 0.0431, wR2 = 0.1048
R indices (all data)	R1 = 0.0649, wR2 = 0.1189
Extinction coefficient	0.00
Largest diff. peak and hole	0.560 and -0.407 e.$Å^{-3}$

Table 9: Atomic coordinates

atom	x	y	z
Br(1)	7833(1)	2979(1)	7431(1)
Cu(1)	6431(1)	2334(1)	7420(1)
N(1)	6161(2)	1893(4)	9364(3)
C(2)	6184(2)	743(4)	9571(3)
C(3)	5936(4)	248(6)	8208(9)
N(4)	6470(2)	683(3)	7441(11)
C(5)	6310(3)	414(5)	5798(9)
C(6)	5727(4)	1231(6)	5240(6)
N(7)	6092(2)	2396(6)	5446(4)
C(8)	5526(2)	3447(5)	5410(5)
C(9)	5196(3)	3632(4)	6831(6)
N(10)	5788(2)	3670(3)	7657(12)
C(11)	5494(5)	3640(5)	9336(7)
C(12)	5486(3)	2367(5)	9752(6)

Table 10: Bond Lengths(Å)

Atom	atom	Distance	atom	atom	distance
Br(1)	Cu(1)	2.5667(5)	Cu(1)	N(10)	1.974(4)
Cu(1)	N(4)	1.991(4)	Cu(1)	N(7)	1.991(4)
Cu(1)	N(1)	2.001(4)	N(1)	C(12)	1.362(6)
N(1)	C(2)	1.4001	C(2)	C(3)	1.504(9)
C(3)	N(4)	1.299(10)	N(4)	C(5)	1.638(13)
C(5)	C(6)	1.513(10)	C(6)	N(7)	1.554(9)
N(7)	C(8)	1.605(8)	C(8)	C(9)	1.501(7)
C(9)	N(10)	1.303(9)	N(10)	C(11)	1.696(12)
C(11)	C(12)	1.584(9)			

Table 11: Bond Angles(°)

atom	atom	atom	angle	atom	atom	atom	angle
N(10)-	Cu(1)-	N(4)	146.36(17)	N(10)-	Cu(1)-	N(7)	84.9(4)
N(4)-	Cu(1)-	N(7)	93.3(4)	N(10)-	Cu(1)-	N(1)	88.6(3)
N(4)-	Cu(1)-	N(1)	74.5(3)	N(7)-	Cu(1)-	N(1)	146.31(15)
N(10)-	Cu(1)-	Br(1)	107.14(10)	N(4)-	Cu(1)-	Br(1)	105.65(10)
N(7)-	Cu(1)-	Br(1)	105.99(12)	N(1)-	Cu(1)-	Br(1)	107.52(10)
C(12)-	N(1)-	C(2)	113.6(3)	C(12)-	N(1)-	Cu(1)	110.4(3)
C(2)-	N(1)-	Cu(1)	112.95(13)	N(1)-	C(2)-	C(3)	105.0(3)
N(4)-	C(3)-	C(2)	97.5(6)	C(3)-	N(4)-	C(5)	110.3(6)
C(3)-	N(4)-	Cu(1)	112.6(5)	C(5)-	N(4)-	Cu(1)	100.5(4)
C(6)-	C(5)-	N(4)	109.2(5)	C(5)-	C(6)-	N(7)	105.5(5)
C(6)-	N(7)-	C(8)	117.2(4)	C(6)-	N(7)-	Cu(1)	102.1(3)

C(8)-	N(7)-	Cu(1)	103.5(3)	C(9)-	C(8)-	N(7)	109.5(4)
N(10)-	C(9)-	C(8)	104.9(6)	C(9)-	N(10)-	C(11)	109.9(5)
C(9)-	N(10)-	Cu(1)	110.6(5)	C(11)-	N(10)-	Cu(1)	105.4(5)
C(12)-	C(11)-	N(10)	105.3(4)	N(1)-	C(12)-	C(11)	109.3(5)

5.9 Conclusions and Further Work

Trans-dioxocyclam based ligands and complexes

We report the first structure of nickel(II) *trans*-dioxocyclam and that of the free ligand. The short amide C-N bond lengths in both structures reflect the dominant tautomeric form. The Ni-N bond lengths to the amide groups are shorter reflecting the stronger interaction. The nickel environment shows significantly less distortion than a recently reported *cis*-dioxocyclam nickel complex. A cyanoethyl derivative was also presented. Future work will focus on further pendant arms and reducing the cyano groups to amine donors.

"Big Macs"

These ligands provide a simple route for preparing dinuclear metal complexes such as dinickel complexes for CO_2 reduction and dicopper complexes as models for biological systems. The copper work was pursued elsewhere in the group and the rather poor solubility limited their use for electrochemical studies[4,12].

Synthesis of dipeptides for the study of metal promoted pipeptide ester hydrolysis

The work demonstrates the efficacy of modern synthetic techniques using protecting group methodology. However, the DCC coupling route chosen led to significant contamination by dicyclohexylurea which proved difficult to remove in the purification steps. An alternative route based on the mixed anhydrides is proposed.

Copper cyclen complexes

In work aimed at functionalising cyclen for MRI applications, interesting structural data on copper cyclen complexes was discovered. The structure of [Cu(II)(cyclen)Br](ClO_4).$NaClO_4$.H_2O was presented. The geometry of the copper environment is square pyramidal consistent with other copper cyclen complexes in the literature. The copper(II) ion lies 0.53Å above the plane due to the small size of the binding cavity. Some minor distortions from ideal geometry as well as a larger than expected Cu-Br bond length were attributed as most probably due to hydrogen bonding effects. Future work will concentrate on functionalising the secondary amines with, for example, acrylonitrile.

5.10 References

1. R. W. Hay and P. R. Norman, *Transition Met. Chem.*, 1980, **5**, 232.
2. Personal communication, S. Ditop, Institute of Physical Chemistry, The University of Kiev, Kiev.
3. Source: The University of Durham, Department of Chemistry, Dr. J. A. Gareth Williams, Metal complexes of macrocyclic ligands; http://www.dur.ac.uk/j.a.g.williams/.
4. T. Clifford, *Ph.D. Thesis*, University of St Andrews, 1996.
5. F. Denat et al., *New J. Chem.*, 2000, **24**, 959.
6. M. Chin et al., *ICA*, 1999, **292**, 257.
7. F. Denat, S. Lacour, S. Brandes, R. Gillard, *Tetrahedron Lett.*, 1997, **38**, 4417.
8. F. Rabiet, F. Denat, R. Gillard, *Synth. Commun.*, 1997, **27**, 9789.
9. T. Sorrel, Tetrahedron, 1989, **45**, 3.
10. D. E. Fenton and H. Okawa [R. W. Hay, J. R. Dilworth and K. B. Nolan (Eds.)] *Perspectives in Bioinorganic Chemistry*, JAI Press, Connecticut, 1993.
11. M. Pietraszkiewics and R. Gasiorowski, *Chem. Ber.*, 1990, **123**, 405.
12. R. W. Hay, A. Danby, T. Clifford *et al.*, *Transition Met. Chem.*, 1995, **20**, 220.
13. R. W. Hay, K. B. Nolan, *J. Chem. Soc., Dalton Trans.*, 1974, 2542.
14. R.W. Hay, M. P. Pujari, *J. Chem. Soc., Dalton Trans.*, 1984, 1083.
15. R. Nakon, R. J. Angelici, *Inorg. Chem.*, 1973, **12**, 1269.
16. J. C. Sheehan, *Chem. Comm.*, 1955, **77**, 1067.
17. P. Greenstein, M. Winitz, *Chemistry of the Amino Acids*, 1961, **vol.2**, Wiley.
18. G. W. Anderson, J. E. Zimmerman, F. M. Callahan, *J. Am. Chem. Soc.*, 1967, **89**, 5012.
19. J. P. Collman and P. W. Schneider, *Inorg. Chem.*, 1966, **5**, 1380.
20. R. W. Hay and P. R. Norman, *J. Chem. Soc., Dalton Trans.*, 1979, 1441.

21. R. W. Hay and P. R. Norman, *Transition Met., Chem.*, 1997, **22**, 248.

22. R. W. Hay et al., *Inorg. Chim. Acta*, 1988, **2**, 100.

23. R. M. Clay et al., *Acta Cryst B*, 1979, 35.

24 D. Parker *et al.*, *J. Chem. Soc., Perkin Trans.*, 1993, **2**, 605.

25. Source: The University of Durham, Department of Chemistry, Professor David Parker, http://www.dur.ac.uk/chemistry/Staff/dp/dp.html

26. M. Zimmer, *Coord. Chem. Rev.*, 2001, **212**, 133.

27. L. F. Lindoy, T. Rambusch, B. W. Skelton and A. H. White, *J. Chem. Soc., Dalton Trans*, 2001, 1857.

28. J. Sprinborg and I. Søtofte, *Acta Chem. Scand.*, 1997, **51**, 357.

29. V. J. Thöm, . C. Fox, J. C. A. Boeyens and R. D. Hancock, *J. Am. Chem. Soc.*, 1984, **106**, 5947.